Structure and Surface Chemistry of Gold-Based Model Catalysts

Jinlong Gong*

Key Laboratory for Green Chemical Technology of Ministry of Education, School of Chemical Engineering and Technology, Tianjin University, Tianjin 300072, China

CONTENTS

1. INTRODUCTION

Gold ($[Xe]4f^{14}5d^{10}6s^1$) is one of the most ancient themes of investigation in science and arts, and its renaissance now leads to an exponentially increasing number of publications, especially in the context of emerging nanoscience and nanotechnology, catalysis, and self-assembled monolayers (SAMs). Gold possesses a rich organometallic and coordination chemistry[1] but has been historically considered as an inert substance because bulk gold surfaces readily chemisorb few molecules.[2] Additionally, gold nanoparticles smaller than 10 nm in diameter are somewhat difficult to synthesize due to the low melting point of gold,[3] which is vital for tuning active sites of a catalyst. Although there were a number of early but scattered investigations regarding the use of gold as a catalyst, none of them showed that gold was superior to other catalysts.[4] This situation was changed by the seminal discoveries by Haruta[5] and Hutchings;[6] they clearly demonstrated the unique chemical properties of gold catalysts. In 1989, Haruta et al. pioneered a method for preparing gold nanoclusters on several metal oxides, which possessed high reactivity for CO oxidation and propylene epoxidation, particularly at low temperatures.[7] Remarkably, the CO oxidation can proceed at temperatures as low as 200 K, which later leads to a series of applications of gold catalysts at and below room temperature.

Since then, gold-based heterogeneous catalysts have attracted much attention, particularly for low-temperature CO oxidation, epoxidation, the water−gas shift reaction, and selective oxidation.[8] These subjects are now more intensively investigated, due to fundamental and applied aspects relevant to the support, particle size and shape, and structural sensitivity, especially in the context of catalysis, surface science, biology, nanoscience, and nanotechnology.[4,9−13] A variety of investigations have attempted to draw the correlation between the electronic and structural properties of the Au surfaces and particles with the catalytic activity. For example, the gold single-crystal surfaces covered with atomic oxygen are highly reactive in a variety of reactions. The particle size of Au clusters and the nature of the support are critical in determining catalytic activity. Moreover, it has been proposed that the interface between the Au nanoparticles and the oxide support are active sites. However, size distribution and shapes of gold nanoparticles often vary widely, and the particle structure, particularly at the metal−oxide interface, is generally not well-defined.[14] Owing to these complexities, the nature of active sites of Au-based catalysts remain unclear.[10] Therefore, detailed mechanistic studies aimed at understanding gold's promising catalytic characteristics are urgently needed. Fortunately, fundamental investigations of reactive chemistry on gold-based model catalysts can provide significant insights into the mechanistic details of these reactions since it is possible to carefully control surface structure and reaction parameters as

well as to circumvent the problem of agglomeration of supported gold nanoparticles in some cases.[15]

There are many excellent reviews regarding gold catalysis;[1,3,4,10−12,16−30] however, these reviews primarily focus on (i) the interaction of gold nanoparticles/clusters with the support (predominantly TiO_2 and CeO_2), (ii) oxidative reactions on high-surface-area catalysts, (iii) theoretical studies, and (iv) organometallic chemistry. For example, a classical review written by Meyer et al. in 2004 deals with the surface structure of gold single crystals and supported gold clusters and primarily focuses on the surface chemistry of CO oxidation.[10] Min and Friend provided an excellent overview on the reactivity of Au(111) and $Au/TiO_2(110)$ with regard to the oxidation of CO and propylene.[19] Indeed, there has been a lack of comprehensive reviews on gold-based *model* systems (e.g., Au single crystals, gold-based inversed catalysts, gold-based bimetallic, and Au clusters supported on various substrates) and their chemical reactivity. Therefore, this review aims to provide an overview of the current status of research regarding the surface chemistry of gold-based model systems. Of particular note, the electrochemistry of gold, optical properties (e.g., photonics and plasmonic),[31] and the formation and application of self-assembled monolayers of various components (particularly thiols)[16,32] require their own separate reviews. The review will focus on issues in structural, electronic, and chemical properties of gold-based model catalysts published through December 2011. Results will be presented from simplicity (gold single crystals) to complexity (deposited gold particles) with a discussion of their relevance to real catalysts.

The review begins with a brief overview of surface structures and electronic properties of various gold single-crystal surfaces. We will also examine adsorption phenomena on Au macroscopic crystalline surfaces. Next, reactive chemistry on gold surfaces will be discussed, particularly recent work on oxidized Au(111) that is relevant to the fundamental underpinnings of gold catalysis. The sections on Au-based inverse and bimetallic model systems will focus on the relationship between gold and the metal oxides or a secondary metal with regard to structure and reactivity and the contribution of these investigations to the catalysis community. Lastly, we will discuss recent progress regarding investigations on the electronic and structural properties of supported gold clusters on various metal oxides and its correlation with reactivity. We will also provide an overview of the challenges and opportunities for research in gold heterogeneous catalysis with an emphasis on the roles that model catalyst systems can play in the near future.

2. SURFACE STRUCTURES OF AU SINGLE CRYSTALS

Gold crystallizes as a face-centered cubic (fcc) structure. Three low Miller indexed surfaces, (100), (110), and (111) (see Figure 1), are usually considered. The coordination number of atoms at the surface for these three different facets is 7 [Au(100)], 11 [Au(110)], and 9 [Au(111)]. The surface energies of gold are 0.08, 0.10, and 0.05 eV/$Å^2$ for the clean (100),[33] (110),[34] and (111)[35] surfaces, respectively. The classical arrangement of the atoms associated with each of the facets is not necessarily the most stable (e.g., minimum surface free energy); therefore, all three surfaces undergo reconstruction.

The (111) facet of gold has the lowest surface energy among other surfaces, as reflected in the growing tendency for thin film in the [111] direction. Gold has the highest ductility and malleability of any element.[38] It is the only metal for which the close-packed (111) surface of an fcc crystal has been observed to
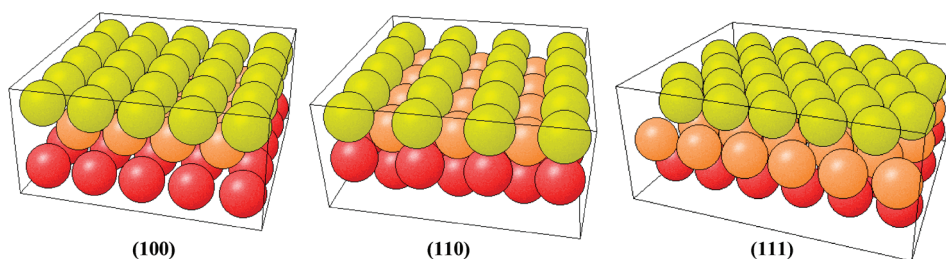
Figure 1. (100), (110), and (111) fcc crystal surfaces. Reproduced with permission from the NIST Surface Structure Database.[36]
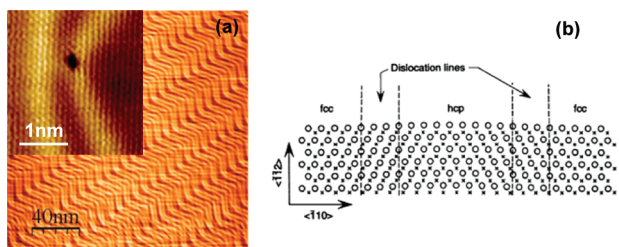

Figure 2. (a) STM image of the reconstructed Au (111) surface. Inset shows atomic resolution of the edge dislocations (depressions) which are present at the elbows of the herringbone reconstruction. (b) In-plane structure of the Au(111) reconstructed surface. The circle and crosses correspond to atoms in the first and second surface layers, respectively. Reproduced with permission from ref 37. Copyright 1992 American Association for the Advancement of Science.

reconstruct,[38] which is attributed to relativistic effects in the large electronic core of gold.[39] The reconstruction of Au(111) has been investigated by low-energy electron diffraction (LEED),[40] helium atom scattering,[38] scanning tunneling microscopy (STM),[37,41,42] and density functional theory (DFT) calculations.[43] Reconstructed Au(111) has a $22 \times \sqrt{3}$ herringbone structure (Figure 2a). This structure is the result of a balance between two opposing tendencies:[44] the surface layer undergoes contraction to compensate for its reduced coordination, whereas opposing this contraction the underlying substrate potential favors a commensurate surface layer.[37] The misfit between the substrate and the surface layer induces a periodic array of pairs of partial dislocations, leading to the separation of alternating domains where surface atoms occupy fcc and hexagonal close-packed (hcp) sites (Figure 2b). The surface atoms at the dislocation lines occupy bridge sites instead of hollow sites.[37] The unit cell of this reconstruction contains 23 surface atoms instead of 22, thus allowing a 4.4% contraction along the $[1\bar{1}0]$ direction in the surface layer.[45]

Reconstruction of the Au(110) surface into the (1×2) pattern is formed by a "missing row" along the $\{1\bar{1}0\}$ direction in the surface layer, which was first observed by Fedak et al. employing LEED[48] and has been intensively studied subsequently[7,12,15−22] [similar superstructures have also been observed on the (110) faces of platinum[49] and iridium[50]]. A schematic of the missing row reconstructed Au(110) (1×2) surface along with an atomic resolution STM image is illustrated in Figure 3. The missing row reconstruction leads to three type of surface atoms (e.g., top, side of row, and trench) with different coordination numbers; this structure is strongly related to the adsorptive behavior of the surface.[51] The sides of the rows in reconstructed surface are similar in structure to the fcc(111) surface and are typically referred to as (111) microfacets.[10] The

arrangement on the surface leads to a distortion in the underlying layers. A variation of the first two layer spacings and a row pairing in the second layer have usually been considered.[52] Moritz and Wolf reported that spacing of the top layer was contracted by ∼20% in the vertical direction, while a lateral displacement of 0.07 Å was observed for the second layer.[52] Additionally, Gritsch et al. found that structural defects such as steps interacted with the reconstruction.[51] The stabilization of the (111) microfacets, at step edges, was generally found to govern the step terrace topography of these surfaces. The presence of trace impurities was correlated with an increase to (1×3) structural units along the $[1\bar{1}0]$ direction, leading at first to a decrease in (1×2) domain size and, at higher densities, to structures such as (1×7), (1×5), and finally a (1×3). This result exhibits periodic arrangements of (1×3) units as the common building principle.[51] For the defect-free surface, the order−disorder transition of the (1×2) reconstruction appears at a critical temperature of (670 ± 20) K.[53]

Compared to the other two low indexed surfaces, the reconstruction of the Au(100) surface is somewhat controversial. A (1×5) reconstruction was first observed by Fedak and Gjostein[48] and soon after by Mattera et al.[55] However, later in 1967, Fedak and Gjostein resolved a splitting in the LEED spots for Au, leading to a (5×20) rather than (1×5) superstructure, and first proposed a hexagonal overlayer on the square substrate mesh as a model for the surface rearrangement.[56] Since then, various models have been put forward including a (5×20) with rotation,[57] a $c(26 \times 68)$,[40] a (24×48) with rotation,[58] and a hexagonal $(5 \times 28)R0.6°$.[59] A (5×20)-based reconstruction is now widely accepted, and the surface can be described as a quasi-hexagonal top layer, in which interatomic distances are shortened by about 4% with respect to the bulk fcc values.[26,32] An atomic resolution STM image of the characteristic (5×20) reconstruction is shown in Figure 4.

The reconstructed surfaces experience various combinations of the above-mentioned structures depending on the surface temperature and the step density.[22,33] The reconstruction is generally limited to the first layer, suggesting that the more compact surface arrangement is favored.[10] However, based on electron density calculations and He diffraction, Rieder et al. showed that the complex LEED patterns observed for Au(100) were due to the secondary structural features such as minor atomic displacements in both topmost and lower layers.[60] Marks and Smith suggested that the reconstruction could be due to Shockley partial dislocations.[61] Their high-resolution electron microscope (HREM) images indicated that small displacements could occur on unreconstructed Au(100). They concluded that a majority of mass transfer for the reconstruction takes place through a mechanism involving the observed dislocations.[61] Using first-principles calculations, Takeuchi et al. ascribed the
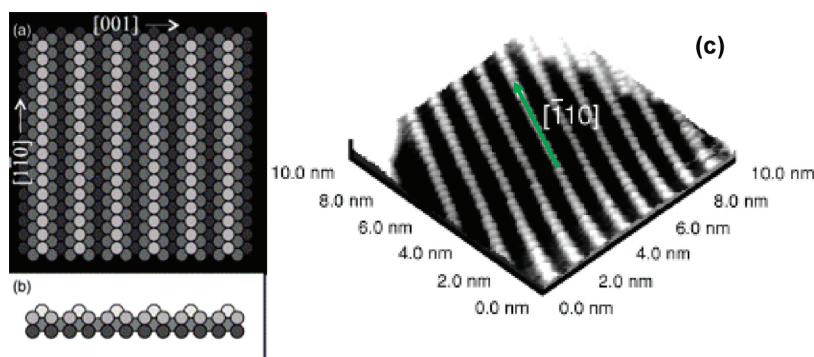
Figure 3. Schematic missing row reconstructed Au(110) (1 × 2) surface with (a) top view and (b) cross-section. Reproduced with permission from ref 46. Copyright 2003 Elsevier. (c) STM image of Au(110) (1 × 2) with an atomic-scale spatial resolution. Reproduced with permission from ref 47. Copyright 2002 American Physical Society.
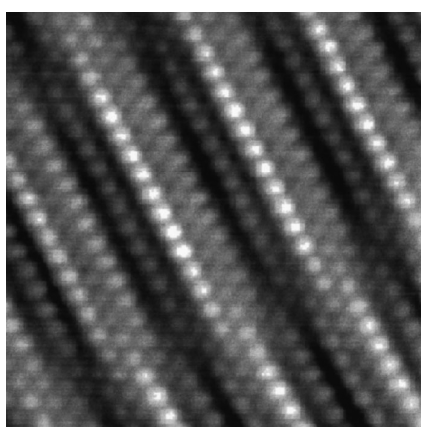

Figure 4. High-resolution STM image of the reconstructed Au(100) (5 × 20) surface (size 5.3 × 5.3 nm^2). Reproduced with permission from ref 54. Copyright 1998 American Physical Society.

reconstruction of Au(100) to its d orbital being involved in bonding,[62] as is the case for Au(111).[33] Mochrie and co-workers studied the reconstruction of Au(100) as a function of temperature employing X-ray scattering and found that above 1170 K the surface undergoes a structural phase transition [i.e., (1 × 1) superstructure] marked by a reduced asymmetry in the specular reflectivity.[63]

3. ADSORPTION OF MOLECULES/ATOMS ON AU SINGLE-CRYSTALLINE SURFACES

3.1. Adsorption of Oxygen

There have been many efforts over the years to investigate the interaction of oxygen with gold surfaces to better understand the unique oxidative catalytic properties of gold catalysts. Gold single-crystal surfaces do not measurably chemisorb oxygen either molecularly or dissociatively under ultrahigh vacuum (UHV) conditions[64] or at elevated temperatures and pressures;[17,65] however, molecular oxygen physically adsorbs up to ~50 K (physisorbed oxygen cannot be transferred to a chemisorbed state by simply annealing the surface).[17,66] Although some earlier investigations reported chemisorption of molecular oxygen on gold surfaces,[67−70] researchers presented evidence later showing that the observed oxygen dissociation was actually induced by calcium[71,72] or silicon[73] impurities.

The inability to populate gold surfaces with oxygen via exposure to gaseous, molecular oxygen has motivated researchers to develop other means of creating atomic oxygen precovered gold surfaces. Successful approaches primarily include thermal dissociation of gaseous O_2 on hot filaments,[74−76] ozone decomposition,[77−80] coadsorption of nitrogen oxides (e.g., NO_2 or N_2O_4) and H_2O,[81,82] O^+ sputtering,[83−86] electron bombardment of condensed oxygen or NO_2,[66,87−90] and a radio frequency (RF) generated oxygen plasma.[91−94] It is notable that the achievable saturation oxygen coverages and surface structures are strongly dependent on the preparation methods and surface temperature.

3.1.1. Thermal Dissociation of Gaseous O_2 on Hot Filaments. Ford et al. first reported the oxidation of gold films by atomic oxygen formed through dissociation of molecular oxygen on a hot metallic filament.[74] As measured by a surface potential method, adsorption of atomic oxygen proceeded from 77 K to room temperature, and desorption began at 400 K.[74] Eley and Moore, however, questioned the preparation method, as they detected metallic oxides on the gold surface originating from the filament.[75] Subsequently, Canning et al. successfully cracked molecular oxygen using a hot platinum filament (1400 K) and exposed atomic oxygen to a polycrystalline gold sample.[76] They showed that the surface oxide completely decomposed upon thermal treatment and oxygen desorbed recombinatively around 650 K (with an activation energy of ~163 kJ/mol).[76] The Madix group later used the same method to populate atomic oxygen on Au(110), which yielded a single desorption peak at 590 K upon heating.[95−97] Davis and Goodman further extended this approach to Au(100) and Au(111) surfaces [a saturation oxygen coverage of 1.5 monolayers (ML) was achieved, Figure 5a and 5b].[98] They observed a peak desorption maximum of 470 K for all oxygen coverages from Au(100), whereas for Au(111) the desorption peak temperature increased with an increase in the oxygen coverage up to 0.5 ML (e.g., 505 K of 0.1 ML vs 535 K of 0.5 ML).[98] No ordered overlayer structure on either surface was observed by LEED.[98]

3.1.2. Oxygen Sputtering. Pireaux et al. deposited atomic oxygen on Au(111) by DC reactive sputtering with oxygen and demonstrated that the formed oxide is Au_2O_3 (auric oxide), which decomposed under thermal treatment in the temperature range of 390−590 K. It was assumed that Au_2O (aurous oxide) is a possible intermediate in this reduction.[83] Gottfried et al. systematically characterized the chemisorbed oxygen species produced by bombardment of a Au(110) (1 × 2) surface with oxygen ions (O^+/O_2^+).[84] Temperature-programmed desorption
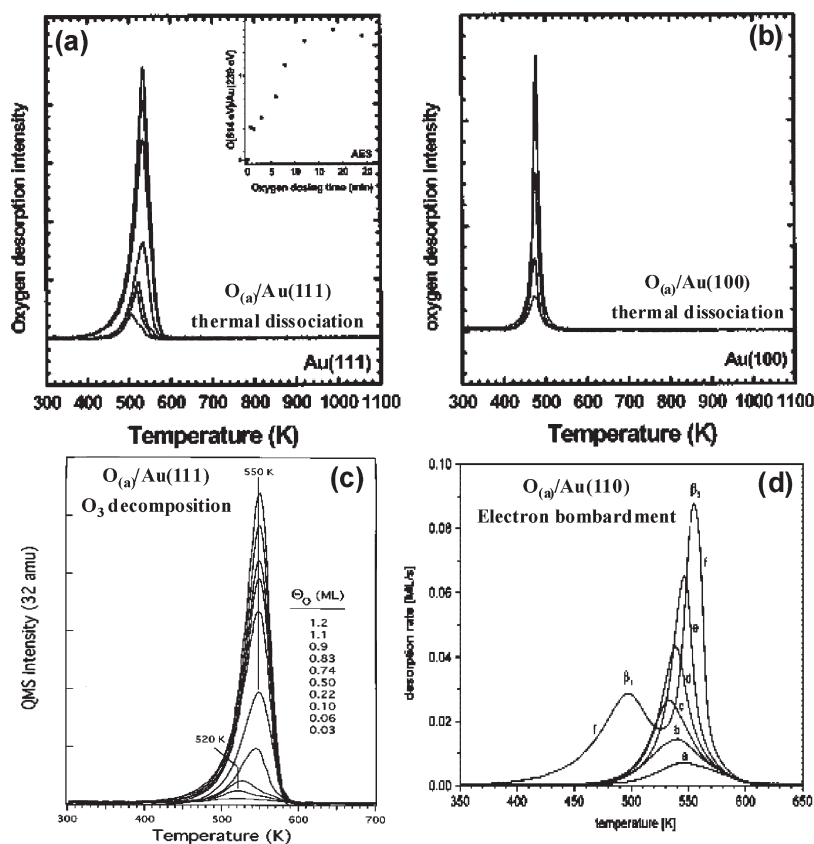
Figure 5. Oxygen TPDs following depositing atomic oxygen on (a) Au(111) and (b) Au(100) via thermal dissociation of gaseous O_2 on a glowing filament (Reproduced with permission from ref 98. Copyright 2000 American Chemical Society.); (c) exposures of ozone on Au(111) at 300 K (Reproduced with permission from ref 79. Copyright 1998 Elsevier.); (d) low-energy electron (500 eV) bombardment of physisorbed oxygen precovered on Au(110) at 28 K. Reproduced with permission from ref 66. Copyright 2002 Elsevier.

(TPD) revealed four states of oxygen desorption appearing at 415, 545, 620, and 680–850 K, respectively. The two peaks at lower temperatures were associated with the surface oxide and chemisorbed oxygen species as reported earlier.[66] The peak at the highest desorption temperature grew and shifted to higher temperatures with an increase in ion energy and sputtering time and thus could be assigned to oxygen atoms dissolved in the bulk.[21]

3.1.3. Ozone Decomposition. Koel's group showed that exposure of Au(111) to ozone (the O−O bond strength in $O_3(g)$ is only 96 kJ/mol) at 300 K formed an atomic oxygen adlayer, which desorbed to produce a single TPD single peak at 550 K (activation energy of 117 kJ/mol based on first-order desorption kinetics).[78,79,81] The saturation coverage of oxygen on Au(111) was about 1.2 ML, and the O_2 TPD peak shifted to lower temperatures at very low coverages (e.g., 0.1 ML) as shown in Figure 5c.[79] The small change in the desorption activation energy for O_2 could be due to inductive electronic effects whereby adsorbed oxygen withdrew charge from Au surface atoms and increases the subsequent interaction between $Au^{\delta+}$ and $O^{\delta-}$.[79] No ordered oxygen overlayer on Au(111) was reported, and a small oxygen coverage (e.g., 0.1 ML) was sufficient to cause the surface reconstruction.[78,79]

Recently, Min et al. showed that oxidization of Au(111) by ozone (which occurs rapidly) leads to the formation of oxidized Au nanoparticles on top of the surface (Figure 6).[101] Release of Au atoms upon oxidation is facilitated by the characteristic "herringbone" structure of clean Au(111) with an excess of 4.5% Au atoms compared to a bulk (111) plane, some of which are weakly bound at "elbow" sites.[102] These gold islands or clusters formed on the Au(111) surface were suggested to consist of either pure gold or gold−oxygen complexes, but the latter is more likely since gold atoms were expected to be highly mobile in the studied temperature ranges (200−400 K) and would diffuse to step edges.[19,99] A narrow size distribution, with the majority of islands having diameters between 1 and 5 nm, is measured following oxidation with ozone at 200 K (Figure 6a).[99] Three distinct types of oxygen—chemisorbed oxygen, surface oxide, and bulk oxide—were identified depending on the coverage and surface temperature (Figure 6e).[29,99,100,103] The chemisorbed oxygen (also called "metastable oxygen species",[19,104] which readily formed at low oxygen coverage and deposition temperature) does not have long-range order and consists of mobile Au−O complexes and disordered Au−O clusters that are ∼5 nm in diameter. The well-ordered two-dimensional (2D) Au−O structure observed when oxidation was carried out using O_3 at 400 K is defined as a surface oxide. The bulk oxide, formed at high coverage and/or deposition temperature, contains oxygen in ordered, three-dimensional (3D) structures.[19] For example, an ordered (1 × 3) structure is observed with both LEED and STM after deposition of 0.3 ML of oxygen via ozone decomposition at 400 K.[99] As will be discussed later, the reactivity of oxygen species on Au surfaces is strongly dependent on the structure. The same group using DFT calculations further
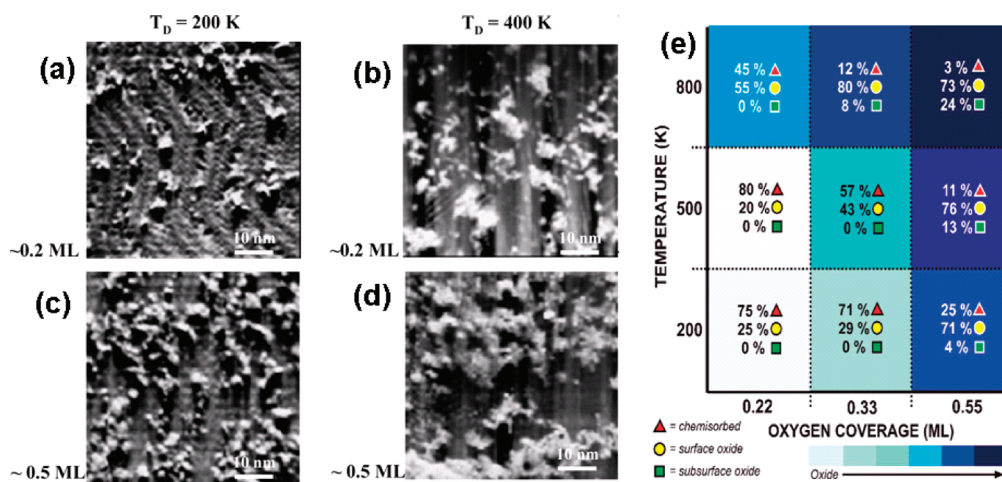
Figure 6. STM images (50 nm × 50 nm) of oxidized Au(111) surfaces where oxygen was deposited at 200 (a and c) and 400 K (b and d) using ozone. Reproduced with permission from ref 99. Copyright 2006 American Chemical Society. (e) Diagram illustrating the percentage of each oxygen type at each dosing temperature and oxygen coverage. Each square is shaded by the amount of oxide character of the surface. Reproduced with permission from ref 100. Copyright 2009 American Chemical Society.

confirmed that the coordination of the gold atoms to which oxygen is bound is an important factor in the energetics of oxygen adsorption.[105] Oxygen interacted favorably with semiundercoordinated gold in the form of terrace vacancies, steps, and 2D islands but not with single adatoms or 3D islands, which suggests that atomic oxygen could break up bigger islands leaving just oxygen bound to 2D islands with three atoms, since oxygen bound to a 3-fold site is more stable.[105] They also showed that atomic oxygen, at low coverages, has a repulsive interaction with adatoms and an attractive interaction with vacancies, this latter interaction being responsible for the release of gold atoms from the surface in the presence of oxygen.[105]

The surface structure of gold indeed affects the nature of oxygen adsorbed on the surface.[106] Kim et al. covered a Au(211) surface with atomic oxygen (with a saturation coverage of ∼0.9 ML) via O_3 decomposition and showed that step sites bound oxygen adatoms more tightly than terrace sites.[107] In the low-coverage regime (θ_O < 0.15 ML), the O_2 TPD peak appeared at 540 K (with a desorption energy of ∼138 kJ/mol) and did not shift with coverage, which was ascribed to oxygen adatoms at the steps on the Au(211) surface. Upon increasing coverages, an additional lower-temperature desorption peak appeared, shifting from 515 to 530 K at saturation coverage, owing to oxygen adsorbed on the (111) terrace sites of the Au(211) surface.[107] LEED patterns indicated an oxygen-induced step doubling on Au(211) at low coverages (0.08−0.17 ML) and extensive disruption of the 2D ordering at saturation coverages of oxygen.

3.1.4. Co-adsorption of Nitrogen Oxides and H_2O.
Wang and Koel pioneered a convenient approach for generating oxygen adatoms on gold in UHV. They examined the coadsorption of NO_2 (or N_2O_4) and water−ice on Au(111) at 86 K and found that adsorbed atomic oxygen up to 0.5 ML could be reliably obtained from this reaction.[81,82,108,109] They noticed in TPD measurements that the atomic oxygen adlayer recombinatively desorbs producing a single peak at ∼520 K.[82,109] Interestingly, oxygen atoms were only formed following multilayer adsorption of NO_2 (present as N_2O_4) and only if the adsorption was on amorphous ice clusters and not crystalline ice.[82,109] It was proposed that the extent of these reactions was proportional to the concentration of "free OH" groups on the ice film, indicating

that water molecules with only two hydrogen bonds were required to initiate these reactions by strongly hydrating N_2O_4.[109]

3.1.5. Electron-Induced Chemisorption of Oxygen.
Gottfried et al. induced chemisorption of oxygen via irradiating a Au(110) surface precovered with physisorbed oxygen with 500 eV electrons at 28 K.[66,87−89] Two desorption peaks for oxygen were observed (Figure 5d); the low-temperature feature appeared at 490 K at high coverage (>1.0 ML) and was assigned to the decomposition of a thermally unstable Au_2O_3 surface oxide, and the second peak at 550 K was associated with chemisorbed oxygen on the surface.[87,88] At monolayer coverage, chemisorbed oxygen lead to a work function increase of 0.9 eV, indicating charge transfer from gold to oxygen.[88]

Electron bombardment of NO_2 condensed on Au(111) at 100 K also leads to the formation of atomic oxygen (with a saturation coverage of ∼0.4 ML) on the surface.[90,110] The peak temperature for O_2 evolution appeared at 550 K (corresponding to a desorption energy of 138 kJ/mol) independent of oxygen coverage, implying pseudofirst-order kinetics for recombinative desorption. Interestingly, Deng et al. showed that, on a reconstructed Au(111)-herringbone surface, the presence of trace oxygen adatoms (prepared by electron bombardment of NO_2) enhanced the dissociation probability of O_2 by at least 3 orders of magnitude compared to the clean surface at 400 K.[90] This observation indicates that O_2 dissociation is very sensitive to the structure of the surface and particularly the creation of small gold islands possibly formed by Au atoms released from the surface.[99,101] Indeed, Mills et al. found that a rough surface (i.e., the presence of coordinatively unsaturated atoms) promotes the adsorption of molecular oxygen.[111] Odd numbers of electrons enhanced the binding of oxygen, although negligible effect was observed on the flat Au(111) surface.[65] The reactivity of rough surfaces and clusters could be due to a highly localized highest occupied molecular orbital (HOMO), which promotes the charge transfer to O_2. In contrast, smooth surfaces cannot chemisorb O_2 because the HOMO is delocalized.[111]

3.1.6. Radio-Frequency-Generated Oxygen Plasma.
Employing a home-built oxygen atom source based on a design by Pollard,[112] Mullins and co-workers populated atomic oxygen
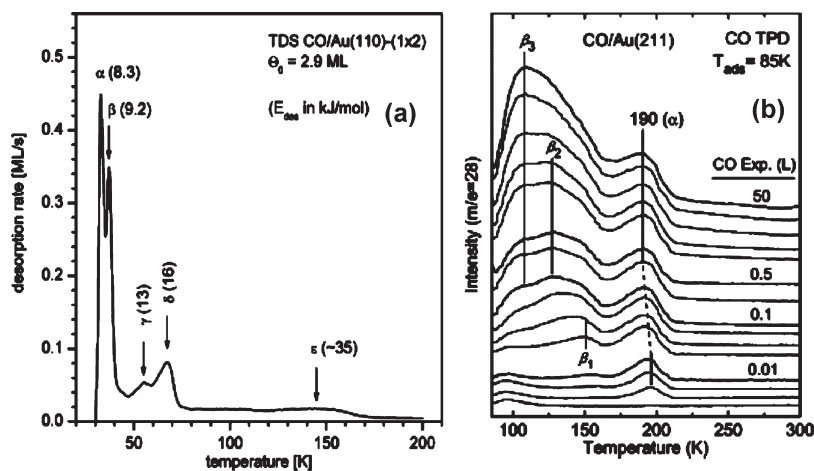
Figure 7. (a) TPD of CO/Au(110) (1 × 2) for an initial coverage of 2.9 ML. The desorption activation energies (kJ/mol) for the first-layer peaks $\gamma - \varepsilon$ were calculated by Redhead analysis; those for α and β were obtained by leading-edge analysis. Reproduced with permission from ref 123. Copyright 2003 Elsevier. (b) CO TPD with various CO exposure (0.0025−50 L) on Au(211) at 85 K. Reproduced with permission from ref 124. Copyright 2006 American Chemical Society.

onto Au(111) using a RF-generated plasma source that produced a supersonic beam of O atoms from an 8% (vol.) O_2 in Ar gas mixture.[91,113,114] A flux of oxygen atoms of ∼0.04 ML/s[115] (1 ML is defined as 1.387×10^{15} molecules/atoms cm^{-2} referring to a single atomic layer of close-packed gold) was typically achieved, and a saturation oxygen coverage was estimated to be ∼2.0 ML.[92−94] Chemisorbed $O_{2,a}$ is present on Au(111) after exposure to the plasma-jet source, but the surface concentration is very small (less than 0.02 ML).[116,117]

Oxygen desorption at low coverage (e.g., 0.16 ML) produces a peak around 520 K, and with increasing oxygen coverages this peak shifts to higher temperatures, indicative of first-order kinetics.[93,118] At saturation coverage, a desorption peak for oxygen was observed at ∼550 K.[93] The desorption activation energy of oxygen from Au(111) based on the Redhead analysis[119] is ∼126 kJ/mol at an atomic oxygen coverage of 0.16 ML, increasing to ∼134 kcal/mol at 1.0 ML, consistent with values reported for oxygen atoms prepared by other methods. DFT calculations show that increasing coverages of oxygen atoms lead to a broadening of the surface atom d-bands and a consequent reduction in the average energy of the d-band center due to conservation of the d-band filling. The reduction in the energy of the d-band center leads to a correlated increase in the adsorption energy.[120]

3.2. Adsorption of Carbon Monoxide

Adsorption of CO has been widely examined as a probe of the surface structure of metals. Early work showed that CO weakly adsorbed on gold films compared to most other metals, and the heat of adsorption of CO was ∼36.7 kJ/mol.[65] On Au(111), CO adsorbs on the surface at cryogenic temperatures (e.g., <77 K) under UHV conditions. However, at elevated pressures, CO strongly interacts with the Au(111) surface.[121] Employing surface X-ray diffraction (SXRD), Peters et al. observed the lattice expansion of Au(111) upon CO exposure between 0.1 and 400 Torr at 300 K, although the long-range herringbone structure was intact.[121] The original reconstruction was disordered when Au(111) was exposed to CO at 80 Torr and 600 K. Since the surface remained disordered after evacuation of the CO, a thermally activated chemical reaction (dissociative adsorption

of CO) was suggested.[121] Recently, in a more careful study by Piccolo et al., CO-induced modification of the surface morphology ($22 \times \sqrt{3} \rightarrow 1 \times 1$ transition) was examined by STM and reflection absorption infrared spectroscopy (RAIRS) when Au(111) was exposed to CO at room temperature and elevated pressures (10^{-3}−10^3 Torr of CO); CO chemisorption is favored at low-coordinated sites, with the classical trend: terraces < steps < kinks < adatoms.[122]

Outka and Madix studied the interaction of CO with Au(110) (1 × 2) at surface temperatures down to 125 K and found no CO adsorption in the investigated temperature range.[95] Recently, in a related lower-temperature study by Gottfried et al., five adsorption states were identified (Figure 7a): α (multilayer at 32 K), β (second layer at 37 K), γ (physisorbed first layer at 55 K), δ (physisorbed first layer at 67 K), and ε (chemisorbed at 145 K).[123] For any coverage studied, no ordered overlayer structures were observed in LEED patterns. The ε peak saturated at ∼0.13 ML, lower compared to CO adsorption on other metals.[65] On the basis of results from ion bombardment experiments (for artificially producing surface defects), the authors conformed that the ε peak was not related to defects.[123] Polarization resolved ultraviolet photoelectron spectroscopy (UPS) measurements indicated that chemisorbed CO on Au(110)[125] orients parallel to the surface,[123] which was further supported by a lack of intensity for the 5σ orbital contribution. Additionally, Goodman and co-workers showed that, with increasing CO coverage, the CO RAIRS absorption shifted red from 2118 to 2108 cm^{-1} on Au(110); they obtained an adsorption energy of 45.6 kJ/mol for the low coverage limit,[126] which is slightly lower than what Gottfried et al. reported (59 kJ/mol).[123]

High coverages of chemisorbed CO on Au(110) could be obtained by raising the CO pressure at elevated temperatures (e.g., 300 K).[127] Jugnet et al. observed two C−O stretching features in their RAIRS study: ν_{CO} of 2110 cm^{-1} at pressures above 10^{-2} Torr attributed to weakly chemisorbed CO (assigned to on-top adsorption), and ν_{CO} of 2141 cm^{-1} at pressures higher than 100 Torr associated with physisorbed CO species.[127] However, the intensity of chemisorbed CO decreased upon increasing exposure time, indicating that CO could dissociate on the surface. STM and polarized RAIRS results confirmed a lifting of terrace
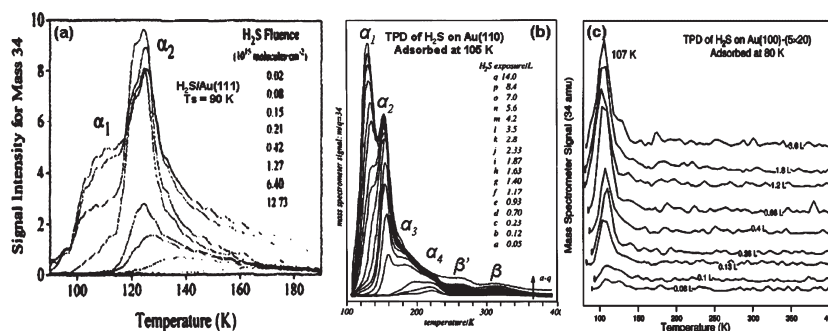
Figure 8. H₂S TPDs following exposures of H₂S on (a) Au(111) at 90 K (Reproduced with permission from ref 152. Copyright 1994 Elsevier.); (b) Au(110) at 105 K (Reproduced with permission from ref 153. Copyright 1991 Elsevier.); and (c) Au(100) at 80 K (Reproduced with permission from ref 155. Copyright 1999 American Institute of Physics.). Detailed explanations regarding various desorption features (α_1, α_2, α_3, etc.) can be found in corresponding references.

anisotropy and surface roughening accompanied by surface carbon deposits under the studied conditions.[127]

The heat of CO adsorption on Au(100) was estimated to be 59 ± 3 kJ/mol,[128] which is consistent with values reported for Au(110)[123] and Au(332) (55 kJ/mol).[129,130] No ordered adsorption structures of Au(100) were observed in LEED patterns.[128]

Kim et al. have recently examined adsorption of CO on a Au(211) stepped surface.[124] Two adsorption states of CO were reported: α (from step sites) and β (from terrace sites) (Figure 7b). RAIRS and TPD results showed that CO was weakly adsorbed at atop sites of Au(211) but was more strongly bound at step sites (50 kJ mol⁻¹) than at terrace sites (27−38 kJ mol⁻¹).[124] The ν_{CO} band underwent a red shift from 2126 to 2112 cm⁻¹ with increasing CO coverage.[124] This could be due to the combination effect of steric repulsion between the filled d band of gold and the CO 5σ.

3.3. Adsorption of Sulfur-Containing Molecules

3.3.1. Sulfur. Sulfur is well-known for its poisoning effect in heterogeneous catalysis; however, the role of sulfur in gold catalysis is fairly unusual due to its promotional effect.[131,132] The Au−S interaction is also one of the most intensively studied systems as it plays an important role in Au ore formation[133] and controls the structure and dynamics of thiol-based self-assembled monolayers.[11,16,32,134−136]

Sulfur adsorbs on Au(111) from either S^{2-}, SH^-,[137] or H₂S[138] in aqueous electrolyte solutions [for electrochemical scanning tunnel microscopy (EC-STM) measurements], or from S_2[139] and SO₂[140,141] in the gas phase. In all cases, the adsorption of sulfur on the surface results in a strong covalent bond and different structures according to the surface coverage. It was believed that sulfur started to physisorb at terraces[142,143] followed by chemisorption at step edges.[144] Rodriguez et al. examined sulfur adsorption (deposited via S_2 gas) on Au(111) with high-resolution photoemission spectroscopy.[139] At small coverages, sulfur adsorbed on fcc hollow sites of the "herringbone" structure of the gold substrate, which was energetically more favorable compared to adsorption on bridge or atop sites.[139,145] Sulfur behaved as a weak electron acceptor but substantially reduces the density-of-states that gold exhibits near the Fermi edge.[78] DFT calculations[139,146] agreed with the earlier report by Gottschlack and Hammer[147] that sulfur preferentially adsorbed at the 3-fold hollow site at low coverages and induced a reconstruction to a $\sqrt{3} \times \sqrt{3}$ R30° pattern as indicated by LEED.[143,148] Upon increasing sulfur coverage, a weakening of

the Au−S bonds was observed that facilitated changes in adsorption site and eventually resulted in S−S bonding. At sulfur coverages above 0.4 ML, S_2 is the more stable species on the gold surface. Formation of S_n (n > 2) oligomers (e.g., tetramer, octamer) occurred at sulfur coverages higher than a monolayer.[139] An S_8 octamer model has been frequently applied for describing rectangular surface features in STM images,[137,138] which were suggested on the basis of a static model that the positions of Au atoms keep intact upon interaction with sulfur.[149] A similar phenomenon was reported for sulfur adsorbed on polycrystalline gold[139] as well as on Au(111) from electrolyte Na₂S solutions.[148] However, a recent study on SO₂ adsorption on Au(111) indicated that the rectangles contain AuS rather than polymeric S (e.g., S_8[137,138]).[141] The AuS is created by a corrosion process accompanied with a reconstruction of the Au surface, resulting in the formation vacancy islands. The AuS stoichiometry was estimated to be 1 at a sulfur coverage of 0.5 ML upon annealing the sample to 450 K.[141] Theoretical calculations showed that the presence of S significantly influences the chemistry of Au(111) (e.g., enhancing the adsorption of CO[150]).[141] Although no conclusive evidence was provided regarding the presence of AuS (the proposed stoichiometry was based on STM images but not spectroscopies), this interesting phenomenon is worth detailed experimental and theoretical investigations.[136] Particularly, the influence of surface temperature, the role of the environment (gas phase or electrolyte solutions), and the energy involved in the chemical reactions should be elucidated.[151]

3.3.2. Hydrogen Sulfide. Unlike many other transition metal surfaces, adsorption of hydrogen sulfide (H₂S) on clean Au(111) (Figure 8a),[152] Au(110) (Figure 8b),[153,154] and Au-(100) (Figure 8c)[155] has been found to be completely reversible. Jaffey and Madix first studied the adsorption of H₂S on Au(110), and they found that H₂S molecularly adsorbed (with the S atom bonding on top sites[156]) with unit sticking probability on the clean surface at 105 K up to completion of the monolayer.[153] They also observed ~2% of a monolayer of H₂S decomposed on Au(110) upon electron bombardment.[153] Hydrogen desorbed at 215 K, suggesting the presence of a decomposition channel, while a desorption feature for H₂S at 270 K was ascribed to a disproportionation reaction of SH groups.[153] However, in a later investigation by Fruhberger et al., Jaffey and Madix's results regarding the electron-stimulated dissociation of H₂S were attributed, rather, to the existence of surface defects, since Fruhberger and co-workers observed similar adsorption behavior
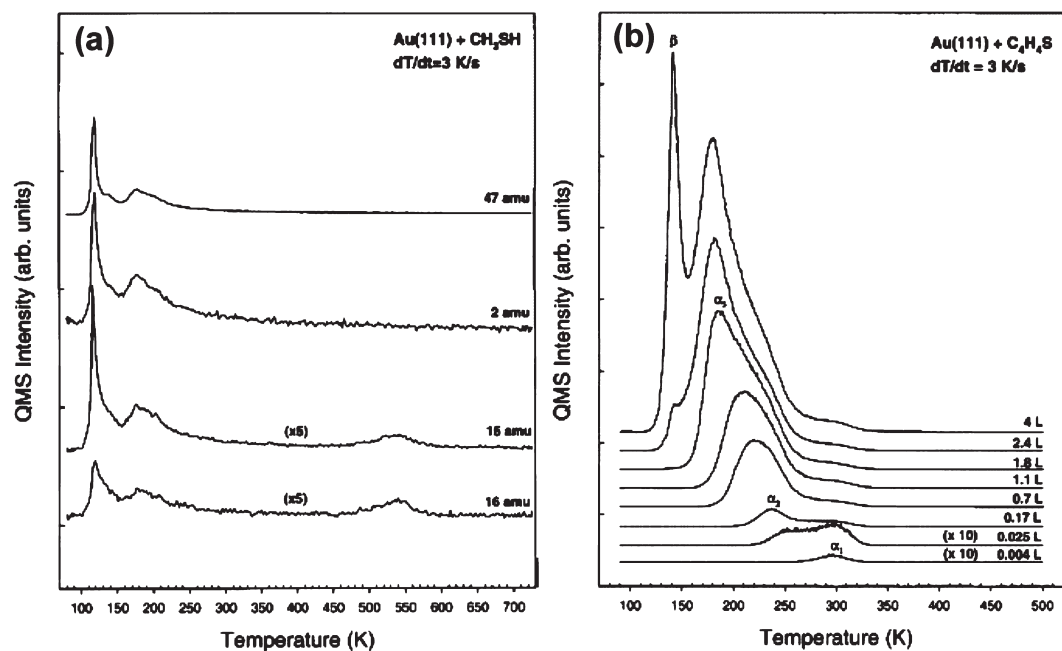
Figure 9. (a) Evolution of hydrogen (2 amu), methyl radical (15 amu), and methane (16 amu) during TPD for 1.5 L methanethiol exposure on Au(111) at 100 K. A very weak peak for desorption of dimethyl disulfide is at ~470 K (not shown). (b) TPD spectra for thiophene adsorption on Au(111) at 100 K as a function of exposure. The parent ion signal (84 amu) was monitored. α_1 was attributed to a defect adsorption state, as also seen on Cu(111).[181] α_2 was assigned to desorption from a chemisorbed monolayer on terraces with a flat-lying adsorption geometry; α_3 can be ascribed to another chemisorbed state on terraces with a tilted adsorption configuration; β was assigned to a physisorbed multilayer of thiophene. Reproduced with permission from ref 163. Copyright 2002 Elesiver.

on their freshly sputtered Au(110) surfaces.[154] Similar phenomena have also been observed on the Au(100)[155] and Au(111)[152] surfaces. Additionally, Bondzie et al. explored the adsorption dynamics of H_2S on clean Au(100) (5 × 20) employing molecular beam techniques.[155] They showed that H_2S adsorption at between 80 and 100 K occurred via a precursor mechanism,[157−162] in which the impinging H_2S molecules initially adsorbed into a mobile, physisorbed precursor state and then migrated on the surface until they either located an empty physisorption site on the surface or desorbed.[155] The initial sticking probability was 0.95 ± 0.05, and it remained constant until the first monolayer of H_2S was adsorbed onto the surface. The apparent sticking probability then dropped to 0.1 ± 0.05 as a dynamic equilibrium was reached between adsorption and desorption into the physisorbed precursor state. At 110 K reversible Langmuir adsorption kinetics were observed due to the much reduced surface residence time in the precursor state.[155]

3.3.3. Sulfur Dioxide. Sulfur dioxide (SO_2) also molecularly adsorbs on defect-free gold single crystals[163] [similar to Ag(100),[164] Ag(110),[165] and Ag(111)[166]]. Rodriguez and co-workers showed that, for SO_2 adsorption at 100 K, only one distinct monolayer peak with a tail extending to higher temperature appears in TPD, in addition to the multilayer desorption feature at ~130 K.[163] The difference in desorption temperature between the monolayer and multilayer is only ~15 K, indicating a weak binding between Au and SO_2. In contrast, a difference of ~50 K was observed on Ag(111), and three submonolayer peaks appeared at 204, 176, and 155 K (from Ag(111)), which were assigned to desorption from defect sites, terraces, and a compressed layer, respectively.[166] More interestingly, sulfur dioxide readily decomposes on copper surfaces [Cu(100)[167,168] and

Cu(111)[168,169]] at temperatures above 200 K with SO or SO_3 as an intermediate. The different behavior of SO_2 on coinage metal surfaces could be due to the differences in the electronic properties of Au, Ag, and Cu (e.g., poor electron donation into the lowest unoccupied molecular orbital (LUMO) of SO_2 leads to weak molecular adsorption of the molecules).[163]

3.3.4. Alkanethiols. For alkanethiols on gold surfaces, it is commonly accepted that stable SAMs involve thiolate radicals upon cleavage of the H—S bond via the reaction shown in eq 1.[32,135]

$$H—(CH_2)_n—S—H + Au \rightarrow H—(CH_2)_n—S—Au + H_2$$
$$(1)$$
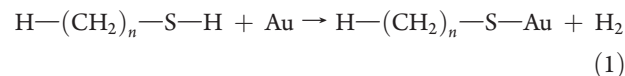
However, even in the simplest scenario—well-characterized surfaces at UHV conditions—several fundamental aspects of the initial stage of adsorption and self-assembly process are still controversial.[135] Ironically, adsorption of methanethiol (CH_3SH), the simplest alkanethiol, on Au(111) is probably the most controversial example. Nuzzo et al. first examined the adsorption of methanethiol and dimethyl disulfide (CH_3SSCH_3) on Au(111) experimentally and found that methanethiol underwent molecular adsorption, while dimethyl disulfide chemisorbed dissociatively.[170] In fact, adsorption of methanethiol has frequently been examined in UHV by exposing the surface to gas-phase dimethyldisulfide,[136] which is dissociated to methanethiolate.[170,171] Similar features of chemisorption of methanethiol on Au(111) were later confirmed by Liu et al. (Figure 9a); however, they also observed the desorption of dimethyl disulfide and methane as decomposition products at 470 and 540 K, respectively, upon CH_3SH exposure on Au(111) at 100 K.[163] Recently, Yates and co-workers showed evidence of no S—H

(or C−S) bond cleavage observed during the adsorption of methanethiol (and CH_3SSCH_3) on the Au(111) surface at temperatures below 220 K.[172] Thus, the decomposition could be attributed to surface defects, as supported by DFT calculations[173−175] that showed the adsorption of SCH_3 is stabilized by about 0.8 eV upon introducing vacancy defects on Au(111).[173] DFT calculations further suggested deprotonation of methanethiol occurs on the terraces of Au(111).[175] The effect of surface defects was also found on the adsorption of thiophene on Au(111), where the main desorption peak at 186 K had a high-temperature shoulder extending out to 330 K (Figure 9b).[163]

More recent DFT calculations showed methanethiol chemisorbs at atop fcc sites without S−H bond scission on the Au(111) terraces [i.e., reaction 1 is not valid].[176] The S−H bond was only broken at defects populated on Au(111).[176] However, ordered structures of chemisorbed methanethiol were observed on Au(111) upon adsorption of dimethyl disulfide on Au(111) at 200 K followed by quenching at 320 K[177] or at room temperature without quenching.[178]

The situation for larger alkanethiols on Au(111) is simpler compared to methanethiol. They can easily chemisorb from the gas or liquid phases at room temperature followed by decomposition.[136,179] Lavrich et al. demonstrated that annealing a decanethiol-covered surface could increase the possibility of cleavage of S−H bonds.[180]

Madix and Jaffey examined the surface chemistry of various thoils on Au(110). They showed that adsorbed ethanethiol on Au(110) underwent S−H bond cleavage below 350 K to form ethyl thiolate; H_2 and H_2S were evolved between 150 and 350 K.[182] Isotopic labeling experiments suggested that H_2S was formed from the transfer of hydrogen atoms in the thiol molecule directly adsorbed to sulfur rather than via the recombination of surface-bound sulfur and hydrogen atoms. Ethyl thiolate further decomposed in the same temperature range, producing a mixture of ethylene, ethane, ethanethiol, and diethyl sulfide. The decomposition kinetics were found to be dependent on surface sulfur coverage.[182] Similar reaction patterns were also observed on benzenethiol (C_6H_5SH)[183,184] and *tert*-butyl thioalcohol [$(CH_3)_3$-CSH].[185] Unlike the complicated chemistry of larger alkanethiols on Au(110), butanethiol exhibited reversible adsorption on *clean* Au(100).[186] However, on a sulfur precovered Au(100) surface, decomposition of butanethiol led to the desorption of 1-butene at 500 K and surface-bound sulfur that could either desorb or diffuse into the bulk above 700 K.[186] Since a small amount of sulfur could induce decomposition, the authors speculated that defects or impurities could be responsible for decomposition on "clean" gold single crystals.[186] These results suggest that the surface chemistry of alkanethiols on gold could be very structurally sensitive.

Details of many other significant aspects concerning organosulfur SAMs on gold single crystal surfaces, such as adsorption dynamics, binding geometry, surface structure, role of defects, and effects of end group and chain saturation, can be found in several excellent reviews.[16,32,134−136]

3.4. Adsorption of Chlorine

Bonding of strongly electronegative halogen atoms on gold surfaces is of fundamental significance in understanding adsorption dynamics. Of particular interest is the interaction of chlorine on Au(111),[103,187−193] which has advantages for various applications: Au(III) chloride has been used as a homogeneous catalyst for many important organic reactions. In heterogeneous chemistry,
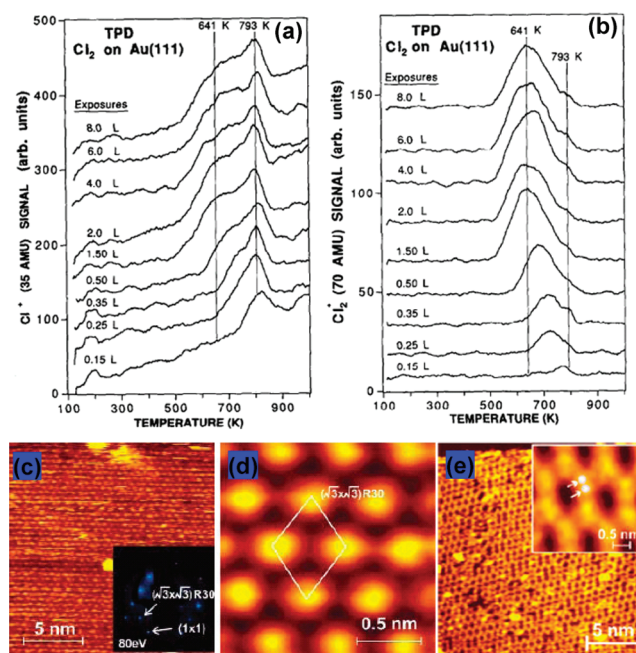
Figure 10. Chlorine TPD spectra of (a) Cl^+ (35 amu) and (b) Cl_2^+ (70 amu) after Cl_2 exposure on Au(111) at 120 K. Reproduced with permission from ref 189. Copyright 1993 Elesiver. STM images of (c) ~0.3 ML and (e) ~0.8 ML (with honeycomb structure) chlorine on Au(111); inset in (c) shows LEED pattern of the surface. (d) Zoom-in image of (c) showing a $(\sqrt{3} \times \sqrt{3})R30°$ atomic arrangement. The inset of (e) shows that each unit in the hexagon adopts a dimer structure. Reproduced with permission from ref 190. Copyright 2008 American Chemical Society.

chlorinating reagents with gold can be used, for instance, to remove mercury emissions from coal-fired boilers.[194] Chlorine also increases the selectivity of styrene epoxidation on Au-(111)[195] and acts as a poison for CO oxidation on supported gold particles.[196]

The interaction of gaseous chlorine (Cl_2) with Au(111) has been examined over the temperature range of 120−1000 K.[188,189] Kastanas and Koel found that chlorine dissociatively adsorbed at all temperatures above 120 K with an apparent activation energy of −8.4 kJ/mol.[189] The saturation coverage of Cl atoms was estimated from Auger electron spectroscopy (AES) calibration to be 2.9 ML. A $(\sqrt{3} \times \sqrt{3})R30°$ LEED pattern was observed at temperatures below 230 K. A structural model was proposed for the LEED pattern in which there were four Cl atoms per unit cell in a closest-packing arrangement with atomic radii of 1.24 Å, giving θ_{Cl} = 1.33 ML.[189] Two desorption features were found— an atomic desorption peak at 790 K (Figure 10a) and a molecular desorption peak at 640 K (Figure 10b)—with desorption activation energies estimated to be 163 and 201 kJ/mol, respectively. Interestingly, no formation of gold chlorides was detected by Kastanas and Koel,[189] whereas in an earlier TPD study Spencer and Lambert found a surface chloride ($AuCl_3$) during chlorine adsorption on Au(111) at 298 K.[188] This contradiction has been addressed by Friend and co-workers via careful DFT and STM investigations,[190,192,193] where they showed that the interaction of chlorine with Au(111) was a rather dynamic process involving multiple stages at different chlorine coverages. At low coverage (e.g., θ_{Cl} < 0.33 ML), Au atoms were released from the herringbone reconstruction to relieve surface stress.

Continuous chlorine adsorption led Cl atoms to bind on top of a Au(111) (1 × 1) layer, ultimately forming the Au(111)-($\sqrt{3} \times \sqrt{3}$)-$R30°$-Cl overlayer at 0.33 ML coverage (Figure 10c and 10d).[190,197] At higher coverage, more Au atoms were removed from the surface and a surface chloride compound was formed (Figure 10e).[103,190]

3.5. Adsorption of Nitrogen-Containing Molecules

Nearly all nitrogen-containing molecules (nitrogen, ammonia, amines, nitrogen oxides, nitriles, etc.) that have been investigated undergo reversible/molecular adsorption on clean gold single-crystal surfaces.

Ammonia binds weakly (with the N atom bound at atop sites[198]) without dissociation to clean Au(111).[199,200] TPD spectra showed a submonolayer peak with a shift to lower temperature (135 → 105 K) with increasing coverage up to one monolayer.[200] Adsorption energies of 26 and 32 kJ/mol were estimated for 1/4 ML and 1/9 ML of ammonia, respectively.[198] Higher NH_3 coverages give rise to a multilayer peak at lower temperature (∼ 90 K).[199,200] Adsorption of amines results in a bond to a gold atom via the nitrogen lone pair, and the NH_2 unit is held parallel to the surface plane while the functional group (e.g, methyl, ethyl, propyl, phenyl) is tilted with respect to the surface normal.[201] Adsorption energetics revealed that preferential binding occurs in undercoordinated sites (e.g, on atop sites).[201] Like ammonia, propylamine weakly adsorbs and desorbs molecularly at ∼140 K.[202] Repeated exposures of propylamine on Au(111) provided reproducible TPD spectra and Auger electron spectra (without cleaning in between) and confirmed that no dissociation products (i.e., residual carbon, surface bound oxygen, and/or nitrogen) remain on the surface.[202]

Koel and co-workers studied the adsorption of nitrogen oxides on Au(111).[108,203] NO_2 adsorbs reversibly, exhibiting a monolayer desorption peak at 220 K (with first-order kinetics and an activation energy of 58 kJ/mol) and a multilayer desorption peak at 150 K.[108,203] Vibrational spectroscopies[108,203,204] and DFT calculations[205] showed that the molecule is uprightly bonded to the surface through its two oxygen atoms. Significant dimerization of NO_2 to N_2O_4 was observed for multilayer films.[206]

Bartram and Koel were unable to observe adsorption of either NO or N_2O on Au(111) for temperatures above 95 K.[203] However, McClure et al. showed that NO molecularly adsorbs on Au(111) at 77 K, and upon heating a peak desorption temperature of ∼150 K was observed.[92] Rienks et al. estimated the strength of NO chemisorption on Au(100) to be 57 ± 4 kJ/mol. They also observed formation of the unreconstructed phase of Au(100) after NO exposure at 170 K.[207] On the stepped Au(310) surface, the desorption maximum of NO at 120 K corresponds to an adsorption energy of 30 kJ/mol.[208]

Koel's group also looked into adsorption dynamics of nitrobenzene ($C_6H_5NO_2$)[209] and nitromethane (CH_3NO_2);[210] they undergo reversible adsorption without decomposition on Au(111). Neither ordered phases nor surface reconstruction were observed for both molecules. For nitrobenzene, three peaks were observed in TPD at 290, 210, and 195 K due to the desorption from monolayer, bilayer, and multilayer, respectively. RAIRS measurements showed that nitrobenzene exhibits a flat geometry for low coverages up to 1.0 ML.[209] For nitromethane, similar desorption features were reported.[210] No significant chemical shifts at monolayer and submonolayer coverages were observed compared to multilayer films. The authors suggested that nitromethane adsorbs on Au(111) with C_s symmetry in monodentate geometry with one oxygen atom (unlike NO_2, which is doubly bonded) binding to the surface with a large tilt of the C−N bond away from the surface normal.[210]

Reversible adsorption of acetonitrile (CH_3CN) and benzonitrile (C_6H_5CN) on Au(100) was examined by Christmann and co-workers.[211] Acetonitrile is oriented preferentially with the nitrogen lone pair being directed toward the surface (with the C−C−N axis), which exhibits a binding energy of 46 kJ/mol.[211] In contrast, benzonitrile interacts significantly more strongly with Au(100) (E_{ad} = 75 kJ/mol) with the molecular plane parallel to the surface bonded through three ring carbon atoms.[211]

Molecular nitrogen only physisorbs on the gold single-crystal surface below 77 K.[17,65] However, via nitrogen ion irradiation (with kinetic energies of 500 eV), Siller et al. demonstrated the presence of two nitrogen species formed on Au(110), which were identified as nitrogen chemisorbed to gold as a nitride (Au_3N is the most likely nitride stoichiometry based on theoretical calculations[212]), and molecular nitrogen trapped beneath the gold surface.[212,213]

3.6. Adsorption of Hydrocarbons and Oxygenates

Understanding adsorption of hydrocarbons and oxygenates on gold surfaces is important with increased interest in exploring partial hydrogenation and oxidation reactions that have been catalyzed by gold. The general consensus is that hydrocarbons and oxygenates weakly and molecularly adsorb on gold single-crystal surfaces.

3.6.1. Hydrocarbons.
Outka and Madix have studied the adsorption of ethylene (C_2H_4) and acetylene (C_2H_2) on Au-(110)[96] and found that acetylene molecularly adsorbs on the surface without decomposition, producing a single broad desorption peak between 125 and 200 K.[96] The plausible explanation for this broad desorption profile was that the non-hydrogen-bonded molecules are so weakly attracted to the surface that they have no well-defined binding site.[96] A rough estimate of the desorption activation energy for acetylene was 42 kJ/mol.[96] A nearly identical desorption feature was observed for ethylene (also with the absence of decomposition products).[69,96]

Davis and Goodman demonstrated that the reversible adsorption of propylene on both Au(111) and Au(100) surfaces was remarkably similar.[98] Energy loss spectra suggested that propylene adsorbs with its molecular plane tilted slightly with respect to the surface normal.[98] Two desorption peaks—a multilayer at 120 K and a monolayer peak at 140−145 K—were observed in TPD. A desorption activation energy of 39 kJ/mol and very small shifts of the vibrational frequencies from their gas-phase values indicated weak interaction between propylene with the surface.[98] DFT calculations yielded a very weak bonding energy (∼0.07 eV) on clean Au(111).[214] The difference between experiment and theory may originate from the failure of the existing functionals to describe dispersion forces.

C_6-based molecules have also been frequently examined on gold surfaces.[69,110,215,216] Nondissociative adsorption of cyclohexene (c-C_6H_{10}), benzene (C_6H_6), and n-heptane (n-C_7H_{16}) was observed on both Au(111) and a stepped Au(766) surface by Chesters and Somorjai.[69] In contrast, naphthalene ($C_{10}H_8$) dissociated on both surfaces at room temperature.[69] Syomin and Koel further showed that cyclohexane (c-C_6H_{12}) and cyclohexene are reversibly adsorbed on Au(111), with desorption peak temperatures of 198 and 213 K from the adsorbed monolayer, respectively, and 143 K from both multilayer films.[215]

Table 1. Desorption Activation Energies for Hydrocarbon Molecules[a]

molecule	observed energy (kJ/mol)	calculated energy (kJ/mol)	deviation (% error)
methane	14.5	14.4	fitted
ethane	24.1	24.1	fitted
butane	40.5	41.4	2.2
hexane	55.9	56.2	0.5
heptane	62.7	62.4	−0.5
octane	69.7	68.6	−1.6
nonane	75.2	74.8	−0.5
decane	80.1	81.0	1.1
dodecane	93.6	93.4	−0.2
ethylene	27.0	24.9	−7.8
trans-2-butene	41.7	43.5	4.3
cis-2-butene	44.5	43.5	−2.2
2-methylpropene	45.4	44.3	−2.4
1-hexene	56.6	57.4	1.4
1-octene	70.1	69.8	−0.4
1-nonene	76.2	76.0	−0.3
1-decene	81.1	82.2	1.4
1-undecene	87.8	88.4	0.7
cyclohexane	50.6	50.4	−0.4
cyclooctane	63.1	67.2	6.5
benzene	57.9	56.7	−2.1
toluene	66.1	66.3	0.3
propylene	35.0	34.2	−2.2
allene	34.2	35.4	3.5
1,3-butadiene	46.2	43.8	−5.2

[a] Reproduced with permission from ref 217. Copyright 1998 American Chemical Society.

Helium atom reflectivity and theoretical modeling have been used to study the adsorption of a series of n-alkanes, 1-alkenes, and cyclic hydrocarbons on Au(111).[217,218] For the long-chain n-alkanes studied (C_6H_{14}–$C_{12}H_{26}$), the physisorption energy increases linearly with the chain length by 6.2 ± 0.2 kJ/mol per additional methylene unit. The physisorption energies of the 1-alkenes (C_6H_{12}–$C_{11}H_{22}$) showed a similar linear dependence on chain length but are slightly higher than those of the corresponding alkanes.[217] A bond-additive model was presented for predicting the adsorption energy of various saturated and unsaturated hydrocarbons.[217] A summary of desorption activation energies for various hydrocarbon molecules is presented in Table 1.

As derivatives of alkanes, the adsorption and reactivity of alkyl iodides on gold surfaces have been investigated due to their importance in radical- and photochemistry. Paul and Bent found that, on a well-annealed (to 900 K) Au(111) surface, CH_3I remains molecularly intact on the surface.[219] However, on sputtered or incompletely annealed surfaces, a small amount of ethane was formed at 270 K, which can be attributed to partial dissociation of CH_3I at defect sites and subsequent coupling of methyl.[219] Interestingly, considerable quantities of ethane were produced from CH_3I adsorption on Au(100). The coupling reaction on Au(100) occurred at 330 K and proceeded slower than that on Au(111), probably due to a stronger Au−CH_3 bond

on Au(100).[219] Additionally, methyl coupling could be blocked by coadsorption of trimethylphosphine (TMP).[219] Higher iodoalkanes were more reactive than iodomethane (e.g., the coupling reaction of iodoethane was about 5 orders of magnitude faster than that of iodomethane).[220,221] For C_2–C_4 iodoalkanes, disproportionation and coupling reactions took place in the same temperature range (260–270 K), although they were not competitive. Iodoethane produced C_2H_4, C_2H_6, and C_4H_{10} at ~270 K on both Au(111)[221] and Au(100).[220] However, the yield of ethene and ethane saturated at a rather low C_2H_5I coverage, whereas the yield of butane continued to increase until the C_2H_5I monolayer was saturated. The coupling reaction was strongly favored on the Au(100) surface, whereas disproportionation reactions readily occurred on Au(111). Further examination of higher iodoalkanes showed an increased preference for disproportionation with increasing carbon number.[65,221] Syomin and Koel observed the formation of biphenyl (with the molecular plane parallel to the surface) from the coupling reaction via iodobenzene decomposition.[222] Iodobenzene partially decomposed at 200–250 K on a roughened surface and at 250–300 K on defect-free, well-ordered Au(111) surfaces; desorption of formed biphenyl occurred at 400 K.[222]

Recently, Xie and co-workers systematically studied SAMs of alkane molecules with different carbon chain lengths (from n-$C_{14}H_{30}$ to n-$C_{38}H_{78}$) on reconstructed Au(111) surfaces using STM (Figure 11).[223,224] Gold reconstruction plays a significant role in formation of SAMs. The alkane monolayers adopt a lamellar structure in which the alkane molecules are packed side-by-side.[224] The carbon skeletons are found to lie flat on the surfaces. The authors also showed that two-dimensional chiral lamellar structures were formed for alkanes with an even carbon number due to the specific packing of alkane molecules in a tilted lamella.[224]

3.6.2. Oxygenates. On clean Au(100), Au(110), and Au-(111) surfaces, oxygenates including alcohols, ketones, aldehydes, and epoxides are weakly adsorbed and desorb molecularly.[81,96,97,115,118,225−229] For example, three states were observed in methanol desorption spectra on Au(111), which are assigned to monolayer (155 K), amorphous multilayers (143 K), and crystallized multilayers (134 K).[227] However, on a stepped Au(310) surface, methanol decomposed via a O−H bond scission (occurred above 150 K), resulting in an adsorbed methoxy species which was stable until 500 K.[230] The structural sensitivity of Au(310) can be attributed to the presence of special sites formed by (110) steps and (100) terraces on the surface. Formaldehyde molecularly desorbs at ~160 K on Au(110) with a single broad peak.[97] Similar to methanol, acetone reversibly adsorbs on Au(111), with thermal desorption peaks at 160, 137, and 132 K corresponding to acetone desorption from the monolayer, second layer, and multilayer, respectively.[225] RAIRS results indicated that acetone binds through the oxygen atom with a tilted geometry at low coverages. Upon increasing coverage to ~1 ML, the orientation changed so that the C−O bond was parallel to the surface and the molecular plane is perpendicular to the surface.[225] Adsorption of acrolein at 80 K on Au(111) gave rise to a series of sharp RAIRS bands due to a CH_2 out-of-plane wagging vibration $[\omega(CH_2)]$ successively with increasing coverage, indicating discrete adsorption states, i.e., $964 \rightarrow 978 \rightarrow 991 \rightarrow 1003$ cm^{-1}.[229] All these states have the molecular plane parallel to the surface; bands at 964 and 978 cm^{-1} are in an isolated state, and the band at 991 cm^{-1} is in an associated state with a two-dimensional arrangement, whereas the band at
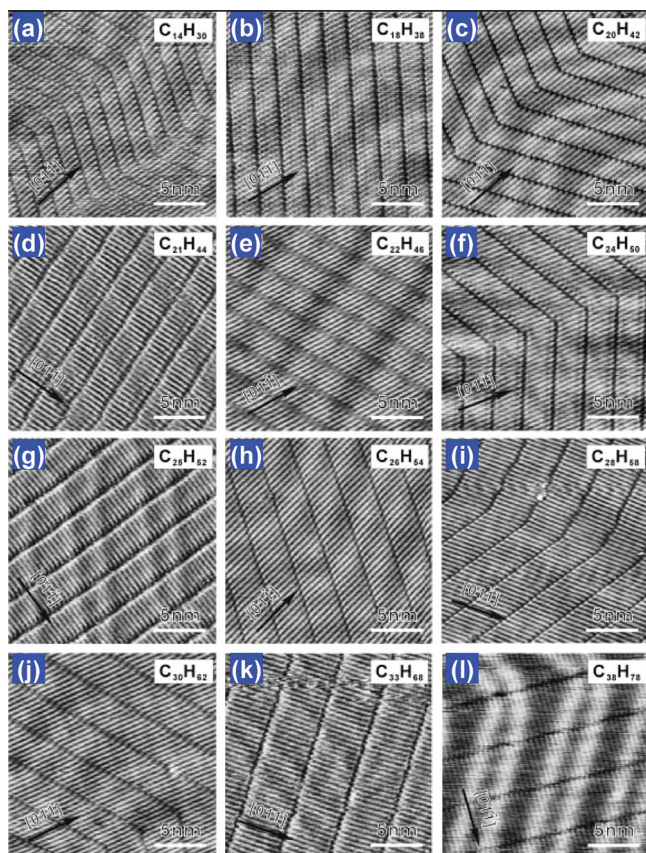
2998

dx.doi.org/10.1021/cr200041p | Chem. Rev. 2012, 112, 2987–3054

Figure 11. STM images of self-assembled *n*-alkanes (from *n*-$C_{14}H_{30}$ to *n*-$C_{38}H_{62}$) on the reconstructed Au (111) surfaces. Images from (b) to (h) exhibit the well-ordered structures of *n*-alkanes for *n* from 18 to 26. Images (a), (i), (j), and (l) are from *n*-$C_{14}H_{30}$, *n*-$C_{28}H_{52}$, *n*-$C_{30}H_{62}$, and *n*-$C_{38}H_{78}$, respectively, and show the representative alkanes for *n* < 18 and *n* > 26 with even *n*. Images (d), (g), and (k) are representative for odd *n* with *n* = 21, 25, and 33, respectively. Arrows on images indicate the [$01\bar{1}$] direction. All images are of 20 nm × 20 nm at the tunneling condition of V_b = 0.1 V, I_t = 1.5 nA. Reproduced with permission from ref 224. Copyright 2004 Wiley-VCH Verlag GmbH & Co. KGaA.

1003 cm^{-1} is due to an ordered multilayered structure.[229] Adsorption of formic acid on gold surfaces was suggested to be structurally sensitive; Outka and Madix showed that formic acid desorbed at 210 (monolayer) and 175 K (multilayers) on Au(110) with dissociation,[97] whereas the formation of formic anhydride as a surface intermediate on Au(111) was reported by Chtaib et al.[231,232] TPD peaks of ethylene oxide on Au(211) appear at 115 K from the multilayer film and 140 and 170 K from the monolayer. Desorption at 140 K was attributed to ethylene oxide desorption from terrace sites and that at 170 K to desorption from step sites.[228]

3.7. Adsorption of Other Molecules

3.7.1. Hydrogen. Molecular hydrogen does not dissociate readily on gold single-crystal surfaces. Sault et al. successfully produced atomic hydrogen on Au(110) via thermal decomposition of dihydrogen on a hot filament; recombinative desorption of hydrogen was observed in a single peak at 216 K.[64] Interestingly, Stobinski found that, while hydrogen and deuterium adsorbed on sintered gold films (deposited on a Pyrex glass cell), molecular chemisorption occurred on as-prepared films at 78 K.[233] Adsorbed hydrogen and deuterium started to desorb at

120 K.[233] The authors suggested this chemisorption occurs on surface Au atoms with low coordination number as a result of formation of AuH_2 complexes, similarly to the compounds arising due to H_2 interactions with isolated Au atoms.[234]

3.7.2. Water. Water reversibly adsorbs and desorbs with a single peak ~160 K on Au(111)[94,199,235,236] and with monolayer (190 K) and multilayer (185 K) peaks on Au(110).[96] Monte Carlo simulations showed that most of the water molecules are adsorbed with the molecular plane parallel to surface, while others adsorb with one of the O–H bonds parallel to the surface and the other bond pointing toward the bulk liquid phase.[237] The fact that H_2O TPD does not display a well-resolved submonolayer peak suggests that H_2O binds more strongly to itself than to the Au substrate, causing it to segregate into 3D islands subsequent to adsorption.[238] STM results showed that that H_2O first adsorbs on Au as a planar, amorphous, monolayer-high film with the subsequent growth of H_2O clusters occurring atop this film.[239] The growth dynamics and structure of amorphous solid water films on gold surfaces is dependent on deposition temperature and conditions.[239,240]

4. REACTIONS ON AU SINGLE-CRYSTALLINE SURFACES

Investigations of surface reactions on gold single crystals have primarily focused on oxidative chemistry. Hydrogenation reactions on gold surfaces are of great interest area but have been rarely explored largely due to the intrinsic inability of gold to dissociate molecular hydrogen (it only significantly adsorbs molecularly at very low temperature).[241] Indeed, theoretical study has revealed that (i) gold has a filled d-band, causing repulsion when hydrogen interacts with the surface due to filling of the antibonding orbital, and (ii) the extent of orbital overlap for gold is high compared to silver or copper, leading to a large orthogonalization energy cost. These factors determines the unique adsorption properties of gold.[241]

Atomic oxygen activates copper, silver, and gold surfaces toward reactions with a variety of molecules. One of the principal mechanisms for this activation is a Brönsted base reactivity where atomic oxygen abstracts an acidic hydrogen atom from an adsorbed molecule.[96,242] In the absence of oxygen adatoms, some of these molecules are completely unreactive, particularly on gold surfaces.[243]

4.1. Reaction of Water and Oxygen Atoms

Water chemisorbs more strongly on oxygen-modified gold surfaces than it does on clean gold. Outka and Madix showed that, following the adsorption of water on an oxidized Au(110) surface, a new water peak was observed at 215 K ascribed to either oxygen-stabilized water or disproportionation of surface hydroxyl groups.[96]

Similar to Au(110), water strongly interacts with oxygen atoms on Au(111) to make a water–oxygen complex or hydroxyls[81,93,94,235,236] as indicated by a new TPD feature with its peak near 175 K, in addition to the water desorption feature at 155 K characteristic of the clean surface (Figure 12a).[94] Water–oxygen interactions also produced oxygen scrambling on Au-(111) as evidenced from isotopic mixing in the oxygen evolution in TPD measurements (Figure 12b and 12c).[94] Oxygen atoms from adsorbed water exchanged with adsorbed oxygen adatoms on Au(111) due to rapid diffusion of transient OH groups with subsequent reversible reactions between two nearby adsorbed
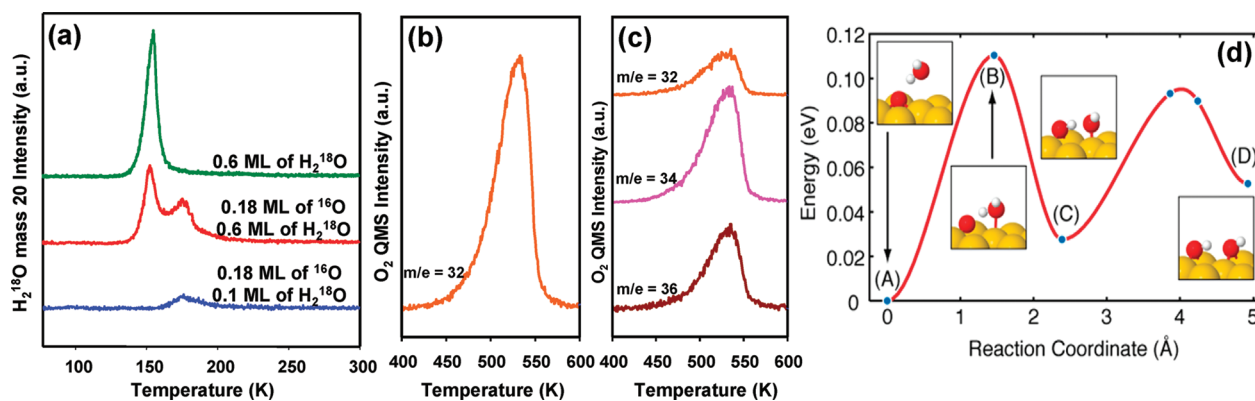
2999

dx.doi.org/10.1021/cr200041p |*Chem. Rev.* 2012, 112, 2987–3054

Figure 12. (a) TPD (β = 1 K/s) of 0.6 ML of $H_2^{18}O$ on clean Au(111) surface (green curve), 0.6 ML of $H_2^{18}O$ on 0.18 ML of ^{16}O covered surface (red curve), and 0.1 ML of $H_2^{18}O$ on 0.18 ML of ^{16}O covered surface (blue curve). TPD (β = 3 K/s) of oxygen after dosing (b) 0.37 ML of ^{16}O and (c) 0.6 ML of $H_2^{18}O$ in addition to 0.37 ML of ^{16}O on Au(111) surface. All exposures at 77 K. (d) The reaction paths of formation of hydroxyls from water and atomic oxygen with a barrier of 0.11 eV. Reproduced with permission from ref 94. Copyright 2008 American Chemical Society.
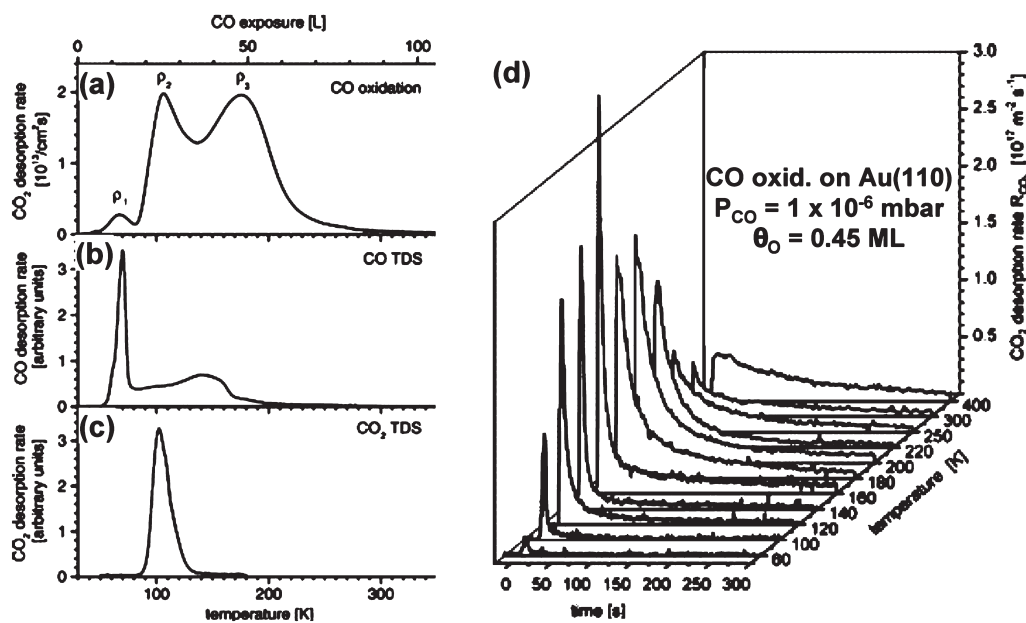
Figure 13. (a) CO_2 production during CO exposure to O/Au(110) (1 × 2) (an initial O coverage of 1.3 ML and a CO pressure of 1×10^{-6} mbar). (b) CO TPD spectrum (1.0 ML initial CO coverage). (c) CO_2 spectrum from a CO_2 and O_a coadsorbed surface (initial CO_2 coverage 1.0 ML, O coverage 1.3 ML). Reproduced with permission from ref 88. Copyright 2003 Elesiver. (d) CO oxidation over O/Au(110) (1 × 2) (an initial O coverage of 0.45 ML and a CO pressure of 1×10^{-6} mbar) as a function of time at various reaction temperatures. Reproduced with permission from ref 89. Copyright 2004 Elesiver.

hydroxyl groups to adsorbed water and oxygen.[94,236] DFT calculations showed that hydroxyls were readily formed by water on oxygen precovered Au(111) due to the small calculated activation barrier of 0.11 eV (Figure 12d).[94] The final state (Figure 12d, point D) of this reaction was only 0.05 eV higher in energy than the initial state (Figure 12d, point A), indicating that hydroxyl formation would be very rapid and reversible between nearby H_2O and O atoms on the surface.[94] Quiller et al. presented details regarding the extent of oxygen exchange and the nature of formed hydroxyls on Au(111) via TPD and RAIRS.[236] They showed that the degree of oxygen exchange depended on the initial coverage of oxygen, the surface temperature when preparing oxygen adatoms, and the water coverage. It was suggested that isolated *stable* hydroxyls may not be formed

and could be more transient in character,[236] which agrees with the result obtained from DFT calculations.[94] They also found that chemisorbed oxygen was critical in the formation of hydroxyls and stabilizing water, whereas gold oxide did not contribute to these effects.[236]

4.2. Oxidation of Carbon Monoxide

4.2.1. Reaction Aspects. CO oxidation was first examined on Au(110) by Madix's group[95] and later by Christmann and co-workers.[89] Outka and Madix observed the production of CO_2 at room temperature on Au(110) precovered with atomic oxygen upon CO exposure.[95] From isotopic experiments with $C^{18}O$ they showed that CO did not dissociate on the surface because $C^{18}O^{16}O$ was the only reaction product evolved.[95] Note that

Figure 14. (a) Initial rate of CO_2 production at 200 K as a function of oxygen coverage for deposition at 200 K (filled circles) and 400 K (open circles), respectively. The atomic oxygen was prepared via ozone decomposition. Reproduced with permission from ref 99. Copyright 2006 American Chemical Society. (b) $CO_2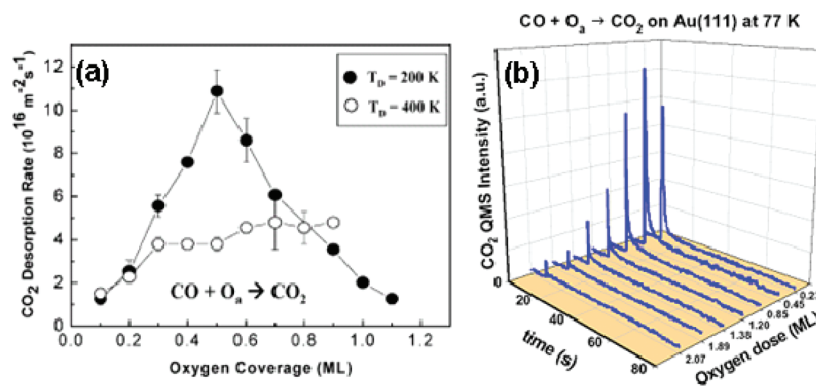$ signal from atomic oxygen precovered Au(111) surfaces at 77 K during CO molecular beam impingement. Atomic oxygen was precovered on Au(111) at 77 K via an O-plasma. The CO beam starts at 10 s for all oxygen coverages. Reproduced with permission from ref 93. Copyright 2007 Springer.

no evidence of carbonate formation ($CO + O_2 \rightarrow CO_3$) was observed, which was proposed as a possible reaction intermediate in CO oxidation.[95] An apparent activation energy of ~41.8 kJ/mol was obtained for an oxygen coverage of 0.25 ML. Interestingly, both instantaneous and initial oxygen coverages determined the reaction rate,[95] which is probably due to the tendency of atomic oxygen to form Au–O islands at high oxygen coverages; CO oxidation occurs via an island consuming mechanism under reaction conditions.[95]

Gottfried et al. scrutinized the same reaction on Au(110), which was precovered with 1.3 ML of atomic oxygen before being exposed to CO.[89,123] Three desorption peaks of CO_2 were observed (Figure 13a–13c). CO_2 from the peak at 105 K could be desorption-limited as this coincided with the desorption temperature of CO_2 from clean Au(110). The small CO_2 peak around 67 K suggested that at least some CO_2 produced was sufficiently excited by the reaction to overcome the desorption barrier. The peak at 175 K was attributed to the reaction-limited production of CO_2.[123] The authors also studied the reaction with an initial oxygen atom coverage of 0.45 ML as a function of temperature and observed CO_2 production over time (Figure 13d).[89] They found that the reaction rate increased with increasing temperature until ~170 K, at which point the production rate of CO_2 began to decrease. The surface reaction was no longer the rate-limiting step at temperatures above 175 K.[89] The surface-bound oxygen enhanced the binding of CO, leading to a decrease in the reaction rate with time.[89] An activation energy was estimated to be 57 kJ/mol.[89]

Likewise, the highest CO_2 production rate on Au(111) was observed at 200 K when the surface was oxidized at 200 K using ozone decomposition.[99] Min et al. investigated the dependence of the rate of CO_2 production on oxygen coverage for the two different temperatures (200 and 400 K) used to prepare the oxygen overlayer (Figure 14a).[99] The initial rate of CO oxidation on the O-covered surface prepared at 200 K reached a maximum at 0.5 ML of oxygen. The initial rate dropped by an order of magnitude for O_a coverages between 0.5 and 1.2 ML for ozone exposures conducted at 200 K. Gong et al. also observed a similar dependence when the Au(111) surface was populated with atomic oxygen via an O-plasma at 77 K (Figure 14b).[93] In contrast, Min et al. observed that the rate of CO_2 production was nearly independent of oxygen coverage if the oxygen layer was prepared with ozone at 400 K. At an oxygen coverage of 0.5 ML,

the rate of CO_2 production for the oxygen layer deposited at 200 K is approximately a factor of 3 greater than for the oxygen layer created at 400 K (Figure 14a). As discussed in the previous section (e.g., Figure 6e), depending on the oxygen coverage, surface temperature, and possibly preparation method, various oxygen states (from chemisorbed to bulk oxide) can be formed upon oxygen deposition. The order of reactivity of atomic oxygen in CO oxidation was classified by Friend and co-workers as chemisorbed (metastable) oxygen > oxygen in a surface oxide (i.e., well-ordered 2D Au–O phase) > oxygen in a bulk gold oxide (i.e., 3D structures containing Au and O).[19,99] Oxide-like domains could predominantly exist at the higher coverages/deposition temperature, while chemisorbed oxygen on Au(111) plays a more dominant role at the lower coverages/deposition temperatures. Additionally, Koel and co-workers observed CO oxidation at 250–375 K on Au(111) populated with atomic oxygen (via ozone decomposition at 300 K) and obtained an apparent activation energy of −10.5 kJ/mol.[81]

Recently, CO oxidation has been investigated on stepped gold single-crystal surfaces.[124,244,245] Koel's group has carried out a transient kinetics study of CO oxidation on Au(211) precovered with atomic oxygen created by ozone decomposition at 85 K.[124,244] CO oxidation on Au(211) was somewhat similar to that on the Au(111) and (110) surfaces. The reaction rate was dependent on the initial oxygen coverage (maximum initial rate of CO_2 production occurred at an oxygen coverage of ~0.5 ML), and the apparent activation energy for CO oxidation was determined to be −7.0 kJ mol^{-1} for an initial oxygen coverage of 0.9 ML.[244] The reaction was proposed to proceed via a Langmuir–Hinschelwood (LH) mechanism with an activation barrier of 20–43 kJ/mol for CO oxidation, which was comparatively lower than the value of 67 kJ/mol predicted on Au(211) by theoretical calculations.[246] Additionally, Fajin et al. calculated the reaction barrier for CO oxidation by molecular or atomic oxygen on a Au(321) surface.[245] They showed that the reaction by atomic oxygen occurred almost without any energy cost on a reconstructed surface, whereas a moderate barrier of 58 kJ/mol was obtained for the direct reaction with molecular oxygen.[245]

4.2.2. Role of Water/Hydroxyl. Water or moisture plays an important role in many oxidative reactions.[247] Understanding the role of water in CO oxidation on gold has been a subject of recent research efforts due to its underlying significance in the
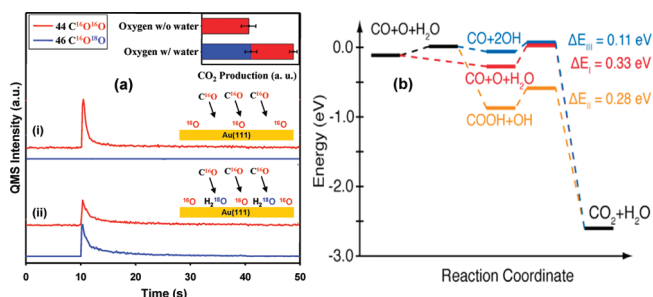
Figure 15. (a) Evolution of CO_2 at 140 K while impinging a continuous CO beam (from 10 to 40 s) at the surface. The red curve represents mass 44 $C^{16}O^{16}O$ and the blue curve represents mass 46 $C^{16}O^{18}O$ with (i) 0.08 ML of ^{16}O preadsorbed, (ii) 0.1 ML $H_2^{18}O$ in addition to 0.08 ML of ^{16}O atoms preadsorbed on Au(111) at 77 K. Reproduced with permission from ref 235 Copyright 2006 American Chemical Society. (b) Energy landscape for three reaction mechanisms of CO oxidation in the presence of H_2O. In pathway I (red), there is no hydrogen transfer from H_2O. In pathway II (orange), hydrogen transfer occurs before CO oxidation. In pathway III (blue), hydrogen transfer occurs concertedly with CO oxidation, leading to the lowest overall barrier for CO oxidation (0.11 eV). Reproduced with permission from ref 94. Copyright 2008 American Chemical Society.

water−gas shift reaction. Date and Haruta showed that the addition of moisture in the feed stream enhances the CO oxidation reaction over supported gold particles by as much as 2 orders of magnitude.[247,248] They postulated that water promotes the reaction by either activating molecular oxygen on the surface or assisting in the decomposition of carbonates that may accumulate on the surface in order to accommodate additional reactants on the surface.[248] Indeed, water reacts with oxygen atoms to form transient hydroxyls, which are directly involved in the reaction of CO oxidation on Au(111)[93,94,235,249,250] as shown from the evolution of $C^{16}O^{18}O$ after $C^{16}O$ impingement on a surface covered with both oxygen ($^{16}O_a$) and isotopically labeled water ($H_2^{18}O$) (Figure 15a). With 0.08 ML of ^{16}O preadsorbed on the surface, $\sim$ 70% more CO_2 production is observed at 140 K when 0.1 ML of water is added to the surface.[235] DFT calculations indicated that, in the presence of H_2O, the barrier for CO oxidation for a selected pathway is reduced to 0.11 eV (see Figure 15b) compared to 0.25 eV for CO oxidation on oxygen precovered Au(111) without H_2O. This reduction is attributed to a concerted hydrogen transfer from one hydroxyl to another that acts to stabilize the transition state for CO oxidation and promote CO oxidation at temperatures as low as 45 K.[94]

Rodriguez and co-workers systematically investigated the role of formate, carbonate, and carboxyl (HOCO) species as possible intermediates in the $OH_{ads} + CO_{gas} \rightarrow CO_{2,gas} + 0.5H_{2,gas}$ reaction on Au(111) using synchrotron-based core level photoemission, near-edge X-ray absorption fine structure (NEXAFS), and RAIRS.[251] Adsorbed HCOO, CO_3, and OH species were prepared by adsorbing formic acid, carbon dioxide, and water on Au(111) precovered with $\sim$0.2 ML of atomic oxygen, respectively (CO_3 formation will be discussed in detail later).[251] The results of NEXAFS, IR, and DFT calculations indicated that the formate adopted a bidentate configuration (η^2-O,O) on Au(111). Since the formate groups are stable on Au(111) up to temperatures near 350 K, it is not likely that formate is a key intermediate for the $OH_{ads} + CO_{gas} \rightarrow CO_{2,gas} + 0.5H_{2,gas}$ reaction at low temperatures.[251] They did not detect HCOO nor CO_3 during the reaction of CO with OH on
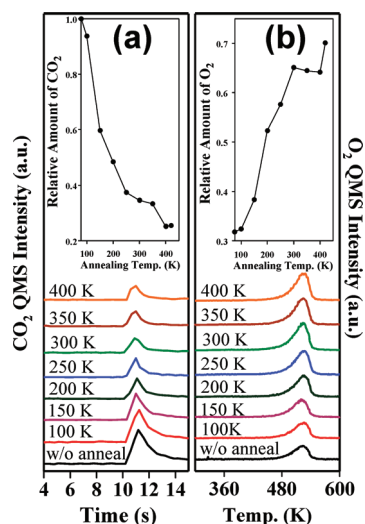

Figure 16. (a) CO_2 evolution at 77 K from 0.37 ML ^{16}O covered Au(111) surfaces annealed to varying temperatures at β = 1K/s and cooled to 77 K in each case before a 10 s CO dose from a molecular beam. (b) TPD spectra of unreacted O_2 remaining on Au(111) after CO oxidation in each of the above cases. The lowest curves represent (a) CO_2 evolution from an unannealed surface and (b) TPD of the remaining oxygen on the unannealed surface. The insets show the normalized amount of (a) CO_2 produced and (b) unreacted oxygen as a function of annealing temperature. Reproduced with permission from ref 252. Copyright 2009 American Chemical Society.

Au(111) at 90−120 K. However, the results of photoemission and IR spectroscopy pointed to HO ↔ CO interactions, consistent with the formation of an unstable HOCO intermediate that has a very short lifetime on the gold surface.[251]

Shubina et al. theoretically studied the interaction of CO with OH and subsequent formation of COOH on Au(110).[249] They found that the reaction barrier within the same unit cell was 0.25 eV.[249] In a similar investigation, Rodriguez showed that in alkaline media CO and OH can enhance each other's binding through what appeared to be a local gold-mediated electron-transfer mechanism that is driven by a change in the local electrostatics, which consequently increased the reaction probability for COOH formation.[250]

4.2.3. Effect of Annealing.
The reactivity of oxygen can be changed by controlling its pre- and postadsorption conditions. Gottfried et al. reported that annealing decreased the intensity of desorption features of CO from the clean Au(110) surface and attributed this effect to a reduction in the surface defect concentration.[123]

Regarding Au(111), atomic oxygen adsorbed at low temperatures (i.e., 77 K) is trapped in a metastable state from which the barrier to further reaction is lowered.[252] Annealing the adsorbed oxygen (from 100 to 400 K) can stabilize the oxygen overlayer, thereby increasing the barrier to reaction; this phenomenon also applies to CO oxidation (Figure 16a). Specifically, CO_2 production decreased with increasing annealing temperature, with the highest CO_2 production occurring when there was no surface annealing.[252] This is consistent with results showing that the amount of unreacted oxygen remaining on the surface after a constant exposure to CO increases with increasing annealing temperature (Figure 16b).

These results could provide insights into the nature of oxygen on gold surfaces related to the catalytic oxidative reactivity. The
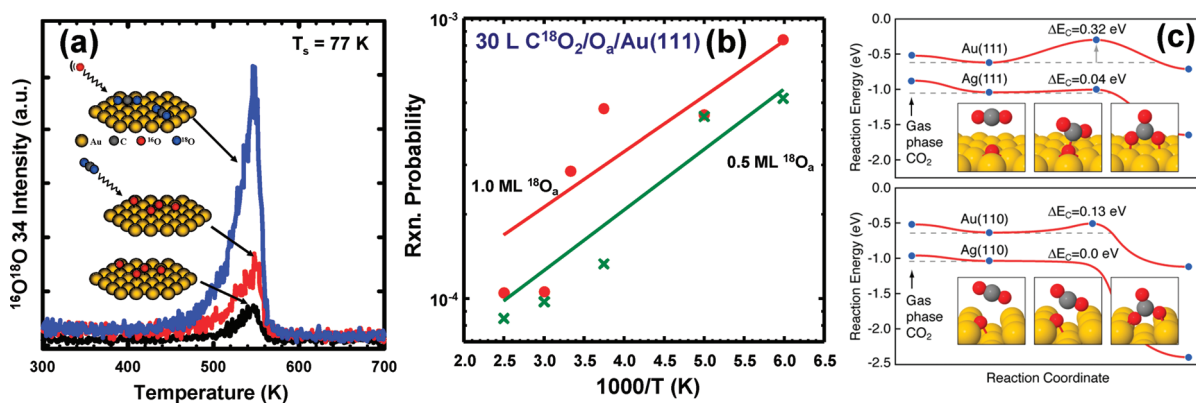
Figure 17. (a) TPD spectra of $^{16}O^{18}O$ after (black curve) dosing 1.3 ML of ^{16}O on clean Au(111); (red curve) backfilling 30 L of $C^{18}O_2$ on Au(111) precovered with 1.3 ML of ^{16}O; (blue curve) dosing 1.3 ML of ^{16}O on Au(111) precovered with 30 L of $C^{18}O_2$ via backfilling. Reproduced with permission from ref 255. Copyright 2008 American Chemical Society. All doses and/or backfillings were done at 77 K, and the heating ramps were 3 K/s. (b) Arrhenius plot of $C^{18}O_2$ reaction probability using a constant $C^{18}O_2$ exposure of 30 L for 1.0 ML (upper plot) and 0.5 ML (lower plot) of atomic oxygen on Au(111). (c) DFT calculations of carbonate formation on Au and Ag (111, upper plot) and (110, lower plot) surfaces. Energy barriers (ΔE_c) are labeled for each reaction pathway. Reproduced with permission from ref 253. Copyright 2008 American Chemical Society.

effect of annealing can be attributed to the relaxation of highly reactive (e.g., metastable oxygen species at low temperatures) into a less reactive state (at high temperatures).[252] At least two discrete atomic oxygen species reside on the surface.[252] As discussed earlier, three types of oxygen on Au were identified as chemisorbed metastable oxygen (indicating oxygen bound to the Au (111) surface or small disordered gold islands), a surface oxide (corresponding to a well-ordered two-dimensional Au–O phase), and a bulk oxide (ordered 3D structures containing Au and O).[99] Upon annealing the O–Au(111) surface from 77 to 400 K, the state of oxygen could undergo a gradual evolution from chemisorbed (metastable) oxygen (i.e., 77–200 K) to Au–O oxides (e.g., 200–400 K) leading to a decrease in the reactivity. It was suggested that the mobility of oxygen species on the surface is crucial to the reactivity. Compared to metastable oxygen, oxygen in ordered structures (i.e., Au–O oxides) is certainly less mobile and would react more slowly with probe molecules.[252]

4.2.4. Formation of Carbonate from CO$_2$ and Oxygen Adatoms.
The carbonate formation and decomposition ($CO_3 \leftrightarrow CO_2 + O_a$) reaction on gold is important regarding low-temperature CO oxidation since it has been considered as a possible reaction intermediate in reactions where CO is involved.[253]

A surface carbonate is readily formed on oxygen-precovered Ag(110) upon exposure to CO_2 at 300 K.[254] In spite of similarities between silver and gold, carbonate formation and decomposition went undetected previously on Au(110)[95] and Au(111)[81] likely due to a low reaction probability. Recently, Ojifinni et al. detected the surface carbonate on Au(111) via reaction of preadsorbed ^{16}O atoms and gaseous $C^{18}O_2$, which decomposes to form either $C^{18}O_2$ or $C^{18}O^{16}O$ while leaving either $^{16}O_a$ or $^{18}O_a$ adatoms on the surface, respectively. Upon heating, the oxygen atoms recombinatively desorb to form $^{16}O_2$ and $^{16}O^{18}O$ (and negligible $^{18}O_2$).[253] Therefore, carbonate formation and decomposition were measured by monitoring the presence of mass 34 ($^{18}O^{16}O$) in the TPD spectra. An increase in $^{16}O^{18}O$ desorption was observed from $C^{18}O_2$ and ^{16}O coadsorbed on Au(111) compared to the solely ^{16}O covered surface (black and red curves in Figure 17a). An Arrhenius plot of

the reaction probability ($\sim 10^{-3}-10^{-4}$) for two oxygen coverages (0.5 and 1.0 ML) yielded similar apparent activation energies of $E_a = -0.15 \pm 0.08$ eV (Figure 17b), suggesting a competition between carbonate formation and CO_2 desorption on the O/Au(111) surface.[253] The difference in carbonate formation on silver and gold is related to surface structure and energetics. DFT calculations provided the difference in energetics and reaction paths for CO_3 formation on Au(111), Au(110), Ag(111), and Ag(110) (Figure 17c).[253] The formation of CO_3 on Ag(110) was spontaneous and occurred with only a very small barrier of 0.04 eV on Ag(111). For Au, however, there was a significant barrier to CO_3 formation [particularly on the (111) surface] and CO_3 was bound much more strongly to Ag than to Au, consistent with the experimental results.[253,254]

Changing the order of deposition of CO_2 and O_a led to different reaction phenomena and mechanisms.[255] By directing an ^{16}O atomic beam toward $C^{18}O_2$ preadsorbed Au(111) (blue curve in Figure 17a), the formed carbonate increased significantly (by a factor of ~ 4) compared to exposing $C^{18}O_2$ to the $^{16}O_a$ precovered Au(111) surface, indicating that the nature of the adsorbed atomic oxygen (i.e., excited or ground state) plays a significant role in carbonate formation reactions.[255] Such a reaction followed a hot-precursor-mediated mechanism.[255] The authors deduced that these results may provide insight into the related reaction between CO and adsorbed molecular oxygen to make CO_2 in which a "hot" oxygen adatom is produced that could encounter other adsorbed moieties on real or model catalysts and react further.

4.3. Selective Oxidation of Olefins
4.3.1. Propylene.
Another area in which supported gold catalysts can potentially enhance catalytic performance is the epoxidation of propylene to propylene oxide.[17] However, the epoxide that is formed on supported Au nanocatalysts is not formed on gold single crystals.[98,256] This difference might be due to the effect of the metal oxide support (e.g., the presence of oxygen vacancies).

Davis and Goodman explored oxidation of propylene on oxygen-covered Au(111) and Au(100).[98] At high oxygen coverage, the reaction yielded combustion products (CO, CO_2, and
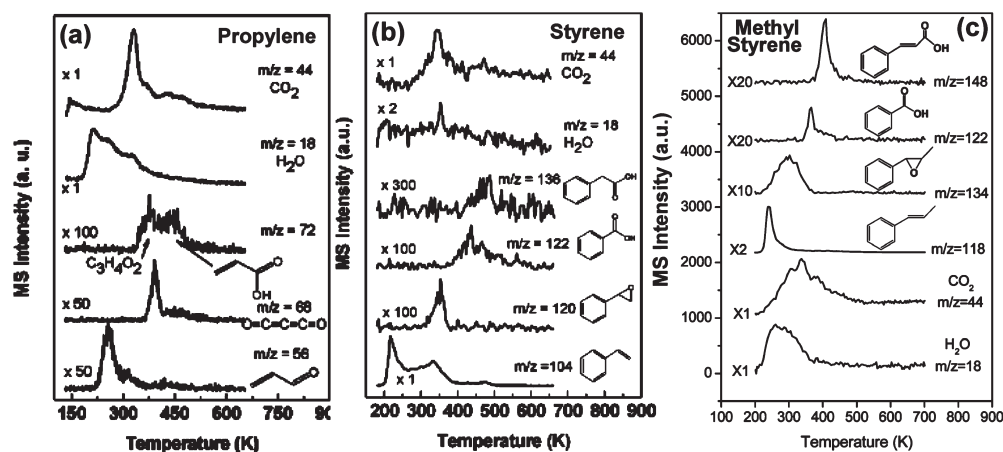
Figure 18. Temperature-programmed reaction spectra of (a) propylene (Reproduced with permission from ref 256. Copyright 2006 American Chemical Society.), (b) styrene (Reproduced with permission from ref 110. Copyright 2005 American Chemical Society.), and (c) *trans-β*-methylstyrene (Reproduced with permission from ref 258. Copyright 2010 American Chemical Society.) on 0.3 ML, 0.2 ML, and 0.2 ML oxygen-covered Au(111), respectively. The adsorption temperature of propylene and styrene was 130 K and of *trans-β*-methylstyrene was 200 K. For all three molecules, multiple layers were adsorbed initially. The heating rate for TPD was ∼10 K/s.

H_2O), whereas a small amount of partial oxidation products with m/z 56 (possibly acrolein) and 58 (possibly propylene oxide) was produced.[98] Interestingly, in a similar but more recent study by Deng et al., the products of partial oxidation of propylene on 0.3 ML atomic oxygen precovered Au(111) were found to be acrolein (desorbed at 255 K), carbon suboxide ($O{=}C{=}C{=}C{=}O$) (390 K), and acrylic acid (440 K) as well as combustion products (Figure 18a).[256] Control experiments suggested that allyloxy was a reaction intermediate formed via insertion of oxygen into the allylic C−H bond, which was subsequently oxidized to acrolein. The similar mechanism was also observed for the activation of phenyl-substituted propenes on atomic oxygen-covered Au-(111).[257] Evolution of gaseous acrolein competed with secondary oxidation to carbon suboxide, acrylic acid, and combustion products.[256] The discrepancy in the two studies might be due to the fact that different methods were used for oxygen deposition (O_2 thermal cracking and deposited at 300 K vs O_3 decomposition at 200 K on the surface) since the structure and morphology of the Au surface strongly depend on the method used for oxygen deposition and the surface temperature.[19]

4.3.2. Styrene. It has been shown that that the reaction of nonallylic olefins with atomic oxygen on coinage metal surfaces is governed by the cycloaddition character of oxygen, leading to the formation of epoxides or other cyclic adducts that incorporate oxygen atoms in the ring.[25] As a representative of nonallylic olefins, styrene oxidation has been studied, and the results are discussed here as an example.

On 0.2 ML atomic oxygen-precovered Au(111), in addition to combustion, a majority portion (∼80%) of the adsorbed styrene was selectively oxidized to styrene oxide, benzoic acid, and benzeneacetic acid (Figure 18 b).[110] Oxametallacycle was a possible intermediate for the formation of styrene oxide on Au(111)[110] as also indicated by DFT calculations,[259] and indeed has been widely adopted by researchers to successfully explain the product distribution in the oxidation of olefins.[25] Reactions of the combustion intermediate, derived from the oxametallacycle via β-H elimination, led to phenylacetaldehyde, phenylketene, and phenylacetic acid as well as adsorbed benzoate and products derived therefrom.[110,260] The activation energy for epoxidation of styrene on Au(111) was 87.4 kJ/mol.[110] Notably, the reaction

pattern on Au(111) is similar to that on Ag(111).[261] The presence of both the C=C bond and allylic C−H bond in bifunctional allylic olefins leads to competing oxidation. Liu et al. studied *trans-β*-methylstyrene on atomic oxygen-precovered Au(111) which undergoes both C=C bond and allylic C−H bond cleavage, resulting in the formation of epoxide, benzoic acid, and cinnamic acid (Figure 18c).[258]

Chlorine coadsorbed on Au(111) significantly enhances the selectivity of styrene epoxidation by inhibiting secondary oxidation, especially combustion and the deposition of residual carbon.[195] The effect of Cl can persist over several turnovers. The authors found a shift in the peak for O_2 evolution from 540 to 525 K when Cl was present, suggesting adsorbed chlorine induced a change in the bonding of O to Au (e.g., distribution and geometric arrangement of the O-covered Au surface).[195] STM experiments indicated that Cl enhanced the dispersion of Au−O complexes on the surface,[191] which would account for the suppression of multiple oxidation steps leading to combustion, formation of organic acids, and nonselective decomposition of the styrene.[195]

Subsurface oxygen on Au(111) created from O_2^+ sputtering had little effect on either the product distribution or the conversion rate of styrene. Surface roughness led to an increase of the overall amount of styrene that was oxidized but reduced the selectivity of the epoxide.[85]

4.4. Oxidative Dehydrogenation of Alcohols

The hydroxyl group is the primary functional group in aliphatic alcohols and has greater gas-phase Brønsted acidity than water. Consequently, the reactions of alcohols on oxygen-covered coinage metal surfaces are initiated by the activation of O−H bonds by adsorbed atomic oxygen to form adsorbed alkoxy and water.[25] Subsequent reaction steps involve C−H bond cleavage; the differences in the product distributions of various alcohols depend on the structure of the alkyl groups as well as the atomic oxygen coverage. The oxidation of alcohols on gold surfaces shares some common character with those on silver and copper, but significant differences have been reported,[25,243] which can be ascribed to the different reactivity of formed alkoxy groups.
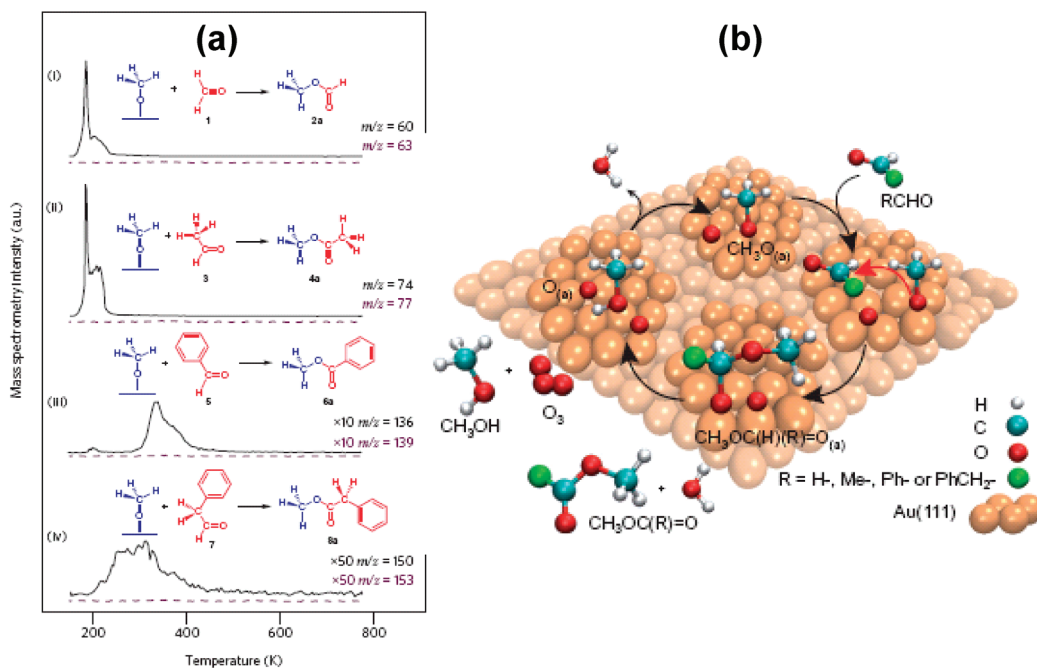
Figure 19. (a) TPD spectra of four esters formed from the cross-coupling of methoxy with aldehydes: (i) formaldehyde, (ii) acetaldehyde, (iii) benzaldehyde, and (iv) benzeneacetaldehyde. Atomic oxygen was generated via ozone decomposition at 200 K; the initial coverage was ~0.05 ML. Methanol and the various aldehydes were sequentially introduced to the O/Au(111) surface at 140 K. (b) Schematic mechanism for coupling of methanol and aldehydes on oxygen-covered Au(111). Reproduced with permission from ref 265. Copyright 2010 Nature Publishing Group.

4.4.1. Methanol. Methanol was oxidized on Au(110) via the activation of the O—H bond by adsorbed atomic oxygen (θ_O = 0.25 ML) to form methoxy at 200 K, which further reacted to from methanol, hydrogen, and methyl formate at 250 K and CO_2 at 350 K.[96] Unlike on Cu(110)[262] and Ag(110),[263] formation of gaseous formaldehyde was not observed. This discrepancy could originate from a fundamental difference in the bonding of methoxy to the gold surface, rendering it more susceptible to attack by the aldehyde.[25] Methoxy decomposed to adsorbed formaldehyde on gold at a lower temperature (250 K) compared to silver, so that its reaction with adsorbed methoxy to form methyl formate was more likely due to a longer surface lifetime during heating. On silver or copper, formaldehyde desorbed much faster at the relatively higher decomposition temperatures of methoxy, although some methyl formate was observed on Ag(110) at sufficiently high coverages of methoxy.[262,263] Notably, formate also existed as a stable intermediate on Au(110) through secondary oxidation of formaldehyde.[96] The decomposition temperature of the formate on Au(110) was 350 K, lower than that observed on Ag(110) (400 K) and Cu(110) (475 K).[97]

The oxidation of methanol on Au(111) also involves the cleavage of the O—H bond forming surface bound methoxy.[81,118,264−266] Gong et al. and Lazaga et al. only detected H_2O, CO, and CO_2 as the decomposed product of methoxy,[81,118] whereas Xu et al. observed the formation of methyl formate (220 K), formaldehyde (250 K), and formic acid (280 K).[264] The formation of methyl formate via coupling of formaldehyde with methanol was attributed to the fact that the decomposition temperature of methoxy via β-H elimination is lower than the desorption temperature of the aldehyde formed.[264] The cross-coupling of methanol with other alcohols such as ethanol and n-butanol has been reported by the same group.[267] There are three possible reasons that can account for the differences in these studies: (i)

the method for preparing oxidzed Au(111) surface was different, possibly leading to differences in the bonding environment of the oxygen; (ii) in the study by Xu et al., methanol was exposed to the surface at a higher temperature (160 K), close to the temperature where water leaves the surface; (iii) the extent of the esterification reaction appears to be low, so the methyl formate may have gone undetected if the mass spectrometer detector is far away from the sample. Remarkably, the selective oxidative coupling of methanol to methyl formate has been reported on nanoporous Au prepared by the dealloying of AuAg alloys, which yields a selectivity to methyl formate above 97% at ~200 K.[268]

Xu et al. creatively designed additional experiments that further proved the coupling mechanism on atomic oxygen cover Au(111).[265,269] They first created a gold surface populated with methoxy that was readily formed from reaction of methanol with oxygen (~0.05 ML) and subsequently used four different aldehydes—formaldehyde, acetaldehyde, benzaldehyde and benzeneacetaldehyde—as probe molecules to investigate the reactivity of methoxy. For all of the aldehydes, they uniquely observed the evolution of respective methyl esters that were selectively formed via cross-coupling of methoxy and aldehydes (Figure 19a).[265] A proposed reaction mechanism under their investigated experimental conditions is shown in Figure 19b.

4.4.2. Ethanol. Interestingly, unlike methanol chemistry on O—Au(111), ethanol was selectively oxidized on Au(111) as indicated by the formation of acetaldehyde and water (Figure 20a) for low oxygen coverages [preadsorbed on Au(111) via O-plasma].[115] No other partial oxidation products, such as methane, ethane, ethylene, ethenol, acetic acid, ethylene oxide, and methyl formate, or C_1-containing species (e.g., CO, CO_2, formaldehyde, and formic acid) were detected during the reaction.[115] A trace amount of ethyl acetate was detected during the reaction. Isotopic experiments provided evidence of the
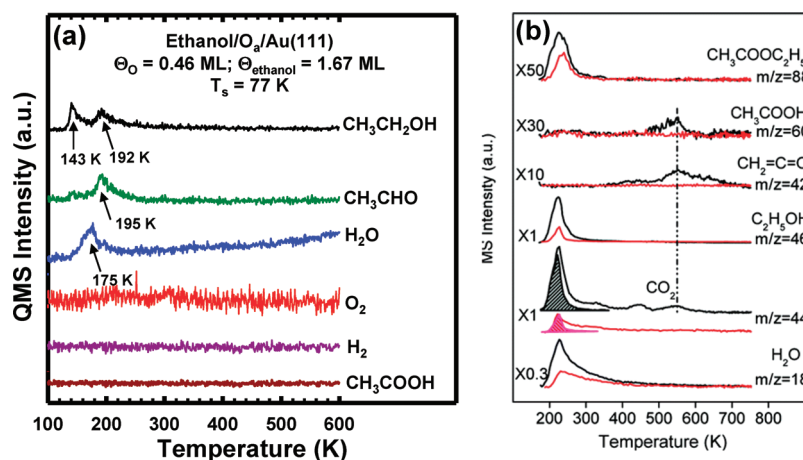
Figure 20. (a) TPD spectra of ethanol (β = 1 K/s) following adsorption of 1.67 ML ethanol on ~0.46 ML atomic oxygen-precovered Au(111) at 77 K. Atomic oxygen was prepared via O-plasma and directed on Au(111) using molecular beam. Reproduced with permission from ref 115. Copyright 2008 American Chemical Society. (b) TPD spectra of ethanol (β = 1 K/s) on O/Au(111) for two different initial oxygen coverages: 0.05 (red) and 0.2 ML (black). Ozone and ethanol were sequentially dosed at a surface temperature of 200 and 180 K, respectively. Reproduced with permission from ref 270. Copyright 2009 American Chemical Society.

absence of cleavage of the C—O and the γ-C—H bonds. At higher oxygen coverages (e.g., 1.0 ML), in addition to acetaldehyde and water, CO_2 was also formed during the reaction due to the cleavage of the γ-C—H bond and the C—C bond.[115] Similar to methanol, a different oxygen preparation method and reaction condition led to a different product distribution. Liu et al. showed that, in addition to molecular acetaldehyde, ethyl acetate (230 K) and acetic acid (450 and 545 K) were formed on Au(111) precovered with 0.4 ML atomic oxygen, when prepared by decomposition of O_3 at 200 K (Figure 20b).[270] At oxygen coverages below 0.1 ML, ethyl acetate was the sole product.[227,270] Friend and co-workers noted that the product distribution under their experimental conditions was in good agreement with those of ethanol oxidation in aqueous solution at 3.5 MPa pressure over supported gold catalysts.[227,271] They, thus, deduced that the mechanistic origin of the formation of ethyl acetate and acetic acid under high pressure, industrial conditions can be well explained by the reaction pathways obtained on single-crystal surfaces, providing an illustration of the link between ultrahigh vacuum studies and heterogeneous catalysis.[25,227]

4.4.3. Other Alcohols. Reactions of other alcohols that have been investigated on preoxygenated gold surfaces include propanol,[226] 2-butanol,[272] allyl alcohol,[256] cyclohexanol,[273] and 2-cyclohexen-1-ol.[273] In all cases, aldehydes or ketones were formed as major products; no ester was produced. The activation energies for β-H cleavage of alkoxys were found to decrease with increasing the chain length, e.g., $E_{methoxy}$ > E_{ethoxy} > E_{butoxy}.[269] Cleavage of the C—O bond was observed since, for example, the oxygen-exchange phenomenon occurs when the Au(111) surface is covered with both $^{18}O_a$ and $C_2H_5CH_{16}OHCH_3$.[272] Propaldehyde was formed at 200 K, acetone at 180 K,[226] 2-butanone at 185 K,[272] and acrolein at 255 K.[256] As for allyl alcohol, in addition to acrolein, at least two other partial oxidation products were detected, acrylic acid and carbon suboxide.[256] Both of them are considered to be produced from secondary oxidation of the intermediate species acrolein. The formation of carbon suboxide could be facilitated by the planar π system in acrolein that brings all the hydrogen atoms close to the surface and makes them subject to attack by excess surface

oxygen.[256] For cyclohexanol and 2-cyclohexen-1-ol, cyclic ketones—cyclohexanone (240 K) and 2-cyclohexen-1-one (240 K)—are the major products of selective oxidation. The produced ketones also experience activation of secondary ring C—H bonds. The product distributions based on TPD spectra reflect a substantial difference in the secondary reactions for these two ketones, which correlate with their gas-phase acidity.[273] The allylic alcohol (2-cyclohexen-1-ol) shows a greater degree of ring C—H activation, yielding the diketone (2-cyclohexene-1,4-dione) and phenol.

From oxidative chemistry of alcohols on gold surfaces, one could learn that adsorbed atomic oxygen acts as a strong Brønsted base that would effectively react with acidic O—H bonds below 200 K to form stable adsorbed alkoxy. The subsequent decomposition of the primary and secondary alkoxy typically occurs via β-H elimination to form acetaldehyde or ketone simultaneously. However, whether the aldehyde evolves into the gas phase depends on (i) the decomposition temperature of alkoxy, (ii) its stability on gold surfaces, (iii) its reactivity with other surface species (e.g., alkoxy or oxygen), and (iv) the presence of other functionalities such as the C═C double bond in the alkyl group.[25] Due to these factors, esters and other products can also be produced dependent on the specific alcohol. Notably, the reaction selectivity and product distribution can be tuned by varying the initial surface coverage of both alcohol and oxygen as well as surface temperature. Selective oxidation to aldehyde or ketone is favorable in oxygen-lean environments.

4.5. Surface Chemistry of Nitric Oxide

Fundamental understanding of NO oxidation is important due its underlying association with NO reduction under oxygen-rich conditions. McClure et al. showed that NO reacted with an atomic oxygen-covered Au(111) surface to form nitrogen dioxide.[92] They observed an increased NO uptake in the presence of oxygen adatoms, likely owing to electronic or structural changes in the Au surface.[92] At temperatures above 200 K, NO_2 production became limited by the surface lifetime of the adsorbed NO species. Below 200 K, nitric oxide can react with surface oxygen to form a chemisorbed NO_2 product.[92] On
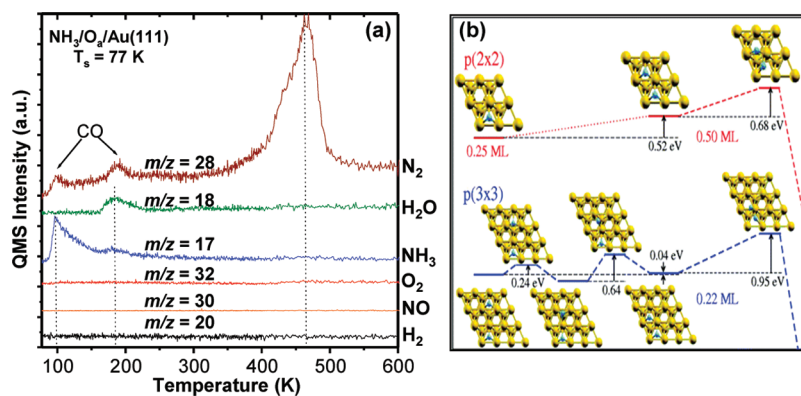
Figure 21. (a) TPD spectra from the adsorption of 0.18 ML of O atoms on Au(111) at 77 K followed by 0.23 ML of NH$_3$ at 77 K. The heating rate was 1 K/s to 400 K, then 3 K/s to 600 K. Reproduced with permission from ref 200. Copyright 2006 American Chemical Society. (b) N−N recombination energy plots at two different coverages: p(2 × 2) and p(3 × 3). Yellow and blue spheres represent Au and N atoms, respectively. Relevant energies are shown in eV. Reproduced with permission from ref 277. Copyright 2006 American Chemical Society.

the basis of an analysis involving a kinetic competition between desorption of the NO molecule and reaction with O adatoms, an activation energy of 0.21 ± 0.02 eV was estimated for the 0.95 ML O/Au(111) surface.[92] This value is comparable to theoretical results obtained from DFT calculations.[274,275]

The Koel group found that, when NO$_2$ was dosed on an oxygen covered Au(111) surface, a second NO$_2$ desorption feature began to appear at 175 K,[81] along with the normal NO$_2$ desorption feature at 225 K. As the atomic oxygen coverage was increased, the normal NO$_2$ desorption feature (~225 K) decreased while the second NO$_2$ desorption feature (~175 K) grew, resulting in complete suppression of the normal TPD feature at oxygen coverages greater than 1.0 ML.[81] Koel and co-workers speculated that this feature may be due to the formation of a nitrate species (NO$_{3,ads}$) on the Au(111) surface, but due to inherent experimental difficulties they were unable to verify this spectroscopically via high resolution electron energy loss spectroscopy (HREELS) measurements.[81]

Interaction of NO with hydrogen adatoms on Au(321) was also studied using DFT calculations.[276] The presence of hydrogen greatly reduced the dissociation barrier of NO on the surface. The kinetically most favorable route was the one producing nitrogen adatoms and water, (i.e., NO* + 2H* → N* + H$_2$O*) via the NOH* intermediate. This reaction was exothermic (1.1 eV), and the energy barriers for the separate NO* + H* → NOH* and NOH* + H* → N* + H$_2$O* reactions were 0.5 eV.[276]

4.6. Selective Oxidation of Ammonia and Amines

Selective catalytic oxidation of ammonia to nitrogen and water is potentially an ideal technology for removing ammonia from oxygen-containing waste gases, thus selectively avoiding the conversion of nitrogen into its oxides. Pt and Ir are the most active catalysts for NH$_3$ oxidation, but they produce significant amounts of nitrogen oxides. However, the selectivity of the catalytic oxidation of ammonia to N$_2$ or to NO on Au(111) was controllable, to some extent, by the amount of surface-bound oxygen.[200] N$_2$ recombination was hindered by a barrier of 0.95 eV, whereas that of NO was 1.03 eV.[200,277] For Au(111) with low oxygen coverages, ammonia selectively decomposed to form water and N$_2$ without any trace of nitrogen oxides (Figure 21).[200] Abstraction of hydrogen from ammonia via the high basic character of O atoms was the initial step in the surface decomposition of NH$_3$.[200,277,278] The formed hydroxyl was also a

stripping agent for NH$_x$ dehydrogenation.[277] Atomic oxygen or hydroxyl-assisted dehydrogenation steps had lower barriers than recombination reactions.

As derivatives of ammonia, amines can be selectively oxidized to the associated nitriles and aldehydes dependent on oxygen coverage.[202] For example, at low oxygen coverage (i.e., θ_O < 0.5 ML) propylamine initially underwent N−H bond breaking to produce propionitrile and water, while the formation of propionitrile, propaldehyde, water, CO, CO$_2$, and N$_2$O was observed at higher oxygen coverages.[202]

Weigelt et al. observed a condensation reaction via covalent interlinking between a dialdehyde and octylamine coadsorbed on Au(111) employing STM.[279] The self-assembled structures of formed diimine were visualized, and the reaction barrier was theoretically estimated to be ~1.2 eV.[279]

4.7. Other Reactions

Rettner and Auerbach studied the reaction dynamics of H atoms with Cl chemisorbed (via Cl$_2$ decomposition at 400 K) on Au(111).[280,281] Employing molecular beam time-of-flight methods with quantum-state-specific detection, they resolved angular and velocity distributions of the HCl product as well as its rotational and vibrational state distributions and thus revealed the concurrence of two dynamically distinct mechanisms (Eley−Rideal and Langmuir−Hinshelwood) during the reaction.[280] The formed HCl via the Eley−Rideal mechanism leaves the surface with a high kinetic energy in a narrow angular distribution that displays a "memory" of the direction and energy of the incident hydrogen atoms. HCl molecules produced through the Langmuir−Hinshelwood mechanism have a near-thermal energy distribution and an angular distribution that is close to that of a cosine function.[280,281]

Outka and Madix explored the oxidation of acetylene adsorbed on oxygen-precovered (θ_O = 0.6 ML) Au(110). Temperature-programmed reaction spectroscopy (TPRS) experiments yielded water (205 K) and carbon dioxide (525 K) as reaction products.[96] Adsorbed acetylene was dehydrogenated in the presence of oxygen to form water, which readily desorbed. Subsequently, the carbon left behind on the surface from further reacted with atomic oxygen at higher temperatures.[96] In a related study, no oxidation reaction occurred when ethylene was adsorbed on the same surface.[96]

Formaldehyde also reacts with atomic oxygen-covered Au-(110). Oxidative products of H$_2$O at 215 K, H$_2$ at 230 K, and CO$_2$, H$_2$O, and HCOOH at 340 K were observed.[97] Another

3007

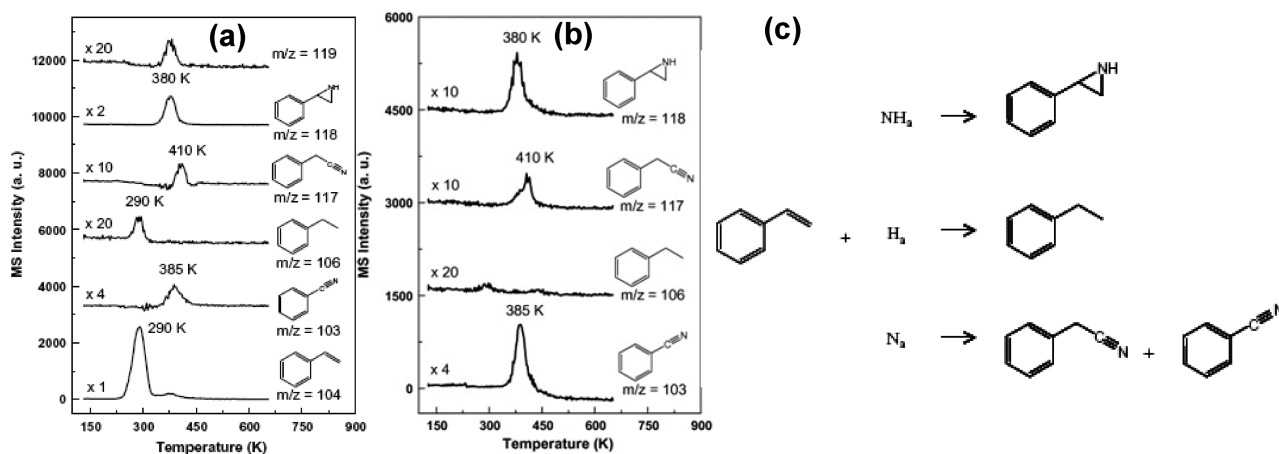dx.doi.org/10.1021/cr200041p | Chem. Rev. 2012, 112, 2987−3054

Figure 22. TPD spectra of styrene on (a) NH_x (predominant) and (b) N_a (predominant) covered Au(111). The surface was prepared by adsorption of NH_3 at 110 K followed by electron bombardment (100 eV) with a total exposure of 1.4×10^{11} electrons/cm^2. The sample in (b) was subsequently heated to 300 K to remove part of adsorbed NH_x. The styrene layer was condensed at 150 K prior to reaction. The average heating rate was 6 ± 1 K/s. (c) Schematic of styrene reactions on NH_x-covered Au(111). Reproduced with permission from ref 282. Copyright 2008 Elsevier.

CH_2O desorption feature evolved at 300 K, probably stabilized on the surface by adsorbed formate groups. The oxidative reaction of formic acid on Au(110) was also reported by the Madix group.[97] Upon heating the sample precovered with 0.25 ML of O atoms and 0.1 ML of formic acid at 100 K, desorption of formed water was observed at 200 K and the formate produced subsequently decomposed to CO_2, H_2O, and formic acid at 340 K with an activation energy of $\sim$84 kJ/mol.[97]

Deng et al. successfully designed experiments in which a nitrogen (N_a and NH_a) functional group could be inserted into styrene on Au(111).[282,283] They first developed a strategy for preparing surface-bound NH and/or atomic nitrogen by electron bombardment of condensed NH_3 at 110 K.[283] The relative concentrations of NH_a and N_a can be varied depending on the temperature used to prepare the surface. Reactions of styrene produced 2-phenylaziridine (380 K), ethylbenzene (290 K), benzonitrile (385 K), and benzyl nitrile (410 K). The formation of 2-phenylaziridine was favored when NH_a was the predominant species (Figure 22a), whereas nitrile (benzo- and benzyl-) formation was favorable when adsorbed N_a was present (Figure 22b). Therefore, the authors concluded that styrene aziridination, hydrogenation, and nitrilation were promoted with adsorbed NH, H, and N, respectively (Figure 22c).

The Friend group has recently reported on the acylation of dimethylamine on oxygen-precovered Au(111).[284] Dimethylamine was initially reacted with O/Au(111) at 120 K, and then formaldehyde was adsorbed on the surface. The selective coupling product, N,N-dimethylformamide [$(CH_3)_2NC(H){=}O$], evolved at $\sim$175 K into the gas phase upon heating the surface. A small amount of N-methylformamide [$H_3NHC(H)O$] was also observed at $\sim$350 K.[284] The selectivity for N,N-dimethylformamide from coupling decreased with the initial oxygen coverage employed. At low initial oxygen coverages (e.g., 0.15 ML), the selectivity approached 100%. As the initial oxygen coverage increased, the selectivity dropped (e.g., 30% at θ_O = 1 ML), where combustion reactions dominated.[284]

5. GOLD-SINGLE-CRYSTAL-BASED INVERSE MODEL CATALYSTS

In this section, we overview the use of low-dimensional nanostructures supported on single-crystal metal surfaces to model catalytically relevant reactions and processes. The so-called inverse model catalyst is a useful concept for studying the chemical properties of the oxide–metal phase boundary and for investigating the promoter effect that the minority oxide phase may exert on the reactivity of multicomponent metal–oxide catalysts.[285] An "inverse model catalyst" consists of a metal-single-crystal surface, which is decorated with a metal oxide (or other metal compounds such as sulfides, carbides, and nitrides) structure: it contains, therefore, the bifunctional site properties of the metal/oxide interface.[286] An important phenomenon affecting the structure and the catalytic performance of oxide-supported metals concerns the encapsulation of metal particles with a thin layer of the support material, which has been suggested to be at the basis of the so-called strong metal–support interaction effect (SMSI).[287−289] Such encapsulation is a more general phenomenon since it occurs frequently when the oxide phase is in a monolayer form. The SMSI effect is frequently used to describe the change in catalytic activity (e.g., favoring hydrogenation) observed when group VIII-B metals supported on reducible oxides (e.g., TiO_2, CeO_2, Fe_2O_3, and V_2O_5) are annealed in a reducing atmosphere.[290]

The interaction of metal oxides, including TiO_2 and CeO_2,[3,291−294] with Au nanoparticles has recently been the subject of intense study. For example, gold nanoparticles supported on metal oxides, particularly TiO_2, are highly active oxidation catalysts, and a pronounced particle size effect was observed (as will be discussed in detail in section 7).[3,291] This finding has caused considerable controversy regarding the underlying reason for the high activity of supported Au nanoparticles. A number of models have been proposed to explain the unusual catalytic properties of gold nanoclusters ranging from metal–support interactions to finite-size effects.[291] Gold-single-crystal-based inverse catalytic systems have attracted attention since they can be used as models for reactivity studies of isolated oxide nanoparticles [Au(111) undergoes surface reconstruction under UHV conditions and is ideally suited as an inert support for the oxidation of metals since neither O_2 nor NO_2 decomposes on the bare surface] and for understanding the metal–support interaction.[295] Gold-based inverse catalysts can also couple the special reactivity of the oxide nanoparticles to the reactivity of gold to produce highly
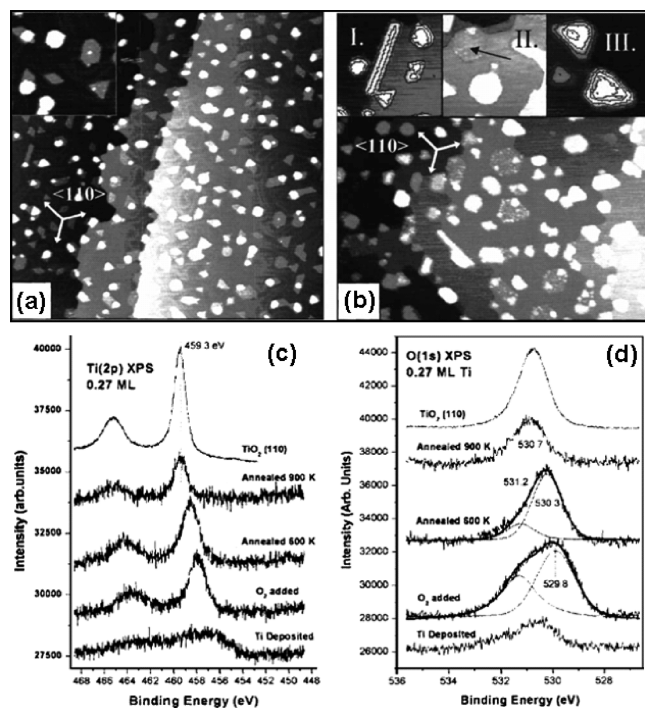
Figure 23. STM images of 2D and 3D titanium oxide nanocrystallites prepared by oxidation (O_2, 5×10^{-5} mbar $\times$ 200 s) of (a) 0.25 ML Ti and (b) 0.5 ML Ti, respectively, followed by annealing at 900 K (10 min). The crystallites are aligned with the substrate and have triangular or hexagonal shape. Additional features such as needlelike crystallites (inset I) and embedded hexagons (inset II) are observed for the higher Ti starting coverage (b). The contour lines, equally spaced by 0.5 nm, are used to visualize the crystallinity of the 3D Ti oxide particles. The images correspond to an area of (a) 160×160 nm^2, inset 32×32 nm^2, and (b) 200×200 nm^2, insets 50×50 nm^2 (I), 52×52 nm^2 (II), and 30×30 nm^2 (III). (c) Ti(2p) and (d) O(1s) XPS spectra collected from TiO$_2$(110), titanium-covered Au(111) surfaces before as well as after oxidation (6.6×10^{-5} mbar $O_2 \times$ 200 s) at 300 K, and subsequent annealing at different temperatures. All the spectra were collected at 300 K. Reproduced with permission from ref 296. Copyright 2005 American Institute of Physics.

active catalysts. One of the characteristics of this system is that oxygen vacancies on the oxide particle can be produced by annealing in vacuum at elevated temperatures or by direct reaction with CO or H$_2$. Supported metal oxides are also easier to reduce than the corresponding bulk phases of the oxides.[295] The reducibility of the oxide/Au(111) systems can be an important property since many bulk oxides exhibit a low reactivity and become chemically active only after the generation of oxygen vacancies.

5.1. TiO$_x$/Au(111) and CeO$_x$/Au(111)

5.1.1. Preparation and Surface Structure.
TiO$_x$ nanoparticles/films on Au(111) are typically formed via subsequent oxidation of titanium particles predeposited on the gold surface.[296,297] Biener et al. used physical-vapor deposition (PVD) of Ti at 300 K preparing regular arrays of titanium nanoparticles at the elbow sites of the herringbone reconstruction of Au(111).[296] After subsequent O$_2$ exposure, two- and three-dimensional titanium oxide nanocrystallites formed with either a triangular or a hexagonal shape during annealing in the temperature range from 600 to 900 K (Figure 23a and 23b). The
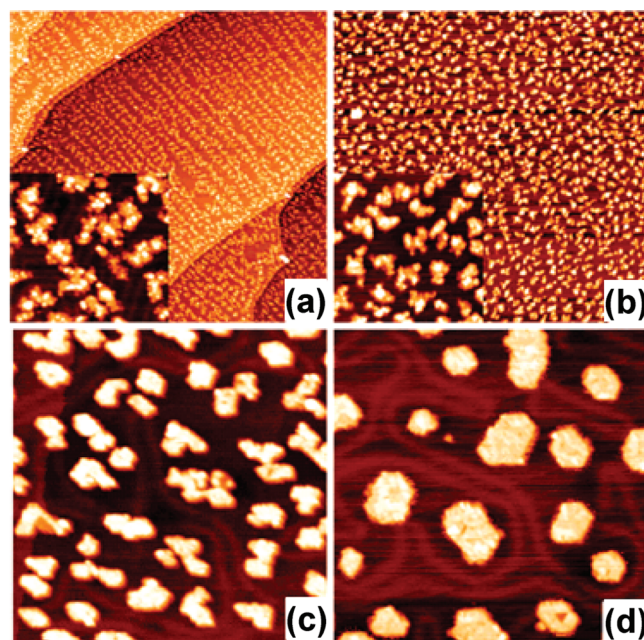
Figure 24. STM images of TiO$_2$ nanoparticles supported on Au(111): (a) prepared by depositing 0.1 ML Ti on a 30 ML thick H$_2$O layer on a Au surface at 90 K and then annealed to 300 K. The size of the TiO$_2$ particles is ~1 nm. The particles preferentially aggregate near the elbow sites of the Au herringbone reconstruction. (b) Prepared by depositing 0.1 ML of Ti onto a 30 ML thick NO$_2$ layer on Au(111) at 90 K and then annealed to 300 K, (c) 500 K, and (d) 700 K. The particle size in (b) is ~1 nm and in (d) is ~5 nm. TiO$_2$ particles prepared by NO$_2$ reactive layers are randomly distributed on the surfaces. The image size of (a) is 400×400 nm^2; the inset is 40×40 nm^2. The image size of (b) is 200×200 nm^2; the inset is 40×40 nm^2. The image sizes of (c) and (d) are 40×40 nm^2. Reproduced with permission from ref 299. Copyright 2005 American Chemical Society.

oxidation state of the titanium oxide nanoparticles varied with annealing temperature (Figure 23c and 23d).[296] Annealing to 900 K resulted in the formation of stoichiometric TiO$_2$ nanocrystals as evidenced by the Ti(2p) binding energies measured via X-ray photoelectron spectroscopy (XPS).[296]

Another method for preparation of compound nanoparticles (e.g., oxides, carbides, sulfides, and nitrides) is reactive-layer assisted deposition (RLAD). In this method, a multilayer of one reactant (e.g., H$_2$O, NO$_2$, and C$_2$H$_4$) is first adsorbed on a support, and the second reactant (i.e., metal atoms) is then deposited onto this layer. After the metal atoms react with the molecular multilayers, raising the substrate temperature causes any unreacted adsorbed molecules and volatile reaction products to desorb from the substrate surface; the final product compound is then left on the surface in the form of an ensemble of nanoparticles. Song et al. employed this method synthesizing TiO$_x$ nanoparticles on Au(111) in which Ti was initially deposited on a multilayer of H$_2$O (or NO$_2$) on a Au (111) substrate at 90 K (Figure 24).[298,299] In the case of a H$_2$O reactive layer, Ti was completely oxidized to stoichiometric TiO$_2$ at room temperature. Intermediate oxidation states such as TiO, Ti$_2$O$_3$, and Ti$_3$O$_5$ were found over the temperature range from 90 to 150 K.[299] At least three distinct morphologies of TiO$_2$ nanocrystallites (5$-$20 nm wide) were formed. The majority of the crystallites (about 70%) had a hexagonal geometry; the atomic structure of these nanocrystals was identified as rutile with a (100) face

3009

dx.doi.org/10.1021/cr200041p |*Chem. Rev.* 2012, 112, 2987–3054
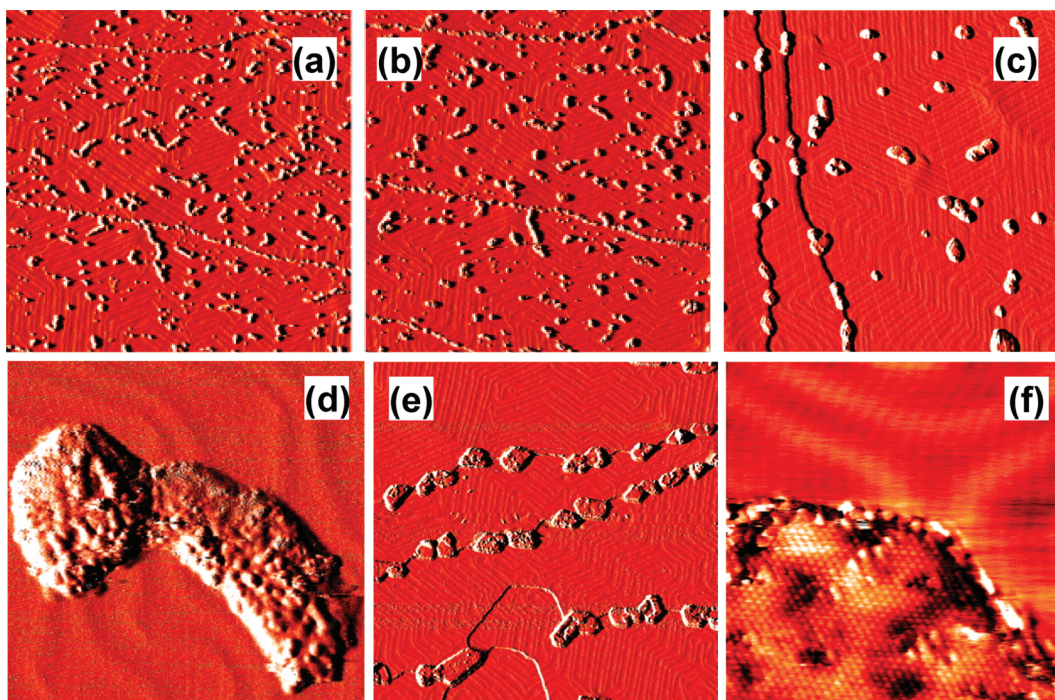
Figure 25. STM images (200 nm × 200 nm) of a Ce/H$_2$O/Au(111) system upon heating to (a) 300 K, (b) followed by subsequent reaction with 10 L of O$_2$. Reproduced with permission from ref 300. Copyright 2007 Elsiever. (c, d) STM images taken after oxidizing a Ce−Au(111) alloy in O$_2$ at 550 K and subsequent annealing to 690 K. The sizes of the images are (c) 200 nm × 200 nm and (d) 25 nm × 27 nm. (e, f) STM images acquired after depositing Ce in an atmosphere of 1.5 × 10^{-7} Torr of O$_2$ at 550 K followed by annealing to 700 K. The sizes of images are (e) 200 nm × 200 nm and (f) 15 nm × 15 nm. Reproduced with permission from ref 294. Copyright 2007 American Association for the Advancement of Science.

parallel to the substrate. The remainder of the crystallites had either a three-dimensional ridgelike morphology, also identified with rutile, or a structure consisting of nanosheets of octagon-shaped TiO$_2$.[298] For the Ti/NO$_2$/Au(111) system, upon reacting with the NO$_2$ reactive layer, Ti (0.1 ML) was fully oxidized to TiO$_2$, even at 90 K, which aggregated randomly on the surface (Figure 24b).[299] Unlike the H$_2$O-layer process, the Au herringbone structure was eliminated immediately after the NO$_2$ deposition because of a much stronger interaction of the NO$_2$ with the Au surface.[299] However, heat treatment of the sample resulted in the reappearance of the herringbone structure, but with a highly disordered state (Figure 24c and 24d).[299] Heat treatment also induced coalescence and ripening of the TiO$_2$ particles for both systems. Upon further annealing to 700 K, the TiO$_2$ particles gradually turned into a flat-crystalline structure,[299] similar to what was observed by Biener et al.[296] This crystalline structure is composed of a mixture of rutile and anatase phases, each having a variety of different exposed facets.[299]

CeO$_x$ supported on Au(111) has been intensively investigated due to the catalytic importance of CeO$_2$ for many reactions, particularly the water−gas shift (WGS) reaction. The RLAD technique has also been used to prepare CeO$_x$/Au(111) model systems.[300,301] Zhao et al. noticed cleavage of the O−H bond breaking and the formation of Ce(OH)$_x$ species upon the adsorption of water at 300 K on disordered Ce−Au(111) alloys.[300] Further thermal treatment to 500−600 K caused the decomposition or disproportionation of surface-bound OH groups to H$_2$ and H$_2$O as well as the formation of Ce$_2$O$_3$ islands on the gold substrate.[300] The intrinsic interactions between Ce and H$_2$O were further explored by inversely depositing Ce atoms on Au(111) precovered with water multilayers; the metal

adatoms were readily oxidized to Ce^{3+}.[300] Upon annealing of the sample to room temperature, finger-like islands of Ce(OH)$_x$ were formed on the gold substrate (Figure 25a). The hydroxyl groups dissociated at 500−600 K, leaving Ce$_2$O$_3$ particles on the surface. In both systems, Ce cannot be fully oxidized by water under UHV conditions. A complete Ce$_2$O$_3$ → CeO$_2$ transformation was seen upon reaction with O$_2$ and NO$_2$ (Figure 25b).[300,302] The formed ceria islands preferentially anchored on defect sites of the gold substrate, and their shape did not change substantially when going from Ce$_2$O$_3$ to CeO$_2$ or vice versa.[302]

The same group developed two different additional procedures to prepare ceria nanoparticles on Au(111).[294,300,302,303] In the first, alloys of Ce/Au(111) were exposed to O$_2$ (∼5 × 10^{-7} Torr) at 500 −700 K for 5−10 min.[300,302] The CeO$_2$ particles grew dispersed on the herringbone structure of Au(111) (Figure 25c) and had a rough three-dimensional structure that did not exhibit any particular face of ceria (Figure 25d).[294] In the second procedure, Ce was vapor deposited onto Au(111) under an atmosphere of O$_2$ (∼5 × 10^{-7} Torr) at 550 K and then heated to 700 K. The CeO$_2$ particles grew preferentially at the steps between the terraces on the Au(111) substrate (Figure 25e) and displayed regions with a CeO$_2$(111) orientation.[294] Groups or clusters of O vacancies were also resolved in STM images (Figure 25f).[294] This result is similar to what was found on bulk CeO$_x$(111).[304] High-resolution XPS showed that Au atoms did not incorporate into the ceria lattice.[300] Au(4f) spectra taken at photon energies of 240−380 eV, probing only two to three layers near the surface, confirmed the absence of the features expected for Au cations incorporated into ceria.[305]

5.1.2. Chemical Properties. Magkoev, employing reflection absorption infrared spectroscopy, showed that CO chemisorbed
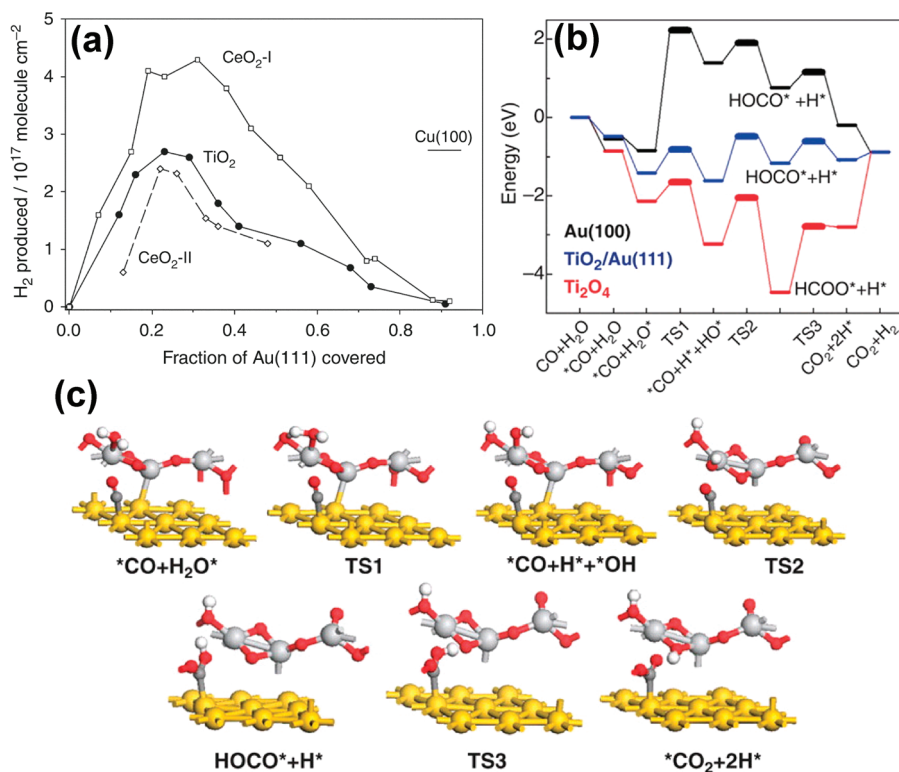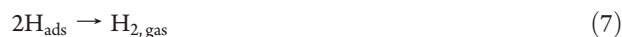
Figure 26. (a) Production of hydrogen during the WGS reaction on a Au(111) surface partially covered with ceria or titania. The ceria nanoparticles were prepared according to two different methodologies denoted as CeO_2–I [alloys of $CeAu_x$/Au(111) were exposed to O_2 (~5 × 10^{-7} Torr) at 500–700 K for 5–10 min] and CeO_2–II [Ce was vapor deposited onto Au(111) under an atmosphere of O_2 (~5 × 10^{-7} Torr) at 550 K and then heated to 700 K]. Each surface was exposed to a mixture of 20 Torr of CO and 10 Torr of H_2O at 573 K for 5 min. (b) Calculated reaction profile for the WGS on Au(100), a free Ti_2O_4 cluster, and TiO_2/Au(111) model catalysts. Transitions states are denoted as TS1, TS2, and TS3. (c) Optimized structures for the different steps of the WGS on TiO_2/Au(111). Large yellow spheres, Au; large gray spheres, Ti; small red spheres, O; small white spheres, H; small dark gray spheres, C. Adsorbed species are denoted by asterisks (*). Reproduced with permission from ref 294. Copyright 2007 American Association for the Advancement of Science.

on the TiO_2/Au perimeter interface, whereas only very weak adsorption was observed on the Au(111) and titania surfaces, respectively.[306] Madix, Friend, and co-workers investigated the reactivity of methanol on TiO_2/Au(111) and compared their results with those from bare TiO_2(110).[307] The TiO_2 nanoparticles on Au(111) produced methane from methanol, while the TiO_2(110) stoichiometric surface did not.[307] This difference was attributed to undercoordinated titanium cations present on facets of the nanoparticles, such as those found on {011}-faceted TiO_2(001) planes, which led to methane formation. The results suggested that the three-dimensional, local structure played a significant role in the reactivity of these nanoparticles toward methanol.[307] Rodriguez et al. found that TiO_2/Au(111) catalysts were highly reactive in the water–gas shift reaction (Figure 26a).[294] This high catalytic activity has been associated with the increase in the concentration of oxygen vacancies, as inferred from XPS measurements, which are most likely located near the oxide–metal phase boundaries. Water dissociated on oxygen vacancies of the TiO_x nanoparticles, and CO adsorbed on gold sites located nearby leading to subsequent reaction steps that took place at the metal–oxide interface (Figure 26b and 26c).[294] The intermediate that preceded the formation of CO_2 and H_2 in the WGS process was a HOCO species (eqs 2–7). CO_x (x = 1, 2) species were observed on the surface of the catalysts after the WGS, and they could be simple spectators when strongly bound to the oxide nanoparticles. In this inverse system, it was believed that

the moderate chemical activity of bulk gold[94,251] was coupled to that of a more reactive titanium oxide.[294]

$$CO_{gas} \rightarrow CO_{ads} \qquad (2)$$

$$H_2O_{gas} \rightarrow H_2O_{ads} \qquad (3)$$

$$H_2O_{ads} \rightarrow OH_{ads} + H_{ads} \qquad (4)$$

$$CO_{ads} + OH_{ads} \rightarrow HOCO_{ads} \qquad (5)$$

$$HOCO_{ads} \rightarrow CO_{2,gas} + H_{ads} \qquad (6)$$

$$2H_{ads} \rightarrow H_{2,gas} \qquad (7)$$

Zhao et al. showed that particles of CeO_2 dispersed on Au(111) did not interact with water at 300 K or higher temperatures and exhibited the same reactivity as the periodic CeO_2(111) surface.[300] On the other hand, the Ce_2O_3/Au(111) and CeO_x/Au(111) (x < 2) surfaces readily dissociated H_2O at 300–500 K due to the presence of oxygen vacancies. Water decomposed into OH groups on Ce_2O_3/Au(111) or CeO_x/Au(111) without completely oxidizing Ce3+ into Ce4+.[300] Annealing to temperatures over 500 K removed the hydroxyl groups, leaving behind CeO_x/Au(111) surfaces, suggesting that the activity of CeO_x/Au(111) for water dissociation could be

3011

dx.doi.org/10.1021/cr200041p |*Chem. Rev.* 2012, 112, 2987–3054

easily recovered.[300] This same group demonstrated that CeO_x/Au(111) showed excellent reactivity in the water–gas shift reaction and were comparable to those of good WGS catalysts such as Cu(111), Cu(100), or Cu nanoparticles dispersed on a ZnO(000$\bar{1}$) (Figure 26).[308] Several potential intermediates including formates (HCOO), carbonates (CO_3), and carboxylates (HOCO) were considered and tested experimentally for the reaction.[303] Adsorption of HCOOH and CO_2 was used to create HCOO and CO_3 on the CeO_x/Au(111) surface, respectively. HCOO had great stability with desorption temperatures up to 600 K, while CO_3 only survived on the surface up to 300 K.[303] Formed OH groups (from the dissociation of H_2O on oxygen vacancies) were stable on the surface up to 600 K and interacted with CO to yield weakly bound intermediates. When there is an abundance of Ce^{4+}, the OH concentration was diminished and the likely intermediates were carbonates. As the surface defects increased, the OH concentration grew and both carbonate and formate species were observed on the surface after dosing CO on H_2O/CeO_x/Au(111).[303]

5.2. MoO$_x$/Au(111)

Mo has three stable oxidation states: Mo^{6+}, Mo^{5+}, and Mo^{4+}. MoO_x nanostructures supported on Au(111) are typically prepared by oxidation of Mo nanoclusters using oxygen or NO_2. Nanoparticles of Mo are prepared on Au(111) generally by two methods: physical-vapor deposition of Mo and chemical-vapor deposition (CVD) through a molybdenum hexacarbonyl precursor [$Mo(CO)_6$]. While bulk MoO_3 is a bilayered material, these MoO_3 clusters exhibit a unique single-layer structure with Au replacing the other half of the bilayer. Epitaxy with the Au(111) substrate is achieved via straining the in-plane Mo–O bonds, which gives rise to electronic properties that are different from bulk MoO_3.[309]

Chang et al. prepared Mo nanoparticles on Au(111) by dissociation of $Mo(CO)_6$ molecules at 500 K.[310] At low coverage (e.g., 0.05 ML), these Mo nanoparticles exhibited very low reactivity toward O_2, and molybdenum oxides were not formed between 300 and 850 K; at higher coverage (e.g., 0.22 ML), O_2 reacted with Mo, partially transforming the metallic Mo to Mo^{4+}.[310,311] However, the Mo particles can be fully oxidized by NO_2 to form MoO_3 at 500 K, as evidenced by both Mo and O photoemission spectra. Formed Mo oxides consisted of two-dimensional islands covering a substantially larger fraction of the Au surface than the metallic Mo, suggesting that the morphology change starts with the diffusion of oxide clusters (ramified-cluster-diffusion mechanism[311]), followed by their breakdown to highly disordered two-dimensional islands of molecular MoO_3.[311] The MoO_3 clusters were stable on the surface below 600 K but disappeared (accompanied by a reduction of Mo^{6+} to Mo^{5+}) on the surface above 700 K.[310] The poor thermal stability of the MoO_x clusters could be due to their limited size or a consequence of weak interactions with the Au(111) substrate.

Friend and co-workers prepared a crystalline MoO_3 structure via repeated cycles of Mo deposition and oxidation, for example, alternate exposures of the Au(111) surface to 1 L of $Mo(CO)_6$ and 10 L NO_2 at 450 K followed by annealing to 600 K for 1 min after every 4 cycles of dosing for a total of 16 cycles.[309,312,313] The location of the deposited Mo clusters dictated the initial nucleation sites as well as the shape and orientation of the MoO_3 islands, which preferentially grew at the step edges.[312] The monolayer MoO_3 islands showed a well-ordered c(4 × 2) LEED pattern indicating the formation of a crystalline epitaxial Mo

oxide.[312,313] Deng later studied the selective reduction of these monolayer nanocrystals of MoO_3 on Au(111) upon annealing at 650 K and above and found that, similar to bulk MoO_3, the reduction of these single-layer MoO_3 nanocrystals proceeded via shear defect formation, which results from one-dimensional ordering and elimination of oxygen vacancies.[313] The oxidation state of Mo associated with these shear-plane defects was +5. The percentage of Mo^{5+} species increased as a function of annealing time, up to a maximum of 50% at 650 K. Further reduction toward Mo_{4+} was not observed.[313]

Nanocrystalline MoO_3 islands on Au(111) were also synthesized by PVD of Mo followed by oxidation using NO_2 at temperatures between 450 and 600 K.[313,314] The main difference between the PVD and CVD methods manifested in the spatial distribution of the Mo clusters on the Au(111) surface prior to oxidation: terrace (PVD) versus step-edge decoration (CVD). The morphology of the MoO_3 islands strongly depends on deposition and oxidation temperatures. For deposition temperatures at 525 K or above, NO_2 induced dealloying of a Mo–Au surface alloy formed during Mo deposition as observed via STM measurements.[314] This, in turn, led to the formation of embedded MoO_3 islands, which nucleated at the steps of Au vacancy islands. The oxidation temperature also affected the growth kinetics of MoO_3 islands: diffusion of MoO_3 precursor species is kinetically controlled at 450 K, which led to an irregular shape of MoO_3 islands with a high aspect ratio. With further annealing the islands changed in size and shape via Ostwald ripening.[314]

5.3. VO$_x$/Au(111)

The V–O phase diagram shows the existence of many stoichiometric compounds such as VO, V_2O_3, VO_2, and V_2O_5.[315] Similar to other oxides, the herringbone reconstruction of Au(111) provides suitable sites for stabilizing the oxide nuclei of vanadium oxides.[316]

The gold–gold distance on the Au(111) surface (2.88 Å) and the average lateral oxygen–oxygen distance on the V_2O_3(0001) surface (2.86 Å) are very close, which is a good base for epitaxial growth. The V_2O_3(0001) film (e.g., 100 Å) on Au(111) can be prepared by evaporation of metallic vanadium (e.g., 50 Å) in an oxygen atmosphere (1×10^{-7} mbar) followed by annealing at 600–700 K in 1×10^{-7} mbar of oxygen for 15 min and annealing in vacuum at 850 K for 10 min.[317–324] The crystalline nature of such films has been verified by the hexagonal superstructure visible in LEED and the well-ordered atomic arrays resolved in the STM (Figure 27a).[320]

The V_2O_3(0001) surface exposes a close-packed layer of vanadyl groups (they are stable on the surface up to temperatures of more than 1000 K),[325] which can form a bulk-truncated O or V termination at strongly oxidizing[320] or reducing conditions (Figure 27b).[326] As will be discussed later, the vanadyl termination is chemically inert due to the closed-shell electronic structure of the V=O groups, and thus surface defects are crucial for adsorption.[317] Two kinds of point defects were identified: vanadyl defects where a complete V=O group is missing and oxygen defects (vacancies) with only the vanadyl oxygen being detached from the V=O. Whereas the former is present naturally in the as-prepared film, the latter needs to be created via electron bombardment. Oxygen defects have been connected with the catalytic activity of the vanadia surface, for instance, in the oxidation of methanol.[327]

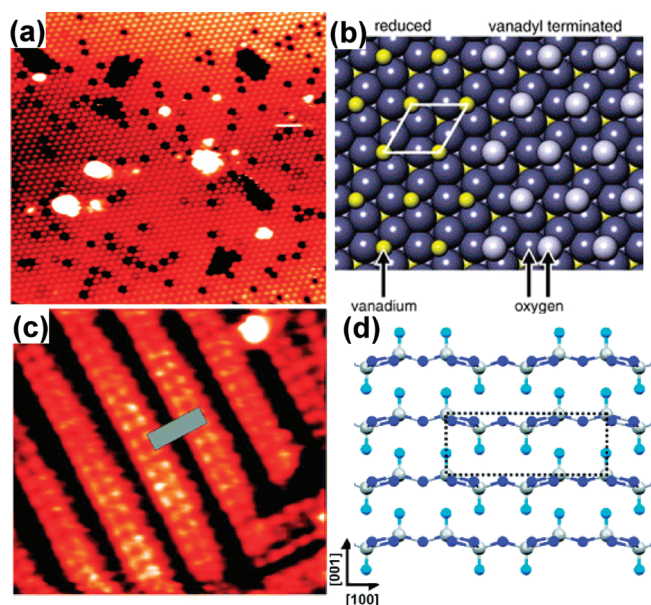Electron bombardment can also remove oxygen atoms of the vanadyl layer, leading to a surface terminated by vanadium

3012

dx.doi.org/10.1021/cr200041p |Chem. Rev. 2012, 112, 2987–3054

Figure 27. (a) STM image (20 nm × 20 nm) of a 10 nm $V_2O_3(0001)$ film grown on Au(111). Reproduced with permission from ref 321. Copyright 2006 Springer. (b) Models of structure of the reduced and the vanadyl-terminated surface. The surface unit cell (5.5 Å × 5.5 Å, angle α = 53.75°) is indicated. Reproduced with permission from ref 318. Copyright 2006 Elsevier. (c) STM image (5 nm × 2.8 nm) of a V_2O_5 (010) film formed by the oxidation of 5.2 ML V/Au(111) under 50 mbar of oxygen. The surface unit cell (3.6 Å × 6 Å) is indicated by a gray parallelogram. (d) Schematic representation of a V_2O_5 single crystal in its stacking along the (010) direction. Gray circles represent V atoms; light and dark blue circles represent O atoms. Reproduced with permission from ref 328. Copyright 2008 American Chemical Society.

atoms.[317] Adsorption of oxygen on reduced $V_2O_3(0001)$ occurs both dissociatively and molecularly. Formation of a negatively charged molecular oxygen species was observed at 90 K. Upon annealing, the oxygen species dissociated, reoxidizing the reduced surface by the formation of vanadyl species.[317] DFT calculations and RAIRS spectra suggested that the surface-bound oxygen species could be η^2-peroxo (O_2^{2-}) lying flat on surface, bonded to the surface vanadium atoms.[317,321]

Water interacts only weakly with the vanadyl-terminated $V_2O_3(0001)$/Au(111) surface and desorbs below room temperature. On the vanadium-terminated reduced surface, water partially dissociates and forms a layer of hydroxyl groups with a surface coverage of ~1.6 molecules per unit cell.[318] These hydroxyls recombinatively desorbed from the surface upon annealing at 600 K. No evidence of surface reoxidation was provided after water desorption.[318] Two factors could account for the different reactivities of the two surfaces: (1) the capping of the vanadium atoms by oxygen atoms on the vanadyl-terminated surface that hinders access to the vanadium atoms in contrast to the situation on the reduced surface, and (2) the lower oxidation state of the vanadium atoms on the reduced surface. Carbon monoxide, propane, and propylene molecules all molecularly adsorb on both oxidized and reduced $V_2O_3(0001)$/Au(111) surfaces; the binding of these molecules to the reduced V-terminated $V_2O_3(0001)$ surface is stronger than that to the oxidized surface.[319]

While the oxidation of vanadium under oxygen pressures in the 10^{-7}–10^{-6} mbar range results in the formation of V_2O_3 and

VO_2, Guimond et al. developed a method for the preparation of fully oxidized, well-ordered $V_2O_5(001)$ thin films on Au(111) by oxidizing physically evaporated vanadium with 50 mbar of oxygen at ~673 K for 10 min.[328,329] Small isolated $V_2O_5(001)$ crystallites started to grow after the completion of a two layer thick $V_6O_{13}(001)$-like interface (following the oxidation of about 1.56 ML V/Au(111)).[329] They had the tendency to grow into large crystallites and "dewet" the interface layer; however, growth by multiple steps of V deposition and oxidation led to flat films having a surface with a low density of point defects (Figure 27c and 27d). Unlike other vanadium oxides, O vacancies on V_2O_5 did not form randomly on the surface but rather appeared as pairs or rows, indicating a concerted reduction process. The films were stable up to 773 K and started sublimating above this temperature. Significant thermally induced reduction of the films occurred above 833 K.[328]

Oxidation of methanol was used as a probe reaction to study the reactivity of $V_2O_5(001)$/Au(111) (grown by three cycles of deposition of 6 Å of vanadium followed by oxidation).[330] TPD showed that fully oxidized, bulk-terminated surfaces were not reactive, whereas reduced surfaces produced formaldehyde (accompanied by water), which desorbed between 400 and 550 K. STM results indicated that methanol formed methoxy groups on vanadyl oxygen vacancies. The methoxy groups can be stabilized at room temperature only when the surface was free of hydroxyl groups since otherwise methoxy and hydroxyl groups may react to form methanol, which desorbed between 230 and 300 K.[330]

5.4. FeO$_x$/Au(111)

Iron- and iron-oxide-based catalysts are widely used in many important industrial processes, such as the synthesis of ammonia, Fischer–Tropsch synthesis, and gas-sensing applications. Iron has two oxidation states, Fe^{2+} and Fe^{3+}. It forms three natural oxides with different stoichiometries and crystal structures— FeO (wüstite), Fe_3O_4 (magnetite), and α-Fe_2O_3 (hematite), and two other artificially synthesized oxides (γ-Fe_2O_3 (maghemite) and ε-Fe_2O_3).[331] Catalytic and chemical properties of iron oxides depend on the oxidation states and crystal structures. This difference is evidenced, for instance, by the experimental observation that $Fe_3O_4(111)$ and α-$Fe_2O_3(0001)$ are capable of chemically adsorbing ethylbenzene and styrene, whereas FeO-(111) is inert to both molecules.[332]

Nanoparticles and thin films of iron oxides such as FeO(111), $Fe_3O_4(111)$, and α-$Fe_2O_3(0001)$ can be synthesized on Au-(111) depending on the growth conditions such as O_2 pressure, oxidation temperature, and Fe coverage.[332] For example, FeO was grown by exposing the Fe nanoparticles to molecular oxygen at 323 K, followed by annealing at 500–700 K. XPS results indicated that FeO was formed after room-temperature oxidation.[333,334] Two-dimensional, bilayer iron oxide particles with irregular hexagonal shape formed after annealing to 700 K (Figure 28a). FeO nanoparticles either resided on the terraces or embedded in the step edges. At Fe coverages above 1 ML, the oxides began to form a continuous film with small islands, which exhibited a moire structure. STM results suggested an overlayer lattice with a short periodicity of 3.3 Å modulated by a larger periodicity of approximately 35 Å.[333]

Changing the oxidizer leads to the formation of iron oxide with a different oxidation state. Deng and Matranga oxidized predeposited Fe particles on Au(111) using NO_2 (1×10^{-8} mbar), at elevated temperature (e.g., 327 to 450 K) followed by
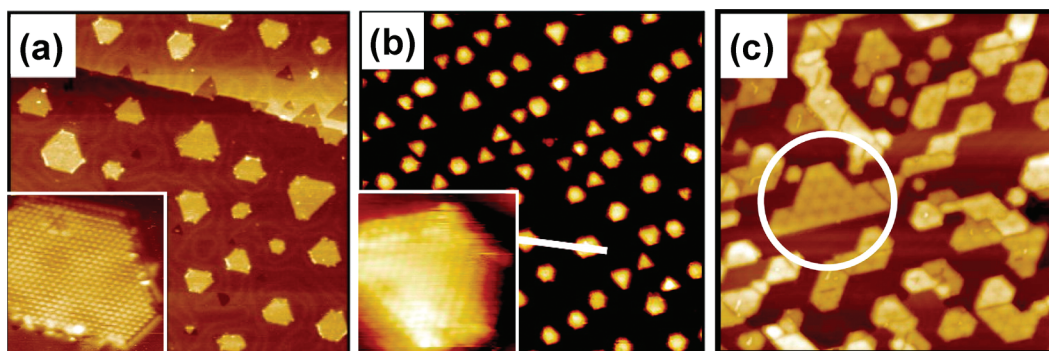
Figure 28. Room-temperature STM images ($100 \, \text{nm} \times 100 \, \text{nm}$) of (a) 0.3 ML FeO, (b) 0.25 ML α-Fe$_2$O$_3$, and (c) 1 ML Fe$_3$O$_4$ on Au(111). Iron oxide particles were prepared from Fe oxidation in (a) oxygen at 323 K and (b) NO$_2$ at an elevated temperature (from 327 to 450 K), followed by annealing in UHV at 700 K. Fe$_3$O$_4$ particles were synthesized from annealing α-Fe$_2$O$_3$ in UHV at 750 K for 10 min. The insets are high-resolution images ($8 \, \text{nm} \times 8 \, \text{nm}$) of (a) FeO and (b) α-Fe$_2$O$_3$ particles. The larger structure highlighted with a circle in (c) displays an ordered hexagonal superstructure. Reproduced with permission from refs (a) 333, (b) 335, and (c) 336. Copyright 2008 Elsevier, 2009 American Chemical Society, and 2010 Elsevier, respectively.

annealing in UHV at 700 K for 10 min, to form α-Fe$_2$O$_3$ nanoparticles, evidenced by the value of binding energy of the Fe $2p_{3/2}$ (710.9 eV) peak and an atomic ratio of O to Fe $\approx$ 1.5:1.[335] STM images revealed an ordered three-dimensional structure of Fe$_2$O$_3$ with an O-terminated (0001) surface on Au(111). The α-Fe$_2$O$_3$ particles adopted either a triangular or hexagonal shape and resided mostly on the terraces of the Au(111) surface (Figure 28b). The morphology of the α-Fe$_2$O$_3$ structures was dependent on the coverage, varying from nanoparticles at low coverage to islands at high coverage. These Fe$_2$O$_3$ structures had nearly identical heights of 5−6 Å at all coverages. showing a hexagonal unit cell with a lattice constant of $\sim$3 Å.[335]

Thermally induced reduction of the α-Fe$_2$O$_3$(0001) nanostructures to Fe$_3$O$_4$(111) occurred upon annealing in UHV to 750 K.[336] XPS measurements yielded the composition of the iron oxide, showing a broadened Fe $2p_{3/2}$ peak owing to the existence of both Fe^{2+} and Fe^{3+} species, and a decrease in atomic ratio of O and Fe (from 1.5 to 1.3). Fe$_3$O$_4$ appeared as nanoparticles at coverages below 1 ML (Figure 28c), and formed thin films on Au(111) at $\sim$2 ML of iron. Two ordered hexagonal superstructures with periodicities of $\sim$50 and $\sim$42 Å were observed on Fe$_3$O$_4$ particles; the 50 Å periodicity was the dominant superstructure observed on the continuous Fe$_3$O$_4$ thin films.[336] The Fe$_3$O$_4$ structures on Au(111) had a hexagonal unit cell with a $\sim$3 Å periodicity.

5.5. MS$_x$/Au(111) (M = Mo, Ti, and Ru)

5.5.1. MoS$_x$/Au(111). Molybdenum sulfide is the most widely used hydrodesulfurization (HDS) catalyst in the chemical and petroleum refining industries. MoS$_x$ can be prepared by chemical-vapor deposition of Mo via decomposition of Mo-(CO)$_6$ at elevated temperature (e.g., 400−500 K) followed by reaction with S$_2$ at 300 K.[337] MoS$_2$ nanoclusters can also be prepared by physical-vapor deposition of Mo in a background of H$_2$S (1×10^{-6} mbar) at 400 K, followed by annealing at 673 K for 15 min while maintaining the H$_2$S background pressure.[338]

Besenbacher and co-workers have systematically studied the atomic-scale structure, surface morphology, and catalytic properties of MoS$_2$ nanoclusters supported on Au(111). These clusters comprised a single S−Mo−S layer oriented with the (0001) facet in parallel with the substrate, and the morphology of the
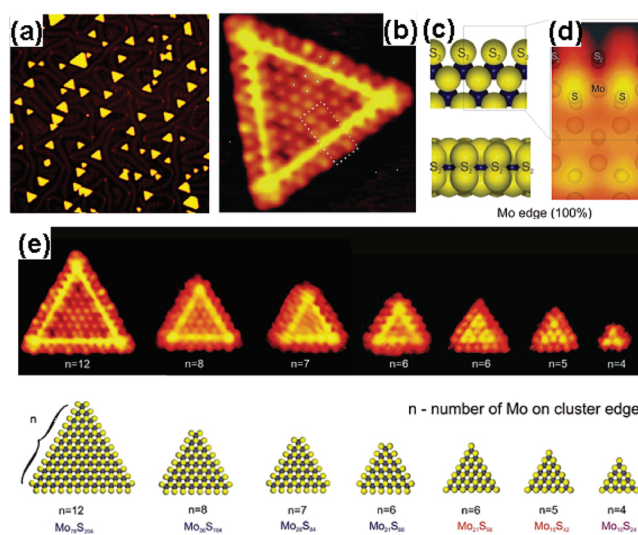
Figure 29. Single-layer MoS$_2$ nanoclusters on Au(111) grown by deposition of metallic Mo on the surface in an H$_2$S atmosphere and subsequent heating to 673 K. (a) STM image ($75 \, \text{nm} \times 72 \, \text{nm}$) showing the predominant triangular shape of MoS$_2$ nanocrystals. (b) Atom-resolved STM image ($4 \, \text{nm} \times 4 \, \text{nm}$) of a single-layer MoS$_2$ nanocluster. (c) Ball model (top view above and side view below) of the edge structure determined as the Mo edge covered with S$_2$ dimers. Mo atoms are shown in blue, and S atoms are yellow. (d) STM simulation of the edge structure based on DFT calculations. (e) STM images of individual clusters illustrating the structural progression of the MoS$_2$ nanocrystals as a function of size, where n denotes the number of Mo atoms on the cluster edge. The lower part shows ball models (top view) associated with the MoS$_2$ triangles observed by STM and the corresponding cluster composition Mo$_x$S$_y$. Reproduced with permission from ref 340. Copyright 2007 Elsevier.

MoS$_2$ nanocluster was triangular independent of the cluster size (Figure 29a).[339−341] The protrusions on the basal plane of the cluster reflected hexagonally arranged S atoms in the topmost layer of MoS$_2$ (Figure 29b). The protrusions at the edges were, however, out of registry with the S protrusions at the basal plane; a characteristic and pronounced bright brim with high electron state density extended along the cluster edge.[342] Both the bright brim and the apparent shifted registry of the edge protrusions can

be traced back to the presence of two distinct one-dimensional electronic edge states on the fully sulfided Mo edges (Figure 29b). DFT calculations regarding the nature of the edge structures[342,343] indicated that only the (100) edges of Mo with a full coverage of sulfur (forming S_2 dimers on the edge) were energetically stable, and STM simulations were consistent with experimental results (Figure 29c and 29d).

Besenbacher and his group also reported an interesting structural size effect on MoS_2 nanoclusters.[340,344] The clusters with an even number of Mo atoms (n = 6, 8, 10, 12, ...) on the edge are more stable, likely due to the formation of a super-structure involving pairing of S_2 dimers, as seen in STM images as alternating bright—dark patterns of the edge protrusions (Figure 29a,e).[344] Figure 29e shows atom-resolved STM images of seven clusters with different size. Notably, for clusters with $n \leq 6$ the authors observed a change in edge structure and brighter appearance of the interior of the cluster, which are likely caused by a structural rearrangement in response to a decrease in the S:Mo.[344] This phenomenon suggests that the bonding energy of sulfur and the tendency to form the catalytically active S vacancies along the cluster edges have a similar dependence on cluster size. Additionally, size-dependent reactivity patterns for MoS_2 nanocrystals should be observed through appropriately tuning the size of the nanoclusters.[340]

It should be mentioned that the electronic edge state is metallic in nature, whereas bulk MoS_2 is a semiconductor with a band gap of 1.2 eV.[341] The fully S-saturated Mo edges (shown in Figure 29c) have been considered the active sites for HDS[345,346] and the hydrogen evolution reaction.[347] They were rather different from that originally assumed, so-called S vacancies on the edges of the clusters as the only type of active site.[345] The evidence was provided via selectively adsorbing thiophene (C_4H_4S) molecules[337] and hydrogen on the MoS_2 clusters, and several bean-like features appeared adjacent to the edges.[345,346] These structures were thiophene-related reaction intermediates originated from partial hydrogenation on the metallic brims. DFT calculations indicated that these reaction intermediates were cis-but-2-ene-thiolates (C_4H_7S-) coordinated through the terminal S atom to the metallic brim, which were formed by a sequential hydrogenation of one of the double bonds in thiophene followed by C—S bond cleavage.[345]

Smaller MoS_x nanoclusters have also been synthesized via mass-selected cluster deposition using a molybdenum target and a sputtering gas of H_2S in Ar.[348] White and co-workers elegantly prepared and characterized Mo_4S_6 clusters supported on Au-(111).[349] These clusters bind strongly to the surface (three times more strongly with the Au(111) than with Mo_6S_8[350]) via three Au—S—Au bridge bonds that slightly distort the cluster geometry but leave the cluster framework intact. Auger spectroscopy and ^{13}CO thermal desorption demonstrated that Mo_4S_6 clusters behaved independently up to coverages of ∼0.15 ML, while at higher coverages, cluster crowding or island formation resulted in no net increase in Mo-atom adsorption sites.[349] CO preferentially binds on the Mo-atom top site (with a binding energy of 0.7 eV) compared to the side sites. In contrast to CO, NH_3 did not adsorb on the clusters at 85 K.[349] This difference suggests the role of Au(111) in modifying the electronic structure and chemical behavior of the supported cluster. The Mo_4S_6 clusters on Au(111) are stable up to 500 K as indicated by CO uptake measurements, which were consistent with diffusion of intact clusters along the Au surface and the formation of 2D islands.[349] Due to the unique stoichiometry of the Mo_4S_6 clusters, aggregates formed by cluster diffusion could exhibit distinctly different
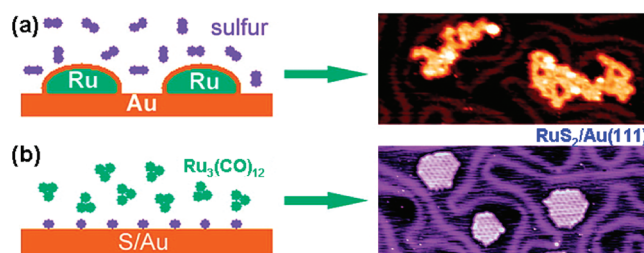

Figure 30. Schematic preventatives of effect of preparation method on surface morphology of Ru_2S nanostructures on Au(111). Reproduced with permission from ref 356. Copyright 2004 American Chemical Society.

chemical behavior compared to MoS_2 nanoclusters or amorphous thin films.

5.5.2. TiS$_2$/Au(111). TiS_2 is a semiconductor with a small band gap and a promising candidate for electronic applications for its two-dimensional electronic structure.[351] The structure of bulk TiS_2 is hcp layers of S atoms with Ti octahedral sites between every other pair of S layers. The lattice constant of the hexagonal unit cell of bulk TiS_2 is 3.45 Å.

TiS_2 has been prepared by conventional CVD or plasma-assisted CVD using $TiCl_4$ and S-containing species (e.g., H_2S and thiols) as precursors. The formed films are, however, typically in an amorphous state and contaminated with carbon and oxygen.[352,353] Remarkably, Biener et al. prepared single-layer, triangular TiS_2 nanocrystallites (similar to MoS_2 nanostructures) on Au(111) by physical-vapor deposition of Ti onto two-dimensional AuS islands followed by subsequent annealing (670—800 K). The well-ordered AuS overlayers (with a S coverage of ∼0.5 ML) were generated by exposing the clean Au(111) surface to SO_2 at a pressure of ∼1 mbar for 15 min at room temperature, followed by annealing at 450 K in UHV for 10 min.[354]

These TiS_2 nanocrystallites have a similar structure to bulk TiS_2. STM and LEED showed a Moire superlattice with a repeat distance of 17.3 Å resulting from the coincidence of five TiS_2 units with six Au atoms.[354] The triangular-shaped islands indicated a preference for one of the two possible edge terminations. The growth of the islands with a preferred orientation upon annealing was consistent with Ostwald ripening.[354]

5.5.3. RuS$_2$/Au(111). Ruthenium sulfide (RuS_2) exhibits the highest catalytic activity for HDS processes among all the transition metal sulfides,[355] making it a promising candidate to replace the current MoS_2-based catalyst in some reactions to meet new and more stringent refinery requirements. Ruthenium sulfide has a pyrite-type cubic structure, where sulfur exists in S_2 discrete units with S—S distances close to an S—S single bond. The RuS_2 single crystal cleaves easily along the (100) plane in an ideal bulk-terminated surface that is unreconstructed and very stable. In contrast, the hexagonal (111) plane is the polar and less stable surface that may exist in several different stoichiometries (e.g., sulfur vacancies).[356] Theoretical calculations have suggested that the (111) plane is responsible for its catalytic activity.[357]

Cai et al. investigated the effect of preparation method on the morphological structure of RuS_2.[356] Upon sulfidation of Ru nanoclusters (with a coverage of ∼0.06 ML) preadsorbed on Au(111) by chemical-vapor deposition of $Ru_3(CO)_{12}$,[358] ruthenium sulfide was formed with small sizes (a diameter of about 1.3 nm, smaller than that of the original Ru nanoclusters) and only a small fraction of flat islands (Figure 30a).[356] This

phenomenon is probably due to the diffusion of ruthenium atoms into the gold lattice, leading to Ru atoms embedded in the gold substrate;[359] during sulfur adsorption, Ru segregated at the surface and reacted with S, producing mainly clustered RuS_2 islands. The sulfide clusters were not uniformly anchored at the elbow sites but sintered and formed islands confined in the fcc region on the Au surface.[356] Interestingly, when $Ru_3(CO)_{12}$ was deposited on a sulfur-modified gold substrate at elevated temperature, flat hexagonal islands of ruthenium sulfide were formed exclusively with a narrow size distribution centered at 30 nm^2 in terms of island area (Figure 30b). The flat islands were single-layer RuS_2 nanocrystals with a (111) surface termination that exhibited an ordered array of sulfur vacancies.

5.6. MoC_x/Au(111)

Transition metal carbides offer advantages of selectivity and resistance to poisoning over the parent metal, and for certain reactions their catalytic behavior approaches and even surpasses that of the group VIII noble metals.[360] Molydenum carbide is one of the most actively studied systems and is active for many reactions such as hydrocarbon conversion, ammonia synthesis, hydrodesulfurization, hydrodenitrogenation, and the water−gas shift reaction.[361,362]

The stoichiometry of bulk molybdenum carbide is Mo_2C, although the phase diagram exhibits a wide range of Mo/C stoichiometry, including MoC (1:1) phases with hexagonal (γ-MoC, η-MoC) and cubic (δ-MoC) structures.[363] Surfaces of the carbide can be carbon or metal terminated, and non-stoichiometric Mo/C ratios were observed on carburized Mo surfaces that exhibited reactivity strongly dependent on the surface composition and annealing temperature.[364,365]

The most common preparation method of molybdenum carbide surfaces is the thermal cracking of ethylene on a molybdenum metal surface at high temperatures.[363,366] However, Mo/Au(111) is less reactive toward most adsorbates, due to spontaneous encapsulation of Mo by Au atoms at temperatures above 300 K, making it impossible to carbide the Mo particles by exposure to simple carbon containing molecules (ethylene, butadiene) at temperatures below which the herringbone structure of the Au(111) substrate is stable (<800 K).[367] Fortunately, Horn et al. successfully generated MoC_x nanoparticles employing the RLAD method via Mo deposition onto a reactive multi-layer of ethylene, which was physisorbed on a Au(111) substrate at low temperatures (<100 K), followed by annealing to 700 K.[363] The resulting clusters had an average diameter of ~1.5 nm and, unlike Mo clusters deposited by PVD, aggregated in the fcc troughs located on either side of the elbows of the reconstructed Au(111) surface. An average Mo/C atomic ratio of 1.2 ± 0.3 was obtained for nanoparticles annealed above 600 K.[363]

The chemical reactivity of these MoC_x nanoparticles was probed via the decomposition of cyclohexene.[367] It was observed that gold encapsulated the MoC_x nanoparticles to some extent upon annealing; this encapsulation can be removed by ion sputtering at room temperature. Au-encapsulated MoC_x nanoparticles were also reactive for the partial dehydrogenation of cyclohexene at 320 K to produce benzene and molecular hydrogen.[367] The overall reactivity was low with only 0.04 ML of cyclohexene undergoing dehydrogenation, whereas the selectivity to benzene was above 95%. The high selectivity originated from Au atoms blocking high reactivity sites on the MoC_x clusters that are otherwise responsible for complete cyclohexene dissociation. Comparatively, MoC_x nanoparticles without Au

encapsulation possessed a higher reactivity with ~0.67 ML of cyclohexene reacting with the surface, but partial dehydrogenation to benzene was only a minor reaction pathway (6%). Most of the cyclohexene either decomposed completely to form surface carbon (35%) and hydrogen or was hydrogenated to cyclohexane (20%).[367]

6. GOLD-BASED BIMETALLIC SYSTEMS

Alloys or bimetallic components have been widely used as heterogeneous catalysts via the addition of a second metal to improve activity and/or selectivity.[368] The complex interplay between elemental constituents that leads to superior catalytic performance has been discussed in terms of ligand and ensemble effects.[369,370] Ligand effects refer to the change in catalytic properties due to electronic interactions between the two elements of a bimetallic alloy. Ensemble effects refer to the spatial distribution of atomic sites that host reactants. Some reactions that require larger ensembles of reactive atoms to catalyze the transformation are halted when the active atom is monodispersed throughout an inert lattice.

Au(111) represents a unique substrate due to the "herringbone" reconstruction (namely, 22 × $\sqrt{3}$ reconstruction). The periodic arrangement of elbows and ridges caused by changes in surface domain orientation induces a long-range order in the reconstructed surface, which often acts as preferential nucleation sites for deposited atoms. Island growth near the elbows of the Au(111) reconstruction has been observed in the deposition of metals such as Pd, Ni, Co, Pt, Fe, V, Mo, Ru, and Ti, but not of the other metals such as Al, Cu, and Ag.[371] The preferential nucleation at elbows of the Au(111) reconstruction is attributed to the higher surface energies and heats of sublimation of grown metals compared to gold,[371] which presents common features such as the position of nucleation sites and island faceting along the close-packed $\langle 1\bar{1}0 \rangle$ directions.[372] Since different gold-based bimetallic systems share many similarities regarding the growth mechanism and surface aggregation,[373] we choose Pd−Au as a representative, considering the increasing attention this system has attracted, to illustrate the various phases of nucleation and growth. Other bimetallic surfaces will also be reviewed individually, but an emphasis will be placed on surface properties and chemistry, from which a general picture could be drawn regarding the growth mechanism of admetals on gold surfaces.

6.1. Pd−Au

Pd−Au is known to form a nearly ideal, completely miscible alloy at all compositions.[374] It can effectively catalyze a number of reactions such as CO oxidation, vinyl acetate (VA) synthesis, cyclotrimerization of acetylene to benzene, selective oxidation of alcohols to aldehydes or ketones, oxidation of hydrogen to hydrogen peroxide or water, and hydrocarbon hydrogenation.[375,376]

The alloy of Pd−Au possesses the same number of valence electrons per atom. The phase diagram of the Au−Pd system has ordered $L1_2$ structures for Au_3Pd and $AuPd_3$ compositions, while for the equiatomic composition the structure has not been determined.[377]

6.1.1. Growth and Surface Structure. Several types of model Pd−Au alloys have been developed including: (1) bulk alloys with specific Pd/Au stoichiometries (e.g., PdAu and Pd_3Au), (2) thin film surface alloys prepared by the deposition of Pd onto a single crystal of Au or vise versa, and (3) Pd and Au thin films synthesized by their deposition onto a refractory metal substrate, for example, molybdenum single crystals. The latter
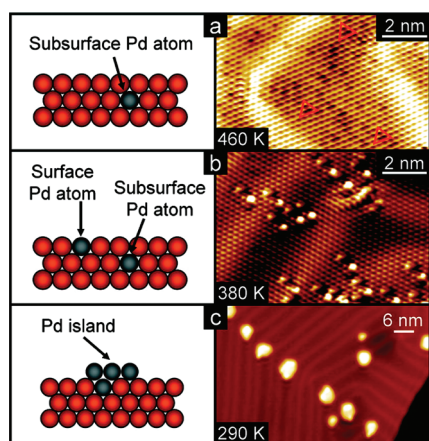
3016

dx.doi.org/10.1021/cr200041p | Chem. Rev. 2012, 112, 2987−3054

Figure 31. Temperature dependence of incorporation site of Pd in Au(111) (side-view schematic and corresponding STM image). (a) After a 0.005 ML Pd deposition of 460 K, the majority of the Pd atoms reside in the subsurface layer and appear in the STM image as three-lobed depressions (highlighted by red triangles). (b) At a lower sample temperature (380 K) during 0.01 ML Pd deposition, Pd atoms are incorporated in the surface and subsurface layers. Subsurface Pd atoms appear as three-lobed features, whereas surface Pd atoms are protrusions. (c) Upon deposition (0.005 ML) at 290 K, Pd atoms exchange place with Au atoms at the edge dislocations and then serve as nucleation centers for the growth of monolayer high islands on top of the Au surface that are a Pd-rich mixture of Pd and Au. Reproduced with permission from ref 379. Copyright 2010 American Chemical Society.

two systems offer considerable flexibility in varying the surface composition simply by varying the deposition and annealing temperature and thus are ideal methods for studying the structure and composition of bare alloy surfaces. A characteristic of the Pd–Au alloy is the significant enrichment of Au on the surface as a consequence of surface free energy minimization (i.e., the surface free energy for Au is 1.63 J/m^2, much lower than the corresponding value for Pd, 2.04 J/m^2).[378]

Pd, the lattice constant of which is about 4.8% smaller than that of Au, grows epitaxially on Au surfaces and forms flat, well-ordered overlayers. While alloy formation takes place for Pd deposition on Au(100) and Au(110), the structure of Pd overlayers on Au(111) is somewhat controversial.

The growth mechanism of evaporated Pd islands on the reconstructed Au(111) 22 × √3 herringbone surface has been studied by STM (Figure 31).[372,379] Atomically resolved STM images at the very early stages of growth at room temperature provide a direct observation of the mechanisms involved in preferential Pd island nucleation at the elbows of the herringbone structure of Au(111) (Figure 31c). At low Pd coverage the herringbone structure remains substantially unperturbed and isolated Pd atoms settled in hollow sites between Au atoms were near the elbows and the distortions of the reconstructed surface.[372,380] In the same regions, at extremely low coverage (0.003 ML) substituted Pd atoms in lattice sites of Au(111) were also observed, suggesting a place exchange mechanism. The substitution plays a fundamental role in the nucleation process, forming aggregation centers for incoming atoms and thus leading to the ordered growth of Pd islands on Au(111). Pd islands were grown in a close-packed arrangement with lattice parameters close to the interatomic distance between gold atoms in the fcc regions of the Au(111) surface.[372,379] Distortion of the herringbone structure for Pd coverages higher than 0.25 ML indicates

strong interaction between the growing islands and the topmost Au(111) layer.[372]

The degree of mixing depends on surface temperature (see Figure 31).[379] Pd deposition at a low temperature (e.g., 80–300 K) yields isolated Pd monomers in the surface layer, and room-temperature alloying resulted in the growth of arrays of Pd islands.[380–385] A maximum in the density of Pd monomers occurs at 0.5 ML Pd on Au(100) and at 1/3 ML Pd on Au(111) (coverages correspond to the Au(100)-c(2 × 2)-Pd and Au-(111)-(√3 × √3)R30°-Pd structures, respectively).[378,383] However, the authors did not observe such well-ordered surface structures, likely because Au and Pd are completely miscible over the entire range of compositions. The lower surface energy of Au favors its surface enrichment.[386] The isolated Pd atoms both in and under the Au surface had an electronic structure almost identical to gold, except for very small charge depletion from the Pd near the peak in the Au surface state. Deposition at a sample temperature of 380 K led to the majority of Pd atoms being alloyed substitutionally into the surface layer in the vicinity of the edge dislocations at the elbows of the herringbone reconstruction (Figure 31b). At high temperatures (>400 K), Pd diffused to more stable sites in the subsurface and bulk of Au (Figure 31a),[379] and a Pd$_2$Au alloy with a (√3 × √3)R30° structure was obtained at a surface temperature of 450 K.[381]

Koel et al. prepared Pd ultrathin films (up to 3 ML) on Au(111) by vapor deposition and studied the growth mechanism over the substrate temperature range 150–650 K.[387] The growth mode of vapor-deposited Pd films on Au(111) at 150 K was described well by an epitaxial layer-by-layer mechanism for the first few layers.[388–391] However, for Pd deposition at substrate temperatures of 300 K and above, low-energy ion scattering (LEIS) spectra using 1 keV Ne$^+$ ions indicated the formation of a surface alloy, with the extent of Au interdiffusion (alloying) increasing with temperature.[387] Annealing at 550 K restores a roughened, Pd overlayer to an atomically flat alloy surface.[385] For higher coverages, the electronic properties of Pd films approach those of macroscopic Pd(111).[392,393]

Several studies have been reported on the deposition of Pd over Au(110) (1 × 2).[394–397] The surface alloy with a (1 × 2) superstructure was formed via a mechanism whereby Pd adatoms fill in the missing rows of the reconstructed Au(110) surface and are subsequently covered by Au atoms. With further Pd deposition (e.g., above 2 ML), a nearly pure Pd layer was formed on top of the initially mixed Pd–Au interface, revealing a (1 × 1) pattern for up to 8 ML Pd.[395]

On the open Au(100) surface, the epitaxial growth of Pd adlayers has been studied by LEED, AES, and STM.[398,399] For the first 6 ML, Pd grew pseudomorphically on Au(100) with a lateral expansion of 4.5% with respect to bulk Pd. The first palladium layer started on both the terrace and gold islands that were formed from the lifting process of the reconstructed Au(100) surface and then proceeded two-dimensionally. The following palladium layer was found to grow mainly from the deposited palladium region on top of the gold islands. The shape of the gold island could be identified even after four palladium layers were deposited.[399] The strain in the expanded commensurate (1 × 1) Pd layers on Au(100) occurred with Pd coverages between 6 and 9 ML by formation of a compressed Pd film with respect to the Au(100) surface, and the compression increased continuously with thickness. For ~20 ML of Pd the lattice constant of the film is nearly identical to bulk Pd, and three-dimensional Pd islands develop at around 30 ML. Due to the
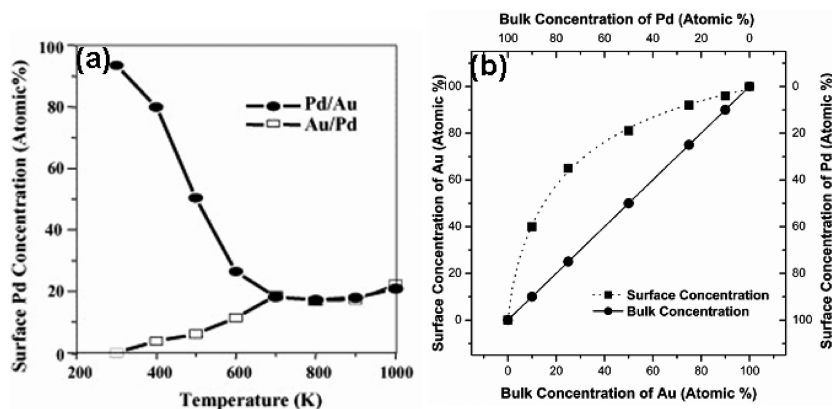
3017

dx.doi.org/10.1021/cr200041p | *Chem. Rev.* 2012, 112, 2987–3054

Figure 32. (a) Surface concentration of Au and Pd (measured by LEIS) of 5 ML Pd/5 ML Au/Mo(110) as a function of annealing temperature. The sample was annealed at each temperature for 20 min. Reproduced with permission from ref 378. Copyright 2006 Elsevier. (b) Surface concentration of various Pd−Au alloys on Mo(110) measured by LEIS compared to the corresponding bulk concentration. The sample was annealed at 800 K for 20 min. Reproduced with permission from ref 416. Copyright 2005 American Chemical Society.

formation of Pd−Au surface alloy, no superstructure was found for coverages from monolayer up to 30 ML Pd on Au(100).[398]

The growth and surface structure of gold particles/films on Pd surfaces have also been studied and characterized by photoelectron spectroscopy,[400−402] LEED,[385,403] LEIS,[404] and STM.[385,405] Taking Au/Pd(111), for example, gold grows in a layer-by-layer fashion (interdiffusion of gold into palladium is negligible) on Pd(111) at 300 K. Upon heating to above 600 K, gold starts to diffuse into the bulk to form a random substitutional surface alloy,[401,403,404,406−408] reflecting bulk miscibilities and the small lattice mismatch of the metal components. Weak repulsion between Au and Pd atoms may drive local ordering.[409] Unlike the Pd/Au(111) system, which forms an ordered ($\sqrt{3} \times \sqrt{3}$)$R30°$ surface alloy upon annealing, Au/Pd(111) shows no ordered LEED patterns except for the substrate (1×1) Bragg spots that are also observed during annealing.[406] STM images demonstrated that a flat alloy surface with no islands on the terraces can only be obtained by annealing at 925 K.[405] It is interesting to note that alloying (intermixing) occurs at a lower temperature than does surface smoothing.

For Au/Pd(110), the surface structure also depends on coverage and annealing temperature.[410−413] The structural transformations were accompanied by an intermixing of gold and palladium at temperatures above 500 K, which can be predicted by the bulk phase diagram.[414] Schmitz et al. found that, for Au coverages below 1.5 ML, the (1×1) overlayer structure was independent of the substrate temperature during gold deposition in the temperature range 130−800 K.[410] A transformation from (1×1) to (1×2) ($\theta_{Au} = 3$ ML) and (1×3) ($\theta_{Au} = 4$ ML) structures was observed upon increasing gold coverage and annealing the surface to temperatures above 300 K. Additionally, a dynamical LEED analysis was performed by Kaukasoina et al., who proposed the formation of a Au/Pd(110) (1×2) structure after annealing of a 2 ML gold film at 640 K.[415] In a medium-energy ion scattering (MEIS) study, the thinnest gold films with anisotropic strain were found to be 25 ML.[412] Three different growth behaviors were proposed by different researchers: a Stranski−Krastanov mode (layer plus island),[410] a Franck−van der Merwe mode (layer by layer),[412] and a multilayer growth mode (0.3−2.5 ML gold).[414]

The surface composition of the Pd−Au alloy was elegantly determined via LEIS by Goodman and co-workers as a function of annealing temperature (Figure 32a).[416] LEIS is inherently sensitive to the outermost layer and is used to correlate the relationship between the bulk and surface compositions.[417] They first confirmed that Pd−Au interdiffusion and/or alloying spontaneously occurred during Pd deposition onto Au films at room temperature (e.g., a 5 ML Pd/5 ML Au/Mo(110)), which yielded mainly flat and ⟨111⟩-like facets nearly independent of substrate.[418,419] Upon annealing, the surface concentration of Pd gradually decreased with an accompanying increase in the Au concentration. Heating the sample to different temperatures allows one to control composition of the alloy in a single experiment. This approach is important because the precise determination of surface coverage of gold or palladium as a function of the fraction of each element in the bulk of the alloy is crucial in understanding the relationship between composition and surface chemistry. The equilibrium surface composition (e.g., $Au_{0.8}Pd_{0.2}$) was reached at 700 K independent of the deposition sequences.[416] Additionally, STM images of the AuPd-(100) surface suggest that the gold and palladium atoms are not randomly distributed. The number of nearest-neighbor (bridge) palladium atoms was lower than expected for a random distribution, and the number of next-nearest neighbor sites was higher.[420] DFT and Monte Carlo simulations explained that this phenomenon could be due to net repulsive interaction between gold atoms in the alloy that leads to a larger proportion of isolated atoms than would be expected from a random distribution.[409] As will be discussed later, the surface composition of the alloy can be affected by the presence of adsorbates. A phase diagram of a surface alloy of Pd−Au supported on Mo(111) was consequently obtained by varying ratios of Pd/Au but maintaining a constant total thickness of 10 ML (Figure 32b).

6.1.2. Chemical Properties. The surface chemistry of the Pd−Au alloy is more complicated due to the coexistence of various active ensembles and changes of these ensembles (e.g., surface segregation) at different reaction conditions. These changes depend on a variety of factors such as reactant pressure, composition, and reaction temperature. The complexity of an alloy catalytic system could mean that the simple structure-insensitivity situation observed for single-metal catalysts may not be retained for the alloy. In other words, reaction kinetics with a bulk alloy may be very different from supported particles due to factors that might affect surface atomic composition and
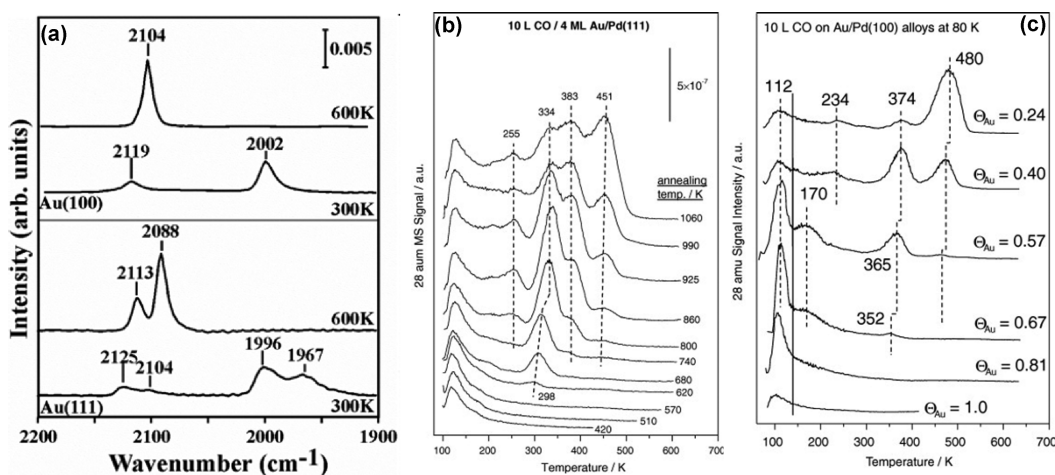
Figure 33. (a) RAIRS spectra for CO adsorption on Pd/Au(100) and Pd/Au(111) surfaces at 100 K showing the presence (300 K anneal) and absence (600 K anneal) of contiguous Pd sites. The Pd/Au(100) and Pd/Au(111) surfaces were prepared by depositing 4 ML of Pd at 100 K, then annealing to 300 and 600 K, respectively, for 10 min. The annealing temperatures are indicated on each spectrum. Reproduced with permission from ref 383. Copyright 2005 American Association for the Advancement of Science. TPD spectra obtained following an exposure of 10.0 L of CO collected at 28 amu on various (b) Au/Pd(111) (annealing to different temperatures yields different surface compositions) and (c) Au/Pd(100) alloys. A heating rate of 3.6 K/s was used. Reproduced with permission from refs (b) 401 and (c) 425. Copyright 2007 and 2010 Elsevier, respectively.

distribution, e.g., very different bulk compositions versus the surface composition for bulk alloys as well as particles.[421]

The temperature-programmed desorption experiment is one of the most useful methods for probing the surface chemistry. However, the interpretation of TPD results of adsorbents from bimetallic systems can be complicated by the continuous change in the surface composition due to alloying occurring during TPD experiments. For example, CO desorption continues until well above the onset of Pd diffusion in the absence of CO. Therefore, TPD measurements may not give a reliable estimate of the different types of a single adsorbent present on the surface and may give a lower bound on the desorption activation energy (since the desorption may be induced by Pd interdiffusion and loss of adsorption sites).

Adsorption and Reaction of CO. Carbon monoxide is very useful for probing the surface structures of alloys since CO stretching frequencies are very sensitive to the nature of the adsorption site. The utility of carbon monoxide as a probe for adsorption sites on gold–palladium alloys has been illustrated in many relevant investigations.[401,406,416,418,422–426]

Gold can modify the CO adsorption capability of Pd. Photoemission and HREELS results indicated that the binding of CO on the Pd monolayer on Au(111) was weaker compared to bulk Pd owing to a decrease in electron density near the Fermi level.[427,428] This was later confirmed by Sellidj and Koel, who showed that the binding energy of CO is slightly reduced at very low Pd coverages.[422] However, if the surface was fully covered with a Pd layer, adsorption of CO was similar to that on Pd(111).

CO RAIRS has been used to quantitatively determine the formation of surface Pd monomers for Pd/Au(100) and Pd/Au(111) (Figure 33a). Intense vibrational features of CO between 1900 and 2000 cm^{-1}, which correspond to CO adsorption on 2-fold bridging and/or 3-fold hollow sites, respectively, were observed for multilayer Pd on Au(100) and Au(111) deposited at or below room temperature.[381,383,387] Upon annealing Pd/Au(100) or Pd/Au(111) at 600 K, the CO features in RAIRS corresponding to bridging and/or 3-fold hollow sites disappear, while the intensity of the features corresponding to

atop sites between 2080 and 2125 cm^{-1} increases significantly. The results indicate that upon annealing contiguous surface Pd ensembles are eliminated, leaving exclusively isolated Pd sites or monomers, i.e., Au_4Pd on Au(100) and Au_6Pd on Au(111).[383] Additionally, due to the presence of gold atoms, the bimetallic PdAu(111) surface was found to have better resistance to sulfur poison than the Pd(111) for CO adsorption.[150]

Desorption features for CO on Au/Pd(111) occur at 120, 255, 334, 383, and 451 K (Figure 33b). The CO desorption peak at 120 K with a 2112 cm^{-1} RAIRS feature was assigned to CO adsorption on gold atop sites.[383,401] The 255 K feature was assigned to CO adsorbed on two adjacent atop sites (with a characteristic RAIRS peak at 2144 cm^{-1}), where one CO desorbed at low temperatures, allowing the second CO to move to a more stable site. The 334, 383, and 451 K features came from desorption on atop (2086–2089 cm^{-1} RAIRS), bridge (1911–1934 cm^{-1} RAIRS), and 3-fold hollow (<1900 cm^{-1} RAIRS) sites of Pd, respectively.[401] DFT calculations reveals that the adsorption site has the considerable influence on the heat of adsorption, while lateral interactions are less important.[424]

The Au/Pd(100) alloy is arguably the simplest alloy surface considering CO occupies only bridge sites on clean Pd(100).[429] CO binds on different sites on Au/Pd(100) alloys dependent upon the surface coverage (or fraction) of Au, and CO desorbs with features at 120, 220, 350, and 480 K (Figure 33c). Li et al. prepared gold–palladium alloys by initially depositing 4 ML of gold on Pd(100) and then by annealing to various temperatures in UHV to produce the desired Au/Pd atomic ratio.[425] The low-temperature features observed at lower palladium coverages are probably due to the presence of low-coordination gold sites that obscure the atop palladium site. Atop palladium sites were occupied as the gold coverage decreased, and CO desorbs at ~350 K, corresponding to a desorption activation energy of ~117 kJ/mol. The 480 K feature is from the CO desorption on palladium bridge sites only for palladium coverages greater than 0.5 ML, indicating that next-nearest neighbor sites are preferentially populated by palladium atoms.[425]

CO also induced a change in surface structure for Pd–Au alloys at certain conditions. At CO pressures lower than

3019

dx.doi.org/10.1021/cr200041p |*Chem. Rev.* 2012, 112, 2987–3054

$\sim 1 \times 10^{-3}$ Torr, Pd segregates to the AuPd(100) surface as evidenced by the enhanced CO RAIRS band intensity on isolated Pd sites with increasing CO pressure,[430] which is consistent with DFT results.[431] However, the extent of segregation was insufficient to form contiguous Pd sites on a well-annealed sample surface. At CO pressures higher than ~ 0.1 Torr, Pd segregation was enhanced such that contiguous Pd sites were formed.[430] The binding energy of CO on contiguous Pd sites is lower than that on isolated Pd sites. These contiguous Pd sites are active in dissociating O_2, providing atomic oxygen for the reaction.[430,432,433] Oxygen adatoms generated at contiguous Pd sites "spills over" to Au/isolated Pd sites to react with chemisorbed CO,[430,432] resulting in enhanced activity compared to Pd crystals.[434] This reaction pathway likely occurs at relatively low temperatures (<400 K) since the weak interaction between CO and Au precludes CO adsorption on Au sites at elevated temperatures.

NO reduction by CO was investigated over a AuPd(100) model catalyst at near atmospheric pressures by Gao and Goodman.[435] The alloy exhibits higher CO_2 formation rates and overall selectivity for N_2 production below ~ 550 K than does pure Pd, although the binding energy of NO on the alloy surface is substantially smaller (i.e., its dissociation tendency is much less). This behavior can be rationalized by the fact that the low CO/NO binding energies with the alloy surface provide a substantial population of empty ensembles for NO dissociation at relatively low temperatures. The reaction orders in CO and NO pressures are vastly different from Pd crystals due to the low-binding energies of CO and NO on the alloy surface. Low-pressure NO promotes the CO + O_2 reaction via gas-phase NO_2 formation; the latter dissociates to form $O_{(ads)}$ more efficiently than does O_2 below ~ 600 K. However, when the NO pressure exceeds a critical value, gas-phase NO_2 causes surface oxidation and thus inhibits CO_2 formation.[435]

Adsorption and Reaction of Hydrogen and Oxygen. Direct synthesis of hydrogen peroxide on supported Pd—Au nanoparticles has attracted considerable attention following the pioneering work by Hutchings and his group.[436] The Pd—Au-based catalysts are highly efficient near room temperature, and, as will be discussed in the next section, the supporting materials play a crucial role in most cases. Possible reaction schemes include a two-step mechanism starting from a superoxo precursor on supported particles and its subsequent reaction with two hydrogen atoms located at neighboring 3-fold positions.[375,437] A competitive reaction involving dioxygen dissociation leads to the nonselective formation of water.[438] The presence of surface gold atoms blocks this dissociation and increases the selectivity toward H_2O_2. Under UHV conditions, Weissman—Wenocur and Spicer investigated the oxidation of hydrogen to water on a $Pd_{0.8}Au_{0.2}(111)$ surface grown on Pd(111). The reaction probability of hydrogen with an adsorbed oxygen layer was lower on Pd—Au compared to Pd.[439] However, Lam et al. had earlier shown that the addition of Au to Pd can significantly enhance its overall catalytic activity for the oxidation of hydrogen with large oxygen excess, and they observed a nearly 2 orders of magnitude increase for $Pd_{0.3}Au_{0.7}$ compared with Pd.[440] This apparent discrepancy can be ascribed to the gold-induced lowering of the O—Pd binding energy through a ligand effect, which would favor hydrogen adsorption, a rate-limiting step only in the conditions of Lam et al.

Piccolo et al. studied the H_2—O_2 reaction over $Pd_{70}Au_{30}(111)$ at *elevated* pressures (0.1—10 Torr) and compared the results to

Pd(111) and Au(111).[441] The presence of palladium atoms promotes the dissociation of hydrogen and oxygen.[442] The activity for hydrogen oxidation followed the order: Pd(111) > $Pd_{70}Au_{30}(111) \gg$ Au(111). This can be explained by an observation that oxygen chemisorption is hindered by surface gold atoms on Pd—Au(111); thus, the majority of hydrogen adatoms are not readily oxidized and, consequently, are free to diffuse into the bulk of the material. For the near-stoichiometric ratio of hydrogen to oxygen, the reaction order with respect to oxygen is unity on both Pd(111) and PdAu(111). Under this condition, dissociative chemisorption of oxygen is the rate-limiting step, which follows a Langmuir—Hinshelwood mechanism.[441] Bulk dissolution of hydrogen strongly competes with its surface oxidation on both Pd(111) and $Pd_{70}Au_{30}(111)$; the latter absorbs more hydrogen than the former in the presence of oxygen. The decrease of the oxidation rate on Pd(111) through the reaction cycles is correlated with an increase in the amount of dissolved hydrogen, until stabilization of the kinetics. Diffusion of dissolved hydrogen atoms toward the surface determines the oxidation rate under low hydrogen pressure.[439,441]

Surface Chemistry Relevant to Synthesis of Vinyl Acetate. Acetoxylation of ethylene to vinyl acetate monomer ($CH_3COOH + C_2H_4 + H_2O \rightarrow CH_3COOCHCH_2 + H_2O$) over Pd—Au-based catalysts is an excellent example of how the addition of Au to Pd can greatly enhance overall catalytic activity of Pd, selectivity, and stability. Commercially, acetoxylation of ethylene to produce vinyl acetate has been carried out on Pd—Au bimetallic nanoparticles supported on silica promoted with potassium acetate (KOAc). Here I will discuss the surface chemistry of acetoxylation, beginning with the simplest phenomenon, namely, the interaction of a single species (e.g., acetic acid, ethylene, and vinyl acetate) with Pd—Au surfaces, then extend discussion to more complex issues such as the nature of the key reaction intermediates, the mechanism, and the active ensemble for reaction on the surface.

Tysoe and his group employing TPD and RAIRS systematically looked at the interaction of ethylene,[407] acetic acid,[408] and vinyl acetate[443] on Au/Pd(111) alloys formed by depositing 5 ML of gold on a Pd(111) surface and annealing to various temperatures in order to obtain a variety of surface compositions. All three molecules adsorb molecularly and desorb intact on Pd—Au surfaces with gold fractions greater than 0.5. Ethylene adsorbs primarily on gold sites for gold coverages greater than ~ 0.7, molecularly desorbing at 200—230 K with activation energies of ~ 50—57 kJ/mol. At gold coverages between ~ 0.5 and ~ 0.7, ethylene adsorbs on palladium sites in a π-bonded configuration, desorbing with an activation energy of between ~ 57 and 62 kJ/mol. Further reducing the gold coverage causes a nearly linear increase in the desorption energy of ethylene with increasing palladium content until it eventually reaches a value of ~ 76 kJ/mol reported for clean Pd(111).[407]

For mole fractions of gold greater than ~ 0.5, acetic acid adsorbs on Pd—Au surfaces molecularly and desorbs intact at ~ 200 K with an activation energy of ~ 52 kJ/mol. The molecule forms a structure of catemers, which depends on gold concentration.[408] When the relative gold coverage is less than ~ 0.33, acetic acid forms η^1-acetate species on the surface upon adsorption at 80 K and annealing to ~ 207 K. Further annealing leads to the decomposition of the η^1-acetate to eventually evolve hydrogen, water, and CO_x or the formation of η^2-acetate species (C—COO plane oriented perpendicularly to the surface).[408,444] The surface coverage of the formed η^2-acetate species increases
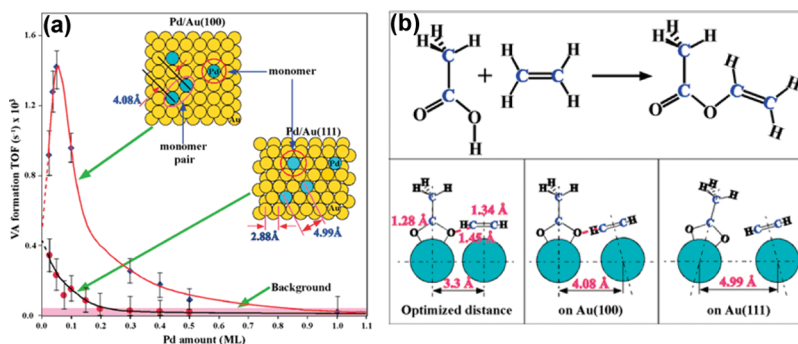
Figure 34. (a) Vinyl acetate formation rates (TOFs) as a function of Pd coverage on Au(100) and Au(111). The VA synthesis was carried out at 453 K, with acetic acid, ethylene, and O_2 pressures of 4, 8, and 2 Torr, respectively. The total reaction time was 3 h. The two insets show Pd monomers and monomer pairs on the Au(100) and Au(111) surfaces. (b) Schematic for VA synthesis from acetic acid and ethylene. The optimized distance between the two active centers for the coupling of surface ethylenic and acetate species to form VA is estimated to be 3.3 Å. With lateral displacement, coupling of an ethylenic and acetate species on a Pd monomer pair is possible on Au(100) but implausible on Au(111). Reproduced with permission from ref 383. Copyright 2005 American Association for the Advancement of Science.

with a decrease in gold concentration in the near-surface region.[408]

Vinyl acetate adsorbs weakly on gold sites on Pd—Au alloys and desorbs at ~210 K (with an activation energy of ~55 kJ/mol), independent of the particle size of the gold ensembles.[443] In contrast, alloying strongly influences the adsorption of VA on palladium. Vinyl acetate desorbs from isolated palladium sites on the alloy with an activation energy of ~70 kJ/mol, close to the value reported on pure Pd(111).[443] With increasing number of palladium dimers and larger ensembles in the alloy, the heat of adsorption of vinyl acetate increases. A maximum value of ~80 kJ/mol was reported at a gold coverage of ~0.5, but without significant thermal decomposition of the vinyl acetate. This result is attributed to the creation of a more distorted vinyl acetate where the acetate group is more remote from the surface due to the rehybridization of the vinyl group. As the gold coverage decreases to ~0.35 and lower, thermal decomposition products, such as methane (~360 K), acetaldehyde (410 K), and hydrogen (>400 K), were found similar to those on Pd(111).[443]

Chen and Goodman nicely draw a correlation between the active site and reactivity in vinyl acetate synthesis and provided a major insight into the mechanism of the promotional effect of gold in a Pd—Au alloy catalyst (Figure 34).[378,383,445] They found that the active site is made up of two noncontiguous, suitably spaced Pd monomers and the role of Au consists of isolating single Pd sites.[383] The pair of isolated Pd sites thus allows the coupling of critical surface species to vinyl acetate monomers and inhibiting byproduct formation (CO, CO_2, and surface carbon) through an ensemble effect.[383] Specifically, both ethylene and CO more weakly bind on a Pd—Au surface without continuous Pd sites compared to a Pd surface. Considering that CO is a reaction intermediate or byproduct in the reaction, the strong interaction of CO on continuous Pd sites may poison the active sites and thus decrease the activity.[446] Additionally, the surface species are different on continuous and isolated Pd. Ethylene and ethylidyne species with the di-σ bonding were formed on continuous Pd sites, which could further decompose into carbon species and thus block and poison the active sites.[378]

The reaction mechanism for vinyl acetate synthesis remains elusive; however, two pathways have generally been considered: (i) adsorption and subsequent activation of ethylene to form a vinyl species, which then couples with a coadsorbed acetate

species to form vinyl acetate,[447] and (ii) adsorbed ethylene reacts with an adsorbed acetate nucleophile to form an ethyl acetate-like intermediate, which then undergoes ß-H elimination to form vinyl acetate.[448] Both mechanisms assume that coupling of a surface ethylenic species and acetate to form vinyl acetate is the rate-limiting step.[383,449,450] A possible coupling reaction between a surface ethylenic and acetate species over a pair of Pd sites is illustrated in Figure 34b. According to the bond lengths of the parent molecular species, the optimum spacing between two active sites for the coupling reaction was estimated to be ~3.3 Å. On Au(100), the spacing between two neighboring Pd monomers is 4.08 Å (Figure 34a, inset), which is close for coupling of the adsorbed surface species. However, the nearest distance between two noncontiguous Pd monomers is 4.99 Å on the Au(111) surface (Figure 34a, inset), which accounts for a much lower rate of vinyl acetate formation compared with Pd/Au-(100).[383] The maximum VA formation rate on a pair of Pd monomers on Pd/Au(100) is almost two orders magnitude higher compared to an isolated Pd site.

Hydrogenation of Alkenes. The surface coverage and binding energy of hydrogen and alkenes control hydrogenation kinetics over Pd/Au bimetallic surfaces.[375,451,452] Piccolo et al. looked at the reactivity of $Pd_{70}Au_{30}(111)$ and $Pd_{70}Au_{30}(100)$ toward the gas-phase hydrogenation of 1,3-butadiene at elevated pressures (~5 Torr) in a static reactor and compared to those of Pd(111) and Au(111).[453] Both surfaces exhibited a (1×1) structure. Annealing the (111) and (110) surfaces to ~723 K led to gold concentrations of 75% and 85% in the top layers, respectively. The fresh Pd—Au(111) surface, highly enriched in gold, was weakly active, probably due to the decreased binding and coverage of hydrogen and/or butadiene molecules in the presence of gold. This finding is consistent with DFT results, indicating that, in increasing the Au surface composition, alkenes (e.g., ethylene) become more weakly bound.[451] The surface was highly activated upon cycling, ascribed to adsorption-induced modifications of the surface. At steady state, the butadiene-to-butenes conversion rate on the fresh model catalysts follows the order: Pd(111) > Pd—Au(110) > Pd—Au(111) > Au(111) ≈ 0. Gold atoms with low-coordination numbers have a positive effect on the reaction process, most likely through stronger adsorption of reactants. Unlike on Pd(111), the production rate of butane was fairly low and the selectivity to butenes reached ~100% on Pd—Au(111).
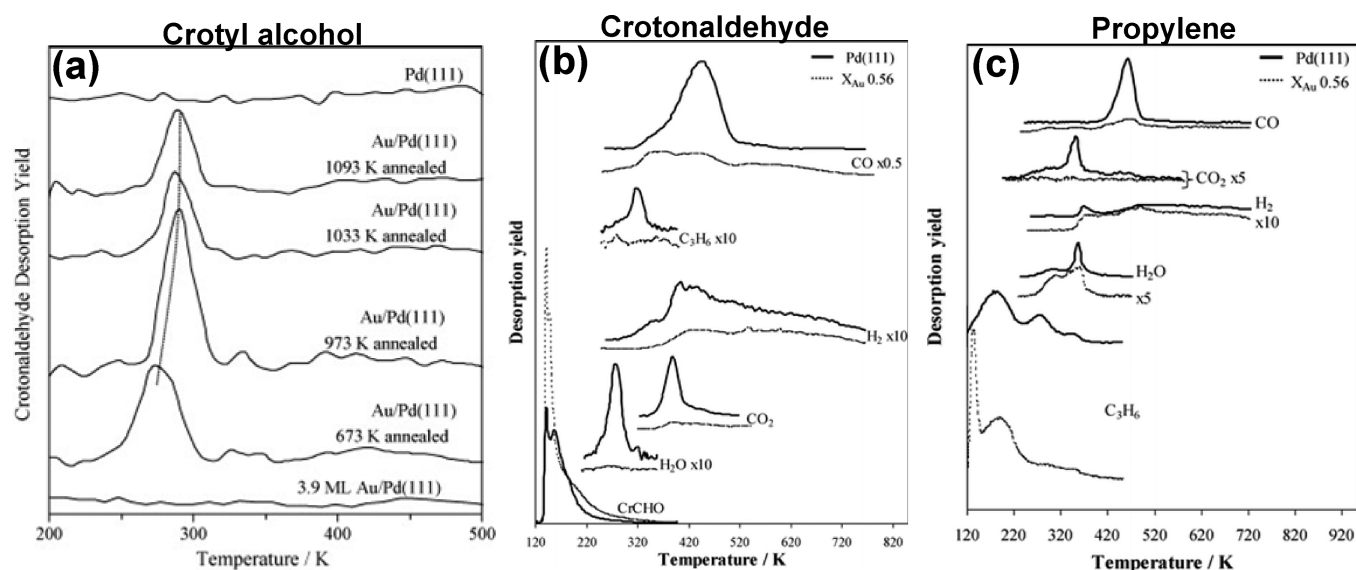
Figure 35. TPD spectra for (a) crotonaldehyde production from a saturated crotyl alcohol adlayer adsorbed on oxygen-precovered 3.9 ML Au/Pd(111) surface alloys at 100 K as a function of annealing temperature. Reproduced with permission from ref 456. Copyright 2009 Elsevier. (b) 3 L crotonaldehyde and (c) 3 L C_3H_6 adsorbed on oxygen-precovered Pd(111) and Au/Pd(111) (X_{Au} = 0.56, obtained upon 4 ML Au film annealed to 773 K) at 120 K. Reproduced with permission from ref 457. Copyright 2010 Royal Society of Chemistry (the PCCP Owner Societies).

Indeed, the presence of gold could facilitate desorption of butenes and thus hamper their hydrogenation to butane. Conversely, low-coordinated sites and surface defects promote butane formation.[453] The authors also noted that hydrogen diffusion toward the bulk Pd—Au surfaces plays a significant role in the reaction. Along with adsorption-induced segregation and/or surface restructuration, the formation of a surface hydride could be responsible for the excellent reactivity of Pd—Au surfaces. Unlike butenes, a high coverage of butadiene molecules sterically hinders hydrogen absorption. The reaction of hydrogen with adsorbed hydrocarbons competes with the absorption process.[453]

Selective Oxidation. Hutchings and co-workers recently discovered a range of bimetallic AuPd catalysts with exceptional activity and selectivity toward the oxidative dehydrogenation of a variety of alcohols and toluenes.[454,455] For example, these metal nanoparticles supported over titania yields up to 25-fold rate enhancements for alcohol aerobic oxidation under mild solvent-free conditions, while the introduction of Au also improves selectivities to aldehydes and ketones compared to monometallic Pd catalysts. Chemical mapping analysis employing high-resolution scanning transmission electron microscopy (STEM) indicated the active nanoparticles comprise a Pd-rich shell encapsulating a Au-rich core, and surface Au atoms could be vital in regulating the electronic structure and thus promoting the reaction over Pd surfaces.[454]

Inspired by this work, Lee et al. employing time-resolved XPS and TPD studied the effect of annealing temperature (leading to different surface compositions of Pd and Au) on the reactivity of selective oxidation of crotyl alcohol ($CH_3CHCHCH_2OH$) to crotonaldehyde (Figure 35a).[456] Crotyl alcohol reversibly chemisorbs over thick gold overlayers epitaxially grown on Pd(111) with 153 K multilayer and 183 K monolayer desorption states[456] and reaction products (e.g., aldehyde and alkene[457]). Gold-rich AuPd surface alloys possessed moderate activity for the oxidative dehydrogenation of crotyl alcohol to crotonaldehyde, which desorbs intact at room temperature with minimal competing

side-reactions. Comparatively, palladium-rich alloy surfaces convert 100% of a crotyl alcohol adlayer to crotonaldehyde, although nearly half of the formed aldehyde subsequently decarbonylates to produce gas-phase CO_x, hydrogen, and propene at 300—450 K (Figure 35b and 35c), leaving small amounts of residual carbon (≤30% of a monolayer). This is a contrast to the surface chemistry of Pd(111) for which only dehydration (butene and water) and decarbonylation (CO and propene) desorption products were observed.[456] The yield of crotonaldehyde increases with an increase in surface Pd content, reaching a maximum for the Au_2Pd_3 surface obtained after being annealed at 973 K (Figure 35a).

Other Reactions. The promotional effect of gold incorporation into Pd surfaces has also been demonstrated for ethyne cyclotrimerization to benzene.[385,406,458] The genesis of Pd_6Au ensembles reduced hydrocarbon decomposition and promoted desorption of benzene, which is consistent with analogous studies on dispersed AuPd colloids.[458] The similar enhancement phenomenon has also been observed for the reaction of propylene oxide and 2-butanol.[459] The surface chemistry of these molecules is strongly affected by the formation of a dilute Au/Pd(111) alloy (with a gold coverage of ~8%) as compared to the chemistry on pure Pd(111).[459] On the alloy surface, propylene oxide decomposes via a proposed oxametallacycle at ~190 K, which finally decomposes at ~250 K to yield adsorbed CO and ethylidyne species; on clean Pd(111), it desorbs without reacting. 2-Butanol completely thermally decomposes on the alloy at exposures below ~0.4 L to yield hydrogen and CO, while any additional adsorption produces 2-butanol by 2-butoxide rehydrogenation or 2-butanone via a β-hydride elimination reaction.[459] Interestingly, Gao et al. showed that propylene oxide does not adsorb strongly enantiospecifically on a 2-butanol-modified surface, and the extent of total decomposition of 2-butanol is not affected by the presence of propylene oxide. However, the reaction of the 2-butoxide species to form 2-butanone or 2-butanol is strongly enantioselective, where values of enantioselective excess of 100% toward the formation of
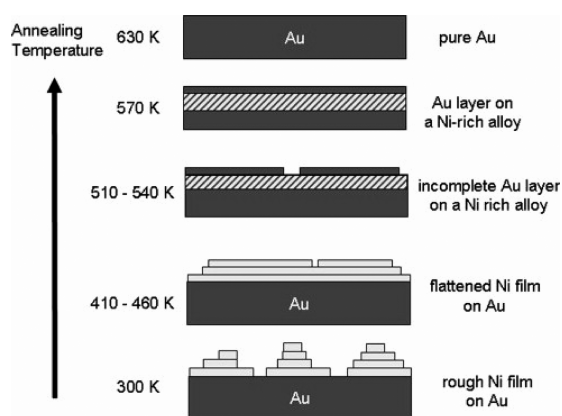
Figure 36. Diagrammatic summary of the effect of annealing an 8 ML Ni film on Au(111). Reproduced with permission from ref 472. Copyright 2010 Elsevier.

R-2-butanol when coadsorbed with R-propylene oxide are found. It is suggested that this is controlled by the initial enantioselective decomposition of 2-butanone, which leaves a surface enriched with the R-2-butoxide species.[459]

6.2. Ni–Au

The bulk Au/Ni phase diagram manifests a large miscibility gap,[460] which suggests no alloy formation at low temperature.[461−463] However, for both Au/Ni(111) and Au/Ni(110) systems, STM,[461,464] AES,[465] LEED,[462,465] LEIS,[462] and theoretical calculations[461,466,467] have confirmed that a surface alloy restricted to the outermost layer is energetically favorable. Both Au and Ni have fcc crystal structures; however, due to a 15.7% lattice mismatch (Au, 4.079 Å; Ni, 3.524 Å), formation of a pseudomorphic Au monolayer on Ni(111) is energetically unfavorable and considerable strain was likely produced at the interface. DFT calculations indicated that it is an activated endothermic process with an activation energy of 1.7 eV.[468] Indeed, Nielsen et al. found that, although Au atoms initially alloy into the Ni(110) surface, phase separation (e.g., dealloying) occurs for gold coverages larger than 0.4 ML, which is due to the surface stress induced by the substituted gold atoms.[464,469] Umezawa et al. reported that the growth of a (9×9) Au overlayer on Ni(111) occurs in two discrete modes, which strongly depend on the growth temperature during deposition.[462] This finding was supported by Jones et al.[470] and Zafeiratos et al.,[471] who concluded that the density of Au is substantially higher in the ultrathin film compared to bulk Au.

The initial growth of Ni forms 2D clusters at the elbows of the Au(111) herringbone reconstruction, which eventually leads to a pseudomorphic structure.[473,474] These clusters influence the growth of subsequent layers of Ni, causing a relatively rough morphology for Ni films (e.g., 8−13 ML).[475,476] Upon annealing, Au diffuses through the Ni films to the surface layer, which eventually generates a Au monolayer on a Ni-rich subsurface region. Complete loss of Ni into the bulk occurs following an anneal to higher temperatures (e.g., 630 K).[476] A diagrammatic representation of the annealing behavior of Ni on Au(111) is illustrated in Figure 36,[472] which was also supported by DFT calculations.[477]

For the reconstructed Au(110) (1×2) surface, submonolayer coverages (e.g., 0.25 ML) of Ni deposited between 130 and 180 K grow in the missing row.[463] After adsorption at 130 K, Ni was very evenly distributed over the surface, and no alloy was formed.

However, island-assisted alloying took place upon increasing the deposition temperature to 300 K.[478] Substitutional Ni atoms are between adislands in the top Au rows of the terrace.[478,479] An asymmetry in their lateral distribution with respect to adislands along the $[1\bar{1}0]$ direction was found, suggesting that these Ni atoms are incorporated during island ripening, when small clusters of adatoms, in a double row configuration, merge to form 2D adislands.[478,480]

Adsorbents can also induce reconstruction of Au−Ni surface. Vestergaard et al. showed that CO induces a phase separation of the surface alloy Au/Ni(111) at high pressures and observed the removal of Ni atoms from the surface layer upon CO exposure.[481,482] DFT calculations indicated that Au atoms bind the CO ~1 eV more weakly than the Ni atoms and that the thermodynamic driving force for the phase separation is the Au-induced compression of the CO overlayer with a resulting dipolar repulsion.[481] Holmblad et al. concluded from a TPD study that the binding energy of a CO molecule is reduced by ~0.3 eV/molecule as the Au concentration in the surface layer increases from 0 to 0.7 ML,[483] which is consistent with theoretical results.[468,484]

Au/Ni(111) has been reported by Lahr and Ceyer to catalyze low-temperature CO oxidation.[485] Through a combination of HREELS and molecular beam scattering, they showed that molecularly adsorbed oxygen is stabilized on the Au/Ni(111) surface alloy at 77 K, which is very reactive for the CO oxidation reaction at low temperature. The necessity of a molecularly adsorbed species, as opposed to gas-phase O_2, for reaction with CO was validated from the absence of reactivity upon exposure of the CO-covered surface alloy to O_2.[485] At an O_2 coverage below 0.5 ML, the reaction probability of CO with molecularly adsorbed O_2 was estimated to be between 0.5 and 1. Between 105 and 125 K, CO_2 production coincides with O_2 dissociation, suggesting a "hot atom" mechanism. Above 125 K, CO and O bound to Au react directly, resulting in CO_2 formation.[485] In an extended study, Knudsen et al. revealed increased low-temperature CO_2 formation upon addition of Au, which blocks active sites for the formation of carbonate.[486] In contrast to the model of molecularly adsorbed O_2 by Lahr et al., DFT calculations suggested that NiO_x surfaces accumulated upon saturation with O_2 play a central role in catalyzing CO oxidation at 100 K.[486]

Addition of gold into nickel decreases the catalytic reactivity. Besenbacher et al. showed that addition of gold to Ni(111) induced a decrease in dissociation activity of methane.[466] The initial sticking probability of methane on a Au/Ni(111) with 0.25 ML of gold decreased to ~10% of the sticking value of the bare Ni(111) surface.[483] DFT calculations demonstrated that the dissociation barrier of CH_4 on a Ni atom (the barrier to dissociation on a Ni(111) atom is ~100 kJ/mol) increased by 16 kJ/mol in the presence of a single Au neighbor.[406,487] Two neighboring gold atoms lead to a 38 kJ/mol increase of dissociation energy. Since the methane molecule interacts with the d states of nickel during dissociation, the loss of activity can be explained by a lowering of the d-band center when Ni is in contact with Au.[466] The gold-covered nickel surface also showed a reduced tendency to bind carbon stronger and form graphite (which accounts for the deactivation of catalyst). The same group further synthesized a conventional Au/Ni/MgAl$_2$O$_4$ catalyst (16 wt % Ni, 0.3 wt % Au) and obtained an enhanced durability compared to a pure Ni catalyst for steam reforming of methane.[466]

The adsorption of α-amino acids and α-hydroxy acids on Raney Ni or supported Ni catalysts has attracted consideration

3023

dx.doi.org/10.1021/cr200041p | Chem. Rev. 2012, 112, 2987−3054

attention for enantioselective catalysis, particularly for the hydrogenation of β-ketoesters.[472] In order to elucidate the effect of Ni alloying with Au on the selectivity of the reaction, Baddeley and co-workers looked at the reaction of tartaric acid (HOOCCHO-HCHOHCOOH)[488] and glutamic acid (HOOCCH$_2$CH$_2$CHN-H$_2$COOH)[472] on Au/Ni bimetallic surfaces. The adsorption of both species is dependent on surface composition and induces the surface segregation of Ni, resulting in active Ni-rich regions of the surface. Taking glutamic acid, for example, adsorption is facile and at 300 K on Ni-rich surfaces, which causes the formation of nickel pyroglutamate species via the dehydration and internal cyclization of glutamate. On the other hand, segregation of Ni to Au-rich bimetallic surfaces was observed upon adsorption of glutamic acid even at 300 K. This is probably due to the formation of nickel pyroglutamate on the surface. Segregation can be reversed by annealing the adsorbate-covered surface to 400 K, the onset temperature for decomposition/desorption of pyroglutamate species.[472]

6.3. Pt—Au

6.3.1. Growth and Surface Structure. Nahas et al. examined the morphology of Pt—Au(111) with low Pt coverages (0.02 ML—0.4 ML) and observed a competition between the ordered growth of nanodots and a random intermixing between Pt and Au via STM.[489] Pt deposition on the Au(111) surface at room temperature shows an ordered growth limited by the insertion of Pt atoms into the surface layer and the subsequent modification of the herringbone surface pattern.[489]

Relatively speaking, the growth mechanism of platinum films of gold surfaces is somewhat controversial. Matthews and Jesser first studied this system by depositing Pt thin films on Au(111) and Au(100) surfaces employing molecular beam epitaxy (MBE), and used ex situ transmission electron microscopy (TEM) to examine morphology of the films.[490] Growth at 313 and 573 K yielded identical results for both surfaces; no 3D nuclei were formed at any stage of growth, and the Pt films remained planar with misfit dislocations (with a spacing of ~25 nm) appearing at a critical thickness of ~1 nm. Accordingly, they suggested the Frank—van-der-Merwe mode (layer by layer) for Pt/Au growth.[490] In contrast, Sachtler et al. examined MBE growth of Pt on Au(100) using in situ LEED and AES and concluded the Volmer—Weber growth mode (island formation) for Pt/Au(100) growth at temperatures between 423 and 473 K.[491] Sugawara and Nittono found, consistent with Matthews and Jesser and at variance with Sachtler et al., that growth occurred via the Frank—van-der-Merwe mode.[492] Recently, Uosaki and co-workers electrochemically deposited Pt thin films to Au(111) at room temperature using electrolytes containing the $[PtCl_6]^{2-}$ complex.[493] They characterized morphological evolution using in situ STM and presented clear evidence of layer-by-layer Frank—van-der-Merwe growth albeit with some increase in surface roughness.[493] In contrast, Waibel et al. performed a very similar study using both $[PtCl_4]^{2-}$ and $[PtCl_6]^{2-}$ containing electrolytes and showed evidence for the Volmer—Weber growth,[494] which was supported by a theoretical study by Chang and Carter.[495] However, simulation studies by Haftel et al. predicted a fairly complex evolution of the Pt film, which could be best described as the Frank—van-der-Merwe growth.[496] Additionally, Pedersen et al. studied the initial growth (up to 2.5 ML) of Pt on Au(111) at 373 K using STM and suggested the growth in the Frank—van-der-Merwe mode. Specifically, marginal surface alloying was limited to the first

monolayer; subsequent monolayers grew as pure Pt with a flat morphology conformal to the substrate without nucleation of islands,.[497] Notably, Mathur and Erlebacher revisited this system with hopes to understand and clarify differences in the growth mode observed in electrochemical deposition studies and in UHV systems .[498] They grew thin (1—10 nm) films of Pt on Au(111) via a PVD method and found that Pt grows in a layer-by-layer growth mode on a smooth Au(111) surface. However, upon exposure of the gold substrate to an acidic environment prior to Pt deposition, the substrate became nanoscopically rough (islanded) and a pseudo-Stranski—Krastanov growth mode (forming both layer and island) was suggested.[498]

The surface structure of gold-covered Pt surfaces has also been investigated dynamically.[499,500] Sachtler and Somorjai showed that deposition of Au on Pt(111) at 300 K produces an epitaxial Au layer consisting of 2D islands that leave large ensembles of Pt(111) uncovered. With increasing coverage of gold, the islands grow until the monolayer is completed, before the second layer begins to form.[499] Adsorption of Au atoms on Pt(100) causes a local lifting of the reconstruction.[500] Rectangular islands with monolayer height were observed during the initial stage of Au deposition. STM images showed that Pt atoms were diffused into the first-layer Au islands, contributing to ~20% of the island area. The first-layer islands preferably nucleate at step edges over flat terraces. Structural defects on Pt surfaces also serve as nucleation sites. Interestingly, growth of the second monolayer islands occurs prior to the completion of the first monolayer.[500] Further growth proceeds in a quasi-layer-by-layer mode; with a film thickness higher than 4 ML, a (1 × 7) surface reconstruction was observed.[500]

The morphology and surface composition of the Au—Pt surface is strongly dependent on temperature, showing an ordering effect at room temperature.[489,499] Kobiela et al. characterized the electronic and surface structures of gold films deposited on Pt(111), and from UPS analysis showed that annealing the surface to 750 K and higher results in diffusion of Au into the Pt bulk (initiated at the step edges).[501] The Au—Pt surface alloy is formed between 950 and 1050 K. At 1150 K the depletion of Au is completed.[501] STM investigations of the alloyed surface showed that the bright areas consist of Au—Pt surrounded by darker patches of clean Pt, suggesting that the Au diffusion into the Pt substrate is initiated at the step edges.[501]

6.3.2. Chemical Properties. In a study of CO adsorption. Pedersen et al. observed a decrease in binding energy of CO for thin platinum films on Au(111).[497] However, as a decline of platinum coverage, the binding strength of CO was decreased, as also confirmed via DFT calculations.[502] A maximum desorption temperature of CO at a 1.3 ML of Pt was ~40 K higher than that of Pt(111).[497] Increase of CO binding energy can be ascribed to a shift in the valence states of the Pt atoms in the Pt—Au surface alloy. The d band shift could be originated from the lattice expansion by the Pt islands.[497,503]

In the opposite case of Au atoms alloyed into a Pt(111) surface, a strong dependence of desorption temperature of CO on Pt concentration in the surface alloy has been reported by Sachtler and Somorjai[499] and later confirmed by Kobiela et al.[501] Particularly, when the Au surface concentration was increased, and thus the Pt ensembles became smaller, CO interacted more strongly with the surface compared to clean Pt(111). This result is in contrast to the Pt—Au(111) system, which can be explained via the mechanism responsible for the increased desorption temperature of CO from the first-layer islands of Pt—Au on
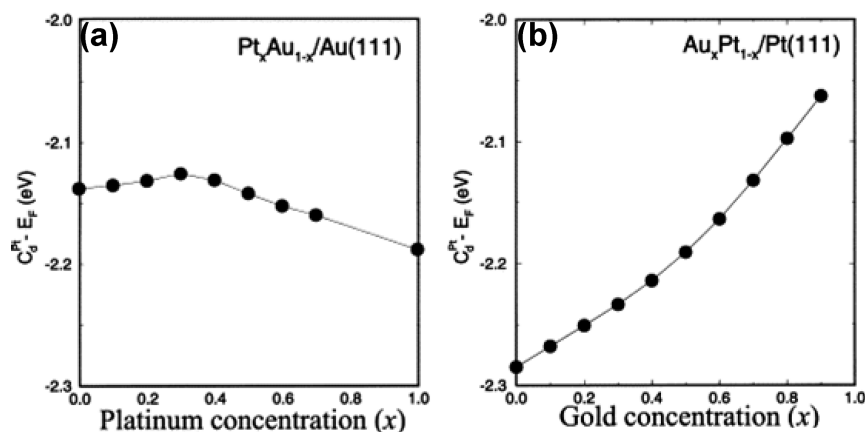
3024

dx.doi.org/10.1021/cr200041p |*Chem. Rev.* 2012, 112, 2987–3054

Figure 37. Ab initio LMTO calculations of the d-band shift of Pt atoms in (a) a Pt–Au alloy on Au(111) and (b) a Pt–Au alloy on Pt(111). On the basis of these calculations, the d-band shift of Pt in Pt–Au alloy on Au(111) is independent of Pt coverage, whereas a strong dependence is shown for Pt in the Pt–Au alloy on Pt(111). This could be an explanation for the observation of a concentration dependence of the CO desorption from a Pt–Au alloy on Pt(111).[499] The increase in CO desorption temperature seen when the Au coverage was increased can be explained by an upward shift of the Pt d-state in the Pt–Au alloy formed. Reproduced with permission from ref 497. Copyright 1999 Elsevier.

Au(111).[497] The concentration dependence of the d-band shift of Pt in a Pt–Au alloy for a Pt–Au alloy on Au(111) and Pt(111) is shown in Figure 37.[497]

One should also note that the CO binding is stronger on both the Pt/Au and the Pd/Au overlayer systems and on the PtAu surface alloys with a coverage of more than 1 ML compared to the pure metal surfaces. This suggests that depositing a more reactive metal on gold surfaces with a larger lattice constant (the lattice constant of Pt is about 5% smaller than that of Au, similar to that of Pd compared to Au) could make it more reactive.[504]

The intermixing of Pt and gold upon annealing the Au–Pt surface to high temperature leads to a reduction of Pt ensembles,[499] which has a profound effect on the catalytic properties. The surfaces with only small Pt ensembles are more active than pure platinum and have a high selectivity for reactions like isomerization, while surfaces with an unaltered site distribution behave as pure Pt.[499,505] Yeates and Somorjai observed a surface structure sensitivity of Au–Pt alloys (Au–Pt(100) and Au–Pt(111)) using *n*-hexane as a probe molecule,[505] which converted into 2- and 3-methylpentane (isomerization), methylcyclopentane (C-5 cyclization), benzene (aromatization), and hydrogenolysis products.[499] The activity of the Au–Pt(100) alloy decreased linearly with increasing surface atom fraction of gold. The Au–Pt(111) alloy showed an enhancement in reactivity as the surface atom fraction of gold was increased from 0 to 0.4, and then fell off with a further increase in the surface concentration of gold atoms.[499]

Introduction of gold onto Pt stepped surfaces in some cases decreases the catalytic reactivity due to the blocking of active sites. Skelton et al. showed that gold deposited on Pt(335) (it has four-atom-wide (111) terraces separated by monatomic (100) steps) blocks the step sites, which are active sites for dissociation of NO, molecular oxygen, and hydrogen on Pt(111) (Figure 38).[506–508] The presence of gold on the Pt(335) surface, therefore, reduces the catalytic reactivity of reactions involving dissociation of adsorbents at step sites, e.g., CO oxidation[507] and hydrogen oxidation.[508] This is consistent with a previous study of CO oxidation on Pt(100) with a submonolayer gold coverage, where the presence of Au atoms essentially reduces the adsorption probability for oxygen and the diffusion coefficient for

chemisorbed CO.[509] Considering the dissociative adsorption of NO (Figure 38a) and oxygen (Figure 38b), for instance, on bare Pt(335) oxygen adsorbs dissociatively above 200 K with recombinative desorption peaks at 700 and 850 K from the terrace and step sites, respectively. Oxygen dissociation takes place predominantly at the step sites, with only a 5% probability of dissociation on the terrace sites. On the 0.3 ML Au/Pt(335) surface, the step sites were filled by Au; however, the saturation oxygen coverage was reduced by only 20% compared to bare Pt(335).[506,507] Desorption of oxygen is also exclusively from the terrace areas of the surface that remain unblocked by the Au. Although the sites at which oxygen would initially dissociate on bare Pt are filled with Au, the oxygen molecules still find dissociation sites, although far less efficiently.[507] Because a partial Au overlayer has a much weaker effect on O₂ dissociation than on NO dissociation, a Pt(335) surface with 0.45 ML Au is at least 100 times more active for O_2 dissociation than for NO dissociation[506] This result could explain how the oxygen-pumping electrodes work in a NO_x sensor.[506]

6.4. Ru–Au

Few studies regarding the structure and reactivity of ruthenium clusters on gold surfaces have been reported, probably due to the relative difficulty in depositing Ru directly from a metal source under UHV conditions. Cai et al. prepared submonolayer Ru nanoclusters on Au(111) via decomposition of Ru₃(CO)₁₂.[358] Carbonyl molecules were partially decomposed after adsorption at room temperature, and Ru preferentially nucleates at the elbow sites of the Au(111) herringbone reconstruction, forming ordered arrays of nanostructures. The decarbonylation was complete at ~500 K, at which aggregation and the emergence of islands of Ru were observed.[358] Surface morphology and the nature of the nucleation sites depend on the deposition conditions. Strbac et al. electrochemically deposited Ru on Au(111) using RuCl₃ and then demonstrated that the nucleation of Ru monolayer islands proceeds mainly in the fcc regions of the reconstructed surface, rather than at the elbow sites of the Au(111) electrode.[510,511]

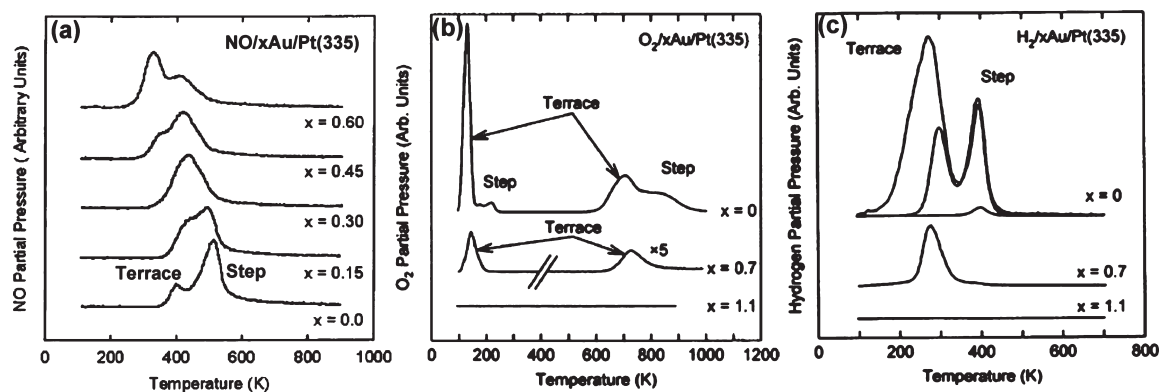The structure of gold deposited on Ru surfaces (e.g., Ru(0001)) is dependent on the surface coverage and temperature.

Figure 38. Desorption of (a) NO, (b) O$_2$, and (c) H$_2$ from Pt(335) and partially Au-covered Pt(335) as a function of Au coverage (denoted as x, ML). The NO dose was sufficient to fill the step sites with just a small amount on the terrace on bare Pt(335). Three H-coverages are shown: 1%, 44%, and saturation. The same scale is used for all curves on bare Pt(335). Reproduced with permission from refs (a) 506, (b) 507, and (c) 508. Copyright 2001, 1999, and 2000 American Chemical Society, respectively.
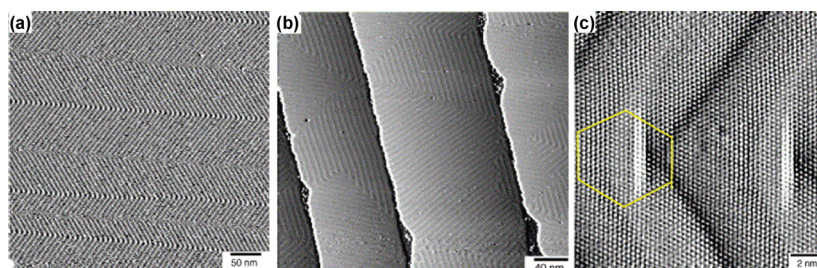

Figure 39. STM images of 1 ML Au film grown on Ru(0001). (a) Herringbones on a large terrace. (b) Random distribution of rotational stripe domains on a narrow terrace. The image is differentiated to show the stripes on all four Ru terraces. (c) Atomic structure of the elbow at the boundary where two stripe domains meet. As shown by the Burgers circuit (yellow line), a perfect edge dislocation exists at the intersection (elbow) of the two partial dislocations. The extra row of atoms at this dislocation core starts on the convex side of the intersecting partial dislocations. The substrate temperature was held at 423 K during Au deposition, and the deposited Au films were flash annealed to ~800 K to achieve a well-ordered surface. Reproduced with permission from ref 512. Copyright 2006 Elsevier.

As a general tendency, lower substrate temperatures favor an island growth of the Au (e.g., Stranski−Krastanov growth mechanism),[513] whereas higher Ru temperatures lead to a more pronounced spreading and dispersion of the Au atoms (e.g., layer-by-layer growth up to 2 ML[514,515]).[516] The hcp(0001) face is a close-packed surface with the same two-dimensional packing of atoms as Au(111). Au wets the Ru surface, but neither forms alloys with Ru nor diffuses into the Ru(0001) substrate.[517] Submonolayer films of Au deposited on Ru(0001) at room temperature form dendritic islands,[518,519] which, upon annealing to 650 K and above, evolve into a herringbone pattern.[512] Figure 39a is an STM image of a 1 ML Au film on a large Ru terrace. The stripe domains are organized into a herringbone pattern with the elbows separated by about 100 nm.[512] On terraces narrower than about 100 nm, the stripe domains are not ordered into a herringbone. Instead, the stripes form random rotational domains with no long-range order (Figure 39b). The average separation of Au atoms along a close-packed row is 2.78 Å (Figure 39c).[512] That is, the Au atoms in a 1 ML film are contracted ~3% relative to bulk Au. Interestingly, a trigonal structure develops when Au grows up to two layers and above on Ru(0001). Considering that the misfit (strain) between bulk Au and bulk Ru is 6.2%, the authors concluded that the interface reconstruction in the first Au layer relaxes the in-plane spacing of the second Au layer to nearly the bulk Au spacing.[512]

The growth of Au on Ru(100) at 300 K was found to follow a nonpseudomorphic, simultaneous multilayer mode,[520] confirmed by oxygen uptake measurements, where Poulston et al. showed that oxygen chemisorption was not completely suppressed up to a Au loading of 2.5 ML.[521] For Au precoverages lower than 2.5 ML, exposure to oxygen resulted in the formation of characteristic O/Ru(100) LEED patterns, c(2 × 4) followed by (2 × 1), indicating oxygen adsorption on free Ru sites. The presence of oxygen on the surface weakens the Au−Ru interaction.[520]

6.5. Cu−Au and Ag−Au

Copper, silver, and gold are metals that have many uses in catalysis and plasmonics. Although they are coinage metals found in the same group of the periodic table, their catalytic behavior, in some cases, is quite different. Heterogeneous copper and silver catalysts are well-established hydrogenation and oxidation catalysts, e.g., in the production of methanol, while nanosized gold has been recognized as an active heterogeneous catalyst more recently.

Cu and Ag have electron affinities that are much smaller compared to Au and thus can donate net electrons when present on gold surfaces.[368] Copper and silver are among metals not preferentially nucleated at the elbows of the Au(111) herringbone surface, macroscopically due to the lower surface energies
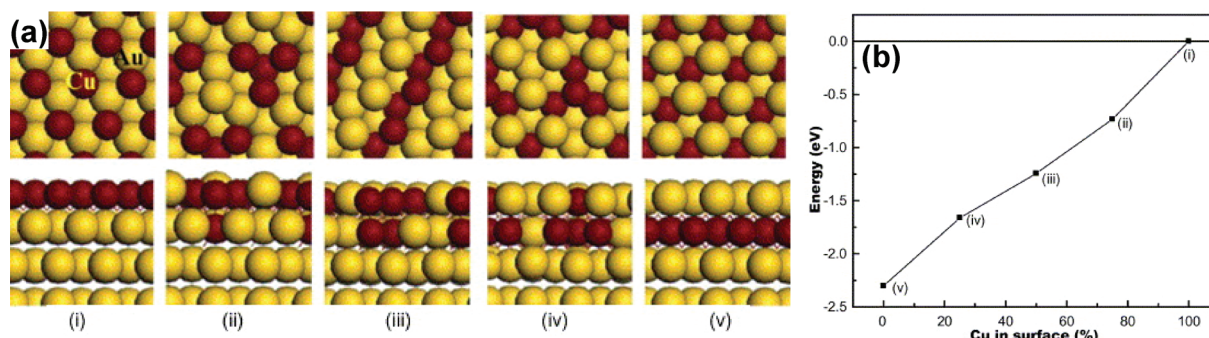
Figure 40. (a) Various optimized configurations for depositing one monolayer of Cu on a Au(111) surface. For each configuration, the upper and the lower drawings display the top and side view, respectively. i, ii, iii, iv, and v correspond to different configurations with a Cu concentration (θ_{Cu}) on the surface of 100%, 75%, 50%, 25%, and 0%, respectively. (b) Calculated surface stability of Cu/Au(111) as a function of θ_{Cu}. Here the stability is expressed in reference to the case of a Cu overlayer on Au(111) with a Cu concentration on the surface of 100% as shown in (i) of (a). Reproduced with permission from ref 526. Copyright 2005 Elsevier.

and heats of sublimation compared to gold.[371] The phase diagram for the Cu—Au binary system (with lattice parameters of 3.615 Å and 4.079 Å, respectively) indicates that they can form a continuous solid solution at high temperature, whereas at lower temperatures superlattices are formed around the Au₃Cu, AuCu, and AuCu₃ compositions.[13,522] Regarding electrochemical deposition, Cu forms ($\sqrt{3} \times \sqrt{3}$) or (1×1) ordered overlayers on Au(111) and no intermixing between Cu and Au was reported.[523,524] Under UHV conditions, reflection high-energy electron diffraction (RHEED) patterns showed that Cu pseudomorphically adsorbed on Au(111) at submonolayer coverages, while intermixing takes place above one monolayer coverage.[525] However, the formation of a pseudomorphic layer at submonolayer coverages is somewhat questionable, because RHEED allows a structural analysis but not an elemental content analysis. Indeed, ISS measurements have clearly shown that Cu intermixes with the Au(111) surface at 300 K or higher temperatures. However, a considerable fraction of Cu is present on the Au(111) surface upon deposition at 100 K.[526] The intermixing and alloy formation at and above room temperature occur for Au/Cu-(100),[527,528] Au/Cu(110),[529] Au/Cu(111),[530] and Au—Cu films.[460] A similar phenomenon has also been reported for silver growth on Au(111) under UHV conditions.[531−533] Theoretical calculations for Cu/Au(111) further showed that Cu atoms penetrating into the substrate are more energetically stable than those staying on the surface (Figure 40).[526,534,535]

Hsieh et al. studied Ag epitaxial overlayers on Au(111) and Au epitaxial overlayers on Ag(111).[536] Ag and Au have a negligibly small lattice mismatch, and the overlayers grow in a layer-by-layer fashion with few stacking faults at the interface under UHV conditions.[532,536−539] At submonolayer coverage, Ag nucleates at steps and grows across terraces; rapid surface diffusion without rapid edge diffusion leads to the formation of finger-like structures.[540] Electrochemical deposition of Ag on Au(111) follows a Stranski—Krastanov mode, where two epitaxial layers of Ag were sequentially formed prior to the heterogeneous nucleation of 3D Ag crystallites which preferentially developed on steps.[541] Similar to Cu—Au, intermixing and alloy formation of the Ag—Au system starts to occur at room temperature. Cu[542] or Ag[543,544] deposited on Au(110) (1×2) at 300 K leads to a Au/Cu/Au(110) or Au/Ag/Au(110) sandwich structure. The introduction of the Cu or Ag underlayer causes the topmost Au layer to change from a missing-row structure to a

more densely packed rotated phase.[542−544] A similar structure has also been reported for the growth of Au on Ag(110)[545] and iron on Au(100).[546]

Zhao et al. examined the chemical properties of Cu/Au(111) using SO₂[526] and glycine[547] as probe molecules. Surface composition has a significant influence on SO₂ adsorption. DFT calculations revealed electronic perturbations in the Cu overlayer contributing to the enhancement of chemical reactivity. The value of θ_{Cu} determines the binding energy of SO₂; the presence of more Cu atoms in the surface leads to stronger bonding energies toward SO₂.[526] Cu/Au(111) also behaves differently from pure Cu. Surprisingly, a temperature increase does not cause cleavage of the S—O bond on the bimetallic surfaces. Instead, the Cu atoms in the surface migrate into Au, accompanied by SO₂ desorption. It is likely that ensembles of the active sites required for the dissociation of SO₂ are not available. For Cu/Au(111), ensemble effects clearly overcome electronic effects.[526] In the Cu submonolayer range, glycine physically adsorbs on Cu/Au(111) in its zwitterionic form ($NH_3^+CH_2COO^-$) and completely desorbs at 350 K.[547] The binding energies of molecules monotonically increase with Cu coverage, and the admetal is alloyed with Au rather than forming overlayers on the Au(111) substrate. Upon increasing the amount of deposited Cu over 1 ML, part of the glycine overlayer transforms from the zwitterionic state to the anionic form ($NH_2CH_2COO^-$) and chemically adsorbs on the surface with the N 1s binding energy shifted by −2.3 eV.[547] Glycine adsorption induces Cu segregation from the subsurface region onto the top layer of the substrate. As the Cu coverage further increases to 6 ML, part of the chemisorbed glycine decomposes upon heating to 450−500 K.[547]

CO adsorption and oxidation were dependent on the local configuration of Au and Ag. On a Au-enriched Ag(110) surface, the presence of Au enhanced CO adsorption. Au substitution into the second Ag subsurface layer led to a lower reaction barrier.[548] While the CO adsorption energy for Au substituted at the second layer was not as strong as that for Au substituted in the top overlayer, it led to the best CO oxidation performance. Although DFT calculations showed that both the ER and LH mechanisms are plausible, the activation barriers of the ER mechanism decrease more upon Au substitution and the ER transition states are energetically more accessible. Therefore, the authors concluded that the ER mechanism plays an increasingly

important (though not necessarily dominant) role in CO oxidation on the Au–Ag(110) bimetallic system.[548]

6.6. Ir–Au

Au is not miscible with Ir. Upon deposition of gold on Ir surfaces (or vice versa), the Au overlayer is compressed due to a lattice mismatch with Ir, where one can expect enhancement of the electron density at the surface.[549]

Ir–Au, however, can form near-surface alloys, and has promise for hydrogen-related applications.[549] Some near-surface alloys bind atomic hydrogen as weakly as the noble metals, while retaining an ability to dissociate molecular hydrogen more readily than the noble metals.[550] Okada et al. prepared Au films (1–10 ML) epitaxially grown (with a (1×1) LEED pattern) on an Ir(111) surface;[551–553] the first Au layer grew in a complete layer at 100 K, whereas higher Au layers were found to grow in a 3D island mode.[554] The island shape and island density strongly depend on the underlying layer and sample temperature. The first-layer islands have a dendritic shape with a triangular envelope. The second-layer islands have a triangular compact shape at 300 K and an irregular compact shape at 100 K, and the third- or higher-layer islands are irregularly shaped at both temperatures.[555] Island density at 100 K is much higher than that at 300 K.

Interestingly, these gold films on Ir(111) were able to dissociate molecular hydrogen.[551–553] The formed hydrogen atoms on Au/Ir(111) recombinatively desorb at lower temperatures (<400 K) than from the Ir(111) surface, suggesting that hydrogenation chemistry (iridium itself has remarkable capability in activating C–C and C–H bonds) could be catalyzed by Au/Ir bimetallic nanoclusters/surfaces.[551] The annealing of the thin Au films induces no changes in the reactivity of hydrogen dissociative adsorption.[551] The authors also suggested that hydrogen can be trapped in the interface between Au and Ir, if hydrogen is first dissociated on Ir and Au is overlaid on the Ir–H system.[552,553,556] Contrary to this behavior, we note that Au overlayers on Pt(111) were not able to dissociate H_2, although Pt itself is active in breaking the H–H bond.[557] The dissociative adsorption of hydrogen on the surface of Au–Ir can be explained by changes in the surface electronic structure induced by the Au overlayer on the Ir surface. Mavrikakis and co-workers observed an upshift in the d-band center of the remaining surface Ir atoms as Au is progressively alloyed into the surface.[558] The center of the d-band of Au–Ir(111) is expected at 4.15 eV below E_F,[559] which is located below the d-band centers of pure Ir (2.11 eV) and pure Au (3.56 eV).

6.7. Na–Au and K–Au

The interaction of alkali metals with gold surfaces has been investigated theoretically and experimentally for decades, because of its importance in catalysis (alkali metals are often used as promoters in many reactions), particularly, fundamental understanding of how surface coverage of alkali metals affects structural properties of surface and consequent reactivities.

Barth et al. observed via STM intermixed layers on Au(111) upon deposition of Na at 300 K.[560,561] A (4×2) metastable substitutional structure evolved at a coverage of 0.5 ML, and a mixed $NaAu_2$ structure was observed in the topmost layer upon annealing the sample to 600 K. The $NaAu_2$ structure with a hexagonal lattice possesses a $(1.08\sqrt{3} \times 1.08\sqrt{3})R30°$ geometry, in which a honeycomb structure of Au atoms is formed and occupied by Na atoms. This lattice mismatch induces a regular hexagonal Moiré pattern with ~38 Å periodicity and ~0.5 Å

corrugation.[562] For K–Au(111), the same group carried out LEED and STM measurements to study coverage–structure dependence at various temperatures.[563] At room temperature, a structural sequence $(22 \times \sqrt{3}) \rightarrow (\sqrt{3} \times \sqrt{3})R30°$ ($\theta_K = 0.33$ ML) $\rightarrow (2 \times 2)$ ($\theta_K \geq 0.5$ ML) was observed by LEED; the $(\sqrt{3} \times \sqrt{3})R30° \rightarrow (2 \times 2)$ structures were assigned to an adlayer and an Au–K intermixed layer from STM experiments.[563]

There is only one alkali metal system for Au(110)—K/Au(110), in which a $c(2 \times 2)$ structure is formed. This structure was first observed by Behm et al. when they deposited 0.5 ML of potassium on Au(110) (1×2) at 100 K followed by flashing to 400 K.[564,565] The $c(2 \times 2)$ structure was interpreted as a result of diffusion of surface Au atoms to occupy the half missing-row sites. This was later confirmed by first-principles total-energy calculations[566] and medium-energy ion-scattering analysis.[567] Barth et al. observed the evolution of Au(110) (1×2) to Au(110) $c(1 \times 2)$ employing STM.[568] At very low coverages (i.e., <0.1 ML), the K atoms stabilize missing-row-type structures with deep (1×3) channels. A (1×2) missing-row structure, identical to that of the clean surface, was found in the coverage range between 0.15 and 0.25 ML. At coverages beyond 0.25 ML, the K atoms disrupt the densely packed Au atomic rows of the surface, and highly anisotropic elements of a $c(2 \times 2)$ structure consisting of a mixed K–Au surface layer are formed.[568]

Surface Au atoms on clean Au(100) are rearranged to a surface structure of (5×20) in the presence of alkali metals. For instance, Neumann et al. based on LEED patterns showed a structural sequence of $(5 \times 20) \rightarrow (2 \times 1) \rightarrow (2 \times 2) \rightarrow (2 \times 2)$ on Au(100) with an increase in Na coverage at 300 K.[569] At a lower deposition temperature (i.e., 130 K), a different sequence was observed, e.g., $(5 \times 20) \rightarrow (5 \times 20) + (1 \times 1) \rightarrow c(2 \times 2)$. However, the structural evolution as a function of K coverage on Au(100) at 300 K is somewhat controversial.[570] Okada et al. reported the sequence of $(5 \times 20) \rightarrow (1 \times 1) \rightarrow (2 \times 1) \rightarrow c(2 \times 8) \rightarrow (2 \times 6)$,[571] while Neumann et al. observed the sequence of $(5 \times 20) \rightarrow (2 \times 1) \rightarrow (4 \times 4)$.[569,572] At low temperatures, results from both groups are consistent. That is, the (5×20) structure gradually changes to a (1×1) structure as the potassium coverage is increased. Higher K coverages lead to the formation of islands of a K-induced reconstruction, which subsequently grow with increasing coverage.[573]

The interaction of acetonitrile and benzonitrile with a potassium covered Au(100) (5×20) surface was studied by Christmann and co-workers in UHV between 100 and 500 K.[574] Both molecules molecularly adsorbed on the surface irrespective of K coverage; potassium only exerts a stabilizing effect on the adsorptive bonding of molecules. Additionally, the same group found that the molecular interaction with coadsorbed alkali metal atoms reduces the C≡N bond length in the acetonitrile molecule by 0.04 Å (Na) and 0.07 Å (K), respectively.[575]

Potassium-precovered Au(111) can also stabilize the binding of CO_2, which leads to the formation of a CO_2^- anion radical. Farkas and Solymosi illustrated that potassium adsorbs in cationic form on Au(111) at low coverage, depolarizing to a neutral metallic state at high coverage based on work function measurements.[576] An enhancement of a weakly held, unperturbed CO_2 also occurred on K-covered Au(111), which was attributed to the formation of an unstable cluster compound $(CO_2)_n \cdot CO_2^-$. The surface concentration and the reactivity of the CO_2^- radical depend sensitively on the K coverage and on the state of potassium. At low K coverages, CO_2^- dissociated into $CO_{(a)}$ and $O^-_{(a)}$. At higher coverages, it disproportionated

3028

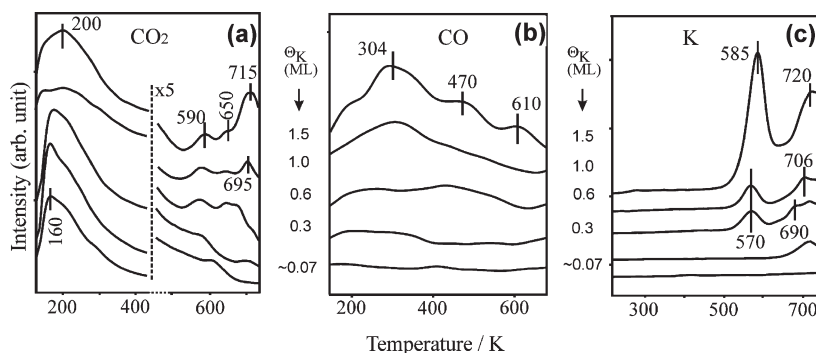dx.doi.org/10.1021/cr200041p |Chem. Rev. 2012, 112, 2987–3054

Figure 41. TPD spectra for (a) CO_2, (b) CO, and (c) K from the CO_2 + K/Au(111) system as a function of K coverage. The CO_2 exposure was 8.0 L. Reproduced with permission from ref 576. Copyright 2009 American Chemical Society.

into stable $CO_3^-{}_{(a)}$ and $CO_{(a)}^-$; these species decomposed to CO_2 and CO and desorbed only above 500 K (Figure 41).[576] Further enhancement of the electron transfer from K-covered Au(111) to CO_2 can be achieved by the illumination of adsorbed CO_2.[577]

6.8. Other Gold-Based Bimetallics

In addition to most gold-based bimetallic systems as discussed above, preference of nucleation at or close to elbows of the Au(111) surface was also reported for many other metals, such as Fe,[333,578] Co,[316,579] Rh,[503,580] Ti,[296] and Mo.[314,338] In contrast, for other metals (e.g., Al,[581] Ce,[302] Ag,[538,540] and Cu[542]) nucleation was found to be homogeneous and independent of the mesoscopic order of the $(\sqrt{3} \times 22)$-reconstruction.[371,373] Generally, metals with higher surface energy than Au(111) will preferentially adsorb at elbow dislocations; the adatoms then become favored nucleation centers for island growth if the bond between adatoms is stronger than that formed with gold atoms.[368,371] This energy balance is inversed for metals that prefer homogeneous nucleation.[371,373] For example, Ce nanoparticles nucleate and grow homogeneously on large terraces of Au(111), and the steps are almost fully decorated by small ceria particles.[302] At low coverage, a larger fraction of the Ce clusters was found at the elbow dislocations while homogeneous nucleation on the terrace sites is less favored. These energetic arguments are fairly universal since they basically can explain all experimental results reported so far.[373]

From a thermodynamic point of view, the growth mode (e.g., layer-by-layer or Frank−van-der-Merwe growth, layer-plus-island or Stranski−Krastanov growth, and island or Volmer−Weber growth) of metal films on gold surfaces heavily relies upon the relative surface free energies of the pure admetal (γ_A), the gold substrate (γ_S), and the interface ($\gamma_{A\text{-}S}$).[368] The ideal layer-by-layer mode is typically applied when $\Delta\gamma = \gamma_A + \gamma_{A\text{-}S} - \gamma_S < 0$. The island mode is expected when $\Delta\gamma = \gamma_A + \gamma_{A\text{-}S} - \gamma_S > 0$. The $\gamma_{A\text{-}S}$ term strongly depends on the nature of the bimetallic bond. The sign and magnitude of this term determines the growth behavior at surfaces. One should note that this analysis model for the growth modes of a metal film on Au surfaces is correct only if thermodynamic equilibrium is established.[368] However, in many cases, film growth occurs under conditions far from equilibrium. For example, in both the Fe/Au(100)[546] and Cu/Au(110)[542] systems, the equilibrium status does not match any of the growth modes described above. Instead, a Au−Cu−Au or Au−Fe−Au sandwich structure was reported at equilibrium conditions.[368] The formation of these

"sandwiches" is thermodynamically driven by the differences in surface free energies between Cu and Au or Fe and Au.

7. GOLD NANOPARTICLES SUPPORTED ON METAL OXIDES

In the real world of heterogeneous catalysis, gold clusters are usually supported on a supporting carrier. Therefore, the role of the support and the origin of differences in catalytic reactivity between gold catalysts on various supports are of particular interest.[3,65] Lack of knowledge regarding the atomic/molecular structure of powdered Au−oxide catalysts and difficulties in controlling particle size, morphology, degree of hydration, etc. render careful and thorough model studies a necessity. Investigations on model systems involving metal particles supported on planar oxide substrates (single crystals or thin films) under well-controlled conditions can provide fundamental knowledge on structure−reactivity dependence of supported gold clusters. Furthermore, surface science studies of planar model catalysts, if designed appropriately, could bridge the materials gap between "real" catalysts and metal single crystals.[65,582−584]

This section reviews the current understanding regarding important features of gold−metal oxide catalysts, particularly model systems. We organize the structure of this section based on the type of metal oxides used to support the gold nanoparticles. We place an emphasis on Au/TiO_2—the most popularly investigated gold catalyst—and discuss a variety of aspects of this system, such as nucleation and growth of gold, electronic properties, and adsorption and reactions of several molecules. We also provide an overview of similar aspects for several other gold−metal oxide model systems (e.g., Au/CeO_2, Au/MgO, and Au/FeO_x), but in a relatively brief manner.

7.1. Nucleation and Growth of Gold

Gold manifests a high electronegativity (2.3 eV) and ionization potential (9.2 eV), which make it a poor electron donor. Consequently, gold weakly interacts with many oxides. Defects such as oxygen vacancies play a crucial role in the adsorption, nucleation, and growth of gold particles on oxide surfaces. Preparation methods, pretreatments, and reaction ambient can all influence the structure and thus reactivity of gold particles on metal oxide surfaces.

7.1.1. Au/TiO_2. Au/TiO_2(110) is the most intensively investigated system among gold model catalysts. Surface structure and the chemistry of the TiO_2(110) rutile surface have been examined in detail with STM and other surface science techniques (see the classic review by Diebold[290]). The TiO_2(110)
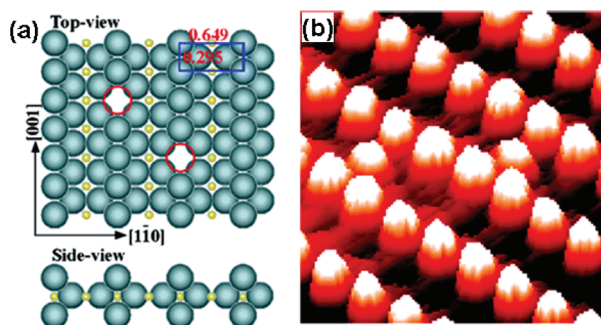
Figure 42. (a) Schematic structural model of $TiO_2(110)$ with empty circles indicating the surface oxygen vacancies and blue rectangle representing a unit cell, and (b) high-resolution STM image of TiO_2-(110). Reproduced with permission from ref 18. Copyright 2006 American Chemical Society.

Figure 43. Densities of oxygen vacancies and Au clusters before and after deposition of ~0:04 ML Au at different temperatures. One ML = 1 vacancy or cluster/$TiO_2(110)$ unit cell = 5.13×10^{14} cm^{-2}. The data were obtained from corresponding high-resolution STM images. Reproduced with permission from ref 594. Copyright 2003 American Physical Society.

(1×1) surface possesses alternating rows of titanium and oxygen atoms with one-half of the titanium atoms covered by bridging oxygen (Figure 42). This unique structure results in the formation of both 6-fold-coordinated Ti (as in the bulk) and 5-fold-coordinated Ti (the bright spot along the rows in Figure 42b)[18] as well as 3-fold-coordinated oxygen (as in the bulk) and 2-fold-coordinated oxygen (bridging oxygen).[290] Due to coordinative undersaturation, the bridge-bonded oxygen atoms can be easily removed to form point defects or color centers (i.e., the additional bright spots between the ordered rows in Figure 42b). Defects of this sort can be created by sputtering with Ar$^+$ or annealing in UHV.[290] The removal of an oxygen atom on the TiO_2 surface causes a redistribution of charge over the Ti ions surrounding the vacancy, leading to negative and positive binding energy shifts in the binding energy of the 5-fold- and 6-fold-coordinated Ti atoms, respectively.[585] A strongly reduced $TiO_2(110)$ surface can form a (1×2) reconstructed structure.[65,290] The nature of surface defects of $TiO_2(110)$ are strongly dependent on sample preparation,[586] which, in turn, affects particle shape, adsorption energy, and electronic structure of deposited Au nanoparticles and thus their catalytic properties. Au nanoparticles on defect-rich titania were found to be much more chemically active than on defect-deficient titania.[132,587]

The initial growth of gold on reduced $TiO_2(110)$ has the following characteristics:[291,586,588−603] (1) Au particle growth at low coverage (<0.1 ML) below room temperature follows a two-dimensional growth mode and then transitions to a three-dimensional growth mode upon increasing coverage; (2) Au particles, during the early stages of growth, are elongated in the direction of bridge-bonded oxygen rows; (3) Au particles nucleate preferably at the sites of oxygen vacancies; and (4) the number of Au particles increases while the average particle size decreases with an increase in the number of oxygen vacancies (schematic shown in Figure 43). Notably, the mode of nucleation and growth of gold particles on $TiO_2(110)$ is dependent on the density of oxygen vacancies on the terrace, which is typically affected by sample preparation conditions (Figure 43).[19,594] In the case that the density of oxygen vacancies on the terraces is low, gold nanoparticles preferentially nucleate and grow on the extended defects (e.g., the step edges of the oxide surfaces).[593]

The critical Au coverage, at which transformation of Au nanoparticles from 2D to 3D growth occurs, increases with increasing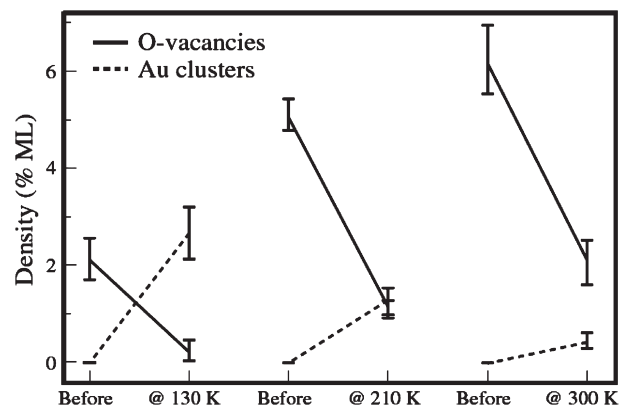 defect density of the TiO_2 surface. On the pristine surface, the critical gold coverage for the transition is ~0.09 ML, whereas ~0.22 ML of Au was reported for the sputtered surface.[590] The critical coverage also decreases with an increase in temperature, e.g., 0.19 ML for gold deposited at 160 K versus 0.09 ML at 300 K.[590] The Au islands grow either larger or thicker as the surface temperature increases.[588]

The crucial role of oxygen vacancies of $TiO_2(110)$ on the growth of gold has been investigated both experimentally and theoretically.[18] DFT calculations have indicated that Au particles bind more strongly to a defect-rich surface and that charge transfer could occur from titania to the Au particles.[594] High-resolution STM coupled with DFT calculations confirmed that bridging oxygen vacancies are the active nucleation centers for the growth of Au nanoclusters on titania, and that each vacancy site can averagely host about three Au atoms.[594] The adsorption energy of a single Au atom on an oxygen vacancy is ~0.45 eV higher compared to the stoichiometric surface.[604,605] While Ti sites along the (001) direction of rows are essentially energetically equal, diffusion along the protruding rows requires a high energy barrier.[604,606] This could explain why gold nanoparticles are frequently elongated in a particular direction on $TiO_2(110)$. Additionally, DFT calculations by Wang and Hwang demonstrated that neighboring oxygen vacancies further increased the interaction between gold and the defect site.[607] A similar phenomena regarding the adsorption of gold on oxygen vacancies has been observed for a $TiO_2(101)$ anatase surface.[608−610]

Semiquantitative analysis of oxygen vacancies on the reduced $TiO_2(110)$ surface has been performed by deposition of Au followed by UPS measurements.[18] Emission at a binding energy of 0.9 eV in UPS spectra was evident from a Ti^{3+} electronic level. Two neighboring Ti atoms are reduced from Ti^{4+} to Ti^{3+} on an oxygen vacancy site. Thes Ti^{3+} defects can be completely reoxidized using oxygen. Upon following deposition of Au, a decrease in the Ti^{3+} intensity suggests that Au atoms adsorb at oxygen vacancy sites.

Figure 44a is a STM image of 0.25 ML (one monolayer corresponds to one Au atom per surface Ti^{4+}) of Au deposited on $TiO_2(110)$ at 300 K followed by annealing at 850 K for 2 min.[291] The atomically resolved $TiO_2(110)$ surface consists of flat terraces with atom rows separated by ~0.65 nm. Au nanoparticles have a

3030

dx.doi.org/10.1021/cr200041p |*Chem. Rev.* 2012, 112, 2987–3054

relatively narrow size distribution, and surface morphologies can be seen as bright protrusions.[18] Schematics of the 1D, 2D, and 3D Au structures with one-, two-, and three-atomic-layer thicknesses are illustrated in Figure 44b–44d.

The nucleation and growth of gold with large coverages (0.2–12 nm) on TiO_2(110) have been examined by Madey and co-workers.[588,611] High-resolution scanning electron microscopy (SEM) images revealed that a new stage of growth started at thicknesses above 1.5 nm. A Volmer–Weber mode has been proposed in the range 160–475 K at these coverages; three-dimensional Au clusters are separated by areas of clean TiO_2 surface.[588] Continued deposition of gold led to a decrease in island density owing to further coalescence, until a granular gold film was eventually formed at a coverage of ~12 nm.[611] Upon annealing these islands, the particle density was intact, whereas the thickness of islands increased, leading to the formation of faceted structures and appearance of more of the TiO_2 surface underneath. This phenomenon agrees with the island thickening model suggested by Campbell for metals grown on oxides[584] but in contrast to the annealing effect at lower coverages, in which both ripening and coalescence led to a decrease in particle density.[65,588]
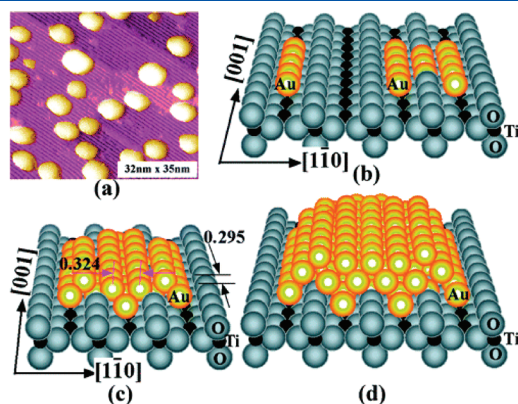

Figure 44. (a) STM image of Au/TiO_2(110) (1 × 1) with a Au coverage of 0.25 ML. Reproduced with permission from ref 291. Copyright 1998 American Association for the Advancement of Science. (b, c, and d) Schematic structural models for 1D, 2D, and 3D structures, respectively, with two-atomic- and three-atomic-layers thick Au particles on TiO_2(110). Reproduced with permission from ref 18. Copyright 2006 American Chemical Society.

Using high-resolution SEM images, the Madey group showed the formation of highly faceted particles of gold on TiO_2(110). When gold nanoparticles were deposited on TiO_2(110) at 300 K followed by annealing to 770 K, the (111)Au//(110)TiO_2 orientation was preferred, while direct deposition at high temperature (e.g., 775 K) preferentially results in the (112)Au//(110)-TiO_2 orientation.[586,612] Similar results were later confirmed by Lazzari et al. using grazing incidence X-ray scattering techniques.[599] No deformation of the Au lattice was found even though there is small strain to overcome for TiO_2 epitaxy, suggesting a weak interaction between gold and titania.[612] The situation, however, is somewhat different on anatase titania. A strong epitaxial relationship between the support and gold was observed due to the small misfit (0.9%) between the Au(111) facet and the TiO_2(112) plane.[613] Even though theoretical studies showed that small gold nanoparticles prefer icosahedral and decahedral shapes,[65] the strong interaction of gold and titania enables the epitaxial growth of large gold particles with a (111) orientation.[612]

7.1.2. Au/CeO₂. In its most stable phase, bulk CeO_2 adopts a fluorite-type $Fm3m$ crystal structure, in which each metal cation is surrounded by eight oxygen atoms.[614] One of the most interesting properties of ceria is its ability to undergo a transition between +4 and +3 states. Ceria is also a wide-band-gap (~5 eV) insulator; thus, one has to overcome sample charging problems, which are usually circumvented by annealing at elevated temperatures (up to 1200 K) leading to a partial reduction of the ceria single crystals.[615] This problem is less critical for thin films of ceria, which possess excellent electrical and thermal conductivity while employing surface-sensitive analytical tools. In addition, oxygen diffusion in the thin films can be easily controlled as opposed to the crystal samples.

Figure 45a shows the structure of a perfect CeO_2(111) surface. The top layer consists of O atoms, but there are holes within this layer leading to the exposure of Ce cations to the second layer. Although both oxygen and cerium vacancies have been considered as the nucleation sites of gold nanoparticles, the cerium vacancy is harder to form and is less stable than the oxygen vacancy, regardless of the presence or absence of gold on the surface.[616,617] DFT calculations on Au atom adsorption on an O vacancy and a Ce vacancy on both CeO_2(111) and CeO_2(110) indicated that Au atom adsorption on a Ce vacancy causes a large distortion on the surface; an oxygen vacancy is produced correspondingly, and an oxygen atom near the Au atom becomes very reactive compared to the stoichiometric surface.[618,619] Gold
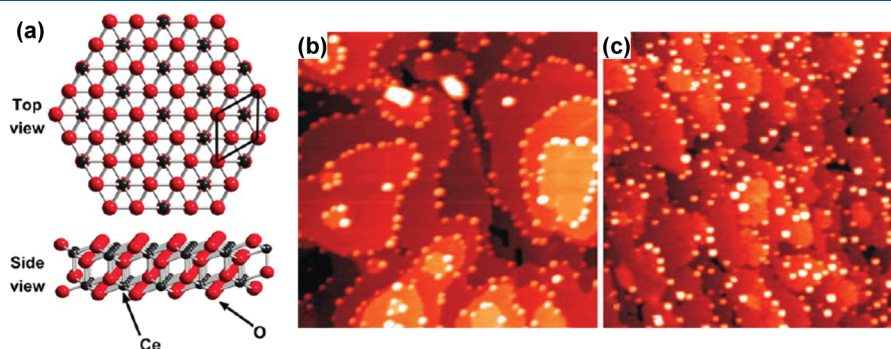
Figure 45. (a) Ball model of an ideal CeO_2(111) surface. The first layer contains only O cations (red spheres) and the second Ce cations (black spheres). Reproduced with permission from ref 616. Copyright 2007 Springer. STM images of 0.1 ML of gold deposited at 300 K on (b) fully oxidized and (c) partially reduced CeO_2(111) films. The reduced film was prepared by oxidation at 4×10^{-8} mbar, which is an order of magnitude lower than used for the fully oxidized film. Image size is 150 × 150 nm². Reproduced with permission from ref 628. Copyright 2007 Springer.

adsorption at the oxygen vacancy site is preferred over that on the cerium vacancy; the latter becomes favorable only near the extreme oxygen-rich limit, which would not be achievable under reaction conditions.[620−623] Additionally, Huang and co-workers have found that Au(I) species and metallic Au nanoparticles compete for the surface oxygen vacancies on CeO_2, and the presence of Au, in turn, promotes the generation and stabilization of these oxygen vacancies.[624]

Rodriguez et al. have demonstrated that gold nucleates on oxygen vacancies forming 3D islands on $CeO_2(111)$ upon depositing gold at 300 K based on XPS analysis.[616,625,626] DFT calculations also suggested that the Ce 4f states play a pivotal role in Au adsorption on the stoichiometric and reduced CeO_2 surfaces.[622] Freund and co-workers have prepared well-ordered $CeO_2(111)$ films epitaxially grown on Ru(0001) and reported on the morphology of deposited Au particles using scanning tunneling microscopy (Figure 45b and 45c).[627−629] The results show that most of the Au particles preferentially nucleate at the step edges of terraces on fully oxidized $CeO_2(111)$, while the particles on terraces presumably grow through the decoration of point defects typically associated with oxygen vacancies on reduced surfaces,[628] which is in good agreement with the theoretical predictions of Castellani et al.[630] The Au particles grow homogeneously on the flat $CeO_2(111)$ terraces only at high coverage, suggesting a 3D growth mode from the onset. A similar observation has also been reported by Weststrate et al on both oxides and reduced $CeO_2(111)$ films.[631,632] Additionally, Akita et al. using high-resolution TEM showed that Au particles on polycrystalline CeO_2 grow by an Ostwald ripening process through surface diffusion forming 3D islands; the hemisphere-like Au clusters have the top facet possessing a hexagonal shape, suggesting a (111) surface and side facet of a (100) feature.[633−635]

7.1.3. Au/MgO. MgO, with its simple rock salt structure, has been considered the prototype of an ionic oxide. Early TEM work illustrated that the interaction between gold particles and MgO could be weak so that deposited particles would diffuse readily on the surface, forming a favorable epitaxial orientation such as $(111)_{Au}//(001)_{MgO}$ or $(110)_{Au}//(110)_{MgO}$.[636] Interestingly, Au particles did not grow epitaxially on air-cleaved MgO crystals, and instead the orientations were random until thick films (100 Å) were formed. Sputtering the MgO substrates with Ar ions prior to gold deposition leads to an increase in the density of Au particles.[637]

Hojrup-Hansen et al. recently have revisited growth of gold nanoparticles on MgO(100) with atomic force microscopy (AFM).[638] They found that the density of clusters rapidly reached saturation with increasing deposition time. Longer deposition time causes a decrease in the cluster density owing to coalescence. The authors thus concluded that nucleation on point defects should be a prevailing process; a homogeneous nucleation mechanism was not supported by their observations.[638] In a similar study, gold particles were found to continuously rearrange to ensure the lowest-energy structure at room temperature.[639] High-resolution electron microscopy images showed that the Au(100) layers and the MgO surface layers were both strained at the interface to compensate lattice constants.[640]

A number of investigations have been reported regarding gold growth on epitaxially grown MgO(100) films. There are well-established recipes to prepare single-crystalline MgO(100) on Mo(100) and Ag(100).[641] The adsorption of Au on MgO(100) films is strongly influenced by the metallic substrate in the limit of

thin MgO films and approaches bulklike properties with increasing MgO layer thickness.[642] The preferential nucleation sites are identified as the low-coordinated oxygen sites located along the oxide step edges.[643] For example, on an 8 ML thin MgO film, Au adsorbs preferentially on oxygen vacancies and annealing to room temperature yields three-dimensional clusters, resembling essentially the situation encountered for Au adsorption on the MgO(100) surface.[644] In contrast, Au adsorption takes place both on magnesium and oxygen sites, and after annealing, clusters stay two-dimensional on a 3 ML thin MgO film. DFT calculations predicted a stabilization of negatively charged 2D particles as opposed to neutral 3D ones on bulklike MgO.[645,646] These results support the suggestion that the properties of Au atoms and clusters can be tuned by the MgO layer thickness.

7.1.4. Au/FeO$_x$. Ordered thin films of iron oxide have recently attracted considerable interest as an oxide substrate for model systems. FeO(111), $Fe_3O_4(111)$, and $Fe_2O_3(0001)$ surfaces can be obtained by varying cycles of iron deposition and subsequent oxidation on a Pt(111) substrate.[332] Similar to other oxide supports, deposited gold nanoparticles on the FeO(111) film first decorate step sites.[647] The density of gold on FeO was approximately one-half that of gold on Al_2O_3/NiAl(110) films[641] with the same deposition rate of Au. This result implies that gold diffusivity on the supports could be fairly different even though they are both very thin and terminated by oxygen.[648] The higher mobility of gold on FeO probably could be due to a lower defect density of the FeO films compared to alumina. Additionally, STM images indicated the formation of monolayer islands of gold on FeO(111) at low coverage.[649] The growth of Au nanoparticles up to 7 nm in diameter was observed with an increase in gold coverage.[650] The (111) top facets of Au could be formed upon epitaxial growth.

$Fe_3O_4(111)$ films grown on Pt(111) yield a regular surface terminated by Fe^{3+} cations.[332] Gold diffusion on $Fe_3O_4(111)$ films is rather limited compared to FeO due to the presence of vacancy defects.[651] A relatively broad distribution of Au particle size was observed for Au/Fe_3O_4 at room temperature. However, heat treatment to 500 K induced an aggregation of Au particles with a average size of ∼4 nm and a narrowing of the size distribution.[647] The histogram analysis based on STM images displayed that the number of layers in the cluster increases as Au particles grow. The annealed particles exhibited mostly ordered hexagonal and trigonal structures. Small lattice mismatch (∼3%) between Au(111) and $Fe_3O_4(111)$ leads to the exposure of the (111) surface of Au nanoparticles.[648]

STM results for $α$-$Fe_2O_3(0001)$ films are rather similar to those found on Fe_3O_4 films. Three-dimensional Au particles are homogenously distributed on the oxide surface with a hemispherical shape. One should note that surface termination of the Fe_2O_3 films is strongly dependent on the preparation conditions,[65,647] and therefore the nucleation phenomenon is currently a subject of investigation.

7.2. Sintering of Au Nanoparticles

Supported Au catalysts are usually much less active than the other supported metal nanoparticles in Pt group. It is primarily due to the poor dispersion of Au particles compared to other supported noble metals originated from the intrinsic properties of Au— the low melting point and weak binding energy of gold to an oxide support. When prepared by the impregnation method, Au particles are usually larger than 30 nm in diameter, whereas Pt clusters have a mean size around 3 nm.[652] Indeed, the

3032

dx.doi.org/10.1021/cr200041p | Chem. Rev. 2012, 112, 2987–3054

melting point of Au is considerably lower compared to Pd or Pt (Au, 1336 K; Pd, 1823 K; Pt, 2042 K). Due to quantum-size effects, the melting point of Au particles with a diameter of 2 nm is even lower (i.e., 600 K[653]). These relatively small Au nanoparticles tend to sinter, forming larger Au particles upon calcination, which causes poor dispersion and low catalytic activity.

7.2.1. Au/TiO$_2$. Since facile sintering is typically considered as a culprit for deactivation of supported Au catalysts, considerable efforts have been made on the understanding of the sintering process and, thus, design and synthesis of sinter-resistant gold-based catalysts. Goodman's group showed that gold nanoparticles deposited at 120 K on a TiO$_2$(001) thin film underwent serious sintering between 120 and 400 K.[654] Zhang et al. reported on substantial agglomeration of Au nanoparticles upon the dosage of 3 ML of gold (5 nm average diameter) followed by annealing at 775 K.[588] However, no encapsulation of gold by TiO$_x$ was detected under reducing or annealing conditions, as has been observed for both platinum and palladium nanoparticles owing to the strong metal support interaction;[65] hence, diffusion of gold particles into the oxide is not likely to occur. STM images witnessed severe sintering upon annealing of gold particles on TiO$_2$(110) up to 773 K;[655,656] the particle density of gold dropped dramatically, and the average particle size increased from 2.7 to 5.5 nm, accompanied with an increase in particle height 0.45 to 0.75 nm. Annealing also leads to the strong binding of gold particles with defects on the TiO$_2$ surface.[655] Interestingly, Lee et al showed that sintering of Au deposited as Au$^+$ at 1 eV kinetic energy is negligible at temperatures of 300 K and below but becomes significant at higher temperature.[657] The possible explanation is that the kinetic energy of Au$^+$ may cause some local disorder that reduces the mobility of gold on the surface.

It is generally agreed that the sintering of titania-supported Au nanoparticles occurs mainly via the Ostwald ripening mechanism.[18,656,658] Ostwald ripening, first described by Wilhelm Ostwald in 1896, describes the energetically preferred mechanism that causes large particles to grow, drawing material from smaller particles, which shrink. This spontaneous process driven thermodynamically takes place since larger particles are more energetically favored due to their smaller ratio of surface area to volume. As the system minimizes its overall energy, molecules or atoms on the surface of the smaller (energetically less favorable) particles diffuse and add to the larger particles. Consequently, the smaller particles continue to shrink, while the larger particles keep growing. Note that particle diffusion to coalescence, where two or more particles merge to form a larger particle, may occur and even dominate under certain reaction conditions. Parker and Campbell have developed an improved kinetic model, based on the pioneering model of Wynblatt and Gjostein, for the sintering of supported metal nanoparticles that can be used to more accurately predict the particle distribution as a function of reaction time.[658,659]

Understanding the sintering of supported Au nanoparticles under reaction conditions is even more important, which has been found to be significantly different than in a vacuum environment (Figure 46). Gold particles on TiO$_2$(110) experience sintering via Ostwald ripening upon exposure to oxygen at room temperature.[660] Oxygen-induced sintering of Au particles, particularly small ones, is likely related to the influence of O$_2$ on the interface bonding since O$_2$ can adsorb and dissociate on Au particles or at the interface of Au/TiO$_2$(110).[3,661] The adsorption and dissociation of O$_2$ could heal the surface defect and restrict the interface bonding between the defects and Au
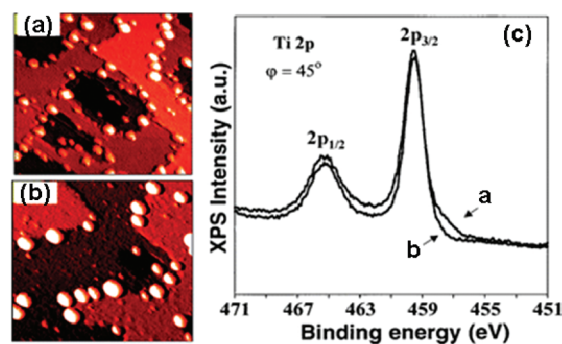

Figure 46. STM images of Au/TiO$_2$(110) (1×1) before (a) and after (b) 120 min of CO−O$_2$ (2:1) exposure at 10 Torr. The Au coverage was 0.25 ML, and the sample was annealed at 850 K for 2 min before the exposures. All of the exposures are given at 300 K. The size of the images is 50 nm by 50 nm. (c) Corresponding core-level spectra (Ti 2p) measured at grazing (45°) emission from the crystal normal. Reproduced with permission from ref 291. Copyright 1998 American Association for the Advancement of Science.

(evidenced by a small shoulder at the low binding energy side of the XPS Ti 2p$_{3/2}$ peak in Figure 46c),[291] which would further destabilize small Au particles due to their low coordination numbers.[662] Ripening in a reactive environment (e.g., O$_2$ and CO) is even stronger.[660,662−664] For example, at a pressure of 10 Torr (2:1 CO/O$_2$) (Figure 46), small clusters grew to from 2.6 to 3.6 nm in diameter and from 0.7 to 1.4 nm in height.[291,660] Surprisingly, several smaller clusters less than 1.5 nm in diameter were also present on the surface. In contrast, no ripening was found for larger particles with an average size of 4.2 nm upon exposure to 10 Torr of oxygen at room temperature, suggesting the ripening process is associated intimately with the reactivity of the particles. Yang et al. suggested that the stabilization of larger Au particles larger than 4.2 nm is less dependent on the interface bond and thus less influenced by oxygen-induced inhibition of the interface bond.[662] Additionally, for gold deposited on *polycrystalline* titania, Sykes et al. observed extreme sintering of gold when exposed to oxygen or air at room temperature. Both Ostwald ripening and coalescence probably account for sintering of the particles.[592]

The mechanism of the ripening process is currently unknown, but the formation of a volatile metal−adsorbate complex (e.g., oxide)—a general explanation for the decay of metal particles—seems unlikely. Au particles supported on TiO$_2$(110) are stable in pure CO gas and have a much slower sintering rate in pure O$_2$ than when subjected to CO oxidation. If the formation of a metal−oxygen complex gives rise to sintering, the presence of CO should inhibit the concentration of the metal−oxygen complex and result in a slower rather than an accelerated sintering rate.[662] Instead, the synergetic sintering effect of a CO and O$_2$ mixture might be explained by a reaction-induced mechanism. DFT results by Liu et al. suggest that CO oxidation on Au/TiO$_2$(110) can proceed with high efficiency without O$_2$ dissociation; the barrier (0.10 eV) for the direct bimolecular pathway to produce CO$_2$ is much lower than the dissociation barrier (0.52 eV) of O$_2$ on Au/TiO$_2$(110).[665] The production of each CO$_2$ molecule releases 2.9 eV.[666] The energy generated from CO oxidation could very well be transferred to electrons at the surface of the Au particles and excite hot electrons, which induce the detachment of Au monomers from supported Au particles, initiating the sintering process.[662,666]
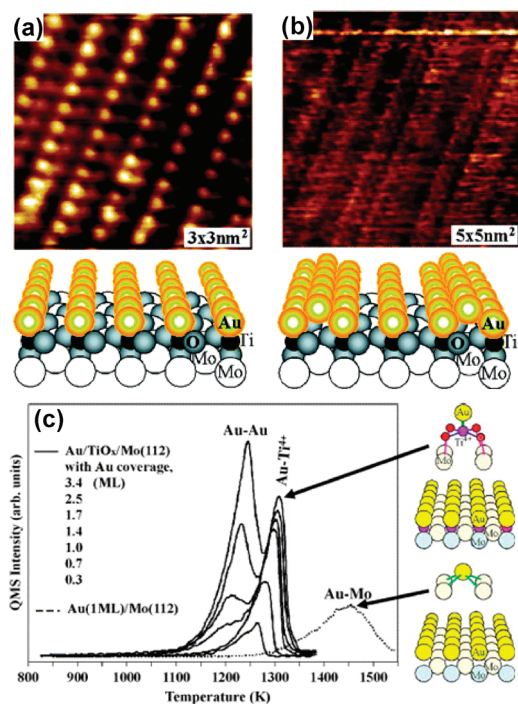
3033

dx.doi.org/10.1021/cr200041p | Chem. Rev. 2012, 112, 2987−3054

Figure 47. Structural model and atomic resolved STM image of (a) Mo(112)-(1 × 1)-(Au,TiO$_x$) and (b) Mo(112)-(1 × 3)-(Au, TiO$_x$). (c) TPD spectra of Au on Mo(112) with coverage of ∼1 ML and on TiO$_x$/Mo(112) with various Au coverages. The binding geometries of Au on the Mo(112) and TiO$_x$/Mo(112) are schematically shown for comparison.[672] Reproduced with permission from ref 668. Copyright 2004 American Association for the Advancement of Science.

Chen and Goodman have researched the design and synthesis of sinter-resistant Au-TiO$_2$-based model catalysts. An excellent example is the preparation of a highly ordered, reduced titania surface on a silica covered Mo(112) substrate (denoted as TiO$_x$−SiO$_2$−Mo(112)).[18,23,667−672] Ti diffuses into the surface producing Ti−O−Si linkages at low coverage and TiO$_x$ 3D islands at a relatively higher coverage.[667,669] In this model, seven Ti atoms decorate every eight Mo atoms along the Mo(112) trough, binding to the surface via Ti−O−Mo bonds and to each other via Ti−O−Ti linkages. On the rutile TiO$_2$(110) surface (Figure 42a), the two Ti atoms nearest to an oxygen vacancy are reduced to Ti^{3+}, whereas a monolayer of reduced Ti^{3+} sites was observed for the (8 × 2) TiO$_x$ surface.[668,670] Accordingly, strong interaction between Au and the TiO$_x$ surface is proposed. As a result, two-dimensional growth of Au up to 1 ML on the TiO$_x$/SiO$_2$/Mo(112) contrasts with the growth of Au on TiO$_2$(110) where 3D clustering occurs at a coverage greater than 0.1 ML.[672] Indeed, formation of well-ordered Au monolayer and bilayer structures with Au completely wetting the surface has been reported upon deposition of Au onto this (8 × 2) TiO$_x$ surface followed by annealing to 900 K.[668] The two ordered structures, designated as (1 × 1) Au−TiO$_x$ and (1 × 3) Au−TiO$_x$, were formed at Au coverages of 1 and 1.3 ML, respectively (Figure 47a and 47b). TPD spectra of gold indicated stronger Au−TiO$_x$ interaction compared with the Au−Au binding (Figure 47c), consistent with the unusual stability of these ordered Au nanofilms.[672]

The addition of a metal (e.g., Pt), which interacts strongly with reducible oxide supports like titania and becomes encapsulated

with a reduced layer of the metal oxide upon heating, into Au-TiO$_2$(110) could somewhat suppress the sintering of Au particles. Chen and co-workers prepared bimetallic Au−Pt clusters on TiO$_2$(110) by depositing Au on existing Pt particles.[673] In contrast, the deposition of Au followed by Pt leads to pure clusters of Pt and Au instead of nucleation of Pt at Au seed clusters. The rate of sintering for the clusters decreases with increasing Pt composition probably due to the formation of stronger Pt−Pt and Au−Pt bonds compared to Au−Au.[673] LEIS spectra demonstrated that the deposition of Au on Pt does not produce core−shell structures with Au on top as predicted for the bulk phase. Instead, surface compositions of the Au−Pt clusters are 10−30% richer in Pt compared to the overall compositions. For the Au−Pt clusters, the extent of encapsulation from SMSI effects is controlled by the Pt composition; reduced titania covers the Pt regions at the cluster surface, but the presence of Au inhibits migration of titania onto the surface of the clusters.[673]

7.2.2. Au/CeO$_2$. Au/CeO$_2$ has relatively better thermal stability compared to Au/TiO$_2$. Lu et al. showed that no sintering of gold particles occurred upon annealing Au/CeO$_2$(111) to 500 K in UHV even for high gold coverages (e.g., 2 ML).[628] Additionally, employing thermal stability measurements in vacuum, Naya et al. revealed that positively charged Au species remain intact at 350 K on reduced CeO$_2$(111) and were finally converted to neutral Au species at 400 K while keeping similar particle size.[674] Gold nanoparticles supported on CeO$_2$(111) are even stable in an O$_2$ ambient up to 10 mbar, while gold sintering starts to occur at CO pressures above ∼1 mbar. Sintering of the Au particles, which mainly proceeds along the step edges of CeO$_2$(111), was observed in a CO and O$_2$ mixture (1:1) at much lower pressure (∼10$^{−3}$ mbar).[628]

Employing high-resolution TEM, Majimel et al. showed that the thermal stability of the gold nanostructures on polycrystalline CeO$_2$ is strongly affected by the particle size. For small nanostructures (<5 nm), reversible shrinkage of gold, layer by layer, onto the ceria surface was observed. The driving forces for the shrinkage are the local temperature rise and the creation of oxygen vacancies on the ceria. For larger particles, a progressive and irreversible encapsulation by a CeO$_{2−x}$ layer was found.[675]

Emergence of gold sintering is more ready under CO oxidation reaction conditions for both Au/ceria and Au/titania systems compared to individual CO and O$_2$ gas exposures. This phenomenon implies that the structural stability of supported Au nanoparticles is inherently dependent on its reactivity.

7.3. Adsorption and Reactions on Supported Au Nanoparticles

7.3.1. Low-Temperature CO Oxidation. *Overview.* The seminal discovery by Haruta that gold nanoparticles supported on metal oxides are highly active for low-temperature CO oxidation has spurred a considerable amount of research directed toward understanding the nature of activity of Au catalysts. However, the factors determining the reactivity of CO oxidation and the reaction mechanism and are still not fully understood. This is partially the complexity of various supports and preparation procedures, which causes contradictory reports on the catalytic reactivity and the dependence of the experimental variables. Both the metal oxide and the Au itself may be important in determining the activity. In particular, edge sites and electronic perturbation of the Au due to its interaction with the support have been suggested to be important for activity. Supported gold catalysts for CO oxidation can be generally
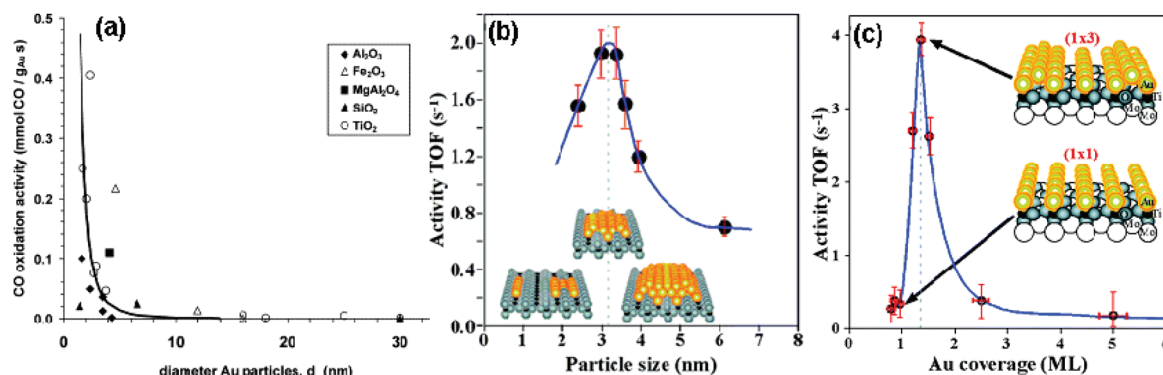
Figure 48. Measured activities (in mmol $CO/(g_{Au}s)$) for CO oxidation at 273 K over different Au-based catalysts as a function of the average particle size (d, in nm). Supports are indicated by the symbol shape. Open symbols are used for reducible supports and solid symbols for irreducible supports. The curve shows a $1/d^3$ guide to the eye, showing that the activity of gold catalysts is approximately proportional with the number of low-coordinated atoms at the corners of the gold particles. Reproduced with permission from ref 686. Copyright 2004 Elsevier. (b) Catalytic activity for CO oxidation as a function of particle size on the $TiO_2(110)$ at 353 K. Reproduced with permission from ref 291. Copyright 1998 American Association for the Advancement of Science. (c) Au coverage on the $Mo(112)$-(8×2)-TiO_x at room temperature. Reproduced with permission from ref 668. Copyright 2004 American Association for the Advancement of Science.

classified into four groups. When carbons (e.g., activated carbon) and polymers (e.g., PMMA and porous coordination polymers) are used as supports, Au nanoparticles are not active at all, even at temperatures above 373 K, strongly indicating the direct involvement of the support in the reaction.[676] On nonreducible metal oxides such as Al_2O_3 and SiO_2, Au nanoparticles are not active at 200 K but exhibit catalytic activity at room temperature in the presence of moisture.[677−679] On reducible metal oxides such as TiO_2, Fe_2O_3, CeO_2, and Co_3O_4, Au nanoparticles smaller than 5 nm are highly active both in the absence and in the presence of moisture. The catalytic activity in terms of turnover frequency sharply increases with a decrease in the mean diameter of Au nanoparticles. The fourth group is Au clusters deposited on metal hydroxides (e.g., $Be(OH)_2$, $Mg(OH)_2$, and $La(OH)_3$);[676] these hydroxides have been found to be effective as supports for Au nanoparticles and exhibit catalytic activity for CO oxidation at 200 K.

In a classical review, Bond and Thompson have summarized the following observations:[8,680] (i) the size of catalytically active gold nanoparticles is dependent on the type of metal oxide support and is typically less than 8 nm in diameter; the highest reactivity has been frequently obtained at sizes of 2−3 nm (Figure 48); and (ii) the preparation method of catalyst, the choice of support, and the pretreatment are crucial factors controlling the reactivity. A possible mechanism involving reaction at the perimeter interface between gold particles and the support has been proposed.[681] Likewise, Haruta has recently concluded that three major factors determine the performance of Au nanoparticles: the particle size of gold, the contact structure to the oxide support, and the nature of the support, with the contact structure being the most important.[682] In contrast to the perimeter model, Goodman's group stated that the primary role of the TiO_x support is to serve as a dispersant and a promoter based on their bilayered Au model in which the access of the support by the reactants is blocked.[668,683] Theoretical calculations also highlight the significance of the interface periphery between gold nanoparticles and the oxide support, e. g., the adsorption tendency of O_2 on finite-size Au particles is increased particularly at low-coordinated sites.[22,684,685]

Nature of the Active Site. Although extensive experimental and theoretical investigations have been performed to elucidate

the origin of the unique activity of supported gold nanoparticles, the nature of the active Au species still remains unclear. Generally, the origins of the catalytic activity of Au have been believed to stem from one or more of three contributions:[18,19,23] (i) quantum size effects; (ii) the presence of low coordination Au sites; (iii) charge transfer between Au and the support (e.g., the oxidation state of gold).

Quantum Size Effect. The activities of highly dispersed Au nanoparticles on oxide surfaces strongly correlate with the Au particle size (for example, see Figure 48).[4,7,8,18−20,23,291,668,685−693] Small Au particles adsorb CO more strongly.[647] Goodman and co-workers achieved the maximum reaction rate for CO oxidation on $Au/TiO_2(110)$ under realistic reaction conditions with Au mean particle size of ~3 nm and a thickness of two atomic layers (Figure 48b).[291] The importance of the thickness of the gold was further comfirmed by the same group based on studies of well-ordered monolayer and bilayer films of Au on a TiO_x thin film grown on $Mo(112)$ (Figure 48c).[668] The activity for CO oxidation at 5 Torr was more than an order of magnitude higher for the gold bilayer compared to a one-layer-thick film. Campbell's group noticed a decreased CO adsorption capacity (but with an enhanced binding energy) over the thinner gold particles.[661] Valden et al. ascribed this maximized activity to the transition between nonmetallic and metallic particles.[687] An increase in the binding energy of CO was observed with declining gold size from 1.8 to 3.1 nm; the maximum reactivity for CO oxidation was obtained with the highest CO binding energy.[691] A similar effect of particle size was also reported by Haruta et al. on the corresponding high-surface-area supported Au/TiO_2 catalyst.[7] The size of gold particles are crucial to the adsorption and activation of molecular oxygen, since CO oxidation to CO_2 at 77 K on $Au/TiO_2(110)$ is only weakly dependent on the particle size when the surface is populated with oxygen atoms.[91,661,694,695]

The size range in which the highest reactivity is attained depends upon the nature of the support and preparation method of the catalyst. For example, for a Au/TiO_2 catalyst prepared using a modified deposition−precipitation method and a new reductive conditioning method, the maximized reactivity was observed with particle sizes below 2 nm.[696] Hutchings and co-workers observed the highest catalytic activity in CO oxidation
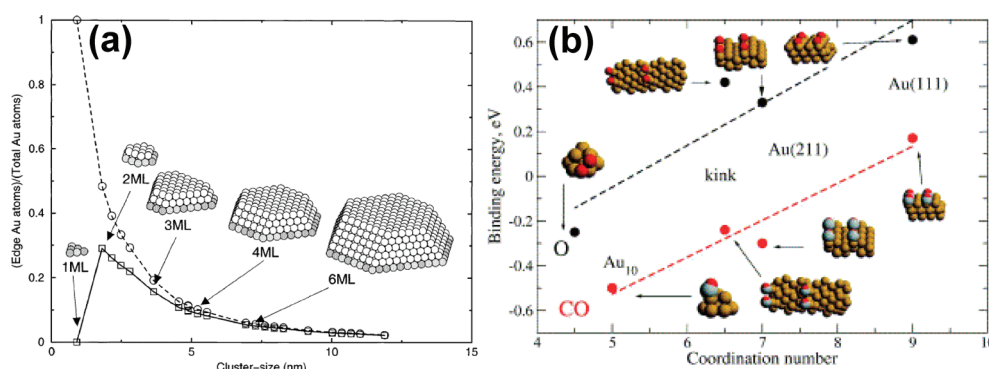
3035

dx.doi.org/10.1021/cr200041p | *Chem. Rev.* 2012, 112, 2987−3054

Figure 49. (a) Calculated step density for Au particles on TiO_2 as a function of particle size. (○) and (□) correspond to the total and "free" step sites on the Au particles. "Free" are the step sites not in direct contact with the support. Lines through the two sets of points are only drawn as a guide to the eye. Insets illustrate the corresponding Wulff constructions for selected particle sizes. Reproduced with permission from ref 2. Copyright 2000 Springer. (b) Correlation between the binding energies, for CO molecules and O atoms, with respect to the coordination number of Au atoms in a series of environments. Binding energies, in eV, reported are referred to gas-phase CO and O_2; for O_2 the energies are given per O atom. Reproduced with permission from ref 686. Copyright 2004 Elsevier.

on FeO_x covered with bilayer gold clusters that are ~0.5 nm in diameter and contain ~10 gold atoms.[697] Several groups used deposition of size-selected cluster cations to study CO oxidation on $Au_n/MgO(100)$[685,698] and $Au_n/TiO_2(110)$,[690,692] observing significant reactivity for clusters as small as Au_8 and Au_1, respectively. In particular, supported Au_{55} clusters (see review[699]) show strong oxidation resistance and unusual chemical behavior.[700]

Low-Coordination Au Sites. The presence of undercoordinated Au atoms at the corner, edge, and surface of small particles could account for the origin of the active sites, at which the binding of CO and O_2 are higher compared to the terrace and the smooth surface.[2,19,23,594,650,686,701-705] Theoretical calculations showed that carbon monoxide and oxygen only adsorb on gold atoms with a coordination number less than 8,[701] which was confirmed by CO IR adsorption on Au nanoparticles supported on TiO_2, ZrO_2, and FeO.[650,706] Mavrikakis et al. predicted from theoretical calculations that a significant number of coordinatively unsaturated gold atoms are present on Au nanoparticles supported on TiO_2.[2] In fact, Figure 49a illustrates that the step density (i.e., the fraction of atoms in gold nanoparticles with seven or less neighbors) increases with a decrease in the particle size (Figure 49a). The importance of coordinatively unsaturated gold sites has been further addressed by (i) calculated results showing that adsorption energies for both CO and O strongly depend on the coordination number of Au,[686] and (ii) experimental observations that nanoporous unsupported gold that is highly active for CO oxidation contains a high density of low-coordinate surface sites, such as step and kink atoms.[707,708] Figure 49b indicates the relationship between the strength of Au−CO and Au−O and the gold coordination number and that binding energies of both O and CO decrease by ~1 eV from Au(111) (with a coordination number of 9) to the Au_{10} cluster (with a coordination number of 4).[19] In contrast, a lower catalytic activity for monolayer Au (coordination number of 3−4) was reported by Chen and Goodman compared to bilayer Au (coordination number of ~6) (Figure 48c).[23] Additionally, although the density of the corner or edge sites increases continuously with a decrease in particle size (Figure 48b), the reactivity of supported Au nanoparticles declines when the size is below 3 nm. Therefore, low-coordinated corner or edge sites of gold alone are not the only factor that determines catalytic activity.[18]

Oxidation State of Active Gold Nanoparticles. The interaction between Au and the support induces a change in electronic structure of Au nanoclusters, which results in high catalytic activities for low-temperature CO oxidation (see refs 4, 19, 20, 23, 26, 65, and 680). In particular, despite a large number of studies, the oxidation state (Au^0, $Au^{\delta-}$, or $Au^{\delta+}$) of the active site of gold particles remains controversial. However, most studies, particularly based on model systems, have shown that metallic or slightly negative Au is responsible for the unique catalytic activities. The oxidation state for Au species is frequently obtained on the basis of the infrared spectra of CO. A blue shift (with respect to CO in the gas phase (2143 cm^{-1})) of the ν_{CO} band typically occurs on electron-rich Au clusters, whereas a red shift has been reported on electron-deficient clusters; the extent of the shift can thus be correlated with the electronic charge on Au. It has been generally accepted that metallic gold possesses a CO stretching band at ~2110 cm^{-1}. The absorption bands in the 2200−2150 cm^{-1} region are usually assigned to $Au^{\delta+}$−CO bonds.[18] Hadjiivanov and co-workers have proposed that the bands at ~2140 cm^{-1} should be originated from CO adsorption on the Au^+ sites on the surface of the metallic Au particles but not on the oxide support.[709] Naya et al. showed that the majority of Au deposited at 85 K on a reduce $CeO_2(111)$ surface is positively charged, giving $\nu(CO)$ peaks at approximately 2130 and 2145 cm^{-1},[674] consistent with a previous CO-XPS study by Weststrate et al.[632] Negatively charged $Au^{\delta-}$−CO species lead to vibrational bands in the range between 1800 and 2050 cm^{-1}.[18,641,644,710] The nature of intermediate bands between 2110 and 2140 cm^{-1} is less understood, which may be associated with partially oxidized gold[711,712] or small metallic Au clusters.[65]

Haruta[3] and Campbell[713] have proposed that the active species could be small metallic gold particles. It is generally believed that the activation of CO occurs on the metallic surface of gold nanoparticles while the boundary between the support and gold is the active site for dioxygen.[3] Goodman and co-workers employing a $Au/TiO_2(110)$ model system found that metallic gold is indispensable to obtain high catalytic activity.[291,668] Gates and co-workers reported that cationic Au was rapidly reduced completely to Au^0 under CO oxidation conditions investigated on $Au/FeO_x/TiO_2$ using extended X-ray absorption fine structure (XANES) and EXAFS.[714] These results

provide strong evidence for the presence of Au^0 rather than cationic Au in the working catalysts. Schwartz et al. performed an X-ray adsorption spectroscopy (XAS) study on Au/TiO_2 catalysts and concluded that oxidized gold may not be necessary for high activity.[715] The necessity of metallic Au for high CO catalytic oxidation rates was also confirmed for Au/TiO_2 by Kung and co-workers based on combinational results from in situ XAS, microcalorimetry, and TEM experiments.[716] With XANES and ^{13}C isotopic transient experiments, Calla et al. also concluded that active Au/TiO_2 and Au/Al_2O_3 catalysts contain predominately metallic Au.[717]

Negatively charged gold particles can also be formed upon transfer electron from defect sites (e.g., oxygen vacancies) to gold nanoparticles. DFT calculations showed that gold atoms can stabilize oxygen vacancies at the $CeO_2(111)$ surface and attract the excess electrons of the defect.[718] Perturbing of the electronic structure of gold (Au^-) via strong interaction between the metal and oxygen vacancies in the oxide could promote the catalytic activity.[713,719] As discussed earlier, the active sites could be located on the perimeter of the gold–oxide interface or Au particles.[713,720,721] Yoon et al. showed that CO oxidation readily occurs on gold octamers (Au_8) supported on MgO(001) that possesses abundant oxygen vacancies (i.e., F centers); in contrast, the similar system nearly free of oxygen vacancies is catalytically inactive.[710] A correlation has been drawn between the activity of Au particles and the surface concentration of F-centers (defects) of a MgO support, indicating a vital role of surface F-centers in Au/MgO catalysts.[644,722] Regarding the monolayer and bilayer structure of gold proposed by Goodman's group, Au monolayer on reduced titania yields a single ν_{CO} mode $(\sim 2107 \text{ cm}^{-1})$ corresponding to CO adsorbed on an atop Au atom. For the bilayer structure, CO can access to both the first and second layers of Au atoms, leading to a broad ν_{CO} feature at 2109 cm^{-1}, which can be split into two bands at 2107 and 2112 cm^{-1}.[668] These two features are ascribed to adsorbed CO on first-layer and second-layer Au, respectively, and CO binds more tightly to the first layer.[668] High-resolution electron energy loss spectroscopy measurements indicated a $Ti^{4+}-O$ vibrational band on the TiO_x surface covered by a gold film, which supports the argument regarding formation of negatively charged Au due to the charge transfer from Ti^{3+} to Au.[871] Additionally, photoelectron spectroscopy has also been employed to study the charge transfer from oxygen vacancies of $TiO_2(110)$ to gold particles.[723]

Electron-rich Au $(Au^{\delta-})$ nanoparticles facilitate activation of CO and adsorb O_2 more strongly; activation of the O–O bond occurs via charge transfer from Au forming a superoxo-like species.[18,686] Moreover, Mullins and co-workers showed that molecularly chemisorbed oxygen on $Au/TiO_2(110)$ can react directly with CO to form CO_2 without O_2 dissociation.[117,724] This agrees with the observation that electron-rich Au facilitates activation of the O–O bond and the reaction pathway for CO oxidation on small Au particles proceeding via a dioxygen species rather than atomic oxygen.[725]

The crucial role of cationic gold (e.g., Au^+ and Au^{3+}) in CO oxidation has been reported in a variety of investigations. The general consensus is that reactivity of supported gold catalysts increases with a decrease in an average particle size of gold, which leads to increased contact perimeter between gold and the support and a change in the electronic nature of the gold atoms.[4] Indeed, the active species in Au catalysts has been suggested to be AuO_x nanoparticles or more specifically cationic
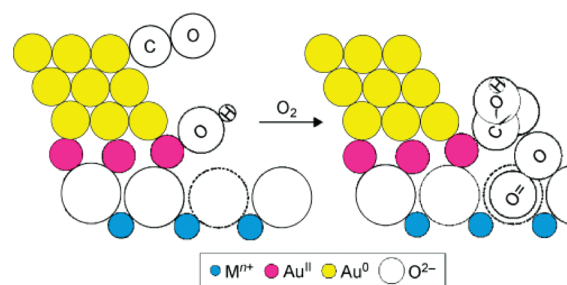

Figure 50. Proposed model for the active site of a supported gold catalyst incorporating the essential features of cationic gold at the interface of the gold nanoparticle with the support, surface vacancies, and the involvement of a hydroxy group. Much of the current experimental evidence is in agreement with this proposal.[680]

species.[23,726−733] Lee and Schwank were among the first to propose that cationic gold is the active sites in Au/MgO and Au/SiO_2.[726] Bond and Thompson have suggested that gold atoms at the peripheral interface of gold and the oxide could be cationic in character, and it is these atoms that are responsible for the activation of dioxygen in oxidative reactions.[680] Kobayashi et al. concluded that cationic gold is the active species for CO oxidation since the highest activity was found on a $Au/Mg(OH)_2$ catalyst with the largest amount of Au^+.[727] Guzman and Gates performed XAS measurements to investigate the valence state of Au particles with a diameter of ~ 3 nm supported on MgO for CO oxidation[728] and found increased formation rate of CO_2 with an increase in Au^+ concentration. Under reaction conditions metallic gold is not likely present; thus, the authors concluded that cationic gold was essential for CO oxidation.[728,734] However, the reaction rate of $\sim 2 \times 10^{-3} \text{ s}^{-1}$ over Au/MgO observed by Guzman and Gates is far lower than rates found for active metallic Au nanoparticles.[18,668] The same group also found both cationic and metallic gold are present in Au/CeO_2 and directly correlated the reactivity for CO oxidation with the Au^{3+} concentration.[293] Hutchings and co-workers investigated the oxidation states of Au in Au/Fe_2O_3 catalysts for CO oxidation using X-ray absorption and Mössbauer effect spectroscopies and showed that the most active catalysts contain abundent Au^{3+} species.[731] These reports, however, cannot rule out the contribution of metallic gold to the catalytic activity; it is very likely that cationic Au may assist metallic Au in catalytic CO oxidation. One should note that the TOF of CO oxidation on 5 wt %Au/Fe_2O_3 in Hutchings' experiments is much lower than those observed for metallic Au catalysts by Haruta and Goodman.[5,291] Boyd et al. showed that Au^+ was active, but again the combined role of cationic gold species with Au^0 could not be ruled out (a schematic proposed by Bond and Thompson is shown in Figure 50).[730] It should be noted that a body of data shows that, although cationic Au is active for CO catalytic oxidation, its activity is significantly lower than the activity of metallic Au nanoparticles.

Although there have been numerous studies to date, including model systems, there is a lack of a definitive study concerning the exact roles of the active oxidation state of gold nanoparticles for CO oxidation. Clearly, it is still an area that attracts much attention in which contributions from surface science can play a significant role.

Role of Moisture. As discussed earlier, a number of investigations have shown that the adsorption and activation of O_2 could

3037

dx.doi.org/10.1021/cr200041p |*Chem. Rev.* 2012, 112, 2987–3054

occur at the interface between gold and oxide support. However, there is a lack of fundamental understanding regarding how the interface area, although limited, is responsible for the activation process.[19,735] It has been shown that adsorbed water, frequently at the interface or the oxide surface, has a promotional effect, particularly when the perimeter of interface is not sufficient to provide enough oxygen for the reaction.[247,677,735−738] Haruta and co-workers demonstrated that turnover rate of CO over Au/TiO$_2$ at 270 K increases in the presence of water (e.g., up to 200 ppm) while the rate decreases at higher water concentrations.[677] The reaction rate with 0.1 ppm of water is 1 order of magnitude higher compared to 3 ppm of water (a typical reaction condition). Gao et al. have shown that the presence of water in the reactant had two effects on reactivity of Au/TiO$_2$(110):[739] (1) a decrease in CO coverage, and (2) the appearance of a carbonate species. The authors noted that since both effects inhibit CO oxidation the promotional effects of water reported previously are probably validated only for adsorption and activation molecular of oxygen. UHV results presented by Ting el al. support the finding by Gao and Goodman in which the production of CO$_2$ decreases on a water precovered surface due to reduced uptake of CO.[740] These results further inferred that carbonate species is first formed on the TiO$_2$ surfaces prior to the diffusion to Au sites and that surface hydroxyl species may play the same promotional role as adsorbed water.

The influence of moisture on CO oxidation is strongly dependent on the type of the oxide support.[19] In a recent theoretical study,[735] Liu et al. showed that oxygen vacancies on TiO$_2$(110) are active sites for the dissociation of water to form hydroxyl species, which are able to facilitate the adsorption of O$_2$ adsorption. The resultant hydrogen atoms induce the charge transfer from the oxide to upcoming oxygen.[19] Bongiorno and Landman using DFT calculations examined the role of water in CO oxidation on gold nanoparticles supported on a perfect MgO(100) surface.[738] They found a hydroperoxyl-like intermediate in the optimized coadsorption configuration and that charge transfer to oxygen induced its activation.

Active Oxygen Species. Numerous attempts have been made to determine the structure of active oxygen, but the nature of active oxygen species in CO oxidation is still elusive. It possibly depends on the structure of the Au species and oxide supports as well as the reaction conditions. Three type of oxygen species—atomic oxygen, activated molecular oxygen, and peroxide-based species—are typically considered catalytic reactive.

Although gold surfaces only weakly bind CO molecules, upon being covered by atomic oxygen it readily catalyzes CO to form CO$_2$.[19,91,661,695] Despite the rapid reaction observed in the presence of atomic oxygen, dissociation of molecular oxygen has been considered as the rate-limiting step. Indeed, dissociation probability of molecular O$_2$ on bulk Au surfaces and supported nanoparticles is fairly low (in the level of $10^{−7}$).[90] However, the presence of undercoordinated Au atoms could promote the dissociation of molecular oxygen.[90,741] Results from DFT calculations showed that activation barriers for O$_2$ dissociation are dependent on coordination number and the lattice constant of of Au[106] and suggested that smaller gold nanoclusters supported on oxides should have a lower barrier for O$_2$ dissociation due to the higher concentration of steps.[2]

Alternatively, molecular oxygen can be dissociatively adsorbed on defect sites (e.g., oxygen vacancies) of reducible oxide supports. It has also been proposed that a peroxo species (−HO$_2$), or its transformative form, could be the active oxygen

species for CO oxidation.[106,117,293,724,738,742] For example, Xu and Mavrikakis observed the reaction of CO with η^1-superoxide or peroxide on Au/CeO$_{2−x}$.[106]

Mullins and co-workers employed molecular beam scattering measurements which showed that molecular oxygen could also directly react with CO on a Au/TiO$_2$(110) surface.[117,724] Theoretical calculations suggested the formation of O−O−CO metastable intermediate (with an activation barrier of ∼0.46 eV) on Au steps[246] or very small gold clusters (e.g., Au$_2^{−}$[743]). This intermediate could further undergo decomposition to form CO$_2$ and adsorbed O; the latter could again readily react with CO.

7.3.2. Propylene Oxidation. The seminal discovery by Haruta et al. regarding selective epoxidation of propylene using gold catalysts has spurred the general interest in this reaction.[744] This reaction shares many similarities to CO oxidation, but mechanistic aspects such as reaction pathways are more complicated. Min and Friend have elegantly reviewed product distributions and possible reaction paths on various gold-based catalysts.[19]

Campbell and his group demonstrated that propylene only adsorbs on the specific sites at the interface between gold particles and the support.[745] With a 1.5 ML gold coverage TiO$_2$(110), two distinct peaks (i.e., 150 and 240 K) were observed from propylene desorption at low coverages. The low-temperature desorption peak was originated from bulk gold surfaces.[98] A third peak appeared at 190 K with an increase in coverage of propylene, corresponding to desorption from titania. The authors speculated that sites located at the particle−support interface could account for the high-temperature peak.[745]

The pathway of propylene oxidation strongly depends on the type of metal oxide.[19] Selective oxidation only occurs when either the anatase phase of TiO$_2$ or titanosilicate is used as a support for gold nanoparticles.[746] Gold nanoparticles supported on TiO$_2$ (anatase) are among the most selective catalysts, in which a 90% selectivity to propylene oxide can be obtained in the presence of both oxygen and hydrogen.[744,747,748] TiO$_2$−SiO$_2$ nanocomposites with mesoporous crystalline structures are active for this reaction as well, and an optimized Ti:Si ratio is typically below 3:100.[749−754] Au/Fe$_2$O$_3$ is not selective to propylene oxide and catalyzes the combustion reaction effectively.[755] Additionally, partial oxidation products such as acetone, acrolein, and C$_2$ oxygenates evolved on Au nanoparticles supported on irreducible oxides (e.g., SiO$_2$, MgO, and MoO$_2$).[755]

Several excellent reviews have pointed out experimental requirements in order to obtain high selectivity to partial oxidation products.[19,747] Both hydrogen and oxygen are essential for high attaining high selectivity of propylene oxide.[756,757] A particle size effect for this reaction require average particle size of gold less than 5 nm to efficiently catalyze the reaction.[758] The selelectivity and reactivity of this reaction also strongly depends on the preparation method of catalysts. Specifically, the deposition−precipitation method is suitable to synthesize catalysts with high selectivity for epoxidation, whereas combustion is predominant for catalysts produced employed the impregnation method.[19] This could be originated from different contact structures (e.g., interface) of gold particles with the oxide support as well as electronic properties of gold and the oxide. Additionally, alkaline ions have often been used as promoters for this reaction.[756,759]

A hydrogen peroxo-like species has been proposed as the active oxygen species for the epoxidation of propylene, although it is largely based on speculations from experimental
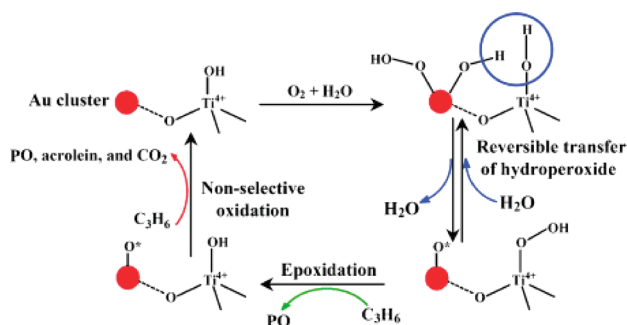
3038

dx.doi.org/10.1021/cr200041p |*Chem. Rev.* 2012, 112, 2987−3054

Figure 51. Possible route for propylene epoxidation with $O_2 + H_2O$ over Au/TS-1 (TS-1 was pretreated by alkaline soultion). Reproduced with permission from ref 759. Copyright 2009 Wiley-VCH Verlag GmbH & Co. KGaA.

results.[759−763] Atomic oxygen could also be reactive for the epoxidation as seen on Ag-based catalysts, and dissociation of O_2 could be the rate-limiting step due to the high activation barrier.[19,759]

The nature of active sites for the epoxidation is still elusive, which needs to be answered in future investigations. As mentioned earier, only TiO_2- or Ti-containing oxide supports promote the reaction, but the differences in elementary steps are not clearly known. Haratu and co-workers proposed a possible reaction pathway for the epoxidation reaction over Au/TS-1 (Figure 51).[759] Specifically, molecular oxygen reacts with H_2O on gold nanoclusters to produce −OOH species; the −OOH species reversibly diffuse from gold surfaces to neighboring Ti sites to form Ti−OOH species, which are responsible for subsequent epoxidation. It is likely that during the reaction O· radicals would be produced and further used to oxidize C_3H_6 to propylene epoxide, acrolein, and CO_2,[764] which was also observed on Au(111).[256] Therefore, selectivity of propylene epoxide should be improved by tuning the reactivity of O radicals over the surfaces of gold nanoclusters.[759] Another puzzle is regarding the exact role of gold nanoparticles in this reaction since bare Ti-containing silica or silicate is highly reactive for the epoxidation.[765,766]

Another issue we need to mention is the underlying basis for the thermal stability of gold catalysts for the oxidation of propylene since the deactivation is frequently reported. Accumulation of byproducts (e.g, carbonates[767]) on active sites or sintering of Au nanoparticles are two major culprits accounting for the deactivation; the former could be the primary reason for the deactivation.[768] High pressures of O_2 under realistic reaction conditions would even accelerate aggregation of gold nanoclusters.

7.3.3. Water−Gas Shift Reaction. Hydrogen energy has attracted much attention for the past few years, particularly considering the depletion of conventional fossil fuels. Commercial production of hydrogen always accompanies a certain level of CO that must be removed, for example, via the water−gas shift reaction, before feeding fuel cells (CO deactivates the Pt-based electrode catalysts). The reaction typically requires a catalyst with superior activity at low temperatures (e.g., below 250 °C).[769] Cu-based catalysts, both pure and supported on metal oxides, fall among the more active and promising for the water−gas shift reaction, although the origin of their reactivity is not fully understood but has been suggested to be highly dependent on the synthesis conditions and/or the nature of

the oxide support.[292,770] Either metallic Cu or Cu^+ cations have been considered as the active sites for the WGS reaction.[292] Oxide mixtures of CuO−ZnO or CuO−ZnO/Al_2O_3 are commercially used for this reaction at temperatures between 450 and 525 K. However, these catalysts are pyrophoric, and standard activation steps before usage are rather lengthy and complicated.[771] Gold nanoparticles supported on oxides possess the required high activity, but the feasibility of using these catalysts under *real* conditions is still questionable.

The use of gold catalysts for the water−gas shift reaction at low temperature was first reported by Andreeva's group for Au/Fe_2O_3 catalysts.[772,773] Subsequently, Venugopal et al. added Ru to Au/Fe_2O_3 catalysts and found a significant enhancement in catalytic performance.[774,775] Hua et al. reported that certain types of metal oxides can also act as promoters for the Au/Fe_2O_3 catalyst.[776] Daniells et al. examined the same catalysts and found that traces of water enhance the reaction at ambient temperature, but much higher temperatures are required at higher concentrations of water.[777] Haruta's group has shown that Au/TiO_2 is also active for this reaction.[778]

CeO_2 has recently attracted considerable interest as a support for the water−gas shift reaction since the seminal discovery by Flytzani-Stephanopoulos and co-workers, who found that Au/CeO_2 was more active than Au/TiO_2.[770,779,780] The same group also reported an enhanced catalytic activity upon treatment of the Au/CeO_2 catalyst with CN^- ions.[292] Most of the gold (e.g., particularly metallic) was leached from this treatment, and the authors proposed that cationic gold could be the active species. Yi et al. illustrated that strong bonded Au_n−O−Ce species could be the active sites for the reaction.[781,782] Indeed, DFT calculations demonstrated that the presence of empty localized nonbonding f states in CeO_2 facilitate the oxidation of Au, thus enabling CO adsorption.[783] The active site for the water−gas shift reaction could consist of Au clusters of 4−6 atoms anchored on an oxygen vacancy on the CeO_2 surface.[4] However, gold cations are not thermally stable at the elevated temperatures at which the water−gas shift reaction is carried out, and thus these theoretical results are more relevant to reactions at ambient temperature, for example, CO oxidation. Haruta and co-workers employing transient experiments with CO and H_2O pulsing into H_2 and He discovered that the WGS reaction took place at the interface of Au nanoparticles and reduced CeO_2 surfaces.[784] Tibiletti et al. used NEXAFS and XANES coupled with theoretical approaches to study Au/CeO_2 catalysts and found that both metallic and cationic gold species could be active for the water−gas shift reaction, although the amount of the oxidized species is below the detection limit of the XANES.[785]

In order to draw a better correlation between WGS activity and surface structure, Rodriguez and his group systematically investigated Au/TiO_2(110) and Au/CeO_x/TiO_2(110) surfaces as a function of Au coverage (Figure 52).[786,787] The Au/TiO_2-(110) systems are active in the WGS reaction, but the reactivity is considerably lower than that of Au/CeO_x/TiO_2(110).[771] The Au/CeO_x/TiO_2(110) catalyst is also more reactive compared to Au/CeO_2(111),[626] Cu/ZnO(000$\bar{1}$),[626] CeO_x/Au(111),[294] and copper single crystals.[626,787] It has been proposed that the concentration of active sites is proportional to the number of ceria regions in contact with gold nanoparticles.[786,788] ISS measurements indicated that only 12% of the titania support was covered by ceria regions; thus, the Au/CeO_x/TiO_2(110) catalyst should be at least 300 times more active than Cu(100) on a per-active-site basis.[626,786] Even more active WGS catalysts
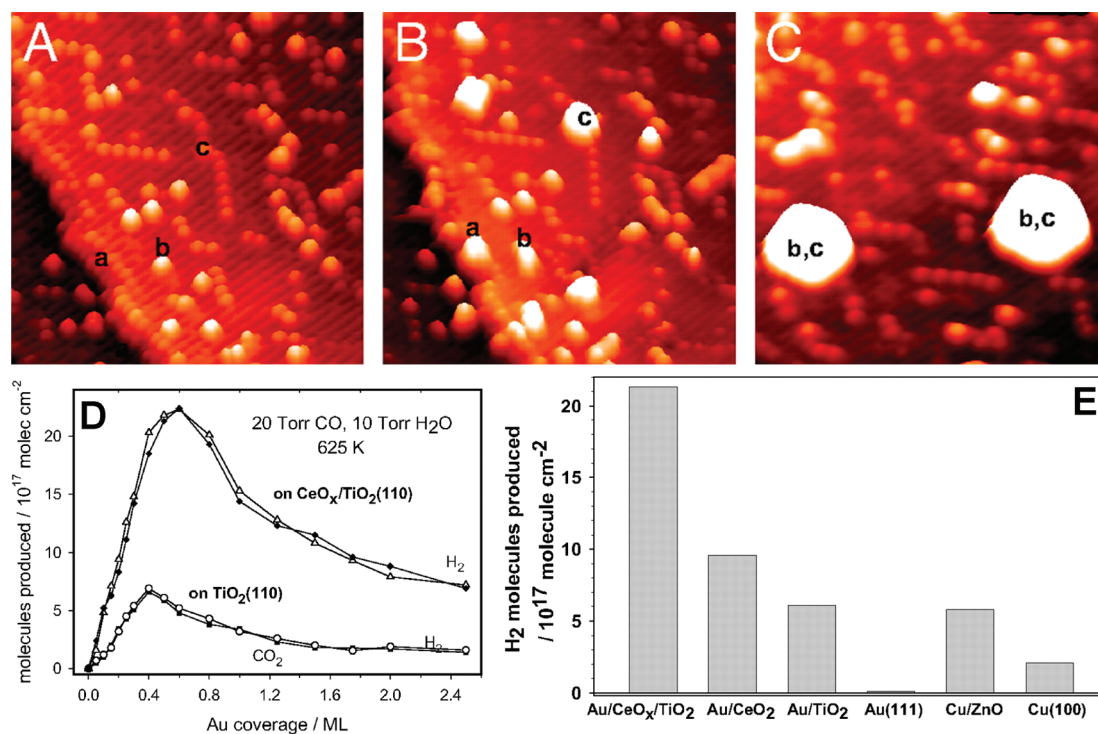
Figure 52. (A−C) Morphology of Au/CeO$_x$/TiO$_2$ (110). (A) STM image of a CeO$_x$/TiO$_2$(110) surface. Ce was deposited at 600 K under an atmosphere of O$_2$ ($\sim$1 × 10^{-7} Torr), and then the sample was annealed at 900 K in O$_2$. (B) STM image for a Au/CeO$_x$/TiO$_2$(110) surface. The gold was deposited on the same area shown in A at 298 K. Approximately 6% of the surface was covered with Au. (C) STM image obtained after annealing the system in B to 600 K. All of the STM images correspond to an area of 20 × 20 nm and imaging conditions of V_t = 1.5 V and I_t = 0.03 nA. (D) The WGS activity of Au/TiO$_2$(110) and Au/CeO$_x$/TiO$_2$(110) as a function of Au coverage. The area of TiO$_2$(110) covered by CeO$_x$ was measured with ISS, before depositing gold, and found to be $\sim$12% of the clean substrate. The reported values for the production of H$_2$ and CO$_2$ were obtained after exposing the catalysts to 20 Torr of CO and 10 Torr of H$_2$O at 625 K for 5 min. The number of H$_2$ and CO$_2$ molecules produced is normalized by the sample surface area. (E) Comparison of the WGS activity of Cu(100), Au(111), and 0.5 mL of Au supported on TiO$_2$(110), CeO$_2$(111), or CeO$_x$/TiO$_2$(110). Reproduced with permission from ref 786. Copyright 2009 the National Academy of Sciences of the United States of America.

were found after depositing Cu and Pt on CeO$_x$/TiO$_2$(110).[788] In the M/CeO$_x$/TiO$_2$(110) (M = Cu, Au, Pt) systems, there is a strong coupling of the chemical properties of the admetal and the mixed-metal oxide.[786,788] The high catalytic activity of M/CeO$_x$/TiO$_2$(110) is likely to be ascribed to the unique chemical properties of the Ce$_2$O$_3$ dimers supported on titania. The dissociation of water is commonly considered as the rate-determining step in the WGS reaction.[789] The Ce^{3+} sites present in CeO$_x$/TiO$_2$(110) easily dissociate water,[788] but highly stable HCO$_x$ species are formed on the oxide surface upon exposure to CO and there is no production of H$_2$ or CO$_2$ gas. The Au/CeO$_x$/TiO$_2$(110) systems are bifunctional catalysts: oxide sites facilitate the adsorption and dissociation of water and CO adsorbs on metal nanoparticles. The subsequent reaction steps happen at interfaces between the oxide and metal nanoparticles. Notably, it has been verified in experiments with high-surface-area powder Pt/CeO$_x$/TiO$_2$ catalysts, which in many aspects show a behavior similar to that seen for Pt/CeO$_x$/TiO$_2$(110) surfaces.[790] The approach could generally apply to catalysts containing ceria,[787] spurring research interests in controlling catalytic activity via coupling appropriate pairs of oxides.

We need to note that even though Au/CeO$_2$ catalysts are significantly more reactive than commercial Cu-based catalysts, they are easily deactivated by carbonates and/or formates.[791]

Stability and Deactivation of Gold Catalysts. Burch[769] and Bond[792] have provided excellent overviews concerning underlying reasons for the deactivation of gold catalysts for the

water−gas shift reaction. The deactivation is generally attributed to the sintering of gold nanoparticles[769,792,793] and changes in the valence state of gold and/or support cations.[780,794] Additionally, formation of the formate species[791] or monodentate CO$_3^-$, at least at high CO$_2$ concentrations[793] could be responsible for the catalyst deactivation. Therein, the formation path of the CO$_3^-$ species is unclear, but it could decompose at higher temperature. Considerable efforts have been made to improve the stability of gold-based catalysts for the WGS reaction. For example, the presence of traces of O$_2$ (e.g., 0.5%) slows down the deactivation of Au/CeO$_2$.[795] Another strategy is to stabilize the Au$^{\delta+}$ species at the interface between gold nanoparticles and the support in order to enhance the binding energy of chemisorbed CO.[783]

Different deactivation mechanisms could be applied to the same catalyst simultaneously dependent on reaction conditions.[769] For instance, sintering of gold nanoparticles became severe at higher temperatures, leading to the irreversible loss of the contact length between gold nanoparticles and the oxide.[785,796−798] At intermediate temperatures, carbonates could be readily formed, which gradually blocks the active sites and causes a slow deactivation.[770,791,795] In the presence of moisture at low temperatures, the irreversible loss of activity could be ascribed to a decrease in surface area of the support.[770] The ultimate loss of reactivity occurs upon the complete destruction of interaction between gold particles and the support.[769]

Proposed Mechanisms for WGS.[769,792]. A large number of investigations have attempted to elucidate the reaction

3040

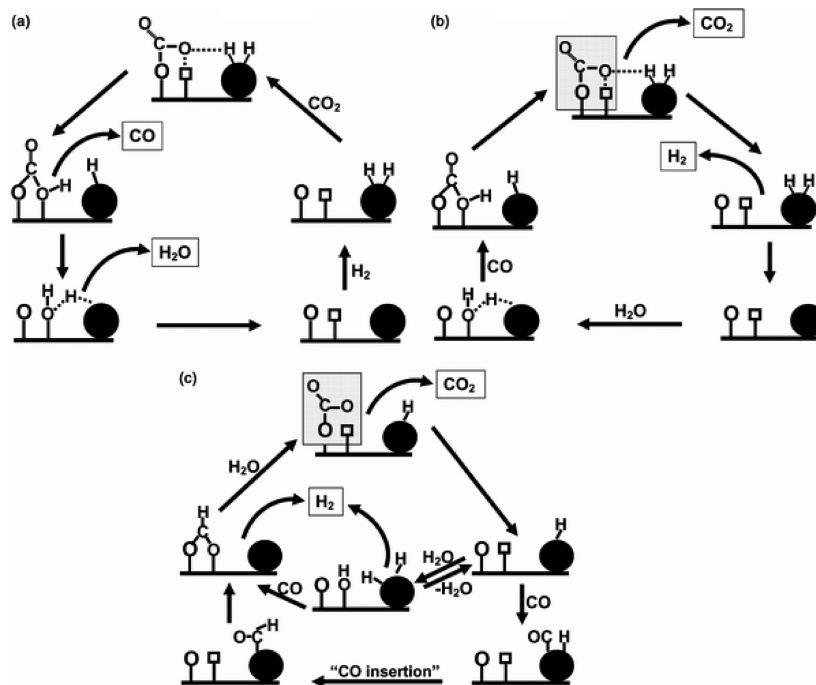dx.doi.org/10.1021/cr200041p |*Chem. Rev.* 2012, 112, 2987−3054

Figure 53. (a) Proposed "carbonate/carboxylate" mechanism for the reverse WGS reaction. (b) Proposed "carbonate/carboxylate" mechanism for the WGS reaction. (c) Proposed "universal" mechanism for the WGS reaction. Note H species attached to Au particles are not intended to imply a stable species, but simply a very transitory species that provides a route to spillover hydrogen and may be formed at surface defects or via assisted adsorption. Reproduced with permission from ref 769. Copyright 2006 Royal Society of Chemistry (the PCCP Owner Societies).

mechanism for the low-temperature WGS reaction over gold-based catalysts.[769,792] In their seminal reviews, Burch[769] and Bond[792] have summarized possible mechanisms for the reaction, among which two types of mechanisms (the redox mechanism and the associative mechanism) are most commonly accepted (Figure 53). Surface carbonates or carboxylates have often been considered as major intermediates involved in the rate-determining step for both mechanisms. As discussed earlier, the mechanistic pathway strongly relies on reaction conditions, and one cannot easily validate a sole mechanism while ruling out others, even for the same catalyst.

A possible universal mechanism for the WGS reaction has been proposed based on experimental and theoretical investigations.[769] We should note that the applicability of any part of this model is a function of the experimental conditions and should include the choice of support (Figure 53). A key part of this universal mechanism is the recognition that all the mechanisms proposed in the literature are subsets of a single process. This is clear from the "formate" model where the decomposition of a "carbonate" is needed to complete the catalytic cycle. Moreover, if the first and last steps are separated in time, then this is a statement of the "redox" model.[769,792]

Figure 53a and 53b represents proposed mechanisms for the reverse and forward WGS reactions, respectively. It is obvious that both carbonates and carboxylates play a crucial role in both cases. The reversibility of this mechanism could help understand the nature of active sites of catalysts for both the forward and reverse reactions. A possible universal mechanism for the WGS reaction proposed based on experimental and theoretical investigations is shown in Figure 53c.[769] The production of formate could be most energetically favorable in this mechanism, particularly when H and CO both adsorbed on the gold surfaces (note that small metallic gold particles can dissociate and adsorb hydrogen[799]).

7.3.4. Adsorption and Reaction of SO_2. SO_2 is a representative of phenomena that the interaction of adsorbates with supported gold nanoparticles is different compared to single-crystal surfaces. Rodriquez et al., employing XPS, observed the dissociation of SO_2 on gold nanoclusters on $TiO_2(110)$ with an average size of 2.6 nm (versus only SO_4 produced on clean $TiO_2(110)$),[132] even though the binding of SO_2 is weak on bulk gold surfaces.[163] The authors proposed that the role of gold is to enhance the exchange of vacancies between the surface and the bulk of TiO_2, while the electronic structure of gold can be, in turn, altered by oxygen vacancies. Indeed, DFT calculations also indicated that the presence of gold nanoparticles on these oxygen vacancies greatly facilitated dissociation of SO_2.[132,616,625] The importance of the oxygen vacancy was also reported for Au/$CeO_x(111)$. The heat of adsorption of SO_2 on Au nanoparticles supported on stoichiometric $CeO_2(111)$ was 4−7 kcal/mol larger compared to Au(111).[625] Negligible decomposition of SO_2 was observed on Au/$CeO_2(111)$; however, upon introduction of oxygen vacancies on the ceria surfaces, SO_2 experienced complete dissociation. AuO_x/CeO_2 were reported to be much less chemically active compared to Au/$CeO_2(111)$ or Au/CeO_{2-x}-(111) catalysts. The active sites in (Au + AuO_x)/ceria catalysts were suggested to be gold nanoparticles in contact with O vacancies.[625]

Rodriguez and co-workers also examined the effect of support by comparing adsorption behaviors of SO_2 on Au/TiO_2 to Au/MgO.[800] No dissociation of SO_2 was observed on Au/MgO, although the heat of adsorption of SO_2 was ∼7 kcal/mol larger than on Au(111). Corner sites (i.e., Au atoms with a low coordination number) on the Au nanoparticles were proposed to be responsible for this difference.[800] Additionally, considering that the particle size of Au was about the same on both substrates, the authors suggested that the metal−support interaction plays a significant role in determining the surface reactivity.[800] One

should also note that an effect of charge polarization induced by Au—C interactions was observed for SO_2 dissociation on a Au—TiC(001) surface.[801]

8. SUMMARIES AND PERSPECTIVES

Heterogeneous catalysis by gold is now under burgeoning development and has been explored via a considerably increased number of experimental and theoretical investigations including both nanosized gold clusters and gold single crystals. It is clear, from the extensive literature presented, that these gold-based model catalysts are very active for low-temperature oxidation of CO, water—gas shift reaction, and oxidations of hydrogen, ammonia, amines, NO, olefins, and alcohols.

From a surface science perspective, it is difficult to standardize preparation techniques and characterize physicochemical properties for real catalyst systems. Indeed, in many cases the various results, which were obtained for the same catalysts but reported by different groups (reproducibility is also an issue[802]), seem to be directly contradictory. Therefore, mechanistic aspects regarding the activity of supported gold nanoclusters are still under debate, particularly for the active site structure, particle size dependence, stability, and molecular oxygen activation process.[10,803] Fortunately, surface science approaches using model systems could make strong contributions with this respect, although both materials and pressure gaps have to be considered.[804,805] The most important characteristic of the model system is that one can start from simplicity to complexity in a stepwise manner, which would, in principle, sort out the effect of each experimental variable via surface phenomena observed. Employing a variety of surface science techniques, we are now somehow able to specifically design and prepare the catalysts with tunable reactivity and selectivity for certain reactions.

The *structural discrepancy* between the practically used conventional catalysts and the planar model systems should always be taken into account. Bridging this materials gap could be even more challenging and complicated than overcoming the pressure gap, which requires systematic work. A comparison of various facets of an oxide support covered with Au nanoclusters of defined size in terms of adsorption and reaction properties could be a first step toward this goal. Subsequently, a better understanding of surface structure and morphology of these catalysts accompanied with detailed kinetic analysis could help design practically relevant Au and oxide catalysts.[806]

One of the major remaining challenges is regarding the structural and electronic nature of the active site for supported gold nanoclusters. Numerous investigations have proved it a highly controversial subject. For example, why high reactivity is typically obtained with restricted gold size range is not yet fully understood.[291,668] We need to recall that in catalytic reactions at least one of the reactants is chemisorbed on gold surfaces, even if it sometimes spills over onto the support. Surface gold atoms, particularly those on sufficiently small particles, lack metallic character due to their low-coordination number and often have better chemisorptive ability.[8] This ability could also be originated from surface mobility and the electronegativity of gold. Additionally, the details of the sintering mechanism and the design/synthesis of functional oxide supports to enhance the gold—support interaction and to retard particle sintering should also be explored. We must recognize that it is difficult to really define active sites because there is no real information about the morphology of the catalytic surfaces under reaction conditions. Detailed in situ STM and/or TEM experiments and quantum mechanical studies of model systems and their interactions with reagent molecules are an urgent necessity.

The activation of molecular oxygen on gold-based materials is obviously another important concern. Both large Au particles and Au single crystals are not active for dissociation of O_2, which could be a key step in reactions. It is clear that the size and shape of gold nanoparticles influence the dissociation of O_2, and the water moiety could also affect interactions of oxygen with oxide support.[19] However, there is no general consensus regarding the identity of active oxygen species for high-surface-area gold-based catalysts;[742] the most frequently suggested adsorbed species include atomic oxygen, hydroperoxy ($\cdot HO_2$) intermediate when moisture is present, and activated molecular oxygen. Detailed mechanistic studies aimed at understanding the identity of the activated oxygen species are urgently required. Model studies on oxidized Au(111) demonstrate, however, that atomic oxygen is very active for low-temperature oxidation reactions, which could illustrate elementary reaction steps on "real" gold catalysts. Further model catalytic studies of oxidative reactions over gold single-crystal supported inverse metal oxide [i.e., TiO_x/Au(111) and CeOx/Au(111)] as well as size-selected Au clusters on metal oxide may help elucidate these mechanistic details and design a more efficient gold catalyst for commercial application.

Even though mechanistic aspects of low-temperature CO oxidation are relatively well manipulated, most other reactions catalyzed by gold are less understood, partially due to the complexity of the reaction system. Taking the propylene oxidation, for example, the underlying basis regarding how Ti-based support promotes catalytic stability of catalysts is not exactly known.[19] Surface science investigations on a number of reactions, including CO preferential oxidation (PROX) in hydrogen-rich gas streams, oxidation of volatile organic compounds (VOCs), and hydrogenation reactions, are fairly limited, which, in turn, renders future model studies an opportunity. Notably, Pan et al. have very recently reported on hydrogenation of acetaldehyde to ethanol on Au(111) precovered with atomic hydrogen.[807] The recent developments in aberration-corrected scanning transmission electron microscopy and X-ray adsorption techniques (e.g., XANES and EXAFS) offer great opportunities to better understand the complexity of practically used catalysts, which is particularly well-exemplified by recent elegant investigations on the Au/TiO$_2$ catalyst.[808] On the one hand, we need to specify the real active species present in practically used catalysts from a mechanistic point of view and to address if this species for all the reactions. After all, it is very likely that several different sites could exist on the same catalyst, at which the activity can be regulated to a specific reaction.[803] This point has not been achieved yet and perhaps represents the current major challenge for gold-based heterogeneous catalysis. Model systems and theoretical studies would be vital in attaining this understanding; contribution of expertise from materials scientists would also be essential to rationally design a catalyst with specific structures and catalytic efficacy. Elegant model and theoretical research will direct the way in this new era of gold catalysis.

Gold-based bimetallics are another subject worth substantial attention. While in many cases addition of an inactive metal leads to a decrease in activity, in some cases there is an initial increase. It has frequently been ascribed to a decrease in the mean size of the active ensemble, which, in turn, minimizes the formation of strongly bonded surface species that could lower the rate of the desired reaction, although sometimes improving its selectivity. The probability of finding an active ensemble of a specified size is a function of the ratio in which the two metals are present, but the

3042

dx.doi.org/10.1021/cr200041p |*Chem. Rev.* 2012, 112, 2987–3054

component of lower surface energy to segregate preferentially at the surface that would occupy low-coordination-number sites. Additionally, a number of reports show that gold can improve the activity of palladium in reaction involving only hydrogen. For instance, bimetallic catalysts containing gold show activity superior to that of either compound separately in the synthesis of hydrogen peroxide and vinyl acetate and several other selective oxidations. However, sound explanations for these effects are not always available even from model systems, although it is clear that the role of gold is to favorably modify the performance of the palladium. Detailed surface science investigations of bimetallic surfaces and supported bimetallic clusters, not limited to the Au–Pd system, would spur considerable interest and attention in the research community.

There are numerous opportunities emerging in gold-catalyzed heterogeneous reactions, particularly, for example, in the field of selective chemical synthesis. Increased attention has been paid to the direct synthesis of hydrogen peroxide and the selective oxidation of OH functional groups.[27,809] Gold catalysts have also been proven to be highly active in the conversion of biorenewable feedstocks such as sugars and glycerol. Additionally, although acetylene is highly reactive on gold catalysts, the reactions of other alkenes have been less reported, which could also be a key opportunity.[803] Other reactions, such as photocatalytic hydrogen production, hydrogenation reactions, and decomposition of halogen-containing compounds, are potentially interesting but are relatively less investigated and thus underdeveloped. Overall, the real opportunity stems from a combination of expertise of synthetic methods and theoretical and experimental model studies.
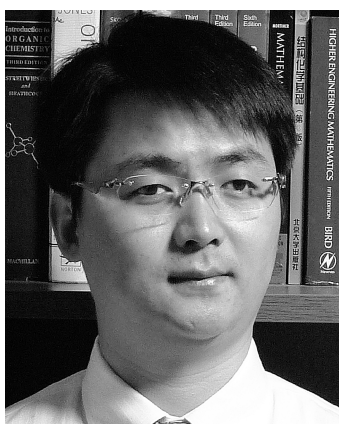
ASSOCIATED CONTENT

Ⓢ Supporting Information

As noted in the Noted Added after ASAP Publication, the original review is available as Supporting Information. This material is available free of charge via the Internet at http://pubs.acs.org.

AUTHOR INFORMATION

Corresponding Author

*E-mail: jlgong@tju.edu.cn. Phone: +86-22-87401818.

BIOGRAPHY

Jinlong Gong studied chemical engineering and received his B.S. and M.S. degrees from Tianjin University and Ph.D. degree from the University of Texas at Austin under the tutelage of C. Buddie Mullins. He was a visiting scientist at the Pacific Northwest National Laboratory in 2007. After a stint with Professor George M. Whitesides as a postdoctoral research fellow at Harvard University, he joined the faculty of Tianjin University, where he is currently a professor in chemical engineering. He is the recipient of a number of awards including a Chinese Government Award for Outstanding Graduate Students Abroad, an International Precious Metals Institute Research Award, and an IUPAC Prize for Young Chemists—Honorable Mention Award. He was elected into the Program for New Century Excellent Talents in University administrated by the Ministry of Education of China in 2010. His research interests in surface science and catalysis include catalytic conversions of green chemicals and energy, novel utilizations of carbon dioxide, and synthesis and applications of nanostructured materials.

REFERENCES

(1) Hashmi, A. S. K. *Chem. Rev.* **2007**, *107*, 3180.
(2) Mavrikakis, M.; Stoltze, P.; Norskov, J. K. *Catal. Lett.* **2000**, *64*, 101.
(3) Haruta, M. *Catal. Today* **1997**, *36*, 153.
(4) Hashmi, A. S. K.; Hutchings, G. J. *Angew. Chem., Int. Ed.* **2006**, *45*, 7896.
(5) Haruta, M.; Kobayashi, T.; Sano, H.; Yamada, N. *Chem. Lett.* **1987**, 405.
(6) Hutchings, G. J. *J. Catal.* **1985**, *96*, 292.
(7) Haruta, M.; Yamada, N.; Kobayashi, T.; Iijima, S. *J. Catal.* **1989**, *115*, 301.
(8) Bond, G. C.; Thompson, D. T. *Cat. Rev.—Sci. Eng.* **1999**, *41*, 319.
(9) Hakkinen, H.; Abbet, W.; Sanchez, A.; Heiz, U.; Landman, U. *Angew. Chem., Int. Ed.* **2003**, *42*, 1297.
(10) Meyer, R.; Lemire, C.; Shaikhutdinov, S. K.; Freund, H. *Gold Bull.* **2004**, 72.
(11) Daniel, M. C.; Astruc, D. *Chem. Rev.* **2004**, *104*, 293.
(12) Gorin, D. J.; Toste, F. D. *Nature* **2007**, *446*, 395.
(13) Bracey, C. L.; Ellis, P. R.; Hutchings, G. J. *Chem. Soc. Rev.* **2009**, *38*, 2231.
(14) Li, Z. Y.; Young, N. P.; Di Vece, M.; Palomba, S.; Palmer, R. E.; Bleloch, A. L.; Curley, B. C.; Johnston, R. L.; Jiang, J.; Yuan, J. *Nature* **2008**, *451*, 46.
(15) Goodman, D. W. *Chem. Rev.* **1995**, *95*, 523.
(16) Poirier, G. E. *Chem. Rev.* **1997**, *97*, 1117.
(17) Bond, G. C.; Louis, C.; Thompson, D. T. *Catalysis by gold*; Imperial College Press: London, 2006.
(18) Chen, M. S.; Goodman, D. W. *Acc. Chem. Res.* **2006**, *39*, 739.
(19) Min, B. K.; Friend, C. M. *Chem. Rev.* **2007**, *107*, 2709.
(20) Kung, M. C.; Davis, R. J.; Kung, H. H. *J. Phys. Chem. C* **2007**, *111*, 11767.
(21) Carabineiro, S. A. C.; Thompson, D. T. In *Nanocatalysis*; Heiz, U., Landman, U., Eds.; Springer-Verlag: New York, 2007; p 377.
(22) Pyykko, P. *Chem. Soc. Rev.* **2008**, *37*, 1967.
(23) Chen, M. S.; Goodman, D. W. *Chem. Soc. Rev.* **2008**, *37*, 1860.
(24) Carabineiro, S. A. C.; Nieuwenhuys, B. E. *Gold Bull.* **2009**, *42*, 288.

3043

dx.doi.org/10.1021/cr200041p | *Chem. Rev.* 2012, 112, 2987–3054

(25) Liu, X. Y.; Madix, R. J.; Friend, C. M. *Chem. Soc. Rev.* **2008**, *37*, 2243.

(26) Fierro-Gonzalez, J. C.; Gates, B. C. *Chem. Soc. Rev.* **2008**, *37*, 2127.

(27) Corma, A.; Garcia, H. *Chem. Soc. Rev.* **2008**, *37*, 2096.

(28) Carabineiro, S. A. C.; Nieuwenhuys, B. E. *Gold Bull.* **2010**, *43*, 252.

(29) Baker, T. A.; Liu, X. Y.; Friend, C. M. *Phys. Chem. Chem. Phys.* **2011**, *13*, 34.

(30) Carabineiro, S. A. C.; Thompson, D. T. In *Gold: Science and Applications*; Corti, C., Holliday, R., Eds.; CRC Press: New York, 2010; p 89.

(31) Ghosh, S. K.; Pal, T. *Chem. Rev.* **2007**, *107*, 4797.

(32) Love, J. C.; Estroff, L. A.; Kriebel, J. K.; Nuzzo, R. G.; Whitesides, G. M. *Chem. Rev.* **2005**, *105*, 1103.

(33) Takeuchi, N.; Chan, C. T.; Ho, K. M. *Phys. Rev. B* **1991**, *43*, 13899.

(34) Lozovoi, A. Y.; Alavi, A. *Phys. Rev. B* **2003**, *68*, 18.

(35) Crljen, Z.; Lazic, P.; Sokcevic, D.; Brako, R. *Phys. Rev. B* **2003**, *68*, 8.

(36) http://www.fhi-berlin.mpg.de/~hermann/Balsac/SSDpictures.html#A.

(37) Hasegawa, Y.; Avouris, P. *Science* **1992**, *258*, 1763.

(38) Harten, U.; Lahee, A. M.; Toennies, J. P.; Woll, C. *Phys. Rev. Lett.* **1985**, *54*, 2619.

(39) Hakkinen, H.; Moseler, M.; Landman, U. *Phys. Rev. Lett.* **2002**, *89*, 4.

(40) van Hove, M. A.; Koestner, R. J.; Stair, P. C.; Biberian, J. P.; Kesmodel, L. L.; Bartos, I.; Somorjai, G. A. *Surf. Sci.* **1981**, *103*, 189.

(41) Woll, C.; Chiang, S.; Wilson, R. J.; Lippel, P. H. *Phys. Rev. B* **1989**, *39*, 7988.

(42) Davis, L. C.; Everson, M. P.; Jaklevic, R. C.; Shen, W. D. *Phys. Rev. B* **1991**, *43*, 3821.

(43) Wang, Y.; Hush, N. S.; Reimers, J. R. *Phys. Rev. B* **2007**, *75*, 4.

(44) El-Batanouny, M.; Burdick, S.; Martini, K. M.; Stancioff, P. *Phys. Rev. Lett.* **1987**, *58*, 2762.

(45) Narasimhan, S.; Vanderbilt, D. *Phys. Rev. Lett.* **1992**, *69*, 1564.

(46) Rost, M. J.; van Albada, S. B.; Frenken, J. W. M. *Surf. Sci.* **2003**, *547*, 71.

(47) Uehara, Y.; Ushioda, S. *Phys. Rev. B* **2002**, *66*, 165420.

(48) Fedak, D. G.; Gjostein, N. A. *Acta Metall.* **1967**, *15*, 827.

(49) Bonzel, H. P.; Ku, R. *J. Vac. Sci. Technol.* **1972**, *9*, 663.

(50) Chan, C. M.; Vanhove, M. A.; Weinberg, W. H.; Williams, E. D. *Solid State Commun.* **1979**, *30*, 47.

(51) Gritsch, T.; Coulman, D.; Behm, R. J.; Ertl, G. *Surf. Sci.* **1991**, *257*, 297.

(52) Moritz, W.; Wolf, D. *Surf. Sci.* **1985**, *163*, L655.

(53) Campuzano, J. C.; Foster, M. S.; Jennings, G.; Willis, R. F.; Unertl, W. *Phys. Rev. Lett.* **1985**, *54*, 2684.

(54) de la Figuera, J.; Gonzalez, M. A.; Garcia-Martinez, R.; Rojo, J. M.; Hernan, O. S.; de Parga, A. L. V.; Miranda, R. *Phys. Rev. B* **1998**, *58*, 1169.

(55) Mattera, A. M.; Goodman, R. M.; Somorjai, G. A. *Surf. Sci.* **1967**, *7*, 26.

(56) Fedak, D. G.; Gjostein, N. A. *Surf. Sci.* **1967**, *8*, 77.

(57) Melle, H.; Menzel, E. *Z. Naturforsch., A: Phys. Sci.* **1978**, *33*, 282.

(58) Binnig, G. K.; Rohrer, H.; Gerber, C.; Stoll, E. *Surf. Sci.* **1984**, *144*, 321.

(59) Yamazaki, K.; Takayanagi, K.; Tanishiro, Y.; Yagi, K. *Surf. Sci.* **1988**, *199*, 595.

(60) Rieder, K. H.; Engel, T.; Swendsen, R. H.; Manninen, M. *Surf. Sci.* **1983**, *127*, 223.

(61) Marks, L. D.; Smith, D. J. *Surf. Sci.* **1985**, *157*, L367.

(62) Takeuchi, N.; Chan, C. T.; Ho, K. M. *Phys. Rev. Lett.* **1989**, *63*, 1273.

(63) Gibbs, D.; Ocko, B. M.; Zehner, D. M.; Mochrie, S. G. J. *Phys. Rev. B* **1988**, *38*, 7303.

(64) Sault, A. G.; Madix, R. J.; Campbell, C. T. *Surf. Sci.* **1986**, *169*, 347.

(65) Meyer, R.; Lemire, C.; Shaikhutdinov, S. K.; Freund, H. *Gold Bull.* **2004**, *37*, 72.

(66) Gottfried, J. M.; Schmidt, K. J.; Schroeder, S. L. M.; Christmann, K. *Surf. Sci.* **2002**, *511*, 65.

(67) Shishakov, N. A. *J. Phys. Chem.* **1960**, *64*, 1580.

(68) MacDonald, W. R.; Hayes, K. E. *J. Catal.* **1970**, *18*, 115.

(69) Chesters, M. A.; Somorjai, G. A. *Surf. Sci.* **1975**, *52*, 21.

(70) Schrader, M. E. *J. Colloid Interface Sci.* **1977**, *59*, 456.

(71) Schrader, M. E. *Surf. Sci.* **1978**, *78*, L227.

(72) Legare, P.; Hilaire, L.; Sotto, M.; Maire, G. *Surf. Sci.* **1980**, *91*, 175.

(73) Pireaux, J. J.; Chtaib, M.; Delrue, J. P.; Thiry, P. A.; Liehr, M.; Caudano, R. *Surf. Sci.* **1984**, *141*, 211.

(74) Ford, R. R.; Pritchar, J. *Chem. Commun.* **1968**, 362.

(75) Eley, D. D.; Moore, P. B. *Surf. Sci.* **1978**, *76*, L599.

(76) Canning, N. D. S.; Outka, D.; Madix, R. J. *Surf. Sci.* **1984**, *141*, 240.

(77) King, D. E. *J. Vac. Sci. Technol., A* **1995**, *13*, 1247.

(78) Parker, D. H.; Koel, B. E. *J. Vac. Sci. Technol., A* **1990**, *8*, 2585.

(79) Saliba, N.; Parker, D. H.; Koel, B. E. *Surf. Sci.* **1998**, *410*, 270.

(80) Nakamura, I.; Takahashi, A.; Fujitani, T. *Catal. Lett.* **2009**, *129*, 400.

(81) Lazaga, M. A.; Wickham, D. T.; Parker, D. H.; Kastanas, G. N.; Koel, B. E. *ACS Symp. Ser.* **1993**, *523*, 90.

(82) Wang, J.; Voss, M. R.; Busse, H.; Koel, B. E. *J. Phys. Chem. B* **1998**, *102*, 4693.

(83) Pireaux, J. J.; Liehr, M.; Thiry, P. A.; Delrue, J. P.; Caudano, R. *Surf. Sci.* **1984**, *141*, 221.

(84) Gottfried, J. M.; Elghobashi, N.; Schroeder, S. L. M.; Christmann, K. *Surf. Sci.* **2003**, *523*, 89.

(85) Zielasek, V.; Xu, B. J.; Liu, X. Y.; Baumer, M.; Friend, C. M. *J. Phys. Chem. C* **2009**, *113*, 8924.

(86) Biener, J.; Biener, M. M.; Nowitzki, T.; Hamza, A. V.; Friend, C. M.; Zielasek, V.; Baumer, M. *ChemPhysChem* **2006**, *7*, 1906.

(87) Gottfried, J. M.; Schmidt, K. J.; Schroeder, S. L. M.; Christmann, K. *Surf. Sci.* **2003**, *525*, 184.

(88) Gottfried, J. M.; Schmidt, K. J.; Schroeder, S. L. M.; Christmann, K. *Surf. Sci.* **2003**, *525*, 197.

(89) Gottfried, J. M.; Christmann, K. *Surf. Sci.* **2004**, *566−568*, 1112.

(90) Deng, X. Y.; Min, B. K.; Guloy, A.; Friend, C. M. *J. Am. Chem. Soc.* **2005**, *127*, 9267.

(91) Kim, T. S.; Stiehl, J. D.; Reeves, C. T.; Meyer, R. J.; Mullins, C. B. *J. Am. Chem. Soc.* **2003**, *125*, 2018.

(92) McClure, S. M.; Kim, T. S.; Stiehl, J. D.; Tanaka, P. L.; Mullins, C. B. *J. Phys. Chem. B* **2004**, *108*, 17952.

(93) Gong, J. L.; Ojifinni, R. A.; Kim, T. S.; Stiehl, J. D.; McClure, S. M.; White, J. M.; Mullins, C. B. *Top. Catal.* **2007**, *44*, 57.

(94) Ojifinni, R. A.; Froemming, N. S.; Gong, J.; Pan, M.; Kim, T. S.; White, J. M.; Henkelman, G.; Mullins, C. B. *J. Am. Chem. Soc.* **2008**, *130*, 6801.

(95) Outka, D. A.; Madix, R. J. *Surf. Sci.* **1987**, *179*, 351.

(96) Outka, D. A.; Madix, R. J. *J. Am. Chem. Soc.* **1987**, *109*, 1708.

(97) Outka, D. A.; Madix, R. J. *Surf. Sci.* **1987**, *179*, 361.

(98) Davis, K. A.; Goodman, D. W. *J. Phys. Chem. B* **2000**, *104*, 8557.

(99) Min, B. K.; Alemozafar, A. R.; Pinnaduwage, D.; Deng, X.; Friend, C. M. *J. Phys. Chem. B* **2006**, *110*, 19833.

(100) Baker, T. A.; Xu, B.; Liu, X.; Kaxiras, E.; Friend, C. M. *J. Phys. Chem. C* **2009**, *113*, 16561.

(101) Min, B. K.; Deng, X.; Pinnaduwage, D.; Schalek, R.; Friend, C. M. *Phys. Rev. B* **2005**, *72*, 4.

(102) Ibach, H.; Bach, C. E.; Giesen, M.; Grossmann, A. *Surf. Sci.* **1997**, *375*, 107.

(103) Baker, T. A.; Friend, C. M.; Kaxiras, E. *J. Chem. Phys.* **2009**, *130*, 084701.

(104) Shi, H.; Stampfl, C. *Phys. Rev. B* **2007**, *76*, 14.

(105) Baker, T. A.; Friend, C. M.; Kaxiras, E. *J. Phys. Chem. C* **2009**, *113*, 3232.

(106) Xu, Y.; Mavrikakis, M. *J. Phys. Chem. B* **2003**, *107*, 9298.

(107) Kim, J.; Samano, E.; Koel, B. E. *Surf. Sci.* **2006**, *600*, 4622.

(108) Wang, J.; Koel, B. E. *J. Phys. Chem. A* **1998**, *102*, 8573.

(109) Wang, J.; Koel, B. E. *Surf. Sci.* **1999**, *436*, 15.

(110) Deng, X. Y.; Friend, C. M. *J. Am. Chem. Soc.* **2005**, *127*, 17178.

(111) Mills, G.; Gordon, M. S.; Metiu, H. *J. Chem. Phys.* **2003**, *118*, 4198.

(112) Pollard, J. E. *Rev. Sci. Instrum.* **1992**, *63*, 1771.

(113) Wheeler, M. C.; Seets, D. C.; Mullins, C. B. *J. Chem. Phys.* **1997**, *107*, 1672.

(114) Wheeler, M. C.; Reeves, C. T.; Seets, D. C.; Mullins, C. B. *J. Chem. Phys.* **1998**, *108*, 3057.

(115) Gong, J. L.; Mullins, C. B. *J. Am. Chem. Soc.* **2008**, *130*, 16458.

(116) Stiehl, J. D.; Kim, T. S.; McClure, S. M.; Mullins, C. B. *J. Phys. Chem. B* **2005**, *109*, 6316.

(117) Stiehl, J. D.; Kim, T. S.; McClure, S. M.; Mullins, C. B. *J. Am. Chem. Soc.* **2004**, *126*, 1606.

(118) Gong, J.; Flaherty, D. W.; Ojifinni, R. A.; White, J. M.; Mullins, C. B. *J. Phys. Chem. C* **2008**, *112*, 5501.

(119) Redhead, P. A. *Vacuum* **1962**, *12*, 203.

(120) Miller, S. D.; Kitchin, J. R. *Surf. Sci.* **2009**, *603*, 794.

(121) Peters, K. F.; Steadman, P.; Isern, H.; Alvarez, J.; Ferrer, S. *Surf. Sci.* **2000**, *467*, 10.

(122) Piccolo, L.; Loffreda, D.; Cadete Santos Aires, F. J.; Deranlot, C.; Jugnet, Y.; Sautet, P.; Bertolini, J. C. *Surf. Sci.* **2004**, *566–568*, 995.

(123) Gottfried, J. M.; Schmidt, K. J.; Schroeder, S. L. M.; Christmann, K. *Surf. Sci.* **2003**, *536*, 206.

(124) Kim, J.; Samano, E.; Koel, B. E. *J. Phys. Chem. B* **2006**, *110*, 17512.

(125) Sandell, A.; Bennich, P.; Nilsson, A.; Hernnas, B.; Bjorneholm, O.; Martensson, N. *Surf. Sci.* **1994**, *310*, 16.

(126) Meier, D. C.; Bukhtiyarov, V.; Goodman, D. W. *J. Phys. Chem. B* **2003**, *107*, 12668.

(127) Jugnet, Y.; Cadete Santos Aires, F. J.; Deranlot, C.; Piccolo, L.; Bertolini, J. C. *Surf. Sci.* **2002**, *521*, L639.

(128) McElhiney, G.; Pritchard, J. *Surf. Sci.* **1976**, *60*, 397.

(129) Ruggiero, C.; Hollins, P. *J. Chem. Soc., Faraday Trans.* **1996**, *92*, 4829.

(130) Ruggiero, C.; Hollins, P. *Surf. Sci.* **1997**, *377–379*, 583.

(131) Bailie, J. E.; Hutchings, G. J. *Chem. Commun.* **1999**, 2151.

(132) Rodriguez, J. A.; Liu, G.; Jirsak, T.; Hrbek, J.; Chang, Z. P.; Dvorak, J.; Maiti, A. *J. Am. Chem. Soc.* **2002**, *124*, 5242.

(133) Phillips, G. N.; Evans, K. A. *Nature* **2004**, *429*, 860.

(134) Delamarche, E.; Michel, B.; Biebuyck, H. A.; Gerber, C. *Adv. Mater.* **1996**, *8*, 719.

(135) Ulman, A. *Chem. Rev.* **1996**, *96*, 1533.

(136) Vericat, C.; Vela, M. E.; Benitez, G. A.; Gago, J. A. M.; Torrelles, X.; Salvarezza, R. C. *J. Phys.: Condens. Matter* **2006**, *18*, R867.

(137) Vericat, C.; Andreasen, G.; Vela, M. E.; Salvarezza, R. C. *J. Phys. Chem. B* **2000**, *104*, 302.

(138) Gao, X.; Zhang, Y.; Weaver, M. J. *J. Phys. Chem.* **1992**, *96*, 4156.

(139) Rodriguez, J. A.; Dvorak, J.; Jirsak, T.; Liu, G.; Hrbek, J.; Aray, Y.; Gonzalez, C. *J. Am. Chem. Soc.* **2003**, *125*, 276.

(140) Heinz, R.; Rabe, J. P. *Langmuir* **1995**, *11*, 506.

(141) Quek, S. Y.; Biener, M. M.; Biener, J.; Bhattacharjee, J.; Friend, C. M.; Waghmare, U. V.; Kaxiras, E. *J. Phys. Chem. B* **2006**, *110*, 15663.

(142) Vericat, C.; Vela, M. E.; Andreasen, G. A.; Salvarezza, R. C.; Borgatti, F.; Felici, R.; Lee, T. L.; Renner, F.; Zegenhagen, J.; Martin-Gago, J. A. *Phys. Rev. Lett.* **2003**, *90*, 075506.

(143) Jackson, D. C.; Chaudhuri, A.; Lerotholi, T. J.; Woodruff, D. P.; Jones, R. G.; Dhanak, V. R. *Surf. Sci.* **2009**, *603*, 807.

(144) Biener, M. M.; Biener, J.; Friend, C. M. *Langmuir* **2005**, *21*, 1668.

(145) Kurokawa, S.; Miyawaki, Y.; Sakai, A. *Jpn. J. Appl. Phys.* **2009**, *48*, 5.

(146) Gonzalez-Lakunza, N.; Lorente, N.; Arnau, A. *J. Phys. Chem. C* **2007**, *111*, 12383.

(147) Gottschalck, J.; Hammer, B. *J. Chem. Phys.* **2002**, *116*, 784.

(148) Vericat, C.; Vela, M. E.; Andreasen, G.; Salvarezza, R. C.; Vazquez, L.; Martin-Gago, J. A. *Langmuir* **2001**, *17*, 4919.

(149) Min, B. K.; Alemozafar, A. R.; Biener, M. M.; Biener, J.; Friend, C. M. *Top. Catal.* **2005**, *36*, 77.

(150) Gan, L. Y.; Zhang, Y. X.; Zhao, Y. J. *J. Phys. Chem. C* **2010**, *114*, 996.

(151) Biener, M. M.; Biener, J.; Friend, C. M. *Surf. Sci.* **2007**, *601*, 1659.

(152) Leavitt, A. J.; Beebe, T. P. *Surf. Sci.* **1994**, *314*, 23.

(153) Jaffey, D. M.; Madix, R. J. *Surf. Sci.* **1991**, *258*, 359.

(154) Fruhberger, B.; Grunze, M.; Dwyer, D. J. *J. Phys. Chem.* **1994**, *98*, 609.

(155) Bondzie, V.; Dixon-Warren, S.; Yu, Y. *J. Chem. Phys.* **1999**, *111*, 10670.

(156) Abufager, P. N.; Lustemberg, P. G.; Crespos, C.; Busnengo, H. F. *Langmuir* **2008**, *24*, 14022.

(157) Seets, D. C.; Wheeler, M. C.; Mullins, C. B. *Chem. Phys. Lett.* **1997**, *266*, 431.

(158) Seets, D. C.; Wheeler, M. C.; Mullins, C. B. *J. Chem. Phys.* **1997**, *107*, 3986.

(159) Seets, D. C.; Reeves, C. T.; Ferguson, B. A.; Wheeler, M. C.; Mullins, C. B. *J. Chem. Phys.* **1997**, *107*, 10229.

(160) Mullins, C. B.; Weinberg, W. H. *J. Chem. Phys.* **1990**, *92*, 3986.

(161) Mullins, C. B.; Weinberg, W. H. *J. Chem. Phys.* **1990**, *92*, 4508.

(162) Mullins, C. B.; Weinberg, W. H. *J. Vac. Sci. Technol., A* **1990**, *8*, 2458.

(163) Liu, G.; Rodriguez, J. A.; Dvorak, J.; Hrbek, J.; Jirsak, T. *Surf. Sci.* **2002**, *505*, 295.

(164) Hofer, M.; Stolz, H.; Wassmuth, H. W. *Surf. Sci.* **1992**, *272*, 342.

(165) Ahner, J.; Effendy, A.; Vajen, K.; Wassmuth, H. W. *Vacuum* **1990**, *41*, 98.

(166) Sun, Z. J.; Gravelle, S.; Mackay, R. S.; Zhu, X. Y.; White, J. M. *J. Chem. Phys.* **1993**, *99*, 10021.

(167) Rodriguez, J. A.; Ricart, J. M.; Clotet, A.; Illas, F. *J. Chem. Phys.* **2001**, *115*, 454.

(168) Polcik, M.; Wilde, L.; Haase, J.; Brena, B.; Cocco, D.; Comelli, G.; Paolucci, G. *Phys. Rev. B* **1996**, *53*, 13720.

(169) Jackson, G. J.; Driver, S. M.; Woodruff, D. P.; Abrams, N.; Jones, R. G.; Butterfield, M. T.; Crapper, M. D.; Cowie, B. C. C.; Formoso, V. *Surf. Sci.* **2000**, *459*, 231.

(170) Nuzzo, R. G.; Zegarski, B. R.; Dubois, L. H. *J. Am. Chem. Soc.* **1987**, *109*, 733.

(171) Hayashi, T.; Morikawa, Y.; Nozoye, H. *J. Chem. Phys.* **2001**, *114*, 7615.

(172) Rzezinicka, I. I.; Lee, J. S.; Maksymovych, P.; Yates, J. T. *J. Phys. Chem. B* **2005**, *109*, 15992.

(173) Molina, L. M.; Hammer, B. *Chem. Phys. Lett.* **2002**, *360*, 264.

(174) Sellers, H. *Surf. Sci.* **1993**, *294*, 99.

(175) Gronbeck, H.; Curioni, A.; Andreoni, W. *J. Am. Chem. Soc.* **2000**, *122*, 3839.

(176) Zhou, J.-G.; Hagelberg, F. *Phys. Rev. Lett.* **2006**, *97*, 045505.

(177) De Renzi, V.; Di Felice, R.; Marchetto, D.; Biagi, R.; del Pennino, U.; Selloni, A. *J. Phys. Chem. B* **2004**, *108*, 16.

(178) Kondoh, H.; Iwasaki, M.; Shimada, T.; Amemiya, K.; Yokoyama, T.; Ohta, T.; Shimomura, M.; Kono, S. *Phys. Rev. Lett.* **2003**, *90*, 066102.

(179) Nuzzo, R. G.; Dubois, L. H.; Allara, D. L. *J. Am. Chem. Soc.* **1990**, *112*, 558.

(180) Lavrich, D. J.; Wetterer, S. M.; Bernasek, S. L.; Scoles, G. *J. Phys. Chem. B* **1998**, *102*, 3456.

(181) Milligan, P. K.; Murphy, B.; Lennon, D.; Cowie, B. C. C.; Kadodwala, M. *J. Phys. Chem. B* **2001**, *105*, 140.

(182) Jaffey, D. M.; Madix, R. J. *Surf. Sci.* **1994**, *311*, 159.

(183) Jaffey, D. M.; Madix, R. J. *J. Am. Chem. Soc.* **1994**, *116*, 3020.

(184) Whelan, C. M.; Barnes, C. J.; Walker, C. G. H.; Brown, N. M. D. *Surf. Sci.* **1999**, *425*, 195.

(185) Jaffey, D. M.; Madix, R. J. *J. Am. Chem. Soc.* **1994**, *116*, 3012.

3045

dx.doi.org/10.1021/cr200041p | *Chem. Rev.* 2012, 112, 2987–3054

(186) Bondzie, V.; Dion-Warren, S. J.; Yu, Y.; Zhang, L. *Surf. Sci.* **1999**, *431*, 174.

(187) Lemoine, D.; Quattrucci, J. G.; Jackson, B. *Phys. Rev. Lett.* **2002**, *89*, 268302.

(188) Spencer, N. D.; Lambert, R. M. *Surf. Sci.* **1981**, *107*, 237.

(189) Kastanas, G. N.; Koel, B. E. *Appl. Surf. Sci.* **1993**, *64*, 235.

(190) Gao, W. W.; Baker, T. A.; Zhou, L.; Pinnaduwage, D. S.; Kaxiras, E.; Friend, C. M. *J. Am. Chem. Soc.* **2008**, *130*, 3560.

(191) Gao, W. W.; Zhou, L.; Pinnaduwage, D. S.; Friend, C. M. *J. Phys. Chem. C* **2007**, *111*, 9005.

(192) Baker, T. A.; Friend, C. M.; Kaxiras, E. *J. Am. Chem. Soc.* **2008**, *130*, 3720.

(193) Baker, T. A.; Friend, C. M.; Kaxiras, E. *J. Chem. Phys.* **2008**, *129*, 104702.

(194) Zhao, Y.; Mann, M. D.; Pavlish, J. H.; Mibeck, B. A. F.; Dunham, G. E.; Olson, E. S. *Environ. Sci. Technol.* **2006**, *40*, 1603.

(195) Pinnaduwage, D. S.; Zhou, L.; Gao, W.; Friend, C. M. *J. Am. Chem. Soc.* **2007**, *129*, 1872.

(196) Oh, H. S.; Yang, J. H.; Costello, C. K.; Wang, Y. M.; Bare, S. R.; Kung, H. H.; Kung, M. C. *J. Catal.* **2002**, *210*, 375.

(197) Zheleva, Z. V.; Dhanak, V. R.; Held, G. *Phys. Chem. Chem. Phys.* **2010**, *12*, 10754.

(198) Bilic, A.; Reimers, J. R.; Hush, N. S.; Hafner, J. *J. Chem. Phys.* **2002**, *116*, 8981.

(199) Kay, B. D.; Lykke, K. R.; Creighton, J. R.; Ward, S. J. *J. Chem. Phys.* **1989**, *91*, 5120.

(200) Gong, J. L.; Ojifinni, R. A.; Kim, T. S.; White, J. M.; Mullins, C. B. *J. Am. Chem. Soc.* **2006**, *128*, 9012.

(201) Hoft, R. C.; Ford, M. J.; McDonagh, A. M.; Cortie, M. B. *J. Phys. Chem. C* **2007**, *111*, 13886.

(202) Gong, J. L.; Yan, T.; Mullins, C. B. *Chem. Commun.* **2009**, 761.

(203) Bartram, M. E.; Koel, B. E. *Surf. Sci.* **1989**, *213*, 137.

(204) Sato, S.; Senga, T.; Kawasaki, M. *J. Phys. Chem. B* **1999**, *103*, 5063.

(205) Lu, X.; Xu, X.; Wang, N. Q.; Zhang, Q. *J. Phys. Chem. A* **1999**, *103*, 10969.

(206) Beckendorf, M.; Katter, U. J.; Schlienz, H.; Freund, H. J. *J. Phys.: Condens. Matter* **1993**, *5*, 5471.

(207) Rienks, E. D. L.; van Berkel, G. P.; Bakker, J. W.; Nieuwenhuys, B. E. *Surf. Sci.* **2004**, *571*, 187.

(208) Vinod, C. P.; Hans, J. W. N.; Nieuwenhuys, B. E. *Appl. Catal., A* **2005**, *291*, 93.

(209) Syomin, D.; Wang, J.; Koel, B. E. *Surf. Sci.* **2001**, *495*, L827.

(210) Wang, J.; Busse, H.; Syomin, D.; Koel, B. E. *Surf. Sci.* **2001**, *494*, L741.

(211) Solomun, T.; Christmann, K.; Baumgartel, H. *J. Phys. Chem.* **1989**, *93*, 7199.

(212) Krishnamurthy, S.; Montalti, M.; Wardle, M. G.; Shaw, M. J.; Briddon, P. R.; Svensson, K.; Hunt, M. R. C.; Siller, L. *Phys. Rev. B* **2004**, *70*, 5.

(213) Siller, L.; Hunt, M. R. C.; Brown, J. W.; Coquel, J. M.; Rudolf, P. *Surf. Sci.* **2002**, *513*, 78.

(214) Chretien, S.; Gordon, M. S.; Metiu, H. *J. Chem. Phys.* **2004**, *121*, 3756.

(215) Syomin, D.; Koel, B. E. *Surf. Sci.* **2002**, *498*, 61.

(216) Mullegger, S.; Winkler, A. *Surf. Sci.* **2006**, *600*, 1290.

(217) Wetterer, S. M.; Lavrich, D. J.; Cummings, T.; Bernasek, S. L.; Scoles, G. *J. Phys. Chem. B* **1998**, *102*, 9266.

(218) Baxter, R. J.; Teobaldi, G.; Zerbetto, F. *Langmuir* **2003**, *19*, 7335.

(219) Paul, A. M.; Bent, B. E. *J. Catal.* **1994**, *147*, 264.

(220) Yang, M. X.; Jo, S. K.; Paul, A.; Avila, L.; Bent, B. E.; Nishikida, K. *Surf. Sci.* **1995**, *325*, 102.

(221) Paul, A.; Yang, M. X.; Bent, B. E. *Surf. Sci.* **1993**, *297*, 327.

(222) Syomin, D.; Koel, B. E. *Surf. Sci.* **2001**, *490*, 265.

(223) Xie, Z. X.; Xu, X.; Tang, J.; Mao, B. W. *J. Phys. Chem. B* **2000**, *104*, 11719.

(224) Zhang, H. M.; Xie, Z. X.; Mao, B. W.; Xu, X. *Chem.—Eur. J.* **2004**, *10*, 1415.

(225) Syomin, D.; Koel, B. E. *Surf. Sci.* **2002**, *498*, 53.

(226) Gong, J. L.; Flaherty, D. W.; Yan, T.; Mullins, C. B. *ChemPhysChem* **2008**, *9*, 2461.

(227) Madix, R. J.; Friend, C. M.; Liu, X. Y. *J. Catal.* **2008**, *258*, 410.

(228) Kim, J. H.; Koel, B. E. *Langmuir* **2005**, *21*, 3886.

(229) Akita, M.; Osaka, N.; Itoh, K. *Surf. Sci.* **1998**, *405*, 172.

(230) Vinod, C. P.; Niemantsverdriet, J. W.; Nieuwenhuys, B. E. *Phys. Chem. Chem. Phys.* **2005**, *7*, 1824.

(231) Chtaib, M.; Thiry, P. A.; Delrue, J. P.; Pireaux, J. J.; Caudano, R. *J. Electron Spectrosc. Relat. Phenom.* **1983**, *29*, 293.

(232) Chtaib, M.; Thiry, P. A.; Pireaux, J. J.; Delrue, J. P.; Caudano, R. *Surf. Sci.* **1985**, *162*, 245.

(233) Stobinski, L. *Appl. Surf. Sci.* **1996**, *103*, 503.

(234) Stobinski, L.; Zommer, L.; Dus, R. *Appl. Surf. Sci.* **1999**, *141*, 319.

(235) Kim, T. S.; Gong, J.; Ojifinni, R. A.; White, J. M.; Mullins, C. B. *J. Am. Chem. Soc.* **2006**, *128*, 6282.

(236) Quiller, R. G.; Baker, T. A.; Deng, X.; Colling, M. E.; Min, B. K.; Friend, C. M. *J. Chem. Phys.* **2008**, *129*, 9.

(237) Neves, R. S.; Motheo, A. J.; Fartaria, R. P. S; Fernandes, F. *J. Electroanal. Chem.* **2008**, *612*, 179.

(238) Thiel, P. A.; Madey, T. E. *Surf. Sci. Rep.* **1987**, *7*, 211.

(239) Ikemiya, N.; Gewirth, A. A. *J. Am. Chem. Soc.* **1997**, *119*, 9919.

(240) Donev, J. M. K.; Yu, Q.; Long, B. R.; Bollinger, R. K.; S. C. Fain, J. *J. Chem. Phys.* **2005**, *123*, 044706.

(241) Hammer, B.; Norskov, J. K. *Nature* **1995**, *376*, 238.

(242) Madix, R. J. *Science* **1986**, *233*, 1159.

(243) Gong, J.; Mullins, C. B. *Acc. Chem. Res.* **2009**, *42*, 1063.

(244) Samano, E.; Kim, J.; Koel, B. E. *Catal. Lett.* **2009**, *128*, 263.

(245) Fajin, J. L. C.; Cordeiro, M.; Gomes, J. R. B. *J. Phys. Chem. C* **2008**, *112*, 17291.

(246) Liu, Z. P.; Hu, P.; Alavi, A. *J. Am. Chem. Soc.* **2002**, *124*, 14770.

(247) Date, M.; Haruta, M. *J. Catal.* **2001**, *201*, 221.

(248) Daté, M.; Okumura, M.; Tsubota, S.; Haruta, M. *Angew. Chem., Int. Ed.* **2004**, *43*, 2129.

(249) Shubina, T. E.; Hartnig, C.; Koper, M. T. M. *Phys. Chem. Chem. Phys.* **2004**, *6*, 4215.

(250) Rodriguez, P.; Koverga, A. A.; Koper, M. T. M. *Angew. Chem., Int. Ed.* **2010**, *49*, 1241.

(251) Senanayake, S. D.; Stacchiola, D.; Liu, P.; Mullins, C. B.; Hrbek, J.; Rodriguez, J. A. *J. Phys. Chem. C* **2009**, *113*, 19536.

(252) Ojifinni, R. A.; Gong, J. L.; Flaherty, D. W.; Kim, T. S.; Mullins, C. B. *J. Phys. Chem. C* **2009**, *113*, 9820.

(253) Ojifinni, R. A.; Gong, J. L.; Froemming, N. S.; Flaherty, D. W.; Pan, M.; Henkelman, G.; Mullins, C. B. *J. Am. Chem. Soc.* **2008**, *130*, 11250.

(254) Guo, X. C.; Madix, R. J. *J. Phys. Chem. B* **2001**, *105*, 3878.

(255) Gong, J. L.; Mullins, C. B. *J. Phys. Chem. C* **2008**, *112*, 17631.

(256) Deng, X. Y.; Min, B. K.; Liu, X. Y.; Friend, C. M. *J. Phys. Chem. B* **2006**, *110*, 15982.

(257) Liu, X. Y.; Baker, T. A.; Friend, C. M. *Dalton Trans.* **2010**, *39*, 8521.

(258) Liu, X. Y.; Friend, C. M. *J. Phys. Chem. C* **2010**, *114*, 5141.

(259) Xue, L. Q.; Pang, X. Y.; Wang, G. C. *J. Comput. Chem.* **2009**, *30*, 438.

(260) Quiller, R. G.; Liu, X. Y.; Friend, C. M. *Chem.—Asian J.* **2010**, *5*, 78.

(261) Klust, A.; Madix, R. J. *J. Am. Chem. Soc.* **2006**, *128*, 1034.

(262) Wachs, I. E.; Madix, R. J. *J. Catal.* **1978**, *53*, 208.

(263) Wachs, I. E.; Madix, R. J. *Surf. Sci.* **1978**, *76*, 531.

(264) Xu, B. J.; Liu, X. Y.; Haubrich, J.; Madix, R. J.; Friend, C. M. *Angew. Chem., Int. Ed.* **2009**, *48*, 4206.

(265) Xu, B. J.; Liu, X. Y.; Haubrich, J.; Friend, C. M. *Nature Chem.* **2010**, *2*, 61.

(266) Xu, B. J.; Haubrich, J.; Baker, T. A.; Kaxiras, E.; Friend, C. M. *J. Phys. Chem. C* **2011**, *115*, 3703.

(267) Xu, B.; Haubrich, J.; Freyschlag, C. G.; Madix, R. J.; Friend, C. M. *Chem. Sci.* **2010**, *1*, 310.

(268) Wittstock, A.; Zielasek, V.; Biener, J.; Friend, C. M.; Baumer, M. *Science* **2010**, *327*, 319.

(269) Xu, B. J.; Madix, R. J.; Friend, C. M. *J. Am. Chem. Soc.* **2010**, *132*, 16571.

(270) Liu, X. Y.; Xu, B. J.; Haubrich, J.; Madix, R. J.; Friend, C. M. *J. Am. Chem. Soc.* **2009**, *131*, 5757.

(271) Jorgensen, B.; Christiansen, S. E.; Thomsen, M. L. D.; Christensen, C. H. *J. Catal.* **2007**, *251*, 332.

(272) Yan, T.; Gong, J.; Mullins, C. B. *J. Am. Chem. Soc.* **2009**, *131*, 16189.

(273) Liu, X. Y.; Friend, C. M. *Langmuir* **2010**, *26*, 16552.

(274) Zhang, W. H.; Li, Z. Y.; Luo, Y.; Yang, J. L. *J. Chem. Phys.* **2008**, *129*.

(275) Torres, D.; Gonzalez, S.; Neyman, K. M.; Illas, F. *Chem. Phys. Lett.* **2006**, *422*, 412.

(276) Fajin, J. L. C.; Cordeiro, M. N. D. S.; Gomes, J. R. B. *J. Phys. Chem. C* **2009**, *113*, 8864.

(277) Lopez, N.; Garcia-Mota, M.; Gomez-Diaz, J. *J. Phys. Chem. C* **2008**, *112*, 247.

(278) Liu, R. Q.; Shen, W.; Zhang, J. S.; Li, M. *Appl. Surf. Sci.* **2008**, *254*, 5706.

(279) Weigelt, S.; Busse, C.; Bombis, C.; Knudsen, M. M.; Gothelf, K. V.; Strunskus, T.; Woll, C.; Dahlbom, M.; Hammer, B.; Laegsgaard, E.; Besenbacher, F.; Linderoth, T. R. *Angew. Chem., Int. Ed.* **2007**, *46*, 9227.

(280) Rettner, C. T. *J. Chem. Phys.* **1994**, *101*, 1529.

(281) Rettner, C. T.; Auerbach, D. J. *Science* **1994**, *263*, 365.

(282) Deng, X.; Friend, C. M. *Surf. Sci.* **2008**, *602*, 1066.

(283) Deng, X. Y.; Baker, T. A.; Friend, C. M. *Angew. Chem., Int. Ed.* **2006**, *45*, 7075.

(284) Xu, B. J.; Zhou, L.; Madix, R. J.; Friend, C. M. *Angew. Chem., Int. Ed.* **2010**, *49*, 392.

(285) Netzer, F. P.; Allegretti, F.; Surnev, S. *J. Vac. Sci. Technol., B* **2010**, *28*, 1.

(286) Freund, H.-J.; Pacchioni, G. *Chem. Soc. Rev.* **2008**, *37*, 2224.

(287) Tauster, S. J.; Fung, S. C.; Garten, R. L. *J. Am. Chem. Soc.* **1978**, *100*, 170.

(288) Tauster, S. J.; Fung, S. C.; Baker, R. T. K.; Horsley, J. A. *Science* **1981**, *211*, 1121.

(289) Goodman, D. W. *Catal. Lett.* **2005**, *99*, 1.

(290) Diebold, U. *Surf. Sci. Rep.* **2003**, *48*, 53.

(291) Valden, M.; Lai, X.; Goodman, D. W. *Science* **1998**, *281*, 1647.

(292) Fu, Q.; Saltsburg, H.; Flytzani-Stephanopoulos, M. *Science* **2003**, *301*, 935.

(293) Guzman, J.; Carrettin, S.; Corma, A. *J. Am. Chem. Soc.* **2005**, *127*, 3286.

(294) Rodriguez, J. A.; Ma, S.; Liu, P.; Hrbek, J.; Evans, J.; Perez, M. *Science* **2007**, *318*, 1757.

(295) Rodriguez, J. A.; Hrbek, J. *Surf. Sci.* **2010**, *604*, 241.

(296) Biener, J.; Farfan-Arribas, E.; Biener, M.; Friend, C. M.; Madix, R. J. *J. Chem. Phys.* **2005**, *123*, 094705.

(297) Potapenko, D. V.; Osgood, R. M. *Nano Lett.* **2009**, *9*, 2378.

(298) Potapenko, D. V.; Hrbek, J.; Osgood, R. M. *ACS Nano* **2008**, *2*, 1353.

(299) Song, Z.; Hrbek, J.; Osgood, R. *Nano Lett.* **2005**, *5*, 1327.

(300) Zhao, X.; Ma, S.; Hrbek, J.; Rodriguez, J. A. *Surf. Sci.* **2007**, *601*, 2445.

(301) Ma, S. G.; Rodriguez, J.; Hrbek, J. *Surf. Sci.* **2008**, *602*, 3272.

(302) Ma, S.; Zhao, X.; Rodriguez, J. A.; Hrbek, J. *J. Phys. Chem. C* **2007**, *111*, 3685.

(303) Senanayake, S. D.; Stacchiola, D.; Evans, J.; Estrella, M.; Barrio, L.; Perez, M.; Hrbek, J.; Rodriguez, J. A. *J. Catal.* **2010**, *271*, 392.

(304) Esch, F.; Fabris, S.; Zhou, L.; Montini, T.; Africh, C.; Fornasiero, P.; Comelli, G.; Rosei, R. *Science* **2005**, *309*, 752.

(305) Wang, X.; Rodriguez, J. A.; Hanson, J. C.; Perez, M.; Evans, J. *J. Chem. Phys.* **2005**, *123*, 221101.

(306) Magkoev, T. T. *Surf. Sci.* **2007**, *601*, 3143.

(307) Farfan-Arribas, E.; Biener, J.; Friend, C. M.; Madix, R. J. *Surf. Sci.* **2005**, *591*, 1.

(308) Rodriguez, J. A.; Graciani, J.; Evans, J.; Park, J. B.; Yang, F.; Stacchiola, D.; Senanayake, S. D.; Ma, S. G.; Perez, M.; Liu, P.; Sanz, J. F.; Hrbek, J. *Angew. Chem., Int. Ed.* **2009**, *48*, 8047.

(309) Quek, S. Y.; Biener, M. M.; Biener, J.; Friend, C. M.; Kaxiras, E. *Surf. Sci.* **2005**, *577*, L71.

(310) Chang, Z.; Song, Z.; Liu, G.; Rodriguez, J. A.; Hrbek, J. *Surf. Sci.* **2002**, *512*, L353.

(311) Song, Z.; Cai, T.; Chang, Z.; Liu, G.; Rodriguez, J. A.; Hrbek, J. *J. Am. Chem. Soc.* **2003**, *125*, 8059.

(312) Biener, M. M.; Friend, C. M. *Surf. Sci.* **2004**, *559*, L173.

(313) Deng, X.; Quek, S. Y.; Biener, M. M.; Biener, J.; Kang, D. H.; Schalek, R.; Kaxiras, E.; Friend, C. M. *Surf. Sci.* **2008**, *602*, 1166.

(314) Biener, M. M.; Biener, J.; Schalek, R.; Friend, C. M. *J. Chem. Phys.* **2004**, *121*, 12010.

(315) Surnev, S.; Ramsey, M. G.; Netzer, F. P. *Prog. Surf. Sci.* **2003**, *73*, 117.

(316) Sebastian, I.; Heiler, M.; Meinel, K.; Neddermeyer, H. *Appl. Phys. A: Mater. Sci. Process.* **1998**, *66*, S525.

(317) Abu Haija, M.; Guimond, S.; Romanyshyn, Y.; Uhl, A.; Kuhlenbeck, H.; Todorova, T. K.; Ganduglia-Pirovano, M. V.; Dobler, J.; Sauer, J.; Freund, H. J. *Surf. Sci.* **2006**, *600*, 1497.

(318) Abu Haija, M.; Guimond, S.; Uhl, A.; Kuhlenbeck, H.; Freund, H. J. *Surf. Sci.* **2006**, *600*, 1040.

(319) Bandara, A.; Abu-Haija, M.; Höbel, F.; Kuhlenbeck, H.; Rupprechter, G.; Freund, H.-J. *Top. Catal.* **2007**, *46*, 223.

(320) Dupuis, A. C.; Abu Haija, M.; Richter, B.; Kuhlenbeck, H.; Freund, H. J. *Surf. Sci.* **2003**, *539*, 99.

(321) Guimond, S.; Abu Haija, M.; Kaya, S.; Lu, J.; Weissenrieder, J.; Shaikhutdinov, S.; Kuhlenbeck, H.; Freund, H. J.; Döbler, J.; Sauer, J. *Top. Catal.* **2006**, *38*, 117.

(322) Simic-Milosevic, V.; Nilius, N.; Rust, H. P.; Freund, H. J. *Phys. Rev. B* **2008**, *77*, 125112.

(323) Lewis, K. B.; Oyama, S. T.; Somorjai, G. A. *Surf. Sci.* **1990**, *233*, 75.

(324) Nilius, N.; Simic-Milosevic, V. *J. Phys. Chem. C* **2008**, *112*, 10027.

(325) Kresse, G.; Surnev, S.; Schoiswohl, J.; Netzer, F. P. *Surf. Sci.* **2004**, *555*, 118.

(326) Schoiswohl, J.; Sock, M.; Surnev, S.; Ramsey, M. G.; Netzer, F. P.; Kresse, G.; Andersen, J. N. *Surf. Sci.* **2004**, *555*, 101.

(327) Nilius, N. *Surf. Sci. Rep.* **2009**, *64*, 595.

(328) Guimond, S.; Sturm, J. M.; Gobke, D.; Romanyshyn, Y.; Naschitzki, M.; Kuhlenbeck, H.; Freund, H.-J. *J. Phys. Chem. C* **2008**, *112*, 11835.

(329) Guimond, S.; Gobke, D.; Romanyshyn, Y.; Sturm, J. M.; Naschitzki, M.; Kuhlenbeck, H.; Freund, H.-J. *J. Phys. Chem. C* **2008**, *112*, 12363.

(330) Sturm, J. M.; Gobke, D.; Kuhlenbeck, H.; Dobler, J.; Reinhardt, U.; Ganduglia-Pirovano, M. V.; Sauer, J.; Freund, H.-J. *Phys. Chem. Chem. Phys.* **2009**, *11*, 3290.

(331) Cornell, R. M.; Schwertmann, U. *The Iron-Oxides*; VCH: Weinheim, Germany, 1996.

(332) Weiss, W.; Ranke, W. *Prog. Surf. Sci.* **2002**, *70*, 1.

(333) Khan, N. A.; Matranga, C. *Surf. Sci.* **2008**, *602*, 932.

(334) Hakkel, O.; Paszti, Z.; Keszthelyi, T.; Frey, K.; Guczi, L. *React. Kinet. Catal. Lett.* **2009**, *96*, 345.

(335) Deng, X.; Matranga, C. *J. Phys. Chem. C* **2009**, *113*, 11104.

(336) Deng, X.; Lee, J.; Matranga, C. *Surf. Sci.* **2010**, *604*, 627.

(337) Rodriguez, J. A.; Dvorak, J.; Jirsak, T.; Hrbek, J. *Surf. Sci.* **2001**, *490*, 315.

(338) Helveg, S.; Lauritsen, J. V.; Laegsgaard, E.; Stensgaard, I.; Norskov, J. K.; Clausen, B. S.; Topsoe, H.; Besenbacher, F. *Phys. Rev. Lett.* **2000**, *84*, 951.

(339) Nielsen, J. H.; Bech, L.; Nielsen, K.; Tison, Y.; Jorgensen, K. P.; Bonde, J. L.; Horch, S.; Jaramillo, T. F.; Chorkendorff, I. *Surf. Sci.* **2009**, *603*, 1182.

(340) Besenbacher, F.; Lauritsen, J. V.; Wendt, S. *Nano Today* **2007**, *2*, 30.

3047

dx.doi.org/10.1021/cr200041p | *Chem. Rev.* 2012, 112, 2987–3054

(341) Lauritsen, J. V.; Bollinger, M. V.; Laesgaard, E.; Jacobsen, K. W.; Norskov, J. K.; Clausen, B. S.; Topsoe, H.; Besenbacher, F. *J. Catal.* **2004**, *221*, 510.

(342) Bollinger, M. V.; Lauritsen, J. V.; Jacobsen, K. W.; Norskov, J. K.; Helveg, S.; Besenbacher, F. *Phys. Rev. Lett.* **2001**, *87*, 196803.

(343) Cristol, S.; Paul, J. F.; Payen, E.; Bougeard, D.; Clemendot, S.; Hutschka, F. *J. Phys. Chem. B* **2000**, *104*, 11220.

(344) Lauritsen, J. V.; Kibsgaard, J.; Helveg, S.; Topsoe, H.; Clausen, B. S.; Laegsgaard, E.; Besenbacher, F. *Nat. Nanotechnol.* **2007**, *2*, 53.

(345) Lauritsen, J. V.; Nyberg, M.; Norskov, J. K.; Clausen, B. S.; Topsoe, H.; Laegsgaard, E.; Besenbacher, F. *J. Catal.* **2004**, *224*, 94.

(346) Lauritsen, J. V.; Nyberg, M.; Vang, R. T.; Bollinger, M. V.; Clausen, B. S.; Topsoe, H.; Jacobsen, K. W.; Laegsgaard, E.; Norskov, J. K.; Besenbacher, F. *Nanotechnology* **2003**, *14*, 385.

(347) Jaramillo, T. F.; Jorgensen, K. P.; Bonde, J.; Nielsen, J. H.; Horch, S.; Chorkendorff, I. *Science* **2007**, *317*, 100.

(348) Patterson, M. J.; Lightstone, J. M.; White, M. G. *J. Phys. Chem. A* **2008**, *112*, 12011.

(349) Lightstone, J. M.; Patterson, M. J.; Liu, P.; Lofaro, J. C.; White, M. G. *J. Phys. Chem. C* **2008**, *112*, 11495.

(350) Popov, I.; Gemming, S.; Seifert, G. *Phys. Rev. B* **2007**, *75*, 7.

(351) Wang, C.; Dotson, L.; McKelvy, M.; Glaunsinger, W. *J. Phys. Chem.* **1995**, *99*, 8216.

(352) Lewkebandara, T. S.; Winter, C. H. *Adv. Mater.* **1994**, *6*, 237.

(353) Cheon, J.; Gozum, J. E.; Girolami, G. S. *Chem. Mater.* **1997**, *9*, 1847.

(354) Biener, M. M.; Biener, J.; Friend, C. M. *J. Chem. Phys.* **2005**, *122*, 034706.

(355) Chianelli, R. R.; Berhault, G.; Raybaud, P.; Kasztelan, S.; Hafner, J.; Toulhoat, H. *Appl. Catal., A* **2002**, *227*, 83.

(356) Cai, T. H.; Song, Z.; Rodriguez, J. A.; Hrbek, J. *J. Am. Chem. Soc.* **2004**, *126*, 8886.

(357) Aray, Y.; Rodriguez, J.; Vega, D.; Coll, S.; Rodriguez-Arias, E. N.; Rosillo, F. *J. Phys. Chem. B* **2002**, *106*, 13242.

(358) Cai, T.; Song, Z.; Chang, Z.; Liu, G.; Rodriguez, J. A.; Hrbek, J. *Surf. Sci.* **2003**, *538*, 76.

(359) Liu, P.; Rodriguez, J. A.; Muckerman, J. T.; Hrbek, J. *Phys. Rev. B* **2003**, *67*, 155416.

(360) Chen, J. G. G. *Chem. Rev.* **1996**, *96*, 1477.

(361) Oyama, S. T. *Catal. Today* **1992**, *15*, 179.

(362) Hwu, H. H.; Chen, J. G. G. *Chem. Rev.* **2005**, *105*, 185.

(363) Horn, J. M.; Song, Z.; Potapenko, D. V.; Hrbek, J.; White, M. G. *J. Phys. Chem. B* **2005**, *109*, 44.

(364) Fruhberger, B.; Chen, J. G. *J. Am. Chem. Soc.* **1996**, *118*, 11599.

(365) Flaherty, D. W.; Berglund, S. P.; Mullins, C. B. *J. Catal.* **2010**, *269*, 33.

(366) Rodriguez, J. A.; Dvorak, J.; Jirsak, T. *Surf. Sci.* **2000**, *457*, L413.

(367) Potapenko, D. V.; Horn, J. M.; White, M. G. *J. Catal.* **2005**, *236*, 346.

(368) Rodriguez, J. A. *Surf. Sci. Rep.* **1996**, *24*, 225.

(369) Campbell, C. T. *Annu. Rev. Phys. Chem.* **1990**, *41*, 775.

(370) Liu, P.; Norskov, J. K. *Phys. Chem. Chem. Phys.* **2001**, *3*, 3814.

(371) Meyer, J. A.; Baikie, I. D.; Kopatzki, E.; Behm, R. J. *Surf. Sci.* **1996**, *365*, L647.

(372) Casari, C. S.; Foglio, S.; Siviero, F.; Li Bassi, A.; Passoni, M.; Bottani, C. E. *Phys. Rev. B* **2009**, *79*, 9.

(373) Brune, H. *Surf. Sci. Rep.* **1998**, *31*, 125.

(374) Weissman-Wenocur, D. L.; Stefan, P. M.; Pate, B. B.; Shek, M. L.; Lindau, I.; Spicer, W. E. *Phys. Rev. B* **1983**, *27*, 3308.

(375) Hutchings, G. J. *Chem. Commun.* **2008**, 1148.

(376) Hutchings, G. J. *Dalton Trans.* **2008**, 5523.

(377) Sluiter, M. H. F.; Colinet, C.; Pasturel, A. *Phys. Rev. B* **2006**, *73*, 174204.

(378) Chen, M. S.; Luo, K.; Wei, T.; Yan, Z.; Kumar, D.; Yi, C. W.; Goodman, D. W. *Catal. Today* **2006**, *117*, 37.

(379) Baber, A. E.; Tierney, H. L.; Sykes, E. C. H. *ACS Nano* **2010**, *4*, 1637.

(380) Stephenson, A. W.; Baddeley, C. J.; Tikhov, M. S.; Lambert, R. M. *Surf. Sci.* **1998**, *398*, 172.

(381) Baddeley, C. J.; Barnes, C. J.; Wander, A.; Ormerod, R. M.; King, D. A.; Lambert, R. M. *Surf. Sci.* **1994**, *314*, 1.

(382) Eguchi, T.; Kamoshida, A.; Ono, M.; Hamada, M.; Shoda, R.; Nishio, T.; Harasawa, A.; Okuda, T.; Kinoshita, T.; Hasegawa, Y. *Phys. Rev. B* **2006**, *74*, 4.

(383) Chen, M.; Kumar, D.; Yi, C.-W.; Goodman, D. W. *Science* **2005**, *310*, 291.

(384) Maroun, F.; Ozanam, F.; Magnussen, O. M.; Behm, R. J. *Science* **2001**, *293*, 1811.

(385) Baddeley, C. J.; Ormerod, R. M.; Stephenson, A. W.; Lambert, R. M. *J. Phys. Chem.* **1995**, *99*, 5146.

(386) Jablonski, A.; Overbury, S. H.; Somorjai, G. A. *Surf. Sci.* **1977**, *65*, 578.

(387) Koel, B. E.; Sellidj, A.; Paffett, M. T. *Phys. Rev. B* **1992**, *46*, 7846.

(388) Kibler, L. A.; El-Aziz, A. M.; Kolb, D. M. *J. Mol. Catal. A: Chem.* **2003**, *199*, 57.

(389) Kibler, L. A.; Kleinert, M.; Randler, R.; Kolb, D. M. *Surf. Sci.* **1999**, *443*, 19.

(390) Naohara, H.; Ye, S.; Uosaki, K. *J. Phys. Chem. B* **1998**, *102*, 4366.

(391) Naohara, H.; Ye, S.; Uosaki, K. *J. Electroanal. Chem.* **2001**, *500*, 435.

(392) Baldauf, M.; Kolb, D. M. *Electrochim. Acta* **1993**, *38*, 2145.

(393) Baldauf, M.; Kolb, D. M. *J. Phys. Chem.* **1996**, *100*, 11375.

(394) Dolle, P.; Baudoing-Savois, R.; De Santis, M.; Saint-Lager, M. C.; Abel, M.; Bertolini, J. C.; Delichere, P. *Surf. Sci.* **2002**, *518*, 1.

(395) Robach, Y.; Abel, M.; Porte, L. *Surf. Sci.* **2003**, *526*, 248.

(396) Martin, D. S.; Blanchard, N. P.; Weightman, P. *Phys. Rev. B* **2004**, *69*, 4.

(397) Kibler, L. A.; Kleinert, M.; Lazarescu, V.; Kolb, D. M. *Surf. Sci.* **2002**, *498*, 175.

(398) Pinheiro, A. L. N.; Zei, M. S.; Luo, M. F.; Ertl, G. *Surf. Sci.* **2006**, *600*, 641.

(399) Naohara, H.; Ye, S.; Uosaki, K. *J. Electroanal. Chem.* **1999**, *473*, 2.

(400) Ormerod, R. M.; Baddeley, C. J.; Lambert, R. M. *Surf. Sci.* **1991**, *259*, L709.

(401) Li, Z. J.; Gao, F.; Wang, Y. L.; Calaza, F.; Burkholder, L.; Tysoe, W. T. *Surf. Sci.* **2007**, *601*, 1898.

(402) Fischer, R.; Fauster, T. *Surf. Rev. Lett.* **1996**, *3*, 1783.

(403) Kuk, Y.; Feldman, L. C.; Silverman, P. J. *Phys. Rev. Lett.* **1983**, *50*, 511.

(404) Li, Z.; Furlong, O.; Calaza, F.; Burkholder, L.; Poon, H. C.; Saldin, D.; Tysoe, W. T. *Surf. Sci.* **2008**, *602*, 1084.

(405) Gleich, B.; Ruff, M.; Behm, R. J. *Surf. Sci.* **1997**, *386*, 48.

(406) Baddeley, C. J.; Tikhov, M.; Hardacre, C.; Lomas, J. R.; Lambert, R. M. *J. Phys. Chem.* **1996**, *100*, 2189.

(407) Calaza, F.; Gao, F.; Li, Z.; Tysoe, W. T. *Surf. Sci.* **2007**, *601*, 714.

(408) Li, Z.; Calaza, F.; Gao, F.; Tysoe, W. T. *Surf. Sci.* **2007**, *601*, 1351.

(409) Boscoboinik, J. A.; Plaisance, C.; Neurock, M.; Tysoe, W. T. *Phys. Rev. B* **2008**, *77*, 6.

(410) Schmitz, P. J.; Leung, W. Y.; Kang, H. C.; Thiel, P. A. *Phys. Rev. B* **1991**, *43*, 8834.

(411) Schmitz, P. J.; Kang, H. C.; Leung, W. Y.; Thiel, P. A. *Surf. Sci.* **1991**, *248*, 287.

(412) Vos, M.; Mitchell, I. V. *Phys. Rev. B* **1992**, *45*, 9398.

(413) Nieminen, J. A. *Phys. Rev. Lett.* **1995**, *74*, 3856.

(414) Kralj, M.; Bailly, A.; Saint-Lager, M. C.; Degen, S.; Krupski, A.; Becker, C.; Dolle, P.; De Santis, M.; Wandelt, K. *Surf. Sci.* **2006**, *600*, 2614.

(415) Kaukasoina, P.; Lindroos, M.; Warren, O. L.; Thiel, P. A. *Surf. Sci.* **1994**, *318*, 243.

(416) Yi, C. W.; Luo, K.; Wei, T.; Goodman, D. W. *J. Phys. Chem. B* **2005**, *109*, 18535.

3048

dx.doi.org/10.1021/cr200041p | *Chem. Rev.* 2012, 112, 2987–3054

(417) Brongersma, H. H.; Draxler, M.; de Ridder, M.; Bauer, P. *Surf. Sci. Rep.* **2007**, *62*, 63.

(418) Wei, T.; Wang, J.; Goodman, D. W. *J. Phys. Chem. C* **2007**, *111*, 8781.

(419) Pluntke, Y.; Kibler, L. A.; Kolb, D. M. *Phys. Chem. Chem. Phys.* **2008**, *10*, 3684.

(420) Han, P.; Axnanda, S.; Lyubinetsky, I.; Goodman, D. W. *J. Am. Chem. Soc.* **2007**, *129*, 14355.

(421) Gao, F.; Wang, Y. L.; Goodman, D. W. *J. Phys. Chem. C* **2010**, *114*, 4036.

(422) Sellidj, A.; Koel, B. E. *Phys. Rev. B* **1994**, *49*, 8367.

(423) Ruff, M.; Frey, S.; Gleich, B.; Behm, R. J. *Appl. Phys. A: Mater. Sci. Process.* **1998**, *66*, S513.

(424) Ruff, M.; Takehiro, N.; Liu, P.; Norskov, J. K.; Behm, R. J. *ChemPhysChem* **2007**, *8*, 2068.

(425) Li, Z.; Gao, F.; Furlong, O.; Tysoe, W. T. *Surf. Sci.* **2010**, *604*, 136.

(426) Xu, J.; White, T.; Li, P.; He, C. H.; Yu, J. G.; Yuan, W. K.; Han, Y. F. *J. Am. Chem. Soc.* **2010**, *132*, 10398.

(427) Shen, X. Y.; Frankel, D. J.; Hermanson, J. C.; Lapeyre, G. J.; Smith, R. J. *Phys. Rev. B* **1985**, *32*, 2120.

(428) Shen, X. Y.; Frankel, D. J.; Lapeyre, G. J.; Smith, R. J. *Phys. Rev. B* **1986**, *33*, 5372.

(429) Szanyi, J.; Kuhn, W. K.; Goodman, D. W. *J. Vac. Sci. Technol., A* **1993**, *11*, 1969.

(430) Gao, F.; Wang, Y.; Goodman, D. W. *J. Phys. Chem. C* **2009**, *113*, 14993.

(431) Soto-Verdugo, V.; Metiu, H. *Surf. Sci.* **2007**, *601*, 5332.

(432) Gao, F.; Wang, Y.; Goodman, D. W. *J. Am. Chem. Soc.* **2009**, *131*, 5734.

(433) Piednoir, A.; Languille, M. A.; Piccolo, L.; Valcarcel, A.; Aires, F.; Bertolini, J. C. *Catal. Lett.* **2007**, *114*, 110.

(434) Zhang, J.; Jin, H. M.; Sullivan, M. B.; Chiang, F.; Lim, H.; Wu, P. *Phys. Chem. Chem. Phys.* **2009**, *11*, 1441.

(435) Gao, F.; Wang, Y. L.; Goodman, D. W. *J. Catal.* **2009**, *268*, 115.

(436) Landon, P.; Collier, P. J.; Papworth, A. J.; Kiely, C. J.; Hutchings, G. J. *Chem. Commun.* **2002**, 2058.

(437) Staykov, A.; Kamachi, T.; Ishihara, T.; Yoshizawa, K. *J. Phys. Chem. C* **2008**, *112*, 19501.

(438) Han, Y. F.; Zhong, Z. Y.; Ramesh, K.; Chen, F. X.; Chen, L. W.; White, T.; Tay, Q. L.; Yaakub, S. N.; Wang, Z. *J. Phys. Chem. C* **2007**, *111*, 8410.

(439) Weissman-Wenocur, D. L.; Spicer, W. E. *Surf. Sci.* **1983**, *133*, 499.

(440) Lam, Y. L.; Criado, J.; Boudart, M. *New J. Chem.* **1977**, *1*, 461.

(441) Piccolo, L.; Piednoir, A.; Bertolini, J.-C. *Surf. Sci.* **2006**, *600*, 4211.

(442) Venkatachalam, S.; Jacob, T. *Phys. Chem. Chem. Phys.* **2009**, *11*, 3263.

(443) Calaza, F.; Li, Z.; Gao, F.; Boscoboinik, J.; Tysoe, W. T. *Surf. Sci.* **2008**, *602*, 3523.

(444) Owens, T. G.; Jones, T. E.; Noakes, T. C. Q.; Bailey, P.; Baddeley, C. J. *J. Phys. Chem. B* **2006**, *110*, 21152.

(445) Chen, M. S.; Goodman, D. W. *Chin. J. Catal.* **2008**, *29*, 1178.

(446) Luo, K.; Wei, T.; Yi, C. W.; Axnanda, S.; Goodman, D. W. *J. Phys. Chem. B* **2005**, *109*, 23517.

(447) Nakamura, S.; Yasui, T. *J. Catal.* **1970**, *17*, 366.

(448) Samanos, B.; Boutry, P.; Montarnal, R. *J. Catal.* **1971**, *23*, 19.

(449) Mazzone, G.; Rivalta, I.; Russo, N.; Sicilia, E. *Chem. Commun.* **2009**, 1852.

(450) Stacchiola, D.; Calaza, F.; Burkholder, L.; Schwabacher, A. W.; Neurock, M.; Tysoe, W. T. *Angew. Chem., Int. Ed.* **2005**, *44*, 4572.

(451) Mei, D. H.; Hansen, E. W.; Neurock, M. *J. Phys. Chem. B* **2003**, *107*, 798.

(452) Pallassana, V.; Neurock, M. *J. Catal.* **2000**, *191*, 301.

(453) Piccolo, L.; Piednoir, A.; Bertolini, J.-C. *Surf. Sci.* **2005**, *592*, 169.

(454) Enache, D. I.; Edwards, J. K.; Landon, P.; Solsona-Espriu, B.; Carley, A. F.; Herzing, A. A.; Watanabe, M.; Kiely, C. J.; Knight, D. W.; Hutchings, G. J. *Science* **2006**, *311*, 362.

(455) Kesavan, L.; Tiruvalam, R.; Rahim, M. H. A.; bin Saiman, M. I.; Enache, D. I.; Jenkins, R. L.; Dimitratos, N.; Lopez-Sanchez, J. A.; Taylor, S. H.; Knight, D. W.; Kiely, C. J.; Hutchings, G. J. *Science* **2011**, *331*, 195.

(456) Lee, A. F.; Hackett, S. F. J.; Hutchings, G. J.; Lizzit, S.; Naughton, J.; Wilson, K. *Catal. Today* **2009**, *145*, 251.

(457) Naughton, J.; Lee, A. F.; Thompson, S.; Vinod, C. P.; Wilson, K. *Phys. Chem. Chem. Phys.* **2010**, *12*, 2670.

(458) Lee, A. F.; Baddeley, C. J.; Hardacre, C.; Ormerod, R. M.; Lambert, R. M.; Schmid, G.; West, H. *J. Phys. Chem.* **1995**, *99*, 6096.

(459) Gao, F.; Wang, Y.; Li, Z.; Furlong, O.; Tysoe, W. T. *J. Phys. Chem. C* **2008**, *112*, 3362.

(460) Santra, A. K.; Rao, C. N. R. *Appl. Surf. Sci.* **1995**, *84*, 347.

(461) Nielsen, L. P.; Besenbacher, F.; Stensgaard, I.; Laegsgaard, E.; Engdahl, C.; Stoltze, P.; Jacobsen, K. W.; Norskov, J. K. *Phys. Rev. Lett.* **1993**, *71*, 754.

(462) Umezawa, K.; Nakanishi, S.; Gibson, W. M. *Phys. Rev. B* **1998**, *57*, 8842.

(463) Hitzke, A.; Hugenschmidt, M. B.; Behm, R. J. *Surf. Sci.* **1997**, *389*, 8.

(464) Nielsen, L. P.; Besenbacher, F.; Stensgaard, I.; Laegsgaard, E. *Phys. Rev. Lett.* **1995**, *74*, 1159.

(465) Nowicki, M.; Rusiniak, L.; Turko, D.; Mroz, S. *J. Electron Spectrosc. Relat. Phenom.* **2006**, *154*, 9.

(466) Besenbacher, F.; Chorkendorff, I.; Clausen, B. S.; Hammer, B.; Molenbroek, A. M.; Norskov, J. K.; Stensgaard, I. *Science* **1998**, *279*, 1913.

(467) Jacobsen, J.; Pleth Nielsen, L.; Besenbacher, F.; Stensgaard, I.; Lagsgaard, E.; Rasmussen, T.; Jacobsen, K. W.; Norskov, J. K. *Phys. Rev. Lett.* **1995**, *75*, 489.

(468) Termentzidis, K.; Hafner, J.; Mittendorfer, F. *J. Phys.: Condens. Matter* **2006**, *18*, 10825.

(469) Umezawa, K.; Nakanishi, S.; Gibson, W. M. *Surf. Sci.* **1999**, *426*, 225.

(470) Jones, T. E.; Noakes, T. C. Q.; Bailey, P.; Baddeley, C. J. *Surf. Sci.* **2006**, *600*, 2129.

(471) Zafeiratos, S.; Kennou, S. *J. Phys. Chem. B* **2002**, *106*, 41.

(472) Trant, A. G.; Jones, T. E.; Noakes, T. C. Q.; Bailey, P.; Baddeley, C. J. *Surf. Sci.* **2010**, *604*, 300.

(473) Chambliss, D. D.; Wilson, R. J.; Chiang, S. *J. Vac. Sci. Technol., B* **1991**, *9*, 933.

(474) Chambliss, D. D.; Wilson, R. J.; Chiang, S. *Phys. Rev. Lett.* **1991**, *66*, 1721.

(475) Katona, G. L.; Erdelyi, Z.; Beke, D. L.; Dietrich, C.; Weigl, F.; Boyen, H. G.; Koslowski, B.; Ziemann, P. *Phys. Rev. B* **2005**, *71*, 115432.

(476) Trant, A. G.; Jones, T. E.; Gustafson, J.; Noakes, T. C. Q.; Bailey, P.; Baddeley, C. J. *Surf. Sci.* **2009**, *603*, 571.

(477) Tan, X.; Yang, G. W. *J. Alloys Compd.* **2009**, *467*, 428.

(478) Hugenschmidt, M. B.; Hitzke, A.; Behm, R. J. *Phys. Rev. Lett.* **1996**, *76*, 2535.

(479) Fan, W.; Gong, X. G. *Appl. Surf. Sci.* **2003**, *219*, 117.

(480) Cullen, W. G.; First, P. N. *Surf. Sci.* **1999**, *420*, 53.

(481) Vestergaard, E. K.; Vang, R. T.; Knudsen, J.; Pedersen, T. M.; An, T.; Lagsgaard, E.; Stensgaard, I.; Hammer, B.; Besenbacher, F. *Phys. Rev. Lett.* **2005**, *95*, 126101.

(482) Zhdanov, V. P.; Vang, R. T.; Knudsen, J.; Vestergaard, E. K.; Besenbacher, F. *Surf. Sci.* **2006**, *600*, L260.

(483) Holmblad, P. M.; Larsen, J. H.; Chorkendorff, I. *J. Chem. Phys.* **1996**, *104*, 7289.

(484) Termentzidis, K.; Hafner, J. *J. Phys.: Condens. Matter* **2007**, *19*, 7.

(485) Lahr, D. L.; Ceyer, S. T. *J. Am. Chem. Soc.* **2006**, *128*, 1800.

(486) Knudsen, J.; Merte, L. R.; Peng, G.; Vang, R. T.; Resta, A.; Lagsgaard, E.; Andersen, J. N.; Mavrikakis, M.; Besenbacher, F. *ACS Nano* **2010**, *4*, 4380.

(487) Kratzer, P.; Hammer, B.; Norskov, J. K. *J. Chem. Phys.* **1996**, *105*, 5595.

(488) Jones, T. E.; Noakes, T. C. Q.; Bailey, P.; Baddeley, C. J. *J. Phys. Chem. B* **2004**, *108*, 4759.

(489) Nahas, Y.; Repain, V.; Chacon, C.; Girard, Y.; Rousset, S. *Surf. Sci.* **2010**, *604*, 829.

(490) Matthews, J. W.; Jesser, W. A. *Acta Metall.* **1967**, *15*, 595.

(491) Sachtler, J. W. A.; Vanhove, M. A.; Biberian, J. P.; Somorjai, G. A. *Surf. Sci.* **1981**, *110*, 19.

(492) Sugawara, A.; Nittono, O. *J. Cryst. Growth* **1991**, *115*, 596.

(493) Uosaki, K.; Ye, S.; Naohara, H.; Oda, Y.; Haba, T.; Kondo, T. *J. Phys. Chem. B* **1997**, *101*, 7566.

(494) Waibel, H. F.; Kleinert, M.; Kibler, L. A.; Kolb, D. M. *Electrochim. Acta* **2002**, *47*, 1461.

(495) Chang, T.-M.; Carter, E. A. *J. Phys. Chem.* **1995**, *99*, 7637.

(496) Haftel, M. I.; Rosen, M.; Franklin, T.; Hettermann, M. *Phys. Rev. B* **1996**, *53*, 8007.

(497) Pedersen, M. O.; Helveg, S.; Ruban, A.; Stensgaard, I.; Lagsgaard, E.; Norskov, J. K.; Besenbacher, F. *Surf. Sci.* **1999**, *426*, 395.

(498) Mathur, A.; Erlebacher, J. *Surf. Sci.* **2008**, *602*, 2863.

(499) Sachtler, J. W. A.; Somorjai, G. A. *J. Catal.* **1983**, *81*, 77.

(500) Berg, C.; Venvik, H. J.; Strisland, F.; Ramstad, A.; Borg, A. *Surf. Sci.* **1998**, *409*, 1.

(501) Kobiela, T.; Moors, M.; Linhart, W.; Cebula, I.; Krupski, A.; Becker, C.; Wandelt, K. *Thin Solid Films* **2010**, *518*, 3650.

(502) Gohda, Y.; Gro, A. *Surf. Sci.* **2007**, *601*, 3702.

(503) Gotsis, H. J.; Rivalta, I.; Sicilia, E.; Russo, N. *Chem. Phys. Lett.* **2007**, *442*, 105.

(504) Gross, A. *J. Phys.: Condens. Matter* **2009**, *21*, 7.

(505) Yeates, R. C.; Somorjai, G. A. *J. Catal.* **1987**, *103*, 208.

(506) Skelton, D. C.; Wang, H.; Tobin, R. G.; Lambert, D. K.; DiMaggio, C. L.; Fisher, G. B. *J. Phys. Chem. B* **2001**, *105*, 204.

(507) Skelton, D. C.; Tobin, R. G.; Lambert, D. K.; DiMaggio, C. L.; Fisher, G. B. *J. Phys. Chem. B* **1999**, *103*, 964.

(508) Skelton, D. C.; Tobin, R. G.; Fisher, G. B.; Lambert, D. K.; DiMaggio, C. L. *J. Phys. Chem. B* **2000**, *104*, 548.

(509) Asakura, K.; Lauterbach, J.; Rotermund, H. H.; Ertl, G. *Surf. Sci.* **1997**, *374*, 125.

(510) Strbac, S.; Magnussen, O. M.; Behm, R. J. *Phys. Rev. Lett.* **1999**, *83*, 3246.

(511) Strbac, S.; Behm, R. J.; Crown, A.; Wieckowski, A. *Surf. Sci.* **2002**, *517*, 207.

(512) Ling, W. L.; Hamilton, J. C.; Thurmer, K.; Thayer, G. E.; de la Figuera, J.; Hwang, R. Q.; Carter, C. B.; Bartelt, N. C.; McCarty, K. F. *Surf. Sci.* **2006**, *600*, 1735.

(513) Bzowski, A.; Sham, T. K.; Watson, R. E.; Weinert, M. *Phys. Rev. B* **1995**, *51*, 9979.

(514) Park, C. *Surf. Sci.* **1988**, *203*, 395.

(515) Steltenpohl, A.; Memmel, N.; Taglauer, E.; Fauster, T.; Onsgaard, J. *Surf. Sci.* **1997**, *382*, 300.

(516) Harendt, C.; Christmann, K.; Hirschwald, W.; Vickerman, J. C. *Surf. Sci.* **1986**, *165*, 413.

(517) Bzowski, A.; Kuhn, M.; Sham, T. K.; Rodriguez, J. A.; Hrbek, J. *Phys. Rev. B* **1999**, *59*, 13379.

(518) Potschke, G.; Schroder, J.; Gunther, C.; Hwang, R. Q.; Behm, R. J. *Surf. Sci.* **1991**, *251*, 592.

(519) Hwang, R. Q.; Schroder, J.; Gunther, C.; Behm, R. J. *Phys. Rev. Lett.* **1991**, *67*, 3279.

(520) Poulston, S.; Tikhov, M.; Lambert, R. M. *Langmuir* **1997**, *13*, 5356.

(521) Poulston, S.; Tikhov, M.; Lambert, R. M. *Surf. Sci.* **1993**, *287*, 969.

(522) Kumar, V.; Bennemann, K. H. *Phys. Rev. Lett.* **1984**, *53*, 278.

(523) Xia, X. H.; Nagle, L.; Schuster, R.; Magnussen, O. M.; Behm, R. J. *Phys. Chem. Chem. Phys.* **2000**, *2*, 4387.

(524) Vasiljevic, N.; Viyannalage, L. T.; Dimitrov, N.; Sieradzki, K. *J. Electroanal. Chem.* **2008**, *613*, 118.

(525) Nakai, Y.; Zei, M. S.; Kolb, D. M.; Lehmpfuhl, G. *Ber. Bunsen-Ges. Phys. Chem. Chem. Phys.* **1984**, *88*, 340.

(526) Zhao, X. Y.; Liu, P.; Hrbek, J.; Rodriguez, J. A.; Perez, M. *Surf. Sci.* **2005**, *592*, 25.

(527) Chambliss, D. D.; Wilson, R. J.; Chiang, S. *J. Vac. Sci. Technol., A* **1992**, *10*, 1993.

(528) Chambliss, D. D.; Chiang, S. *Surf. Sci.* **1992**, *264*, L187.

(529) Kyriakou, G.; Williams, F. J.; Tikhov, M. S.; Wander, A.; Lambert, R. M. *Phys. Rev. B* **2005**, *72*, 4.

(530) Noakes, T. C. Q.; Bailey, P. *Thin Solid Films* **2001**, *394*, 15.

(531) Borensztein, Y.; Lopez-Rios, T.; Vuye, G. *Phys. Rev. B* **1988**, *37*, 6235.

(532) Cercellier, H.; Fagot-Revurat, Y.; Kierren, B.; Malterre, D.; Reinert, F. *Surf. Sci.* **2004**, *566*, 520.

(533) Lipphardt, U.; Engelhard, H.; Westhof, J.; Goldmann, A.; Witzel, S. *Surf. Sci.* **1993**, *294*, 84.

(534) Papathanakos, V.; Evangelakis, G. A. *Surf. Sci.* **2002**, *499*, 229.

(535) Lei, H. L.; Hou, Q.; Hou, M. *J. Phys.: Condens. Matter* **2000**, *12*, 8387.

(536) Hsieh, T. C.; Chiang, T. C. *Surf. Sci.* **1986**, *166*, 554.

(537) Cercellier, H.; Didiot, C.; Fagot-Revurat, Y.; Kierren, B.; Moreau, L.; Malterre, D.; Reinert, F. *Phys. Rev. B* **2006**, *73*, 16.

(538) Dovek, M. M.; Lang, C. A.; Nogami, J.; Quate, C. F. *Phys. Rev. B* **1989**, *40*, 11973.

(539) Eisenhut, B.; Stober, J.; Rangelov, G.; Fauster, T. *Phys. Rev. B* **1994**, *49*, 14676.

(540) Chambliss, D. D.; Wilson, R. J. *J. Vac. Sci. Technol., B* **1991**, *9*, 928.

(541) Corcoran, S. G.; Chakarova, G. S.; Sieradzki, K. *Phys. Rev. Lett.* **1993**, *71*, 1585.

(542) Hugenschmidt, M. B.; Ruff, M.; Hitzke, A.; Behm, R. J. *Surf. Sci.* **1997**, *388*, L1100.

(543) Hirschorn, E. S.; Miller, T.; Sieger, M.; Chiang, T. C. *Surf. Sci.* **1993**, *295*, L1045.

(544) Hirschorn, E. S.; Lin, D. S.; Hansen, E. D.; Chiang, T. C. *Surf. Sci.* **1995**, *323*, L299.

(545) Hayoz, J.; Pillo, T.; Fasel, R.; Schlapbach, L.; Aebi, P. *Phys. Rev. B* **1999**, *59*, 15975.

(546) Bader, S. D.; Moog, E. R. *J. Appl. Phys.* **1987**, *61*, 3729.

(547) Zhao, X. Y.; Rodriguez, J. *Surf. Sci.* **2006**, *600*, 2113.

(548) Chou, J. P.; Pai, W. W.; Kuo, C. C.; Lee, J. D.; Lin, C. H.; Wei, C. M. *J. Phys. Chem. C* **2009**, *113*, 13151.

(549) Greeley, J.; Mavrikakis, M. *Nat. Mater.* **2004**, *3*, 810.

(550) Kandoi, S.; Ferrin, P. A.; Mavrikakis, M. *Top. Catal.* **2010**, *53*, 384.

(551) Okada, M.; Nakamura, M.; Moritani, K.; Kasai, T. *Surf. Sci.* **2003**, *523*, 218.

(552) Okada, M.; Ogura, S.; Dino, W. A.; Wilde, M.; Fukutani, K.; Kasai, T. *Appl. Catal., A* **2005**, *291*, 55.

(553) Okada, M.; Ogura, S.; Dino, W. A.; Wilde, M.; Fukutani, K.; Kasai, T. *Appl. Surf. Sci.* **2005**, *246*, 68.

(554) Ogura, S.; Fukutani, K. *J. Phys.: Condens. Matter* **2009**, *21*, 8.

(555) Ogura, S.; Fukutani, K.; Okada, M. *Top. Catal.* **2007**, *44*, 65.

(556) Okada, M.; Moritani, K.; Kasai, T.; Dino, W. A.; Kasai, H.; Ogura, S.; Wilde, M.; Fukutani, K. *Phys. Rev. B* **2005**, *71*, 4.

(557) Ogura, S.; Fukutani, K.; Wilde, M.; Matsumoto, M.; Okano, T.; Okada, M.; Kasai, T.; Dino, W. A. *Surf. Sci.* **2004**, *566*–*568*, 755.

(558) Ferrin, P. A.; Kandoi, S.; Zhang, J. L.; Adzic, R.; Mavrikakis, M. *J. Phys. Chem. C* **2009**, *113*, 1411.

(559) Ruban, A.; Hammer, B.; Stoltze, P.; Skriver, H. L.; Norskov, J. K. *J. Mol. Catal. A: Chem.* **1997**, *115*, 421.

(560) Barth, J. V.; Brune, H.; Schuster, R.; Ertl, G.; Behm, R. J. *Surf. Sci.* **1993**, *292*, L769.

(561) Barth, J. V.; Behm, R. J.; Ertl, G. *Surf. Sci.* **1995**, *341*, 62.

(562) Barth, J. V.; Behm, R. J.; Ertl, G. *Surf. Sci.* **1994**, *302*, L319.

(563) Barth, J. V.; Schuster, R.; Behm, R. J.; Ertl, G. *Surf. Sci.* **1996**, *348*, 280.

(564) Behm, R. J.; Flynn, D. K.; Jamison, K. D.; Ertl, G.; Thiel, P. A. *Phys. Rev. B* **1987**, *36*, 9267.

(565) Flynn, D. K.; Jamison, K. D.; Thiel, P. A.; Ertl, G.; Behm, R. J. *J. Vac. Sci. Technol., A: Vac. Surf. Films* **1987**, *5*, 794.

(566) Ho, K. M.; Chan, C. T.; Bohnen, K. P. *Phys. Rev. B* **1989**, *40*, 9978.

(567) Haberle, P.; Gustafsson, T. *Phys. Rev. B* **1989**, *40*, 8218.

(568) Barth, J. V.; Schuster, R.; Wintterlin, J.; Behm, R. J.; Ertl, G. *Phys. Rev. B* **1995**, *51*, 4402.

(569) Neumann, A.; Schroeder, S. L. M.; Christmann, K. *Phys. Rev. B* **1995**, *51*, 17007.

(570) Tochihara, H.; Mizuno, S. *Prog. Surf. Sci.* **1998**, *58*, 1.

(571) Okada, M.; Iwai, H.; Klauser, R.; Murata, Y. *J. Phys.: Condens. Matter* **1992**, *4*, L593.

(572) Schroeder, S. L. M.; Neumann, A.; Solomun, T.; Lenzsolomun, P.; Christmann, K. *Surf. Sci.* **1995**, *337*, 285.

(573) Barth, J. V.; Schuster, R.; Behm, R. J.; Ertl, G. *Surf. Sci.* **1994**, *302*, 158.

(574) Solomun, T.; Baumgartel, H.; Christmann, K. *J. Phys. Chem.* **1991**, *95*, 10041.

(575) Neumann, A.; Rabus, H.; Arvanitis, D.; Solomun, T.; Christmann, K.; Baberschke, K. *Chem. Phys. Lett.* **1993**, *201*, 108.

(576) Farkas, A. P.; Solymosi, F. *J. Phys. Chem. C* **2009**, *113*, 19930.

(577) Farkas, A. P.; Solymosi, F. *J. Phys. Chem. C* **2010**, *114*, 16979.

(578) Voigtlander, B.; Meyer, G.; Amer, N. M. *Surf. Sci.* **1991**, *255*, L529.

(579) Voigtlander, B.; Meyer, G.; Amer, N. M. *Phys. Rev. B* **1991**, *44*, 10354.

(580) Altman, E. I.; Colton, R. J. *Surf. Sci.* **1994**, *304*, L400.

(581) Fischer, B.; Brune, H.; Barth, J. V.; Fricke, A.; Kern, K. *Phys. Rev. Lett.* **1999**, *82*, 1732.

(582) Goodman, D. W. *J. Phys. Chem.* **1996**, *100*, 13090.

(583) Freund, H. J. *Surf. Sci.* **2002**, *500*, 271.

(584) Campbell, C. T. *Surf. Sci. Rep.* **1997**, *27*, 1.

(585) Bredow, T.; Pacchioni, G. *Chem. Phys. Lett.* **2002**, *355*, 417.

(586) Cosandey, F.; Madey, T. E. *Surf. Rev. Lett.* **2001**, *8*, 73.

(587) Eyrich, M.; Kielbassa, S.; Diemant, T.; Biskupek, J.; Kaiser, U.; Wiedwald, U.; Ziemann, P.; Bansmann, J. *ChemPhysChem* **2010**, *11*, 1430.

(588) Zhang, L.; Persaud, R.; Madey, T. E. *Phys. Rev. B* **1997**, *56*, 10549.

(589) Lai, X.; St Clair, T. P.; Valden, M.; Goodman, D. W. *Prog. Surf. Sci.* **1998**, *59*, 25.

(590) Parker, S. C.; Grant, A. W.; Bondzie, V. A.; Campbell, C. T. *Surf. Sci.* **1999**, *441*, 10.

(591) Guo, Q. L.; Luo, K.; Davis, K. A.; Goodman, D. W. *Surf. Interface Anal.* **2001**, *32*, 161.

(592) Sykes, E. C. H.; Williams, F. J.; Tikhov, M. S.; Lambert, R. M. *J. Phys. Chem. B* **2002**, *106*, 5390.

(593) Santra, A. K.; Kolmakov, A.; Yang, F.; Goodman, D. W. *Jpn. J. Appl. Phys.* **2003**, *42*, 4795.

(594) Wahlstrom, E.; Lopez, N.; Schaub, R.; Thostrup, P.; Ronnau, A.; Africh, C.; Laegsgaard, E.; Norskov, J. K.; Besenbacher, F. *Phys. Rev. Lett.* **2003**, *90*, 026101.

(595) Lopez, N.; Norskov, J. K.; Janssens, T. V. W.; Carlsson, A.; Puig-Molina, A.; Clausen, B. S.; Grunwaldt, J. D. *J. Catal.* **2004**, *225*, 86.

(596) Maeda, Y.; Fujitani, T.; Tsubota, S.; Haruta, M. *Surf. Sci.* **2004**, *562*, 1.

(597) Pillay, D.; Hwang, G. S. *Phys. Rev. B* **2005**, *72*, 6.

(598) Okazawa, T.; Fujiwara, M.; Nishimura, T.; Akita, T.; Kohyama, M.; Kido, Y. *Surf. Sci.* **2006**, *600*, 1331.

(599) Lazzari, R.; Renaud, G.; Jupille, J.; Leroy, F. *Phys. Rev. B* **2007**, *76*, 18.

(600) Yu, X.; Xu, L. S.; Zhang, W. H.; Jiang, Z. Q.; Zhu, J. F.; Huang, W. X. *Chin. J. Chem. Phys.* **2009**, *22*, 339.

(601) Shibata, N.; Goto, A.; Matsunaga, K.; Mizoguchi, T.; Findlay, S. D.; Yamamoto, T.; Ikuhara, Y. *Phys. Rev. Lett.* **2009**, *102*, 4.

(602) Pabisiak, T.; Kiejna, A. *Phys. Rev. B* **2009**, *79*, 10.

(603) Carrettin, S.; Hao, Y.; Aguilar-Guerrero, V.; Gates, B. C.; Trasobares, S.; Calvino, J. J.; Corma, A. *Chem.—Eur. J* **2007**, *13*, 7771.

(604) Lopez, N.; Norskov, J. K. *Surf. Sci.* **2002**, *515*, 175.

(605) Chretien, S.; Metiu, H. *J. Chem. Phys.* **2007**, *127*, 13.

(606) Giordano, L.; Pacchioni, G.; Bredow, T.; Sanz, J. F. *Surf. Sci.* **2001**, *471*, 21.

(607) Wang, Y.; Hwang, G. S. *Surf. Sci.* **2003**, *542*, 72.

(608) Vittadini, A.; Selloni, A. *J. Chem. Phys.* **2002**, *117*, 353.

(609) Matthey, D.; Wang, J. G.; Wendt, S.; Matthiesen, J.; Schaub, R.; Laegsgaard, E.; Hammer, B.; Besenbacher, F. *Science* **2007**, *315*, 1692.

(610) Gong, X. Q.; Selloni, A.; Dulub, O.; Jacobson, P.; Diebold, U. *J. Am. Chem. Soc.* **2008**, *130*, 370.

(611) Zhang, L.; Cosandey, F.; Persaud, R.; Madey, T. E. *Surf. Sci.* **1999**, *439*, 73.

(612) Cosandey, F.; Zhang, L.; Madey, T. E. *Surf. Sci.* **2001**, *474*, 1.

(613) Akita, T.; Tanaka, K.; Tsubota, S.; Haruta, M. *J. Electron Microsc.* **2000**, *49*, 657.

(614) Trovarelli, A. *Catal. Rev.—Sci. Eng.* **1996**, *38*, 439.

(615) Ganduglia-Pirovano, M. V.; Hofmann, A.; Sauer, J. *Surf. Sci. Rep.* **2007**, *62*, 219.

(616) Rodriguez, J. A.; Wang, X.; Liu, P.; Wen, W.; Hanson, J. C.; Hrbek, J.; Perez, M.; Evans, J. *Top. Catal.* **2007**, *44*, 73.

(617) Laguna, O. H.; Romero Sarria, F.; Centeno, M. A.; Odriozola, J. A. *J. Catal.* **2010**, *276*, 360.

(618) Chen, Y.; Hu, P.; Lee, M. H.; Wang, H. F. *Surf. Sci.* **2008**, *602*, 1736.

(619) Nolan, M.; Verdugo, V. S.; Metiu, H. *Surf. Sci.* **2008**, *602*, 2734.

(620) Zhang, C. J.; Michaelides, A.; King, D. A.; Jenkins, S. J. *J. Am. Chem. Soc.* **2010**, *132*, 2175.

(621) Zhang, C. J.; Michaelides, A.; King, D. A.; Jenkins, S. J. *J. Phys. Chem. C* **2009**, *113*, 6411.

(622) Zhang, C.; Michaelides, A.; King, D. A.; Jenkins, S. J. *J. Chem. Phys.* **2008**, *129*, 8.

(623) Hernandez, W. Y.; Romero-Sarria, F.; Centeno, M. A.; Odriozola, J. A. *J. Phys. Chem. C* **2010**, *114*, 10857.

(624) Qian, K.; Lv, S.; Xiao, X.; Sun, H.; Lu, J.; Luo, M.; Huang, W. *J. Mol. Catal. A: Chem.* **2009**, *306*, 40.

(625) Rodriguez, J. A.; Perez, M.; Evans, J.; Liu, G.; Hrbek, J. *J. Chem. Phys.* **2005**, *122*, 4.

(626) Rodriguez, J. A.; Liu, P.; Hrbek, J.; Evans, J.; Perez, M. *Angew. Chem., Int. Ed.* **2007**, *46*, 1329.

(627) Lu, J. L.; Gao, H. J.; Shaikhutdinov, S.; Freund, H. J. *Surf. Sci.* **2006**, *600*, 5004.

(628) Lu, J. L.; Gao, H. J.; Shaikhutdinov, S.; Freund, H. J. *Catal. Lett.* **2007**, *114*, 8.

(629) Baron, M.; Bondarchuk, O.; Stacchiola, D.; Shaikhutdinov, S.; Freund, H. J. *J. Phys. Chem. C* **2009**, *113*, 6042.

(630) Castellani, N. J.; Branda, M. A.; Neyman, K. M.; Illas, F. *J. Phys. Chem. C* **2009**, *113*, 4948.

(631) Weststrate, C. J.; Westerstrom, R.; Lundgren, E.; Mikkelsen, A.; Andersen, J. N. *J. Phys. Chem. C* **2009**, *113*, 724.

(632) Weststrate, C. J.; Resta, A.; Westerstrom, R.; Lundgren, E.; Mikkelsen, A.; Andersen, J. N. *J. Phys. Chem. C* **2008**, *112*, 6900.

(633) Akita, T.; Okumura, M.; Tanaka, K.; Kohyama, M.; Haruta, M. *J. Mater. Sci.* **2005**, *40*, 3101.

(634) Akita, T.; Tanaka, K.; Kohyama, M.; Haruta, M. *Catal. Today* **2007**, *122*, 233.

(635) Akita, T.; Tanaka, K.; Kohyama, M. *J. Mater. Sci.* **2008**, *43*, 3917.

(636) Metois, J. J.; Heinemann, K.; Poppa, H. *Appl. Phys. Lett.* **1976**, *29*, 134.

(637) Green, A. K.; Dancy, J.; Bauer, E. *J. Vac. Sci. Technol.* **1970**, *7*, 159.

(638) Hojrup-Hansen, K.; Ferrero, S.; Henry, C. R. *Appl. Surf. Sci.* **2004**, *226*, 167.

(639) Kizuka, T.; Tanaka, N. *Phys. Rev. B* **1997**, *56*, R10079.

(640) Pauwels, B.; Van Tendeloo, G.; Bouwen, W.; Kuhn, L. T.; Lievens, P.; Lei, H.; Hou, M. *Phys. Rev. B* **2000**, *62*, 10383.

(641) Risse, T.; Shaikhutdinov, S.; Nilius, N.; Sterrer, M.; Freund, H.-J. *Acc. Chem. Res.* **2008**, *41*, 949.

(642) Sterrer, M.; Risse, T.; Heyde, M.; Rust, H. P.; Freund, H. J. *Phys. Rev. Lett.* **2007**, *98*, 206103.

(643) Benia, H. M.; Lin, X.; Gao, H. J.; Nilius, N.; Freund, H. J. *J. Phys. Chem. C* **2007**, *111*, 10528.

(644) Sterrer, M.; Yulikov, M.; Fischbach, E.; Heyde, M.; Rust, H. P.; Pacchioni, G.; Risse, T.; Freund, H. J. *Angew. Chem., Int. Ed.* **2006**, *45*, 2630.

(645) Ricci, D.; Bongiorno, A.; Pacchioni, G.; Landman, U. *Phys. Rev. Lett.* **2006**, *97*, 036106.

(646) Lin, X.; Yang, B.; Benia, H. M.; Myrach, P.; Yulikov, M.; Aumer, A.; Brown, M. A.; Sterrer, M.; Bondarchuk, O.; Kieseritzky, E.; Rocker; Risse, T.; Gao, H. J.; Nilius, N.; Freund, H. J. *J. Am. Chem. Soc.* **2010**, *132*, 7745.

(647) Shaikhutdinov, S. K.; Meyer, R.; Naschitzki, M.; Bäumer, M.; Freund, H. J. *Catal. Lett.* **2003**, *86*, 211.

(648) Starr, D. E.; Shaikhutdinov, S. K.; Freund, H. J. *Top. Catal.* **2005**, *36*, 33.

(649) Nilius, N.; Rienks, E. D. L.; Rust, H. P.; Freund, H. J. *Phys. Rev. Lett.* **2005**, *95*, 4.

(650) Lemire, C.; Meyer, R.; Shaikhutdinov, S. K.; Freund, H. J. *Surf. Sci.* **2004**, *552*, 27.

(651) Gatel, C.; Snoeck, E. *Surf. Sci.* **2007**, *601*, 1031.

(652) Haruta, A. *Chem. Rec.* **2003**, *3*, 75.

(653) Buffat, P.; Borel, J. P. *Phys. Rev. A* **1976**, *13*, 2287.

(654) Xu, C.; Oh, W. S.; Liu, G.; Kim, D. Y.; Goodman, D. W. *J. Vac. Sci. Technol., A* **1997**, *15*, 1261.

(655) Kitchin, J. R.; Barteau, M. A.; Chen, J. G. G. *Surf. Sci.* **2003**, *526*, 323.

(656) Mitchell, C. E. J.; Howard, A.; Carney, M.; Egdell, R. G. *Surf. Sci.* **2001**, *490*, 196.

(657) Lee, S.; Fan, C. Y.; Wu, T. P.; Anderson, S. L. *Surf. Sci.* **2005**, *578*, 5.

(658) Parker, S. C.; Campbell, C. T. *Top. Catal.* **2007**, *44*, 3.

(659) Parker, S. C.; Campbell, C. T. *Phys. Rev. B* **2007**, *75*, 15.

(660) Lai, X. F.; Goodman, D. W. *J. Mol. Catal. A: Chem.* **2000**, *162*, 33.

(661) Bondzie, V.; Parker, S.; Campbell, C. *Catal. Lett.* **1999**, *63*, 143.

(662) Yang, F.; Chen, M. S.; Goodman, D. W. *J. Phys. Chem. C* **2009**, *113*, 254.

(663) Kolmakov, A.; Goodman, D. W. *Catal. Lett.* **2000**, *70*, 93.

(664) Kolmakov, A.; Goodman, D. W. *Surf. Sci.* **2001**, *490*, L597.

(665) Liu, Z. P.; Gong, X. Q.; Kohanoff, J.; Sanchez, C.; Hu, P. *Phys. Rev. Lett.* **2003**, *91*, 266102.

(666) Ji, X.; Zuppero, A.; Gidwani, J. M.; Somorjai, G. A. *J. Am. Chem. Soc.* **2005**, *127*, 5792.

(667) Min, B. K.; Wallace, W. T.; Goodman, D. W. *J. Phys. Chem. B* **2004**, *108*, 14609.

(668) Chen, M. S.; Goodman, D. W. *Science* **2004**, *306*, 252.

(669) Chen, M. S.; Goodman, D. W. *Surf. Sci.* **2005**, *574*, 259.

(670) Chen, M. S.; Wallace, W. T.; Kumar, D.; Yan, Z.; Gath, K. K.; Cai, Y.; Kuroda, Y.; Goodman, D. W. *Surf. Sci.* **2005**, *581*, 115.

(671) Chen, M. S.; Cai, Y.; Yan, Z.; Goodman, D. W. *J. Am. Chem. Soc.* **2006**, *128*, 6341.

(672) Chen, M. S.; Luo, K.; Kumar, D.; Wallace, W. T.; Yi, C. W.; Gath, K. K.; Goodman, D. W. *Surf. Sci.* **2007**, *601*, 632.

(673) Park, J. B.; Conner, S. F.; Chen, D. A. *J. Phys. Chem. C* **2008**, *112*, 5490.

(674) Naya, K.; Ishikawa, R.; Fukui, K. *J. Phys. Chem. C* **2009**, *113*, 10726.

(675) Majimel, J.; Lamirand-Majimel, M.; Moog, I.; Feral-Martin, C.; Treguer-Delapierre, M. *J. Phys. Chem. C* **2009**, *113*, 9275.

(676) Takei, T.; Okuda, I.; Bando, K. K.; Akita, T.; Haruta, M. *Chem. Phys. Lett.* **2010**, *493*, 207.

(677) Date, M.; Okumura, M.; Tsubota, S.; Haruta, M. *Angew. Chem., Int. Ed.* **2004**, *43*, 2129.

(678) Han, Y. F.; Zhong, Z. Y.; Ramesh, K.; Chen, F. X.; Chen, L. W. *J. Phys. Chem. C* **2007**, *111*, 3163.

(679) Zhong, Z. Y.; Highfield, J.; Lin, M.; Teo, J.; Han, Y. F. *Langmuir* **2008**, *24*, 8576.

(680) Bond, G. C.; Thompson, D. T. *Gold Bull.* **2000**, *33*, 41.

(681) Green, I. X.; Tang, W. J.; Neurock, M.; Yates, J. T. *Science* **2011**, *333*, 736.

(682) Haruta, M. *CATTECH* **2002**, *6*, 102.

(683) Choudhary, T. V.; Goodman, D. W. *Appl. Catal. A-Gen.* **2005**, *291*, 32.

(684) Molina, L. M.; Rasmussen, M. D.; Hammer, B. *J. Chem. Phys.* **2004**, *120*, 7673.

(685) Arenz, M.; Landman, U.; Heiz, U. *ChemPhysChem* **2006**, *7*, 1871.

(686) Lopez, N.; Janssens, T. V. W.; Clausen, B. S.; Xu, Y.; Mavrikakis, M.; Bligaard, T.; Norskov, J. K. *J. Catal.* **2004**, *223*, 232.

(687) Valden, M.; Pak, S.; Lai, X.; Goodman, D. W. *Catal. Lett.* **1998**, *56*, 7.

(688) Kung, H. H.; Kung, M. C.; Costello, C. K. *J. Catal.* **2003**, *216*, 425.

(689) Campbell, C. T.; Grant, A. W.; Starr, D. E.; Parker, S. C.; Bondzie, V. A. *Top. Catal* **2000**, *14*, 43.

(690) Lee, S. S.; Fan, C. Y.; Wu, T. P.; Anderson, S. L. *J. Am. Chem. Soc.* **2004**, *126*, 5682.

(691) Meier, D. C.; Goodman, D. W. *J. Am. Chem. Soc.* **2004**, *126*, 1892.

(692) Tong, X.; Benz, L.; Kemper, P.; Metiu, H.; Bowers, M. T.; Buratto, S. K. *J. Am. Chem. Soc.* **2005**, *127*, 13516.

(693) Miller, J. T.; Kropf, A. J.; Zha, Y.; Regalbuto, J. R.; Delannoy, L.; Louis, C.; Bus, E.; van Bokhoven, J. A. *J. Catal.* **2006**, *240*, 222.

(694) Bondzie, V. A.; Parker, S. C.; Campbell, C. T. *J. Vac. Sci. Technol., A* **1999**, *17*, 1717.

(695) Stiehl, J. D.; Kim, T. S.; Reeves, C. T.; Meyer, R. J.; Mullins, C. B. *J. Phys. Chem. B* **2004**, *108*, 7917.

(696) Schumacher, B.; Plzak, V.; Kinne, M.; Behm, R. J. *Catal. Lett.* **2003**, *89*, 109.

(697) Herzing, A. A.; Kiely, C. J.; Carley, A. F.; Landon, P.; Hutchings, G. J. *Science* **2008**, *321*, 1331.

(698) Sanchez, A.; Abbet, S.; Heiz, U.; Schneider, W. D.; Hakkinen, H.; Barnett, R. N.; Landman, U. *J. Phys. Chem. A* **1999**, *103*, 9573.

(699) Schmid, G. *Chem. Soc. Rev.* **2008**, *37*, 1909.

(700) Boyen, H. G.; Kastle, G.; Weigl, F.; Koslowski, B.; Dietrich, C.; Ziemann, P.; Spatz, J. P.; Riethmuller, S.; Hartmann, C.; Moller, M.; Schmid, G.; Garnier, M. G.; Oelhafen, P. *Science* **2002**, *297*, 1533.

(701) Lopez, N.; Norskov, J. K. *J. Am. Chem. Soc.* **2002**, *124*, 11262.

(702) Janssens, T. V. W.; Carlsson, A.; Puig-Molina, A.; Clausen, B. S. *J. Catal.* **2006**, *240*, 108.

(703) Chretien, S.; Buratto, S. K.; Metiu, H. *Curr. Opin. Solid State Mater. Sci.* **2007**, *11*, 62.

(704) Janssens, T. V. W.; Clausen, B. S.; Hvolbaek, B.; Falsig, H.; Christensen, C. H.; Bligaard, T.; Norskov, J. K. *Top. Catal.* **2007**, *44*, 15.

(705) Hvolbaek, B.; Janssens, T. V. W.; Clausen, B. S.; Falsig, H.; Christensen, C. H.; Norskov, J. K. *Nano Today* **2007**, *2*, 14.

(706) Grunwaldt, J.-D.; Maciejewski, M.; Becker, O. S.; Fabrizioli, P.; Baiker, A. *J. Catal.* **1999**, *186*, 458.

(707) Zielasek, V.; Jurgens, B.; Schulz, C.; Biener, J.; Biener, M. M.; Hamza, A. V.; Baumer, M. *Angew. Chem., Int. Ed.* **2006**, *45*, 8241.

(708) Xu, C. X.; Su, J. X.; Xu, X. H.; Liu, P. P.; Zhao, H. J.; Tian, F.; Ding, Y. *J. Am. Chem. Soc.* **2007**, *129*, 42.

(709) Centeno, M. A.; Hadjiivanov, K.; Venkov, T.; Klimev, H.; Odriozola, J. A. *J. Mol. Catal. A: Chem.* **2006**, *252*, 142.

(710) Yoon, B.; Hakkinen, H.; Landman, U.; Worz, A. S.; Antonietti, J.-M.; Abbet, S.; Judai, K.; Heiz, U. *Science* **2005**, *307*, 403.

(711) Manzoli, M.; Boccuzzi, F.; Chiorino, A.; Vindigni, F.; Deng, W.; Flytzani-Stephanopoulos, M. *J. Catal.* **2007**, *245*, 308.

(712) Carrettin, S.; Concepcion, P.; Corma, A.; Lopez-Nieto, J. M.; Puntes, V. F. *Angew. Chem., Int. Ed.* **2004**, *43*, 2538.

(713) Campbell, C. T. *Science* **2004**, *306*, 234.

(714) Carrettin, S.; Hao, Y.; Aguilar-Guerrero, V.; Gates, B.; Trasobares, S.; Calvino, J.; Corma, A. *Chem.—Eur. J.* **2007**, *13*, 7771.

(715) Schwartz, V.; Mullins, D. R.; Yan, W.; Chen, B.; Dai, S.; Overbury, S. H. *J. Phys. Chem. B* **2004**, *108*, 15782.

(716) Yang, J. H.; Henao, J. D.; Raphulu, M. C.; Wang, Y.; Caputo, T.; Groszek, A. J.; Kung, M. C.; Scurrell, M. S.; Miller, J. T.; Kung, H. H. *J. Phys. Chem. B* **2005**, *109*, 10319.

(717) Calla, J. T.; Bore, M. T.; Datye, A. K.; Davis, R. J. *J. Catal.* **2006**, *238*, 458.

(718) Hernandez, N. C.; Grau-Crespo, R.; de Leeuw, N. H.; Sanz, J. F. *Phys. Chem. Chem. Phys.* **2009**, *11*, 5246.

3052

dx.doi.org/10.1021/cr200041p | *Chem. Rev.* 2012, 112, 2987–3054

(719) Vijay, A.; Mills, G.; Metiu, H. *J. Chem. Phys.* **2003**, *118*, 6536.

(720) Remediakis, I. N.; Lopez, N.; Norskov, J. K. *Angew. Chem., Int. Ed.* **2005**, *44*, 1824.

(721) Hakkinen, H. *Chem. Soc. Rev.* **2008**, *37*, 1847.

(722) Yan, Z.; Chinta, S.; Mohamed, A. A.; Fackler, J. P.; Goodman, D. W. *J. Am. Chem. Soc.* **2005**, *127*, 1604.

(723) Minato, T.; Susaki, T.; Shiraki, S.; Kato, H. S.; Kawai, M.; Aika, K. I. *Surf. Sci.* **2004**, *566*, 1012.

(724) Stiehl, J. D.; Gong, J. L.; Ojifinni, R. A.; Kim, T. S.; McClure, S. M.; Mullins, C. B. *J. Phys. Chem. B* **2006**, *110*, 20337.

(725) Chen, M. S.; Goodman, D. W. *Catal. Today* **2006**, *111*, 22.

(726) Lee, J. Y.; Schwank, J. *J. Catal.* **1986**, *102*, 207.

(727) Kobayashi, Y.; Nasu, S.; Tsubota, S.; Haruta, M. *Hyperfine Interact.* **2000**, *126*, 95.

(728) Guzman, J.; Gates, B. C. *J. Am. Chem. Soc.* **2004**, *126*, 2672.

(729) Daniells, S. T.; Overweg, A. R.; Makkee, M.; Moulijn, J. A. *J. Catal.* **2005**, *230*, 52.

(730) Boyd, D.; Golunski, S.; Hearne, G. R.; Magadzu, T.; Mallick, K.; Raphulu, M. C.; Venugopal, A.; Scurrell, M. S. *Appl. Catal., A* **2005**, *292*, 76.

(731) Hutchings, G. J.; Hall, M. S.; Carley, A. F.; Landon, P.; Solsona, B. E.; Kiely, C. J.; Herzing, A.; Makkee, M.; Moulijn, J. A.; Overweg, A.; Fierro-Gonzalez, J. C.; Guzman, J.; Gates, B. C. *J. Catal.* **2006**, *242*, 71.

(732) Camellone, M. F.; Fabris, S. *J. Am. Chem. Soc.* **2009**, *131*, 10473.

(733) Skoda, M.; Cabala, M.; Matolinova, I.; Prince, K. C.; Skala, T.; Sutara, F.; Veltruska, K.; Matolin, V. *J. Chem. Phys.* **2009**, *130*, 7.

(734) Guzman, J.; Gates, B. C. *Angew. Chem., Int. Ed.* **2003**, *42*, 690.

(735) Liu, L. M.; McAllister, B.; Ye, H. Q.; Hu, P. *J. Am. Chem. Soc.* **2006**, *128*, 4017.

(736) Park, E. D.; Lee, J. S. *J. Catal.* **1999**, *186*, 1.

(737) Costello, C. K.; Yang, J. H.; Law, H. Y.; Wang, Y.; Lin, J. N.; Marks, L. D.; Kung, M. C.; Kung, H. H. *Appl. Catal., A* **2003**, *243*, 15.

(738) Bongiorno, A.; Landman, U. *Phys. Rev. Lett.* **2005**, *95*, 106102.

(739) Gao, F.; Wood, T. E.; Goodman, D. W. *Catal. Lett.* **2010**, *134*, 9.

(740) Yan, T.; Gong, J. L.; Flaherty, D. W.; Mullins, C. B. *J. Phys. Chem. C* **2011**, *115*, 2057.

(741) Kim, J.; Dohnalek, Z.; Kay, B. D. *J. Am. Chem. Soc.* **2005**, *127*, 14592.

(742) Zope, B. N.; Hibbitts, D. D.; Neurock, M.; Davis, R. J. *Science* **2010**, *330*, 74.

(743) Hakkinen, H.; Landman, U. *J. Am. Chem. Soc.* **2001**, *123*, 9704.

(744) Hayashi, T.; Tanaka, K.; Haruta, M. *J. Catal.* **1998**, *178*, 566.

(745) Ajo, H. M.; Bondzie, V. A.; Campbell, C. T. *Catal. Lett.* **2002**, *78*, 359.

(746) Liu, T.; Hacarlioglu, P.; Oyama, S. T.; Luo, M. F.; Pan, X. R.; Lu, J. Q. *J. Catal.* **2009**, *267*, 202.

(747) Sinha, A. K.; Seelan, S.; Tsubota, S.; Haruta, M. *Top. Catal.* **2004**, *29*, 95.

(748) Stangland, E. E.; Stavens, K. B.; Andres, R. P.; Delgass, W. N. *J. Catal.* **2000**, *191*, 332.

(749) Mul, G.; Zwijnenburg, A.; van der Linden, B.; Makkee, M.; Moulijn, J. A. *J. Catal.* **2001**, *201*, 128.

(750) Uphade, B. S.; Yamada, Y.; Akita, T.; Nakamura, T.; Haruta, M. *Appl. Catal., A* **2001**, *215*, 137.

(751) Sinha, A. K.; Seelan, S.; Akita, T.; Tsubota, S.; Haruta, M. *Catal. Lett.* **2003**, *85*, 223.

(752) Sinha, A. K.; Seelan, S.; Tsubota, S.; Haruta, M. *Angew. Chem., Int. Ed.* **2004**, *43*, 1546.

(753) Taylor, B.; Lauterbach, J.; Blau, G. E.; Delgass, W. N. *J. Catal.* **2006**, *242*, 142.

(754) Sacaliuc, E.; Beale, A. M.; Weckhuysen, B. M.; Nijhuis, T. A. *J. Catal.* **2007**, *248*, 235.

(755) Grzybowska-Swierkosz, B. *Catal. Today* **2006**, *112*, 3.

(756) Huang, J. H.; Takei, T.; Akita, T.; Ohashi, H.; Haruta, M. *Appl. Catal., B* **2010**, *95*, 430.

(757) Jiang, J.; Oxford, S. M.; Fu, B. S.; Kung, M. C.; Kung, H. H.; Ma, J. T. *Chem. Commun.* **2010**, *46*, 3791.

(758) Taylor, B.; Lauterbach, J.; Delgass, W. N. *Appl. Catal., A* **2005**, *291*, 188.

(759) Huang, J. H.; Akita, T.; Faye, J.; Fujitani, T.; Takei, T.; Haruta, M. *Angew. Chem., Int. Ed.* **2009**, *48*, 7862.

(760) Ojeda, M.; Iglesia, E. *Chem. Commun.* **2009**, 352.

(761) Bravo-Suarez, J. J.; Bando, K. K.; Lu, J. Q.; Fujitani, T.; Oyama, S. T. *J. Catal.* **2008**, *255*, 114.

(762) Bravo-Suarez, J. J.; Bando, K. K.; Lu, J. I.; Haruta, M.; Fujitani, T.; Oyama, S. T. *J. Phys. Chem. C* **2008**, *112*, 1115.

(763) Clerici, M. G.; Bellussi, G.; Romano, U. *J. Catal.* **1991**, *129*, 159.

(764) Nijhuis, T. A.; Sacaliuc-Parvulescu, E.; Govender, N. S.; Schouten, J. C.; Weckhuysen, B. M. *J. Catal.* **2009**, *265*, 161.

(765) Liu, Y.; Murata, K.; Inaba, M.; Mimura, N. *Catal. Lett.* **2003**, *89*, 49.

(766) Murata, K.; Kiyozumi, Y. *Chem. Commun.* **2001**, 1356.

(767) Konova, P.; Naydenov, A.; Tabakova, T.; Mehandjiev, D. *Catal. Commun.* **2004**, *5*, 537.

(768) Nijhuis, T. A.; Weckhuysen, B. M. *Chem. Commun.* **2005**, 6002.

(769) Burch, R. *Phys. Chem. Chem. Phys.* **2006**, *8*, 5483.

(770) Fu, Q.; Deng, W. L.; Saltsburg, H.; Flytzani-Stephanopoulos, M. *Appl. Catal., B* **2005**, *56*, 57.

(771) Rodriguez, J. A.; Evans, J.; Graciani, J.; Park, J. B.; Liu, P.; Hrbek, J.; Sanz, J. F. *J. Phys. Chem. C* **2009**, *113*, 7364.

(772) Andreeva, D.; Idakiev, V.; Tabakova, T.; Andreev, A. *J. Catal.* **1996**, *158*, 354.

(773) Boccuzzi, F.; Chiorino, A.; Manzoli, M.; Andreeva, D.; Tabakova, T.; Ilieva, L.; Iadakiev, V. *Catal. Today* **2002**, *75*, 169.

(774) Venugopal, A.; Scurrell, M. S. *Appl. Catal., A* **2004**, *258*, 241.

(775) Venugopal, A.; Scurrell, M. S. *Appl. Catal., A* **2003**, *245*, 137.

(776) Hua, J.; Zheng, Q.; Zheng, Y.; Wei, K.; Lin, X. *Catal. Lett.* **2005**, *102*, 99.

(777) Daniells, S. T.; Makkee, M.; Moulijn, J. A. *Catal. Lett.* **2005**, *100*, 39.

(778) Sakurai, H.; Ueda, A.; Kobayashi, T.; Haruta, M. *Chem. Commun.* **1997**, 271.

(779) Fu, Q.; Weber, A.; Flytzani-Stephanopoulos, M. *Catal. Lett.* **2001**, *77*, 87.

(780) Fu, Q.; Kudriavtseva, S.; Saltsburg, H.; Flytzani-Stephanopoulos, M. *Chem. Eng. J.* **2003**, *93*, 41.

(781) Yi, N.; Si, R.; Saltsburg, H.; Flytzani-Stephanopoulos, M. *Appl. Catal., B* **2010**, *95*, 87.

(782) Yi, N.; Si, R.; Saltsburg, H.; Flytzani-Stephanopoulos, M. *Energy Environ. Sci* **2010**, *3*, 831.

(783) Liu, Z. P.; Jenkins, S. J.; King, D. A. *Phys. Rev. Lett.* **2005**, *94*, 196102.

(784) Sakurai, H.; Akita, T.; Tsubota, S.; Kiuchi, M.; Haruta, M. *Appl. Catal., A* **2005**, *291*, 179.

(785) Tibiletti, D.; Fonseca, A. A.; Burch, R.; Chen, Y.; Fisher, J. M.; Goguet, A.; Hardacre, C.; Hu, P.; Thompsett, D. *J. Phys. Chem. B* **2005**, *109*, 22553.

(786) Park, J. B.; Graciani, J.; Evans, J.; Stacchiola, D.; Ma, S. G.; Liu, P.; Nambu, A.; Sanz, J. F.; Hrbek, J.; Rodriguez, J. A. *Proc. Natl. Acad. Sci. U.S.A.* **2009**, *106*, 4975.

(787) Rodriguez, J. A.; Stacchiola, D. *Phys. Chem. Chem. Phys.* **2010**, *12*, 9557.

(788) Park, J. B.; Graciani, J.; Evans, J.; Stacchiola, D.; Senanayake, S. D.; Barrio, L.; Liu, P.; Sanz, J. F.; Hrbek, J.; Rodriguez, J. A. *J. Am. Chem. Soc.* **2010**, *132*, 356.

(789) Gokhale, A. A.; Dumesic, J. A.; Mavrikakis, M. *J. Am. Chem. Soc.* **2008**, *130*, 1402.

(790) Gonzalez, I. D.; Navarro, R. M.; Wen, W.; Marinkovic, N.; Rodriguez, J. A.; Rosa, F.; Fierro, J. L. G. *Catal. Today* **2010**, *149*, 372.

(791) Kim, C. H.; Thompson, L. T. *J. Catal.* **2005**, *230*, 66.

(792) Bond, G. *Gold Bull.* **2009**, *42*, 337.

3053

dx.doi.org/10.1021/cr200041p |*Chem. Rev.* 2012, 112, 2987–3054

(793) Karpenko, A.; Leppelt, R.; Cai, J.; Plzak, V.; Chuvilin, A.; Kaiser, U.; Behm, R. J. *J. Catal.* **2007**, *250*, 139.

(794) Silberova, B. A. A.; Makkee, M.; Moulijn, J. A. *Top. Catal.* **2007**, *44*, 209.

(795) Deng, W. L.; Flytzani-Stephanopoulos, M. *Angew. Chem., Int. Ed.* **2006**, *45*, 2285.

(796) Luengnaruemitchai, A.; Osuwan, S.; Gulari, E. *Catal. Commun.* **2003**, *4*, 215.

(797) Jacobs, G.; Chenu, E.; Patterson, P. M.; Williams, L.; Sparks, D.; Thomas, G.; Davis, B. H. *Appl. Catal., A* **2004**, *258*, 203.

(798) Schubert, M. M.; Venugopal, A.; Kahlich, M. J.; Plzak, V.; Behm, R. J. *J. Catal.* **2004**, *222*, 32.

(799) Bus, E.; Miller, J. T.; van Bokhoven, J. A. *J. Phys. Chem. B* **2005**, *109*, 14581.

(800) Rodriguez, J. A.; Perez, M.; Jirsak, T.; Evans, J.; Hrbek, J.; Gonzalez, L. *Chem. Phys. Lett.* **2003**, *378*, 526.

(801) Rodriguez, J. A.; Liu, P.; Vines, F.; Illas, F.; Takahashi, Y.; Nakamura, K. *Angew. Chem., Int. Ed.* **2008**, *47*, 6685.

(802) Wolf, A.; Schuth, F. *Appl. Catal., A* **2002**, *226*, 1.

(803) Hutchings, G. J.; Brust, M.; Schmidbaur, H. *Chem. Soc. Rev.* **2008**, *37*, 1759.

(804) Somorjai, G. A.; Rupprechter, G. *J. Phys. Chem. B* **1999**, *103*, 1623.

(805) St Clair, T. P.; Goodman, D. W. *Top. Catal.* **2000**, *13*, 5.

(806) Christmann, K.; Schwede, S.; Schubert, S.; Kudernatsch, W. *ChemPhysChem* **2010**, *11*, 1344.

(807) Pan, M.; Flaherty, D. W.; Mullins, C. B. *J. Phys. Chem. Lett.* **2011**, *2*, 1363.

(808) Rashkeev, S. N.; Lupini, A. R.; Overbury, S. H.; Pennycook, S. J.; Pantelides, S. T. *Phys. Rev. B* **2007**, *76*, 035438.

(809) Della Pina, C.; Falletta, E.; Prati, L.; Rossi, M. *Chem. Soc. Rev.* **2008**, *37*, 2077.

NOTE ADDED AFTER ASAP PUBLICATION

The original review that was published ASAP on April 27, 2011, contained material inappropriately cited. The author has rewritten the review to correct the content and to be in compliance with the ACS Ethical Guidelines to Publication of Chemical Research. The original review is available as Supporting Information for this corrected version.

3054

dx.doi.org/10.1021/cr200041p |*Chem. Rev.* 2012, 112, 2987–3054